UNIVERSITÀ DEGLI STUDI DI PADOVA

UNIVERSITÀ DI PADOVA FACOLTÀ DI INGEGNERIA

DIPARTIMENTO DI INGEGNERIA DELL'INFORMAZIONE

SCUOLA DI DOTTORATO IN INGEGNERIA DELL'INFORMAZIONE

CURRICULUM IN SCIENZA E TECNOLOGIA DELL'INFORMAZIONE

XXX Ciclo

Network Science for IoT

Dottorando

ANNA VALERIA GUGLIELMI

Supervisore:

Dr. Leonardo Badia

Direttore della Scuola:

Ch.^{mo} Prof. Andrea Neviani

Anno Accademico 2016/2017

Abstract

The research work presented in this thesis is based on the concept and defintion of network that can spread in several and different real world contexts. Indeed, we can refer to a network in a telecommunications sense considering a collection of transmitters, receivers, and communication channels that send or are used to send information to one another. However, as a matter of fact, in nature there are other several examples of networks: the human brain is one of them. The relationship between the actors in Hollywood can be studied in terms of network as well, a generic social community can be compared to a network, eco-systems are networks of species. The recent Network Science aims at studying all these systems using a set of common mathematical methods. In the following of the thesis, we will focus on some of well known telecommunications networks issues using standard telecommunications procedures to address them, with relevant reference to video flow transmissions and management of electric vehicles networks. At the same time, different models aiming at reach the same goals in contexts that may differ from a telecommunications setup can be used. In more details, we will evaluate queueing systems, jamming problems, groups recognition in networks, and mobile computing using game theoretic approaches. It is worth noting that this aspect can be also seen in a reverse order. Indeed, we will discuss how standard telecommunications analysis can be used to investigate on problems not directly related to a telecommunications background. In particular, one of our future purposes is to investigate on the brain connectivity that is raising significant interest in the recent scientific society.

Il lavoro di ricerca presentato in questa tesi è basato sul concetto e definizione di rete che può spaziare in diversi contesti del mondo reale. Infatti, facciamo riferimento ad una rete di telecomunicazioni se consideriamo una collezione di trasmettitori, ricevitori e canali di comunicazione che trasmettono o vengono usati per trasmettere informazioni. Tuttavia, anche in natura si possono trovare diversi esempi di rete: ad esempio il cervello umano è uno di questi. O ancora le relazioni tra gli attori ad Hollywood può essere studiato in termini di rete, una generica comunità sociale può essere comparata ad una rete, gli eco-sistemi sono da considerare come reti di specie. Network Science è la disciplina scientifica che si propone di studiare tutti questi sistemi usando un insieme comune di modelli matematici. In questa tesi ci focalizzeremo su alcune ben note problematiche relative a reti di telecomunicazioni usando classici metodi e modelli nati nell'ambito delle telecomunicazioni per analizzarle; in particolare, valuteremo trasmissioni video e la gestione di reti di veicoli elettrici. Allo stesso tempo, si può pensare di applicare a queste, o simili, tematiche modelli diversi che si propongono di raggiungere gli stessi obiettivi ma in contesti che possono differire da quelli propri delle telecomunicazioni. Più approfonditamente, valuteremo per mezzo di approcci basati sulla teoria dei giochi sistemi a coda, problemi di jamming, riconoscimento di gruppi nelle reti e il mobile computing. E' bene notare che il punto di vista di quanto appena discusso può essere invertito. Infatti, discuteremo inoltre come sia possibile applicare una classica analisi nell'ambito delle telecomunicazioni per investigare su problemi che non sono direttamente collegati ad un ambiente delle telecomunicazioni. In particolare, uno dei nostri futuri obiettivi è quello di valutare la connettività tra le varie aree che si possono definire nel cervello, tematica che recentemente sta acquistando un significativo interesse nella società scientifica.

Contents

List of Figures

List of Tables

Chapter 1

Introduction

Recently one of the scientific areas that is raising significant attractiveness in the research community is the *Network Science*. Consider the society requiring cooperation between billions of individuals, or communications infrastructure integrating billions of cell phones with computer and satellites. Consider for example the ability to reason and comprehend our world requiring the coherent activity of billions of neurons in our brain, or the fact that our biological existence is based on the interactions between thousands of genes and metabolites within our cells. All these surronding systems are hopelessly complicated and are collectively called complex systems, catching the difficulty to derive their collective behavior from a knowledge of their components. Given the significant role of complex systems in our daily life, in science and in economy, their understanding, mathematical description and prediciton, and lastly control are some of the major intellectual and scientific challenges of the 21st century. Indeed, the network that encodes the interactions between genes, metabolites, and proteins integrating these elements into live cells, called cellular network, is a prerequisite for our life. The neural network capturing the connections between neurons holds the key of our understanding of how the brain works and to our consciousness. The social network, as the sum of all professional, friendship, and family ties, is the fabric of the society determining the spread of knowledge, behavior, and resources. Communications networks describing the interactions between communication devices are the heart of the modern communication system. The network of generators and transmission lines, named power grid, provides energy virtually to all modern technology.

Networks are further at the heart of some of the most innovative technologies of the 21st century, empowering everything from Google to CISCO, Facebook, and Twitter. Networks dominate science, technology, nature, and business to a much higher degree than it may be highlighted through a casual inspection. Therefore, we will not understand complex systems around us if we do not develop a deep understanding of the networks behind them. Despite the obvious diversity of complex systems, the evolution and structure of the networks behind each system is driven by a common set of laws and principles. Consequently, even if form, size, nature, age, and scope of real networks may differ, most networks are based on common organizing principles and, once we overlooked the components nature and the precise character of their interactions, the resulting networks are more similar than different from each other.

The key discovery of Network Science on which this thesis is based is that "*the architecture of networks emerging in various domains of science, nature, and technology are similar to each other, a consequence of being governed by the same organizing principles. Consequently we can use a common set of mathematical tools to explore these systems* [1]."

Several issues might characterize complex systems and the role of the Network Science is to deal with them [1]. For example, to fully understand how our cells work and the origin of disease, a complete list of genes is not enough. Indeed, we further need an accurate map of how genes, proteins, metabolites and other cellular entities interact with each other. Most cellular processes, from food

processing to sensing changes in the environment, rely on molecular networks and the breakdown of these networks is responsible for human diseases. As a consequence, the increasing awareness of the relevance of molecular networks has led to the development of network biology aiming at understanding the behavior of cellular networks. A parallel movement, called network medicine, aims to uncover the role of networks in human disease. Moreover, networks play an important role in drug development. The ultimate purpose of network pharmacology is to develop drugs that can cure diseases without significant side effects.

Another example of Network Science application is related to the terrorism, an affliction of our days requiring significant resources to combat it worldwide. Network thinking is increasingly used in the arsenal of various law enforcement agencies in charge of responding to terrorism. The aims are to disrupt the financial network of terrorist organizations and to map adversarial networks, allowing to uncover the role of their members and their capabilities. In the military doctrine, network concepts, leading to the so-called network-centric warfare, aim at fighting low intensity conflicts against terrorist and criminal networks employing decentralized flexible network organization.

A network perspective can be used also dealing with epidemic spread. While the H1N1 pandemic was not as devastating as it was feared at the beginning of the outbreak in 2009, it has a special role in the history of epidemics. Indeed, it is the first pandemic whose course and time evolution was accurately predicted months before the pandemic reached its peak. Understanding the role of transportation networks in the spread of viruses was the key factor that made its prediction possible. In general, before 2000 epidemic modeling was dominated by compartment-based models, which assume that everyone can infect everyone else in the same socio-physical compartment. A fundamental change has been brought by the emergence of a network-based framework, offering a new level of predictability. Nowadays, epidemic prediction is one of the most active applications of Network Science.

The human brain, made of hundreds of billions of interlinked neurons, is one of the least understood networks from the Network Science perspective. Indeed, we are interested in maps telling us which neurons are linked together. The only fully mapped brain available for research is that of the C. elegans worm, consisting of only 302 neurons. Detailed maps of mammalian brains could allow the understanding and curing of numerous neurological and brain diseases. Consequently, brain research could turn it into one of the most prolific application area of Network Science. In 2010 the National Institutes of Health in the U.S. has initiated the Connectome project aiming at developing technologies that could provide accurate neuron-level maps of mammalian brains.

In the *Information Communication Technology* (ICT) context, the most well known example of network is the *Internet*. Its advent in the 70s can be seen as the first building block for the spread and development of *telecommunication networks*. Afterwards, in the 80s and 90s further advancements were made thanks to the revolution in personal communications brought by mobile phone networks. Nowadays, communication networks pervade every ICT system: the Internet, mobile networks, smart grids, and smart transportation systems are just some examples. In the next future, we can foresee further applications involving, for example, network virtualization, distributed assessment, and the transfer of energy via radio.

Before the emergence of the Internet and other data networks, *telecommunication* had a clear meaning: the telephone (and before it the telegraph) was an application of technology that allowed people to communicate at a distance by voice (and earlier by encoded electronic signals), and telephone service was provided by the *Public Switched Telephone Network* (PSTN). Nowadays, with the term telecommunication we refer, in general, to the transmission of signals, messages, sounds and images or intelligence of any nature by wired, radio, optical, or other electromagnetic systems. Indeed, more recently, communications at a distance have expanded to include e-mail, instant messaging, Web browsing, video conferencing, data transport, and several forms of distributed collaboration, allowed by transmission media that have further expanded from traditional copper wires to include microwave, terrestrial wireless, hybrid fiber/coaxial cable, satellite, and broadband fiber transport.

The general exchange of information between communication participiants, either electrically over physical media, such as cables, or via electromagnetic radiation, involves the use of a technology, and, usually, we refer to telecommunications, i.e., in its plural form, because it entails many different technologies. In this context, a telecommunications network can be defined as a collection of transmitters, receivers, and communcations channels that send or are used to send general messages to one another. The main goal of the telecommunications is to provide reliable, affordable, fair, widespread devices and technologies that allow people all around the world to communicate, work together, solve problems, or just keep in touch. Consequently, several mathematical and engineering methods and models have been properly designed to address standard issues related to telecommunications aim.

One of the most addressed problems, which we may deal with when considering a transmission of information content, is *errors detection* and *errors correction*. It usually holds that information contents are divided into several packets in order to allow the different nodes in the network to share a communication channel in a non-deterministic manner (i.e., packet swithching). In particular, *Automatic Repeat Request* (ARQ) is an error control technique exploiting feedback information about faulty reception of some packets to trigger their retransmissions [2, 3]. The most efficient basic implementation of the ARQ mechanism is the *Selective Repeat* ARQ (SR ARQ) that specifically retransmitts only those packets who are reported to be in error [12]. Recently, there has been a renewed interest for ARQ, also including hybrid ARQ techniques, where plain retransmission schemes are coupled with *Forward Error Correction* (FEC) [4, 5, 17, 6, 16, 29]. ARQ-based error control is used in high-quality multimedia applications [7] and included in the evolution of the *Universal Mobile Telecommunications System* (UMTS) towards *High Speed Packet Access* (HSPA) and the so-called recent *Long Term Evolution* (LTE) [8].

It is meaningful to investigate on multimedia contents, particularly video, in order to understand their behavior and analytically characterize their performance since they are expected to be the dominant traffic component over future generation networks. Unfortunately, most of the research on multimedia transmission just resort to simulation, without strong analytical support for systematic evaluations. Regarding this, we believe that the reason why multimedia content is difficult to be characterized in an analytical manner is related to the incremental nature of source coding applied to such flows. Indeed, video flows are normally obtained through incremental encoders such as those defined by *Moving Picture Experts Group* (MPEG) [9]. As a result, it is worth noting that different packets have different roles within the video flow and, therefore, the performance of an error correction scheme, such as ARQ, cannot be simply described as a residual error probability. From a networking standpoint, it matters evaluate whether the missing packets belong to an independently encoded, rather than an incremental frame [17]. It is further unclear how to apply ARQ-like techniques to such flows. A counter-argument that is often raised against retransmission-based error control for video is that it would cause delay to grow, which is not acceptable for real-time content, such as video content.

In such a background, our objective is to propose a mathematical model exploiting discrete-time Markov chains to represent the SR ARQ retransmission mechanism for multimedia content. This aspect requires to keep into account interdependences of packets in the source coding [6], and to further evaluate their impact at the receiver's side in case a packet is missing, which will also be differently evaluated depending on the kind of packet. One of the main hurdles for ARQ evaluations is that classical investigations do not directly apply as the flow consists of different types of packets. Neverthless, by means of the use of a synthetic description of the inherent structure of the packet group (i.e., the alternation of independently encoded packets and dependently encoded packets), which we call macroscopic representation [29], we are able to greatly simplify the system analysis. Furthermore, another side purpose of this study is to disprove the claim according to which retransmission-based error control would cause a growing delay for video. Indeed, we show that ARQ can be applied quite easily if selective retransmissions are carefully chosen.

The telecommunications world is not only limited to ensuring the correct transmission and re-

ception of any kind of information contents by means of a communication channel. Indeed, another recent telecommunications aim is to advance and promote significant technology progresses in green communications and networks including wireline, optical, and wireless communications and networks. In this setup, green communications and networking means sustainable, energy-efficient, energy-aware, and environmentally aware communications and networking. Therefore, innovations, new technologies, new concepts, and new principles toward a sustainable ICT are needed. The major topics of interest includes (but are not limited to) green wireline, optical, and wireless communications and networks; network and physical layer design, strategies, algorithms, protocols, and scheduling that consider environmental factors; energy-efficient and energy-aware heterogeneous networks, self-organized, and low-power sensor networks; energy efficiency in machine-to-machine communications, cooperative communications, and smart grid networks; energy harvesting, storage, and recycling for network cross-layer optimization; environmentally-aware designs of communications and networking devices and systems; and communications and networking for environmental protection monitoring.

Among these, nowadays *electric vehicles* (EVs) networks are raising significant interest in the scientific research community. Indeed, recently alarming pollution levels and increasing world-wide oil demand are two major circumstances that lead several countries to search for alternate energy sources and decrease carbon dioxide emissions, especially from car transportation, which makes use almost exclusively of internal combustion vehicles [33]. In this context, EVs represent a promising technological choice to decrease pollution and reduce fossil fuel consumption [34]. Neverthless, their limited autonomy, long recharging times, and scarceness of recharging points pose challenges that prevent them from being suitable for many car users. Indeed, a phenomenon named *range anxiety* may arise: customers are wary of practicality, and, as a matter of fact, EVs market becomes a niche market [36]. As a consequence, public investments for a better service are discouraged, and this, in turn, further decreases the attractive aspect of EVs for the average customer. Several practical solutions are sought to avoid this problem. Above all, it may be thought of enhancing the battery capacity, reducing the charging time, or increasing the frequency of charging points. In this context, our aim is to discuss how these aspects can be integrated by a proper Markov model, thereby offering a neat analytical solution to investigate all these problems.

Another significant aspect of a network is that it might be made up of different entities that refer to different technologies, referring to a telecommunications context, and which may aim to provide or require different services with likely different goals. Therefore, keeping the network intelligence spread throughout the entire network is both a low-cost management solution and the proper way to involve the increased computational power of communication devices. Consequently, the need for scalability of modern communication networks has led to the practical establishment of several distributed management algorithms.

To mathematically characterize this aspect, it might be useful to consider a joint combination of several different theories that may be not directly related to the standard set of telecommunications methods and models. Basically, one of the purposes now is related to the further evaluation of classical telecommunications issues from a more general standpoint. We plan to consider the implementation of procedures that are far away from the standard procedures used to deal with these problems because of a different context of application but that work towards the same goal.

As a practical example, it is well known that *queueing system theory* develops to predict behaviors of systems subject to randomly arising demands. This was the spirit of the early contributions by Erlang in 1909 [49], the works by Pollaczek and Khinchine in the 1930s [40], and subsequent studies [50, 51]. Today, queueing theory finds many applications in management of communication networks or air traffic, planning of manufacturing systems, computer program scheduling, and facility dimensioning. However, the idea to use a mathematical theory to make predictions on the behavior of multiple agents is also shared by *game theory* [72], which is now becoming more and more commonly applied to telecommunications problems [52]. It will be discussed in the following of this thesis that, differently

from standard queueing theory, which still adopts a system view, game theory is even more extreme in considering that individual agents, called *players*, interact according to their particular interests, which may be different for every one of them [41].

For this reason, we consider the joint application of both theories to a scenario including multiple candidate servers, whose objective is to provide some services to their clients that, e.g., can be thought to be packets arriving at the system for transmission. We refer to this scenario as an *uplink case*. Each server represents an option available for the clients and has its own specific success probability of service completion. In this context, we model this situation as a game, where the servers are the players and they can decide to be *inactive* or *active*; staying active has a fixed local cost for the server, while a successful task completion is beneficial for the whole system. Clearly, in a system with centralized supervision, it would be best to only keep active the best server, which means the one with the highest successful probability. However, this is hindered by two facts: (i) servers act selfishly, as in any game theory setup; (ii) servers do not even know who the best server is, since they actually do not know each other's characteristics. In addition to the uplink scenario, we further consider a *downlink case*, where multiple candidate clients require services to some servers. Consequently, we investigate on how a server can strategically establish to which of the clients is better to offer a service by making some considerations regarding the system dynamics. Then, the service required, for example, downloading a specific video, might be shared later by the clients.

To further support the idea that theories spanning different environments can be jointly combined towards a common goal, we focus on other problems properly related to telecommunications networks applying a game theoretic point of view. One of these is the so-called *jamming* problem, a *security* issue that can be seen as another application of game theory to wireless networks. Indeed, it describes a situation where a legitimate transmitting network is contrasted by a malicious attacker whose purpose is to disrupt communications [54]. This scenario, if properly formulated, might involves just two agents, i.e., a legitimate network user and the malicious adversary, and, consequently, can be analyzed in terms of a two-player game. We consider two different setups, such as a general wireless network and an underwater acoustic sensor network, which differ in the communication channel used by the proper nodes in the network for communicating [62, 64, 73, 74]. The purpose is to evaluate the effect of the nodes' position on the resulting equilibrium conditions and to investigate the dependence of the equilibria of the game on the actual position of the jammer itself. The game theoretic character comes into play by representing uncertainty about the position information of the nodes. These evaluations can be useful in properly determing the countermeasures (if it's possible) that might be taken against the malicious jammer in order to limit its effects on the communications.

In terms of network security, further unprecedented challenges are posed by the sudden expanding of social mobile networking. Also in this context, we might have malicious adversaries that can steal sensible information and/or disrupt services due to the connection to unprotected wireless hotspots and the interaction with other nodes in the network [83]. Moreover, nodes are usually unaware of the purposes of the agents they are interacting with; therefore, legitimate transmitting nodes can be contrasted by malicious attackers acting, again, with the purpose of disrupting communications. For this reason, another goal is to use game theory for the identification of malicious nodes. With respect to previous similar formulations, a wider array of action options for the network's agents is considered, notably we include a choice about whether to engage or not in packet exchanging, as well as malicious activity and its prevention. As a consequence, this leads to a structured analysis of the considered game, resulting in different equilibrium conditions. More in general, regarding the application of game theory to jamming problems previously discussed, we considered as the critical parameter the uncertainty of the agents' positions in the network, whereas now we focus on the likelihood that the unknown agent is malicious. Indeed, we consider a scenario in which a legitimate server being unaware of the nature of its clients has to decide whether to transmit a packet, or monitor the network, or do nothing. On the other hand, the generic client's possible set of actions is to correctly forward the

packet if it's necessary and if it's not malicious, or forward it adding errors if it has a malicious nature, or, finally, just ignore the received packet.

In general, these evaluations based on different critical parameters used to characterize the system and the objective of the game applied, beyond the design of proper countermeasures against a malicious node, allow us to see how in some cases the malicious behavior of the nodes are tolerated since a trade-off between their presence and the effect of damages that they caused are reached.

Strongly related to what has just been discussed, but on a different matter, the problem of recognizing groups of similar nodes within a mobile social network has been considered. Indeed, as a general track it can be stated that the nodes of networks, especially social networks, most of the time can be classified according to either some attributes that they show, or preferences that they have [96, 116]. These attributes/preferences can be seen, e.g., in terms of friendship relationship with other nodes as we consider in our investigation. However, due to the fact that it may happen to have imperfect communication (e.g. because of limited communication range), each node has just a partial view of the network and it is aware only of its relationships with the immediate neighbors. Depending on how large the communication range actually is, the problem can be in principle solved by clustering nodes by classifying the friendship relationships. Our analysis shows how a simpler procedure based on exchange of social information in a collaborative fashion is able to achieve better results than more expensive clustering algorithms. Even better, these two approaches can be combined by applying a clustering after the exchange of a given amount of social information, thus improving the overall results. This approach can be enriched considering the presence in the network of a given number of malicious nodes, which is the key factor that allows us to link this analysis to the previous investigations. The intent of these malicious nodes might be, for example, to forward erroneous social information to a chosen set of nodes in the network in order to compromise the network information belonging to this set of nodes. With this assumption, it is still possible to evaluate the effects of transmitting/forwarding malicious information in a network.

In the present thesis, both recent addressed problems and guidelines for future research will be described and discussed. These guidelines if on one hand aim to continue on the path already traced by the previous tackled research topics, on the other hand are an effort to start a new research path where a telecommunications point of view might be used to deal with problems not directly related to telecommunications networks.

Following the same path of the current research, we propose as one of the future works the investigation on *Mobile Cloud Computing* (MCC) and *Mobile Edge Computing* (MEC) by means of game theory. We will discuss in more detail later at the end of the thesis MCC and MEC [112, 113]. However, just to give an initial general idea, it is worth saying that in such contexts the mobile device users that are in the network can decide to offload the computation of tasks to a remote cloud instead of the local execution on the device (holding for MCC). They also have the opportunity to offload the computation tasks to a server located at the edge of the network named the edge server (holding for MEC). Keeping in mind that both of them have advantages and disadvantages (e.g, the remote cloud has more computation capability with respect to the edge server, whereas the edge server is nearest to the users with respect the remote cloud), our objective is to combine MCC and MEC assuming that each mobile device user in the network has three different options for a computation task: locally on the mobile device, computation offloading to the edge server, or computation offloading to the remote cloud.

The analysis that will be shown is just an initial simple analysis that can be further improved if we decide to consider in our evaluations the human aspects beyond the device. To do so, more sophisticated games must be addressed. For this reason, for example, it may be thought to use *Evolutionary game theory* (EGT) [114]. In general, EGT is the game theory application to evolving populations in biology. It defines a framework of contests, strategies, and analytics into which Darwinian competition can be modeled. Consequently, it differs from classical game theory because it

focuses more on the dynamics of strategy change that is influenced by the frequency of the competing strategies in the population. In this way the dynamics of our system can be better taken into consideration allowing us to model more accurately our system. Moreover, a further combination of game theory and *reinforcement learning* in terms of *dynamic programming* might be conceived in order to find the best policies using the former and to describe the internal dynamics using the latter.

In order to apply telecommunications techniques in other domains, it is worth reminding that the concept of network is not only related to an information technology context. As already pointed out, network studies concern several research fields, from technology to biology. Nowadays, researchers of different scientific fields focus on relevant open problems, the solution of which is to be sought in the holistic behavior of networks. Some questions must be considered: *how can the interactions between malfunctioning nodes in a complex generic network result in cancer?*, *how and why do we see such a quick spread in some social systems and communication systems, for example involving epidemic diseases or viruses in computer?*, *how can some networks work even when most of the nodes are corrupted?*. These problems can involve the comparison between networks of different nature that have, however, similar structure and organization.

Since the first studies on graph theory integrated with stochastic models, scientists have referred to *complex networks* as graphs with non trivial characteristics and with some connection schemes between the components that are neither purely regular nor completely random [130, 131]. The comparison between these first studies has led to the surprising discover that many networks, starting from the World Wide Web to the metabolic system in the cell or the collaboration degree between actors in Hollywood, are dominated by a small number of nodes, called hubs, that are connected to many other areas of the same network. In this way, *scale-free networks* and the *small world property* have been proposed. In the last few years, researchers have studied and described the *bio-inspired networking* [132], where architectural solutions based on the evolution of living being networks are used to find solutions suitable for complex networks even related to research fields different from biology.

In the light of this scientific evolution, we suggest a twofold objective: on one hand, to thoroughly investigate models for these particular networks to understand their structure and evaluate their performance in terms of communication networks; on the other hand, to consider the application of techniques typically related to communication networks in order to optimize complex systems, with particular reference to neural systems. This joint study may be useful to yield scientific contributions in both fields, in an interdisciplinary fashion. In general, in the literature there are several examples of analysis of the cells network structure in the living beings in terms of complex network [133]. The interaction of these cells, in addition to their behaviors, is also investigated. Some other works focused on the study of the several malfunctioning that can affect the neural network. Indeed, in the last years there has been an exponential increase in *human neuroscientific research*. This is due to the extensive availability of non-invasive techniques for measuring brain activity and structure, such as neuroimaging and neurophysiological recordings, producing large datasets of spatio-temporal data. Moreover, it is generally accepted that the brain can likely be modeled as a complex network and, in the literature, there can be found several description of the relationship between the brain system and a complex network.

Recently, one of the areas that is raising significant interest is that of *brain connectivity*; one of the goals of connectivity analysis is to make the most of the rich datasets that neuroscientists collect by evaluating the spatio-temporal dynamics in the data [134]. In particular, we will focus on the investigation of functional and effective connectivity in the brain. The former is the temporal correlation in the activity of two brain regions, regardless of whether they have direct anatomic links or not, the latter describes directed causal influences one brain area produces in another. The common denominator to the different types of brain connectivity is the fact that, in all instances, the system can be characterized and described as a network and in this way brain properties can be examined under formal mathematical network theories. As a final consideration, complex network analysis has

emerged as an important tool to characterize brain connectivity and, since a description that consider every single components of a system is not suitable for complex systems, a holistic standpoint must be used in studying these aspects of the brain.

The rest of this thesis is organized as follows. In Chapter 2 some classical issues related to the telecommunications are addressed using standard models properly linked to the telecommunications context; in Chapter 3 we will show how a theory born in economic environment, i.e., game theory, can be used to deal with telecommunications problems; future research interests are discussed in Chapter 4; and, finally, some concluding remarks can be found in Chapter 5.

Chapter 2

Classical telecommunications models and methods applied to telecommunications network issues

In this Chapter we deal with some known issues related to video traffic transmissions and management of EVs networks. Our purpose is to investigate on these topics via Markov model approach in order to evaluate how some parameters describing the system setup might affect the network performance. In particular, we show how a hybrid SR ARQ scheme with unequal error protection can be applied to the transmission of video flows over the wireless channel to address the problems of different packet encoded techniques without interfering with the proper real-time aspect of multimedia contents. We further investigate on a environment made up of EVs for assessing and possibly improving their performance, with particular reference to the evaluation of their autonomy and the resulting range anxiety worrying the customers.

2.1 A Markov Analysis of Automatic Repeat Request for Video Traffic Transmission

According to several recent investigations, video traffic is steadily growing.[1] The annual Cisco report forecasts a huge increase due to the massive use of tablets and similar devices [10]. By 2019, nearly a million minutes of video content will cross the network, accounting for 80% of global traffic.

In this scenario, transmission paradigms to avoid network congestion and convey data correctly and efficiently become essential. We focus on error control techniques, which are exploited to attain the reliable data delivery. Usually, FEC is employed, but some contributions argued that ARQ is better, or useful as well [29].

If the data flow is packet-switched, both FEC and ARQ introduce redundancy in the individual packets, but for different purposes. FEC uses error correcting codes to recover the original data without any further interaction with the transmitter. On the other hand, ARQ uses codes for error detection: if the received packets are corrupted, the receiver asks for their retransmission. This means that a bidirectional interaction happens between the sender and the receiver, where the latter replies to each packet, at least from a conceptual point of view, with positive or negative acknowledgments, denoted as ACKs or NACKs, respectively, depending on the absence or presence of residual errors in the packet. We focus on a SR ARQ approach [12]. Consequently, whenever the transmitter receives a NACK, it selectively retransmits the erroneous packet only, i.e., the one that caused the NACK.

[1] This section is taken from "Markov Analysis of Video Transmission based on Differential Encoded HARQ" published in IEEE WoWMoM.

A combined solution for error control is *Hybrid* ARQ (HARQ), which combines FEC and ARQ. In this case, redundancy is introduced in the packets with a twofold purpose. First of all, the receiver checks data integrity and tries to recover corrupted data, according to FEC scheme. In case the number of errors is higher than the correction capability of the code, but not of its detection capability, the receiver sends a retransmission request to the transmitter as per the ARQ [13]. In the following investigation we concentrate on this approach, which has been shown to contain the delay introduced by a basic ARQ scheme.

It is well known that video contents usually impose strict constraints on transmission time and may need a non-homogeneous error control, due to the presence of packets with different relevance in the video flow. Hybrid schemes are particularly suitable for dealing with such requirements. We consider a video flow made up by packets of different kinds and we assume that the error control mechanism distinguishes among them applying a hybrid SR ARQ scheme.

The procedure used to encode video packets belonging to the same flow involves their different nature [14]. We classify them having in mind the MPEG standard, or any similar technique. According to this, MPEG leverages temporal redundancy between subsequent frames by introducing three types of frames: I (Intra), P (Predicted), and B (Bidirectionally predicted) [15]. For each of them, a distinct compression strategy is used. An I-type frame is processed using *Intra-frame* techniques, which means by considering the frame as a stand-alone unit and by simply removing the spatial redundancy (similar to what done for a JPEG picture). P-type and B-type frames are compressed through *Inter-frame* techniques, i.e., by considering predictions with respect to temporally preceding and/or subsequent frames. Both spatial and temporal redundancy are removed. As a consequence, a video sequence is divided into smaller subsets, each of which is called a *Groups of Pictures* (GoP), where the three types of frames alternate based on a specific pattern.

We model a multimedia flow as a sequence of packets that are sent from a source to a destination. We distinguish between A-packets, that, similar to I-frames of MPEG standard, are autonomous and are encoded independently from the others, and B-packets, that, like P- and B-frames, are encoded incrementally based on an A-packet. One independent A-packet and several B-packets incrementally encoded from it are bundled together in a *packet-group*. Our analysis, as well as the terminology, are directly inspired by [16, 17], even though the investigation of those papers is different. Similar approaches have been used also by [18, 29]. This two-level approach, which considers packet dependence limited within a packet-group, allows for a tractable analysis, while still accounting for the system memory introduced by packet interdependencies. However, the ARQ scheme introduces other memory effects due to retransmissions. Furthermore, since a successful detection of an A-packet is needed to correctly decode a B-packet, the hybrid SR ARQ scheme ought to keep this difference into account.

In this context, we propose a mathematical model for the analysis of a hybrid SR ARQ scheme applied to the transmission of video content over a wireless channel. A Markov chain, whose main parameters are the average error burst length and the steady-state error probability, is used to model the channel. We describe a finite-state machine tracking the transmission state of packets for which the transmitter is still waiting for the related ACK/NACK (i.e., the *pending packets*). On the contrary from previous contributions, our finite-state machine is analytically tractable even for systems with relatively large memory, that is with long round-trip time and large size of the packet-group, within the limits of a Markov analysis. Moreover, we propose a macroscopic Markov chain to model the whole video transmission system with the aim of quantifying some indicative performance metrics, namely throughput, average number of transmissions, and packet discarding probability, via Markov analysis. We pinpoint the effect of the channel parameters on video quality and we extract some useful considerations about the implementation of the HARQ scheme in real scenarios. Our analysis is orthogonal to the presence of dynamic adaptations to channel and source conditions at the physical layer. The model can be extended to also include rate optimization and adaptive modulation and coding techniques exploiting the knowledge of the system state to further enhance video transmission

in a cross-layer context [19].

In the literature, several papers treat the analysis of error control techniques for wireless connections through mathematical models of the whole transmission system. Based on these models, it is possible to evaluate some performance metrics, such as throughput and delay.

The papers most directly related to our contribution are [29], [16], and [20]. Indeed, in all these papers HARQ for video transmission with selective retransmission and unequal error protection is considered, proving that retransmission-based techniques can be jointly used with pure FEC to improve the transmission. The proposed unequal error protection technique, that consists of retransmitting only the independently encoded packets and discarding the incremental ones, was first introduced in [16], and it is the same considered here. However, the present work is different from all these previous contributions. For example, [16] does not consider any analytical modeling of the Markov chain. Subsequently, [29] gives a full Markov model but for complexity reasons the round-trip time is limited to two packets. Finally, [20] extends this analysis to longer packet-groups, but internal limitations of the model still limit the maximum number of retransmissions and/or packet interdependencies. To the best of our knowledge, our analysis is the first to relax all these constraints and give a general evaluation where the only limit is the computational complexity of the resulting Markov chain.

Other papers are significant to our investigations, since they also focus on an ARQ mechanism applied to video transmission, which poses two challenges: (i) how to introduce retransmission while at the same time still meeting the delay constraints of a real time application such as video; (ii) how to differentiate among packets, since multimedia packets have different roles within the video flow.

For example, in [21], the authors try to reduce the delay and buffer size needed by the ARQ approach by using a Multi-ARQ scheme and a rescheduling technique for transmitting video streams over wireless channels. A video stream is divided into three sensitivity classes and the unequal error protection is applyed to them, using ARQ-schemes with higher reliability for higher sensitive portions of video data. In particular, SR ARQ is adopted for high sensitive video data, while no ARQ scheme is applied to low sensitive video data. Therefore, a differentiation mechanism is applied to reduce delay, but this refers to the flow as a whole.

In addition to this, in [22] a prioritized ARQ scheme enhancing the error robustness of streaming video is defined. The proposed priority based retransmission scheme is adopted with packet importance information. The estimation of the error propagation effect caused by the loss of a packet determines the level of packet importance. Lost packets with higher impact values can be retransmitted, while regular packets of less importance can be discarded to make room for retransmissions. A two-state Markov model analogous to ours is used to generate the channel packet loss patterns. However, the importance level is specified individually for each packet, while we consider multiple levels depending on the structure of the packet-group. A similar priority model for the packets also appear in [23], where the highest priorities are given to the packets whose loss has stronger effect in the perceived video quality.

[24] proposes an alternative model where ARQ is better matched with delay constraints typical of video content by setting a retransmission limit that may force to drop some packet if it is expected that they will not meet a pre-defined real-time deadline. In this case, the prioritization of packets is purely based on delay aspects, not on their video characteristics.

Our proposal can also be related to the context of unequal error protection for video. About that, the authors of [25] proposed a more detailed unequal error protection scheme than ours. They considered the impact of error propagation on the video quality, that is a very important issue [18]. However, our model, based on a two-level abstraction, does not allow to explore this issue in more depth. An analogous proposal, involving also a more comprehensive cross-layer optimization, is suggested by [26]. Neverthless, these proposals are limited to FEC, without any discussion on whether this can be iteratively modified through ARQ. For this reason, we believe that our proposal can be seen (in addition to theirs) as a complementing extension of their unequal error protection schemes.

Other related papers suggest possible expansions in line with our work at the network [27] and transport layer [93]. They basically identify a possible development of hybrid ARQ in the application of network coding, and also envisione a streaming control mechanism where ARQ is actually selectively applied but controlling, and possibly choking, the stream if delay constraints risk not to be met. Our proposed scheme can be superimposed to improve the performance of these scenarios as well.

The rest of this Section is organized as follows. In Sub-section 2.1.1, we illustrate the HARQ transmission model and we specify the considered assumptions. Sub-section 2.1.2 presents the macroscopic HARQ system description and its evaluation as a result of Markov analysis. Sub-section 2.1.3 discusses some numerical results; finally, Sub-section 2.1.4 draws some conclusions.

2.1.1 Assumption and model of ARQ transmission

The analyzed system consists of a transmitter and a receiver. The transmitter sends a multimedia flow to the receiver through the wireless channel, which is modeled as a noisy and correlated channel with known statistics. The flow is subdivided into packets, each of them representing an encoded information unit. As it is generally the case in ARQ analysis, we assume that the *Heavy Traffic* condition holds, i.e., the transmitter's queue is always backlogged and, thus, there are always packets to transmit.

The system adopts a hybrid SR ARQ technique with unequal error protection. Therefore, the receiver checks packets integrity upon reception. Whenever errors are detected, it tries to reconstruct the original data by exploiting the redundancy of channel coding in a FEC-like fashion. The transmitter is then informed about correct or incorrect packet reception through selective acknowledgments sent on a feedback channel. The feedback channel is assumed not to be instantaneous and *error-free*, which is reasonable due to the short length of ACK/NACK messages. In the literature, there are examples of investigation about the consequences of errors affecting feedback messages [30]. The main conclusion is that the impact of errors roughly consists in a re-scaling of the error probability on the forward channel.

We consider two different types of packets, denoted as A and B. A-packets are *independently encoded*, meaning that they are stand-alone data units that can be decoded without requiring that any other packet is decoded first. Conversely, a B-packet is *incrementally encoded* from a single A-packet; thus, to be decoded, its correct reception is not sufficient, as the generating A-packet must be correctly received as well. Without loss of generality, it is assumed that A- and B-packets have the same length[2] and that, for each A-packet, the number of B-packets incrementally encoded from it is ℓ, $\ell \in \mathbb{N}, \ell \geq 1$. An $(\ell+1)$-element set consisting of an A-packet and its corresponding B-packets is referred to as a *packet-group*. B-packets are transmitted after the corresponding A-packet. As a consequence, A-packets and B-packets alternate within the data flow according to a precise pattern, which consists of an A-packet followed by ℓ B-packets. Apart from that, there is no dependence between B-packets. These assumptions are not restrictive, as the analysis could still be performed considering more interdependences among packets, only with more involuted math. Moreover, note that the *packet-group* can be considered as the analogous of a GoP in *MPEG*.

We assume that time is slotted and a slot is equal to the time needed to transmit a packet of either type. When a packet is transmitted, the corresponding acknowledgment arrives after a number m of slots equal to the *round-trip time*, which coincides with the ARQ window. This implies that, at any time instant, the number of pending packets does not exceed m. Without loss of generality, we consider $m = M(\ell + 1) + 1$, with $M \in \mathbb{N}, M \geq 1$. If the round-trip time is not an integer multiple of the time slot, M may still be chosen such that m is the smallest integer higher than the round-trip time.

[2] In reality, the lengths of these packets are not explicitly considered in the model. As long as the channel quality stays approximately constant throughout each packet transmission, considering different packet lengths just complicates the model without adding any significant insight. See [29] for a detailed discussion on this point.

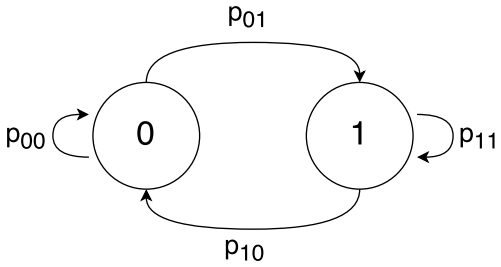

Figure 2.1: Markov representation of the channel (channel chain).

The unequal error protection requires that the A-packets for which the transmitter receives a NACK are retransmitted; erroneous B-packets are instead discarded. There are essentially two motivations for differentiating between A- and B-packets. First, A-packets are more important; indeed, to correctly decode B-packets it is necessary to successfully decode their corresponding A-packet. Second, the retransmission of all types of packets may lead to queue instability and long delays. Provided that retransmissions can be triggered for A-packets only, just a fraction of $\frac{1}{\ell+1}$ packets may undergo retransmissions and a system in which no additional delay increase occurs can be designed.

To avoid delay increases, we assume that retransmissions of A-packets are prioritized, replacing transmissions of B-packets in some following packet-group [16]. Moreover, A-packets can be retransmitted at most r times. We assume that the maximum number of transmissions r of a given A-packet satisfies $r \leq \ell + 1$. A packet-group always starts with a new A-packet, dubbed a "fresh" A-packet. If a fresh A-packet α_1 transmitted at slot k is followed by ℓ B-packets and is in error, then the packet-group transmitted at time slot $k + M(\ell + 1)$ through $k + (M + 1)(\ell + 1) - 1$ will contain two A-packets. A fresh A-packet, α_2, in slot $k + M(\ell + 1)$, i.e., in head position, and the second A-packet, α_1 at its first retransmission, in slot $k + M(\ell + 1) + 1$, in place of the first B-packet incrementally encoded from α_2. If α_1 results in error again, its second retransmission replaces the second B-packet in the packet-group transmitted at slot $k + 2M(\ell + 1)$ through $k + (2M + 1)(\ell + 1) - 1$, and so on. It follows that an A-packet at its nth retransmission is transmitted in place of the nth B-packet of a packet-group, exactly m slots after the beginning of its last transmission. The number of transmissions already performed by an A-packet can be recognized as its position within a packet-group. In fact, a fresh A-packet occupies the head position. If retransmitted, it shifts one position to the right, moving to the second position. If retransmitted again, it shifts to the third, and so on. This means that when a retransmitted A-packet reaches the end position of a packet-group it can no longer be retransmitted and is discarded if in error. B-packets fill the empty slots not used for retransmissions. In particular, for each fresh A-packet, at least $\ell - r + 1$ B-packets are transmitted.

To determine the outcome of packet transmissions, we model the channel state evolution through a discrete-time Markov chain (DTMC). This DTMC, referred to as *channel* chain, has two states: state 0, representing the error-free channel, and state 1, representing an erroneous channel. The channel DTMC is depicted in Fig. 2.1. This is a model similar to the Gilbert Elliot model, however, in our model a transmission performed when the channel is in state 0 or 1 is always successful or always erroneous, respectively [31]. The channel state is constant within each time slot, and makes transitions from a slot to the next according to the one-step transition probability matrix $\mathbf{P}$, which completely characterizes the channel chain. $\mathbf{P} = \{p_{ij}\}$, $i, j \in \{0, 1\}$, where p_{ij} is the probability of going from state i to state j in a single step,

$$\mathbf{P} = \begin{pmatrix} p_{00} & p_{01} \\ p_{10} & p_{11} \end{pmatrix}. \tag{2.1}$$

Also note that transitions to K slots ahead are governed by the K-step transition probability matrix $\mathbf{P}^K$.

Matrix $\mathbf{P}$ can be used to infer information about the average number of consecutive erroneous slots, which we refer to as the *burstiness* B, and the packet error probability at steady-state, which we denote as ε. The burstiness quantifies the channel correlation and its value is $B = \frac{1}{p_{10}}$. The steady-state packet error probability is $\varepsilon = \frac{p_{01}}{p_{10}+p_{01}}$.

Even though the model seems simple, it allows to investigate the impacts of both the average error rate ε and the channel correlation, related to the burstiness B.

2.1.2 Macroscopic HARQ system description and performance metrics

Since the considered HARQ scheme uses selective retransmissions based on packet type and the channel has a non-zero round-trip time, our analysis requires to track previously transmitted packets. Indeed, in order to determine which packet should be transmitted at a generic slot k, it is necessary to know which type of packets have been transmitted at slot $k-m$ (i.e., the slot in which the packet was transmitted, whose acknowledgment is received at the beginning of slot k) through slot $k-1$. The reception of an ACK or NACK at the beginning of slot k then triggers the transmission of a new packet (A or B) or the retransmission of an already transmitted A-packet. Correspondingly, the model of the whole transmission system needs to memorize the types of pending packets, i.e. those for which the transmitter has not received the feedback message yet, and the channel state during their transmission [12].

As a first step, we define a finite-state machine that models the possible pending packets configurations, i.e. the possible sequences of A-packets and B-packets that at a given time slot k could be pending. Transitions occur at each time slot, leading to a new pending packet configuration that depends on ACK or NACK reception, with the ACK or NACK corresponding to the oldest pending packet at time slot k (i.e., that sent in slot $k-m+1$). We refer to the machine states as *machine stages* and we indicate the number of machine stages as L. Each machine stage stands for a possible pending packets configuration and is denoted by a vector $\boldsymbol{\sigma} = [\sigma_0\, \sigma_1\, \ldots\, \sigma_{m-1}]$ of length m, with $\sigma_j \in \{0, 1, \ldots, r\}, 0 \leq j \leq m-1$. Considering that at time slot k the finite-state machine is in stage $\boldsymbol{\sigma}(k)$, we have that each $\sigma_j(k)$, for $0 \leq j \leq m-1$, identifies the type of packet transmitted at slot $k-m+1+j$ and the number of transmissions that this packet has already undergone. More precisely, $\sigma_j(k) = 0$ if the packet transmitted in slot $k-m+1+j$ is a B-packet; $\sigma_j(k) = n, n \in \{1, 2, \ldots, r\}$ if the packet transmitted in slot $k-m+1+j$ is an A-packet at its nth transmission. Note that the last element, $\sigma_{m-1}(k)$, refers to the packet transmitted at slot k, while the first element, $\sigma_0(k)$, refers to the packet transmitted at slot $k-m+1$, for which the transmitter receives the corresponding feedback at the end of slot k.

The number of machine stages, which influences the overall system complexity, can be obtained by considering that for any choice of the parameters ℓ, r, M, and thus $m = M(\ell+1)+1$, the finite-state machine would pass through $\ell+1$ different machine stages only, provided that the channel was error-free. To see it, consider a pending packets configuration that contains fresh A-packets only and where the packet in head position is of type A. We indicate such configuration as $\mathcal{C}$. Since no retransmitted A-packet is present, the number of B-packets associated to each A-packet is ℓ. Therefore, the vector representation of $\mathcal{C}$ contains M consecutive sequences $[1\,0\,\ldots\,0]$ with ℓ zeros, the last one followed by value 1. Now, suppose that the channel is error-free. This implies that no NACK is received and that the finite-state machine indefinitely transits over the same cycle of $\ell+1$ stages. The first one coincides with $\mathcal{C}$. The following ones can be obtained orderly by shifting one position to the left the values in the vector representation of the preceding stage, removing the first element and adding a 0 in last position. Since the number of shifts to the left that can be applied to the vector representation of $\mathcal{C}$ before returning to $\mathcal{C}$ itself is $\ell+1$, this is also the number of machine stages in the considered cycle, which we refer to as *ideal cycle*, since the channel is assumed to be error-free.

From the ideal cycle, we can derive the total number of stages of the finite-state machine for all pending packet configurations. The idea is to sum the number of stages of the idle cycle and the

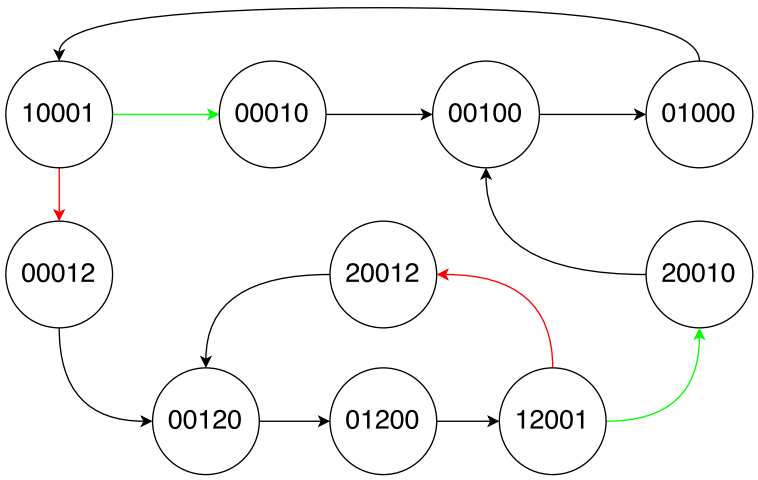

Figure 2.2: Graphical display of the finite-state machine of pending packets configurations; $\ell = 3$, $r = 2$, $M = 1$, $m = M(\ell + 1) + 1 = 5$, $L = 10$.

number of stages that the machine may pass through when the channel resulted to be erroneous in at least one pending packet transmission (and thus, the assumption of error-free channel is removed). The stages in this last set have an associated vector representation where the 1s are the same in number and position as those on one of the stages of the idle cycle, while some 0 element is replaced by a value $x \in \{2, \ldots, r\}$, due to retransmissions of A-packets.

Consider for example the simplest case $r = \ell + 1$ e $M = 1$. The number of machine stages with a vector representation where 1s are placed as in $\mathcal{C}$ are 2^ℓ, including $\mathcal{C}$. The number of machine stages with a vector representation where 1s are placed as in the stages following $\mathcal{C}$ in the ideal cycle is $2^{\ell+1}$ for each stage, including the stage of the ideal cycle. Thus, the total number of machine stages in this simple case is given by $L = 2^\ell + \ell(2^{\ell+1})$.

The same rationale, i.e. the definition of the idle cycle and the determination of stages *affine* to the stages of the idle cycle, can be applied to compute the total number of stages of a generic finite-state machine with arbitrary parameters. The following expression holds $L = [(r-1)2^r + (\ell - r + 2)2^{r-1}](2^{r-1})^{M-1} = (r + \ell)2^{M(r-1)}$.

Fig. 2.2 shows an example of finite-state machine considering $\ell = 3$, $r = 2$, $M = 1$, $m = M(\ell + 1) + 1 = 5$, $L = 10$. In Fig. 2.2, green arrows identify the transitions that occur when the transmitter receives an ACK for an A-packet; red arrows describe the transitions that occur when the transmitter receives a NACK for an A-packet that has not yet reached the maximum number r of transmissions. Black arrows represent transitions that occur when an ACK/NACK is received for a B-packet or when an ACK/NACK is received for an A-packet that has already been transmitted the maximum number of times, i.e., 2 times in the considered example. These last ones are forced transitions.

Given the channel DTMC and the finite-state machine of pending packets configurations, we develop a macroscopic DTMC that models that entire transmission system and which we refer to as HARQ chain, analogously to [16][20]. The HARQ chain allows for the computation of the system steady-state probabilities which, in turn, are employed to compute three networking performance metrics, namely throughput, average number of transmissions to correctly deliver an A-packet, and A-packet dropping probability.

At each time slot k, the HARQ chain's state is described by a vector $\mathbf{S}(k) = [\boldsymbol{\sigma}(k)\, b_0(k)\, \ldots\, b_{m-2}(k)\, c(k)]$ subdivided into three different parts, each of which carries a specific information. $\boldsymbol{\sigma}(k)$ is the finite-state machine stage, as discussed previously. $\mathbf{b}(k) = [b_0(k)\, \ldots\, b_{m-2}(k)]$ describes the channel states from slot $k-m+1$ through $k-1$. In particular, $b_j(k) = 0$ if the channel at slot $k-m+1+j$ was error-free, and thus the packet transmitted at that slot was correctly received; $b_j(k) = 1$ if the channel

at slot $k-m+1+j$ was erroneous, and thus the packet transmitted at that slot was erroneously received. $c \in \{0,1\}$ indicates the channel state at slot k. The number of HARQ chain's states, N, can be obtained as $N = L \cdot 2^{m-1} \cdot 2$, where L is the number of machine stages of the finite-state machine. The value of N also reflects in the computational complexity of our model. As we will show later, we require the computation of steady-state probabilities, obtained by solving a linear system associated with a $N \times N$ matrix. This matrix is sparse and, as a consequence, we can compute the solution efficiently by using procedures whose (both space and time) complexity is $O(N)$. Moreover, N depends exponentially on m; however, it is possible to approximate this exponential dependence with a linear one, thereby decreasing the computational complexity, following the approach of [32].

At time slot k, $\boldsymbol{\sigma}(k+1)$ is univocally determined by $\boldsymbol{\sigma}(k)$ and the value of $b_0(k)$, which indicates whether the oldest pending packet at time slot k has been correctly received or, instead, needs to be retransmitted. Indeed, when $\boldsymbol{\sigma}(k)$ represents a set of pending packets with an A-packet in its head position and $b_0(k) = 1$, the A-packet retransmission is scheduled at time slot $k+1$, provided that this A-packet has not reached the maximum number r of allowed transmissions. The elements $b_j(k+1)$, $0 \leq j \leq m-3$, depend on the values of elements $b_j(k)$, $1 \leq j \leq m-2$, and on the value of $c(k)$. Finally, the value of $c(k+1)$ depends on the value of $c(k)$, according to the channel transition probability matrix $\mathbf{P}$.

The transition matrix $\mathbf{T}$ of the HARQ chain can be defined by observing that, given state $\mathbf{S}(k) = [\boldsymbol{\sigma}\, b_0 \ \ldots\ b_{m-2}\, c]$ (where we omit the dependance on k in the right-hand side of the equality for notation simplicity), the only admitted transitions towards a future state $\mathbf{S}(k+1)$ include

- $\mathbf{S}(k+1) = [\boldsymbol{\sigma}_c\, b_1 \ \ldots\ b_{m-2}\, c\, 0]$ with probability p_{c0}
- $\mathbf{S}(k+1) = [\boldsymbol{\sigma}_c\, b_1 \ \ldots\ b_{m-2}\, c\, 1]$ with probability p_{c1}
- $\mathbf{S}(k+1) = [\boldsymbol{\sigma}_e\, b_1 \ \ldots\ b_{m-2}\, c\, 0]$ with probability p_{c0}
- $\mathbf{S}(k+1) = [\boldsymbol{\sigma}_e\, b_1 \ \ldots\ b_{m-2}\, c\, 1]$ with probability p_{c1}

where $\boldsymbol{\sigma}_c$ and $\boldsymbol{\sigma}_e$ represent the pending packets configurations at time slot $k+1$ when the received feedback at the end of slot k is an ACK or NACK, respectively. Equivalently, they represent the pending packets configurations at time slot $k+1$ when $b_0(k) = 0$ and $b_0(k) = 1$, respectively. Table 2.1 shows $\boldsymbol{\sigma}_c$ and $\boldsymbol{\sigma}_e$ for each possible $\boldsymbol{\sigma}$, considering $\ell = 4$, $r = 3$, $M = 1$, $m = M(\ell+1)+1 = 6$, $L = 28$.

The HARQ chain is irreducible (there is a connection between each state) and each state is recurring (the probability that the system comes back to a state is 1 for each state). As a consequence, we can evaluate the steady-state probabilities $\boldsymbol{\pi} = [\pi_0\, \pi_1\, \ldots\, \pi_{N-1}]^T$, i.e. the probabilities that the system is in a certain state at time slot k, for large k. We solve the system $\mathbf{T}\boldsymbol{\pi} = \boldsymbol{\pi}$, under the constraint that elements in $\boldsymbol{\pi}$ sum to 1. We use $\boldsymbol{\pi}$ to determine the performance metrics, as explained in the following.

With respect to throughput, i.e., the amount of data correctly delivered in unit time, positive contributions are given by correct transmissions of A-packets and B-packets for which the corresponding A-packet has been correctly delivered. To quantify such contributions, we need to inspect the HARQ chain's states. If $\sigma_0 \in \{1, 2, \ldots, r\}$ and $b_0 = 0$, then the HARQ chain's state corresponds to a successful reception of an A-packet. Therefore, the throughput includes the sum of the steady-state probabilities associated to the HARQ chain's states in which $\sigma_0 \in \{1, 2, \ldots, r\}$ and $b_0 = 0$. If $\sigma_0 \in \{1, 2, \ldots, r\}$ and $b_0 = 1$, then the HARQ chain's state corresponds to a failed reception of an A-packet. In this case, if $\sigma_0 = r$, then the contribution to the throughput is zero; if $\sigma_0 \in \{1, 2, \ldots, r-1\}$, then further considerations need to be made, as it will be explained in the next paragraph. If $\sigma_0 = 0$ and $b_0 = 1$, then the HARQ chain's state corresponds to a failed reception of a B-packet and the throughput remains unchanged. If $\sigma_0 = 0$ and $b_0 = 0$, then the HARQ chain's state corresponds to a correct reception

Table 2.1: Table of the σ-transitions for $\ell = 4$, $r = 3$, $M = 1$, $m = M(\ell + 1) + 1 = 6$, $L = 28$.

$\boldsymbol{\sigma}$	**Configuration**	$\boldsymbol{\sigma}_c$	$\boldsymbol{\sigma}_e$
0	100001	1	5
1	000010	2	2
2	000100	3	3
3	001000	4	4
4	010000	0	0
5	000012	6	6
6	000120	7	7
7	001200	8	8
8	012000	9	9
9	120001	10	11
10	200010	2	12
11	200012	6	15
12	000103	13	13
13	001030	14	14
14	010300	18	18
15	000123	16	16
16	001230	17	17
17	012300	19	19
18	103001	22	23
19	123001	20	25
20	230010	21	26
21	300100	3	3
22	030010	21	21
23	030012	24	24
24	300120	7	7
25	230012	24	27
26	300103	13	13
27	300123	16	16

of a B-packet, which contributes to throughput on condition that the corresponding A-packet has successfully reached the destination.

In the following, we consider a system with parameters $\ell = 4$, $r = 3$, $M = 1$, $m = M(\ell+1)+1 = 6$ and we illustrate some examples of computations for throughput contributions. Consider $\boldsymbol{\sigma} = 000010$. The first packet of this configuration is of type B. The HARQ's chain states with such $\boldsymbol{\sigma}$ and $b_0 = 1$ do not contribute to throughput.

If $\boldsymbol{\sigma} = 000010$ and $b_0 = 0$, then we need to consider the transmission outcome of the A packet from which the B packet has been incrementally encoded. By observing $\boldsymbol{\sigma}$, we can deduce that an ACK has been sent for that A-packet. If this was not the case, the pending packets configuration would have been $\boldsymbol{\sigma} = 000012$. Therefore, the steady-state probabilities of the HARQ chain's states with $\boldsymbol{\sigma} = 000010$ and $b_0 = 0$ are added to the throughput.

Consider now $\boldsymbol{\sigma} = 000012$. The A-packet from which the B-packet in head position has been incrementally encoded is at its second transmission. If $b_0 = 0$ and $c = 0$ (i.e., the transmission of the A-packet is successful), then these states give a positive contribution to throughput. If $c = 1$, further reasonings are needed; the A-packet is transmitted for the third (and last, since we are assuming $r = 3$) time after 6 time slots starting from the current time slot, k. Therefore, if $c(k + 6) = 1$, there

is no throughput contribution. Otherwise, if $c(k+6)=0$, there is a positive contribution that can be obtained, for every state with $\boldsymbol{\sigma}=000012$, $b_0=0$, and $c=1$, by multiplying the steady-state probability of such states by $\mathbf{P}^6(1,0)$ (i.e., the entry at row 1 and column 0 in $\mathbf{P}^6$).

Finally, consider $\boldsymbol{\sigma}=000120$. Similar observations hold. However, in this case the transmission outcome of the A-packet is described by b_4. Therefore, if $b_0=0$ and $b_4=0$, the contribution is positive, independently of c. Whereas, if $b_0=0$ and $b_4=1$, the contribution is positive if and only if the transmission of the A-packet after 5 time-slots from the current one is successful. In this case, the contribution is computed by summing the stationary probabilities associated to the states with $b_0=0$, $b_4=1$, and $c=1$ multiplied by $\mathbf{P}^5(1,0)$ and those associated to the states with $b_0=0$, $b_4=1$, and $c=0$ multiplied by $\mathbf{P}^5(0,0)$.

Another relevant metric is the average number of transmissions, which is however interesting only for A-packets, because B-packets are always transmitted just once. We define the conditional probabilities $\pi(n|A)$, $n=1,\ldots,r$, as the probabilities that the system is observed when an A-packet is at its n^{th} transmission. Such probabilities are evaluated as the ratio between the sum of the steady-state probabilities of the HARQ chain's states with $\boldsymbol{\sigma}$ such that $\boldsymbol{\sigma}_0=n$ and the sum of the steady-state probabilities of the HARQ chain's states with $\boldsymbol{\sigma}$ such that $\boldsymbol{\sigma}_0\in\{1,\ldots,r\}$. For the following numerical choices of the parameters $\ell=4$, $r=3$, $M=1$, $m=M(\ell+1)+1=6$, for example, the conditional probabilities can be expressed as, see [20]:

$$\pi(1|A)=\frac{p_1+p_2+p_3}{p_1+2p_2+3p_3}\pi(2|A)=\frac{p_2+p_3}{p_1+2p_2+3p_3}\pi(3|A)=\frac{p_3}{p_1+2p_2+3p_3} \tag{2.2}$$

where p_1, p_2, and p_3 are the probabilities that an A-packet is transmitted exactly one, two, three times, respectively. By solving the above system of equations 2.2, the average number of transmissions of A-packets can be derived as $p_1+2p_2+3p_3$. Analogous computations can be done for a system with different parameters.

Finally, when an A-packet reaches its rth transmission and is still in error, it is dropped. The probability of dropping an A-packet, denoted as $P_{\text{drop, A}}$, is computed as the sum of the steady-state probabilities of the HARQ chain states with a pending packets configuration corresponding to an A-packet at its last transmission and with the channel state equal to 1 during this transmission. Thus,

$$P_{\text{drop, A}}=\sum_{i=0}^{N-1}\chi(\sigma_{i,0}=r\ \ \&\ \ b_{i,0}=1)\pi_i \tag{2.3}$$

where $\chi(\cdot)$ is an indicator function, taking value is 1 if the inner condition is true and 0 otherwise; $\sigma_{i,0}$ and $b_{i,0}$ are the head elements of $\boldsymbol{\sigma}$ and $\boldsymbol{b}$, respectively, in the ith HARQ chain's state.

2.1.3 Numerical results

We consider a system with exemplifying parameters. Our aim is to evaluate a setup sufficiently complex to give a detailed description of the HARQ operations and performance, but, at the same time, tractable enough to be solved easily, without involving high computational power. This setup can be modified to different cases of interest. In particular, it can be tuned to mimic real traffic traces; as illustrated in [29], using real traffic traces for the evaluations only involves a careful choice of the parameters' values. In light of this, we analyze a system where the number of B-packets incrementally encoded from an A-packet is $\ell=4$, the maximum number of transmissions for A-packets is $r=3$, the packet group length is $\ell+1=5$ packets, the round-trip time is equal to $m=M(\ell+1)+1=6$ time slots, and $M=1$. It follows that the number of pending packets configurations is $L=28$ and that the number of HARQ chain states is $N=28\cdot 2^5\cdot 2=1792$.

As a first set of results, we show how metrics vary depending on the steady-state error probability ε for different values of the burstiness B; then, similarly, we show how metrics vary depending on B for many values of ε.

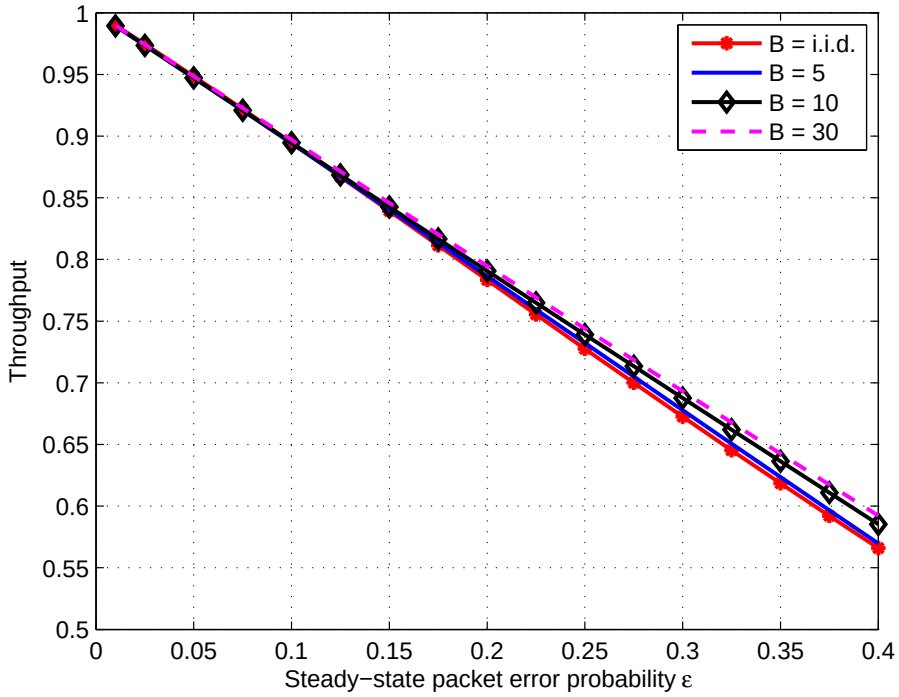

Figure 2.3: Throughput *vs.* ε for various values of B.

We consider ε varying from 0.01 to 0.4. As for the burstiness B, i.e., the average number of consecutive erroneous time slots, we consider the values $5, 10, 30$, and also we consider the special case where $B = \frac{1}{1-\varepsilon}$, which is referred to as the *i.i.d.* case, since in this case the channel is just a binary memoryless symmetric channel with identical error probability ε regardless of the state of the system. The aim is to highlight the differences between performance in case of error bursts with length comparable with the length of a packet group ($B = 5, 10$), in case of error bursts significantly longer than packet groups ($B = 30$), and in the i.i.d. case, i.e., the case of independent and identically distributed errors.

In Fig. 2.3, each curve represents the throughput for variable ε and fixed B. We can notice that the throughput decreases as ε increases. Indeed, the increase in packet error probability causes the reduction of packets correctly delivered to the receiver and, correspondingly, a throughput decrease. It is worth observing, temporarily neglecting the i.i.d. case, that for fixed ε, the throughput increases as B increases. In fact, the channel correlation causes the temporal axis to be roughly subdivided into blocks, each of which can be considered correct or incorrect. Erroneous blocks, i.e., the ones where the channel is bad, do not bring any contribution to the throughput; correct blocks, i.e., the ones where the channel is good, determine the successful deliver of a sequence of packets, giving a relevant contribution. In the i.i.d. case, it results that the throughput is higher than that obtained with a correlated channel for small values of ε. However, if ε increases, the performance over correlated channel becomes better than over i.i.d. channels. In Fig. 2.4 we underline these last considerations by reporting the ratio between the actual throughput and the value $1 - \varepsilon$, which is the throughput in the i.i.d. case without distinction between A- and B-packets and without limits on transmissions. We conclude that the channel correlation does not necessarily imply a degradation of the system performance. Conversely, the throughput is higher than the i.i.d. case if the channel error probability at steady-state is not too small.

In Fig. 2.5 we show the average number of transmissions of an A-packet for varying ε and fixed B.

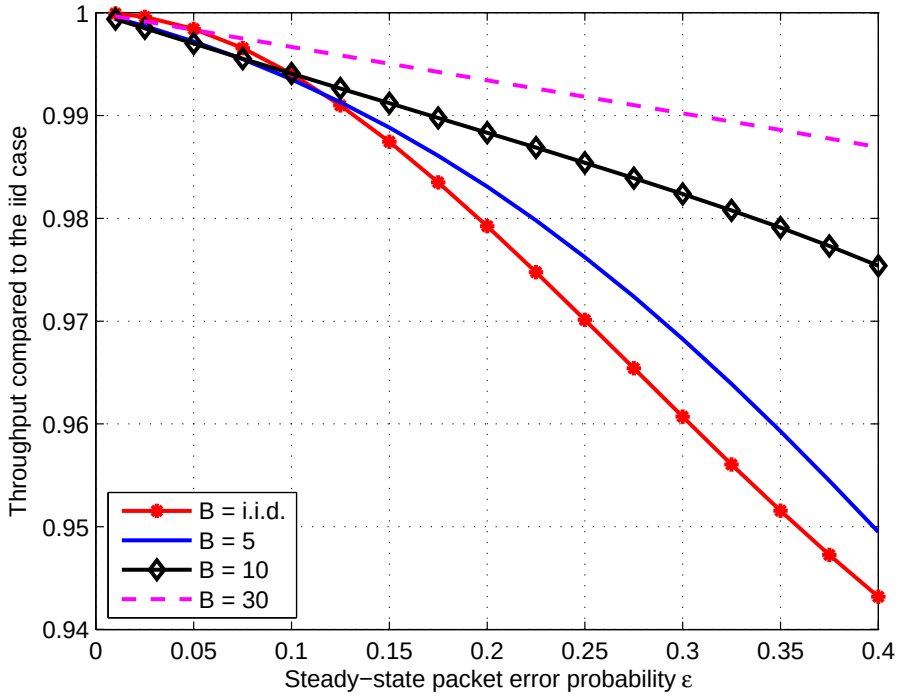

Figure 2.4: Throughput compared to the i.i.d. case *vs.* ε for various values of B.

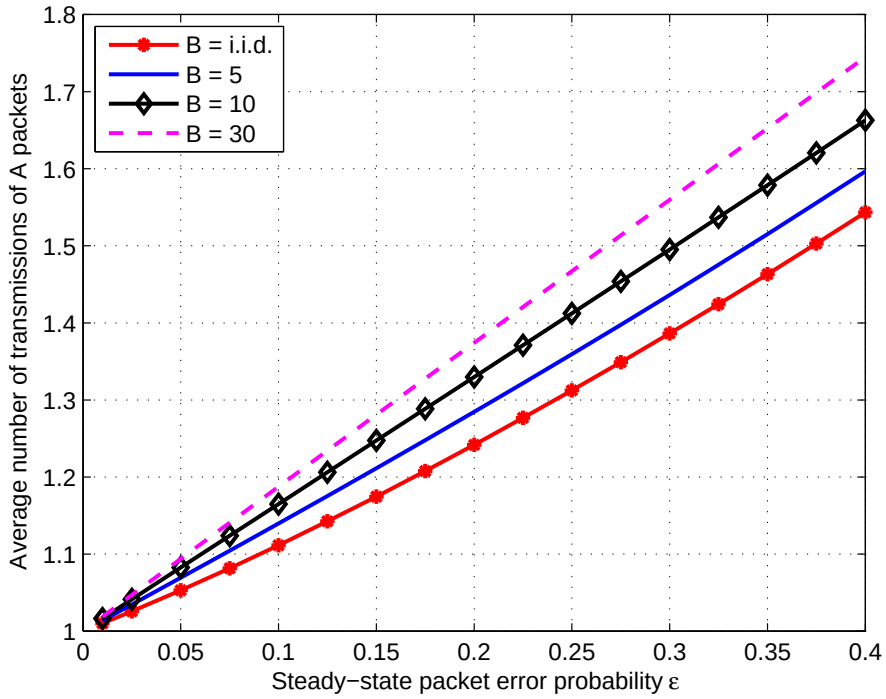

Figure 2.5: Average no. of A-packet transmissions *vs.* ε for various values of B.

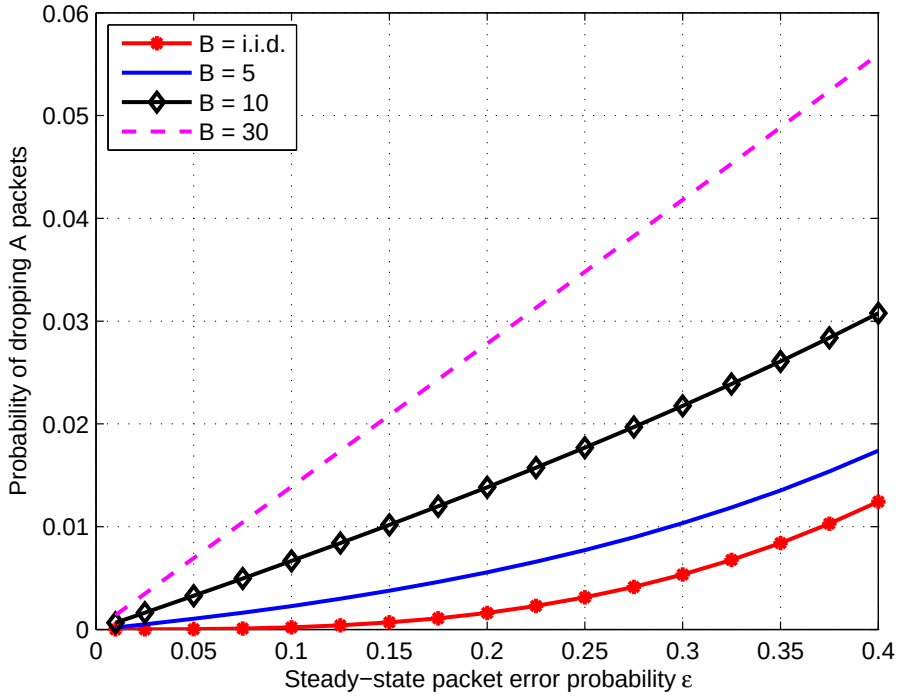

Figure 2.6: Probability of dropping an A-packet *vs.* ε for various values of B.

According to the fact that a higher error probability implies a higher number of failures in A-packet transmissions, we observe that the average number of transmissions increases as ε increases, following a coarsely linear trend. Moreover, for fixed ε, the average number of transmissions is higher for higher burstiness. Indeed, if the channel is correlated and an A-packet is erroneously received, the greater the correlation, the higher the probability that the following transmissions are erroneous.

In Fig. 2.6 we illustrate the probability of dropping an A-packet. It can be observed that this probability increases as ε increases, for each value of B. Indeed, the increase in ε implies an increase in the average number of transmissions and in the probability that an A-packet is erroneously received at its last transmission. Furthermore, for values of B nearly equal to the packet-group length (i.i.d. errors, or $B = 5$, or $B = 10$) the dropping probability increases slowly as ε increases for small values of ε, whereas it increases faster for higher values of ε. For values of B higher than the packet-group length ($B = 30$), the dropping probability increases roughly linearly as ε increases. Finally, we can observe that the dropping probability is very small in any case. This fact agrees with the previous results. Indeed, the average number of transmissions is less than 1.8 (see Fig. 2.5) and the maximum number of transmissions is 3. Thus, the third transmission of an A-packet and its failure are unlikely events.

We now discuss the numerical results obtained by varying B in the range $[\frac{1}{1-\varepsilon}, 30]$ for a fixed ε value chosen within set $\{0.1, 0.2, 0.3\}$. In Fig. 2.7 we report the ratio of the actual throughput and that obtained in the i.i.d. case without distinction between A- and B-packets and without limits on transmissions. The variability interval of the throughput increases as ε increases. In fact, the curve for $\varepsilon = 0.1$ remains nearly constant. More precisely, the throughput initially decreases, it assumes its minimum values for B values comparable with the packet-group length, and then it increases very slowly. The curves for higher values of ε show that in these cases the throughput assumes its smallest values for B roughly corresponding to the i.i.d. case and that it then increases as B increases. This increase is faster for B values lower than, say, 20, and is lighter for higher values. In any case, the

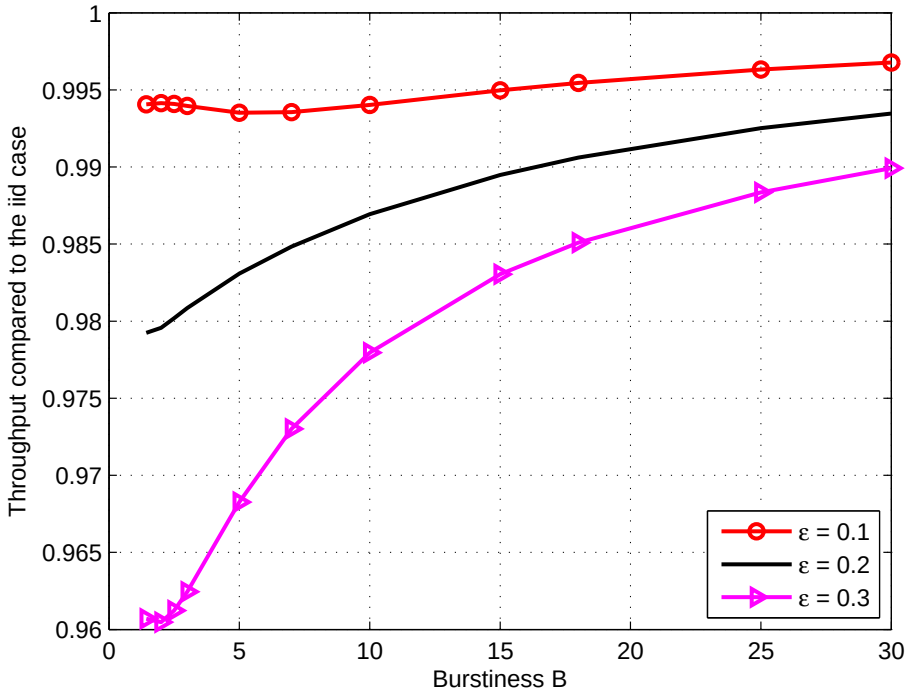

Figure 2.7: Throughput compared to the i.i.d. case *vs.* B for various values of ε.

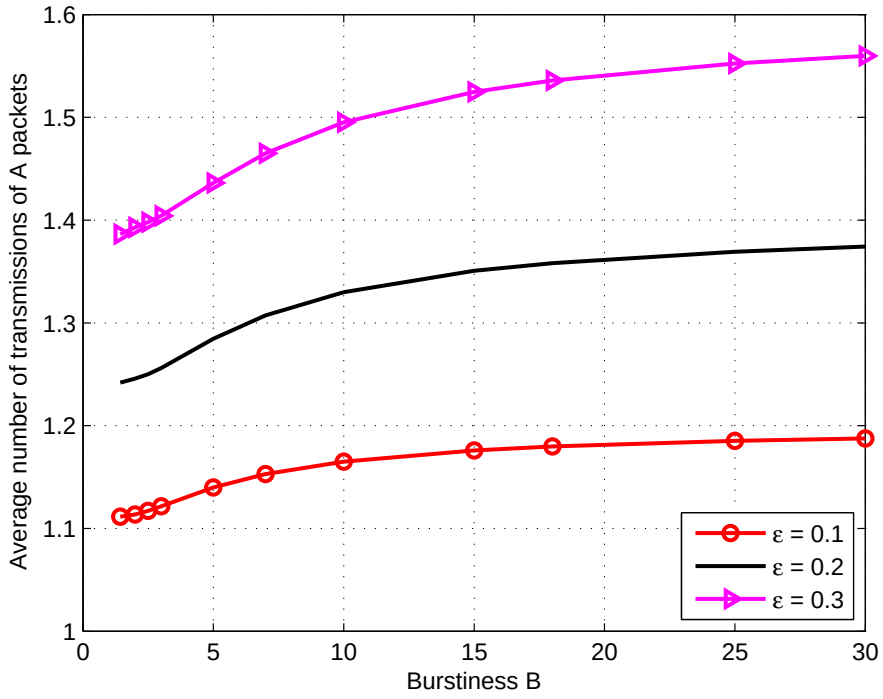

Figure 2.8: Average no. of A-packet transmissions *vs.* B for various values of ε.

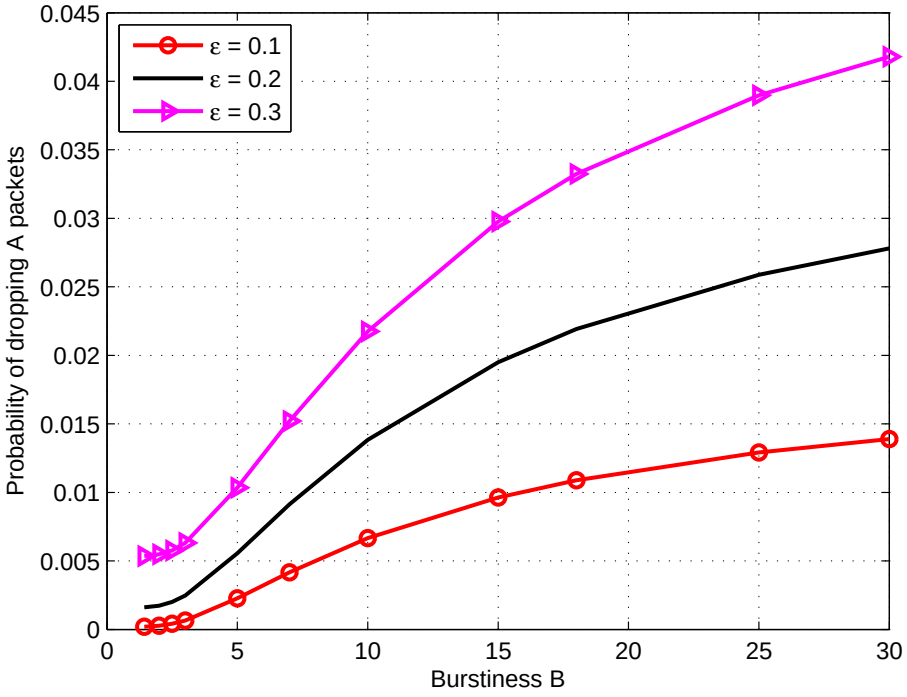

Figure 2.9: Probability of dropping an A-packet *vs.* B for various values of ε.

throughput seems to tend to an asymptotic value.

Finally, in Fig. 2.8 and Fig. 2.9 we report the average number of transmissions and the dropping probability of an A-packet. These figures confirm the previous results. Moreover, it can be observed that the range of values assumed by either performance metric is larger for higher ε. From Fig. 2.8 we can also deduce that the average number of transmissions becomes almost constant for high values of B (say, higher than 10, twice the length of a packet group). The dropping probability of an A-packet in Fig. 2.9 is roughly constant for values of B around the i.i.d. case; it quickly increases until B reaches value 10 and it increases more slowly for higher values of B.

2.1.4 Conclusions

In this Section, we presented a Markov framework for the performance evaluation of a hybrid SR ARQ scheme with unequal error protection applied to the transmission of multimedia contents over the wireless channel. We considered a video flow divided into independent and incrementally encoded packets. Our basic assumption is that the HARQ scheme privileges the transmission of independent packets, due to their more relevant role. As a consequence, independent packets are the only ones to be selectively retransmitted, if in error.

Since we aim to avoid delay increases, we assumed that retransmissions replace transmissions of incrementally encoded packets and that the admissible retransmissions are limited. We modeled the entire transmission system using a macroscopic Markov chain, including the Markov chain representation of the channel and a finite-state machine identifying the possible pending packets configurations.

As performance metrics, we considered the throughput, average number of transmissions, and dropping probability of independent packets. We reported and commented the results for a system with fixed parameters. We found that channel correlation may be beneficial to increase throughput and, therefore, the transmission speed. On the other hand, we verified that correlation has a worsening effect

on the average number of transmissions and the dropping probability, since these quantities increase as the channel burstiness increases. In video transmissions, retransmissions lead to undesirable delays and dropped independent packets cause an irreversible loss of information, which, in turn, compromises the quality of the video. A tradeoff between transmission speed and reproduction quality has thus emerged. Moreover, the adopted approach can be extended to better describe the performance of more specific video transmission protocols operating on possibly correlated channels.

2.2 Markov models for electric vehicles: the role of battery parameters and charging point frequency

Two of the major reasons that lead many nations to search for alternate energy sources and decrease carbon dioxide emissions, especially from car transportation which makes use almost exclusively of internal combustion vehicles (ICVs), are the alarming pollution levels and increasing world-wide oil demand.[3] This problem is especially heavy in the United States, causing 30% of world greenhouse gases emissions, and also in Europe, where the 20-20-20 directive set a goal for the reduction of fossil fuel usage of 20% and replacement with renewable energies (increased by 20%) by year 2020 [33].

In this background, EVs may be seen as a technological solution not only to decrease pollution, but also to reduce usage costs for the end user. EVs can diminish carbon dioxide emissions by 50% and have four to six times lower per-km cost than traditional ICVs [34]. Moreover, EVs can also be integrated with Internet of Things (IoT). To avoid, for example, the frequent electric vehicle theft and traffic accident problems, EV monitoring system could be designed based on the IoT technology [35]. Yet, some hurdles to a widespread diffusion of EVs are represented by limited autonomy, long recharging times, and, finally, scarceness of recharging points.

These aspects involve a limited applicability of EVs, so that a vicious circle arises. The diffidence of the customers towards their practicality especially due to their limited autonomy, a phenomenon known as *range anxiety* [36], leads to a niche market. As a consequence, public investments for a better service are discouraged, and this, in turn, further decreases the palatability of EVs for the average customer. As a matter of fact, preliminary sociological studies have shown that EV users often limit the usage and do not fully exploit the vehicle autonomy, fearing they will not find a recharging point before the battery runs out of charge. Furthermore, long recharging times are distasteful to the users, since they prevent an intense usage and independence in other daily activities.

Considering a modeling standpoint, several intervention points where these aspects can be tackled might be defined. It can be thought of improving the battery efficiency, either increasing its capacity, or making it faster to recharge, or both. At the same time, more charging points can be deployed, increasing, in this way, their availability. With nowadays technology, the cost-benefit relationship of these actions can be rather variable, being also connected with the subjective perception of the end users. Investigating them with an adequate level of details would involve several related economic and social aspects that are out of the scope of our investigation. However, we aim at giving a preliminary contribution for what concerns the technical evaluation of these elements. To do so, we discuss the capability of stochastic models and, in particular, of Markov chains to integrate all of them in a comprehensive description.

In general, Markov models have been used for quantitative evaluation of urban transportation practices. Particularly, there are studies proposing a Markov model to characterize EV behaviors in urban mobility scenarios [37]. Inspired by these descriptions, we propose an enlarged Markov chain where we consider that also the battery management can be integrated. In particular, we discuss the accuracy of the model, and show that even a loose time granularity may still correctly reflect average

[3] This section is taken from "Markov Models for Electric Vehicles: the Role of Battery Parameters and Charging Point Frequency" published in IEEE CAMAD.

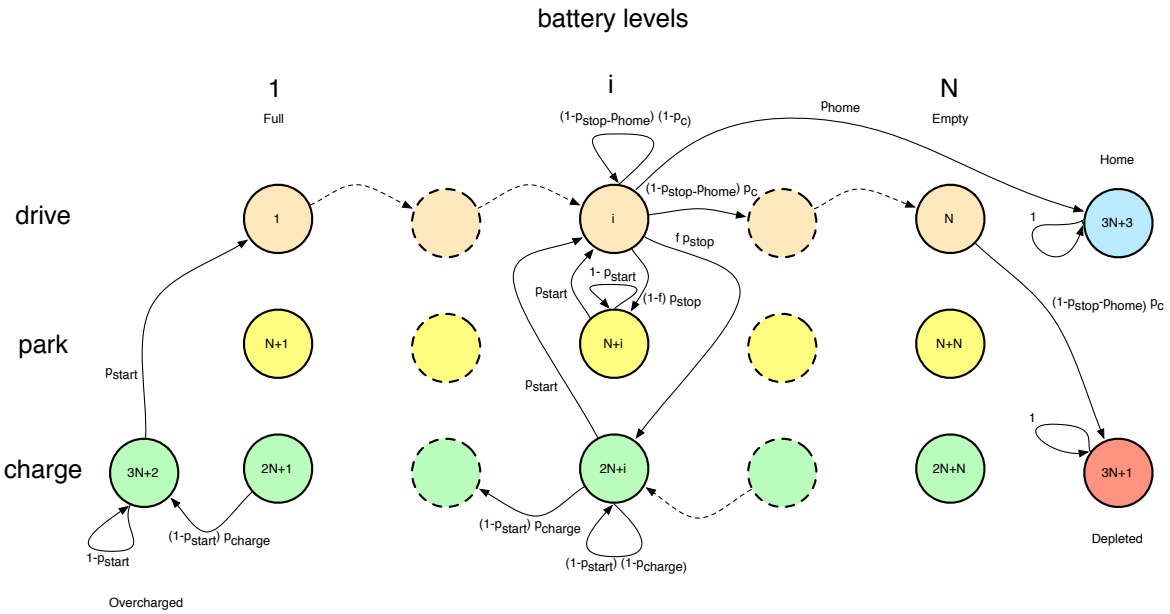

Figure 2.10: The resulting system Markov Chain with $3N + 3$ states.

performance of the EV, especially for the metrics of interest related to range anxiety. Moreover, we show how the model can be properly tuned to investigate the impact of three key aspects mentioned above, i.e.: (i) autonomy of the battery; (ii) speed of battery recharging; (iii) frequency of recharging points.

Our proposed Markov model can be further extended to several more advanced evaluations, still conserving a fully analytical formulation that gives a powerful description, but without requiring an excessive computational cost. In particular, more advanced behavioral patterns of the EV users can be considered, as well as more traffic dynamics and intensities over the day. Also, complex battery effects can be introduced instead of the simple model where the battery charge increases when the EV is parked in a charging point and decreases as the EV moves, by considering leakage or stabilization effects. Finally, the model can be further integrated within stochastic optimization frameworks [38], in order to devise intelligent algorithms for maximum energy efficiency and/or autonomy.

The rest of the Section is organized as follows. Sub-section 2.2.1 describes the system model; in Sub-section 2.2.2 the numerical results are shown; and, finally, in Sub-section 2.2.3 we draw some concluding remarks.

2.2.1 System model

To represent the daily activity of an EV, we consider the following simplified model. We assume that the EV drives through a urban scenario during a day, cyclically alternating being parked and on the move. The EV is considered to always leave from and return to the owner's home, where a charging point is available, in the morning and at the end of the day, respectively. Thus, at the beginning of each day cycle, its battery is fully charged. The duration of the entire daily activity is random, but its expected value is a working day period, so as to model the condition where the vehicle returns home at night after a determined average time. Also, some (but not all) of the parking area within the city have a charging point where the EV's battery can be replenished. To relate this analysis to the study of range anxiety, our objective is to study the probability of running out of all the charge in the battery before the day ends, called p_d. This probability depends, among other aspects, on the length of the chosen path for that day, the number of driving routines performed, the battery models,

and the fraction of parking spots that are charging points. Moreover, we want to study especially the impact on p_d of increasing the charging speed or the battery capacity. We model this scenario with a discrete Markov Chain, making a transition every Δ_t seconds, in which we consider that the EV can operate under three conditions: *Drive*, that is, the EV moves consuming battery; *Charge*, whenever the EV stops in a parking spot that is equipped with a charging point, so that the battery is recharged; and, finally, *Park*, if the EV stops in a parking position without any charging. In addition to this, we describe the battery as an energy queue, having multiple possible charge levels, which are a quantization of the battery charge. We set N as the number of levels, which means we consider levels from 1 to N, with 1 representing the highest charge, i.e., 100% of the battery. The transitions between the three conditions happen according to an independent underlying Markov process, for which several characterizations exist in the literature [37]. Note that this part of the model can be enlarged with additional conditions describing different ways of operating the EV, but such an extension would add little to the description made above. Thus, we can define transitions from i to j, with i, $j \in$ D,C,P, where D, C, P stand for *Drive*, *Charge*, and *Park*, respectively. These three conditions further define macro-blocks of the Markov chain, in which we combine the condition (D, C, or P) with the charge level k.

It is worth noting that the charge level can only increase (or otherwise stay constant) if the condition is C; conversely, it can only decrease (or again stay constant) in condition D. When the system condition is P, we assume that neither discharge nor charge of the battery take place. It would be possible to also include other effects, such as charge balancing or leakage, but their effect is marginal with respect to charge and discharge caused by actual stationing at a charging point and driving, respectively, so we leave their inclusion for future work.

Under these assumptions, the Markov Chain would consist of $3N$ states, but we consider three additional states: the *Depleted* state identifies the situation in which an EV is in condition D with an empty battery and is therefore forced to stop, a condition that causes serious dissatisfaction to the user; the *Overcharged* state, representing a scenario in which the EV is in condition C with the battery fully charged, and therefore may have a higher probability of leaving the charging spot; and finally, the *Home* state, which corresponds to the situation in which the EV eventually arrives home at the end of the day if its operation is not terminated sooner by encountering the *Depleted* state. In other words, the *Home* state describes the service termination for the day in the ideal usage conditions. From the modeling stand point, it is just one of the possible exit states from a D condition, which corresponds to the EV heading back home instead of temporarily parking. Thus, the Markov chain has $3N + 3$ states, with *Depleted* and *Home* being absorbing states. Fig. 2.10 shows the resulting diagram of the Markov chain and its transitions.

The *Depleted* state is considered to characterize the range anxiety, since the owner of the EV would like to complete its daily route without being absorbed into it. For this reason, since the chain is ultimately absorbed by either the *Depleted* or the *Home* state, we define as p_d the probability that the former occurs, whereas $1-p_d$ describes the probability of ending in the *Home* state, as is desirable.

For the sake of simplicity, we consider the transitions among the system conditions to be independent of the EV charge level. In other words, we assume that the driver is actually oblivious to the state of the battery, which does not influence his/her behavior. It would be easy to improve the description of the model by considering a higher likelihood of moving towards a charging point when the charge level is low. Such a characterization would surely be possible within a Markov approach akin to our model, but it would require some assumptions on the driver's behavior (e.g., his/her risk aversion and/or the desire to avoid the *Depleted* state as much as possible), which in turn would need some supporting experimental data. Since all these characterizations are related to the range anxiety of the users, we prefer to keep this concentrated in the simple evaluation of p_d with independence between the system condition and the battery charge level.

As a result, we can describe the entire system through few simple parameters. In particular, we

define p_{start} as probability that when the system is in conditions C or P, the engine is turned on and a corresponding state with the same charge level, but under condition D, is entered. As said above, this value is the same regardless of the actual charge level of the battery. Also, we assume that this is the exit probability from state *Overcharged*, even though it would be easy to change this, for example, by assuming that a fully charged EV leaves the charging spot immediately with probability 1.

Quite similarly, we define the probability that the EV leaves condition D as a constant term p_{stop}; in this case, the system condition becomes P or C, which in turn depends on how broad is the fraction f of electrified parking. We assume that charging stations are uniformly distributed across the areas where the EV can park, thus condition D is left towards C with probability fp_{stop}, and towards P with probability $(1-f)p_{stop}$. However, another exit options exists from condition D, which is the probability to enter the absorbing *Home* state, which happens with probability p_{home}. Note that this parameter can be set depending on the desired average duration of a daily cycle not interrupted by absorption to the *Depleted* state; in particular, in the following we chose it so that the EV stays out for an average of 12 hours. Finally, the two remaining parameters are the probabilities that the EV battery charge decreases or moves to a higher level, things that may happen when the system condition is D or C, and which are denoted by symbols p_c and p_{charge}, respectively.

Such a Markov chain can be solved very easily through standard stochastic process analysis to find, among other metrics of interest, the value of p_d. The number of states N does not heavily impact on the complexity of the solution, as will be further discussed next. Technically speaking, this happens because the transition matrix related to the Markov model is sparse; indeed, the process can be seen as a Quasi-Birth-and-Death process similar to those in [39]. In the following, we discuss the application of our model and the extraction of p_d as a range anxiety analysis. We preliminary investigate the quantization granularity required to have an accurate model, and afterwards we show that our proposed model is able to keep into account the impact of battery capacity, recharge speed, and frequency of the charging spots.

2.2.2 Numerical results

First of all, we consider the impact of quantization parameters in the model previously proposed. The model accuracy heavily depends on the choice of Δ_t and N, which do not refer to real characteristics of the EV system, but are just chosen so as to make the model tractable. Also, in order to have a better understandable model, we introduce further parameters that characterize the system more descriptively, as opposed to the transition probabilities of the Markov chain.

The chosen parameters are the EV autonomy in km from a full battery, denoted as A; the average recharge time, denoted as T_{charge}, to reach the state *Overcharged* from an empty battery assuming no change of condition occurs; the average length of the paths that the EV drives and their average number within a day, denoted as L and n, respectively; the duration of the daily hours, denoted as H; the average EV speed v.

In particular, we can introduce $H^* = H(1 - \frac{Ln}{Hv})$ as the time fraction in which the EV is not driving. Thus, we can write the following relationships, which directly follow from their definitions.

$$p_{start} = \frac{n\Delta t}{H^*} \tag{2.4}$$

$$p_{stop} = \frac{v\Delta t}{L}\frac{n-1}{n} \tag{2.5}$$

$$p_{home} = \frac{v\Delta t}{L}\frac{1}{n} \tag{2.6}$$

$$p_c = \frac{v\Delta t}{A/N} \tag{2.7}$$

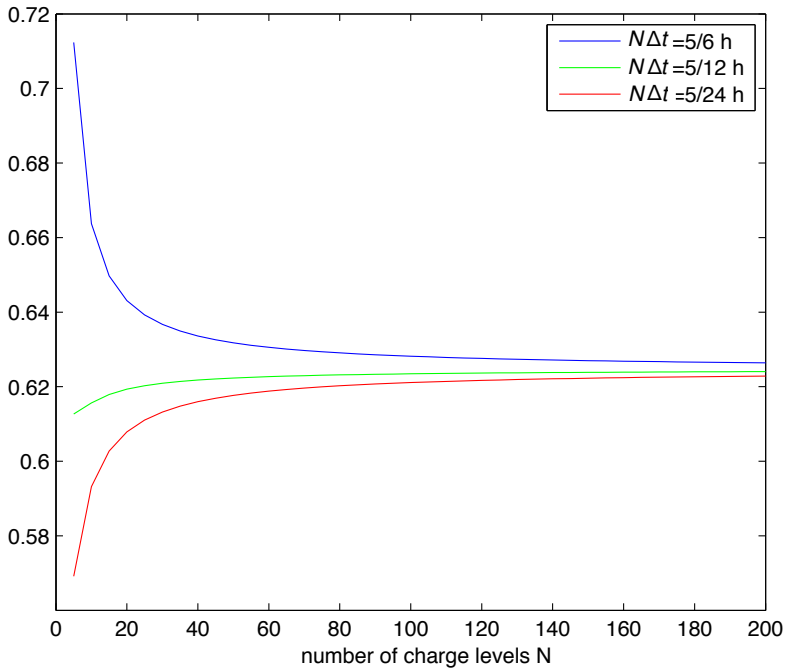

Figure 2.11: Probability of successful service completion within the day (i.e., the battery is not fully depleted), varying discretization parameters Δt and N.

$$p_{charge} = \frac{\Delta t}{T_{charge}/N} \tag{2.8}$$

In the following, if not specified otherwise, we assume these values, that can be seen as a reasonable choice: $A = 100km$, $T_{charge} = 2h$, $L = 25km$, $n = 8$, $H = 12h$, $v = 50km/h$, $f = 0.5$. These are sample values useful to give a proof of concept for the model; more realistic results can be used if available. For what concerns the evaluations of the quantization accuracy, similar results have actually been obtained in a wide range of parameters. Thus, we can plot in Fig. 2.11 the probability of successful service completion, in other words, the probability that the EV at the end of the day is not found in the *Depleted* state, i.e., $1 - p_d$. This is shown by considering different choices of Δ_t and N. Regardless of the actual value of the metric, from the figure it is evident that, when the number of levels N is sufficiently high, granularity in time only has a marginal effect. This is likely to happen because the considered time interval of a daily cycle is sufficiently large to make a time quantization interval of several seconds acceptable. Conversely, from the figure it appears that a sufficiently high value of N is required. As a result, in the following we use $N = 100$ and $\Delta_t = 15$ seconds.

Now, we explore some building aspects of the model in more depth. The impact of the battery capacity on the range anxiety is related to the width of the Markov chain: the higher the number L of battery levels, or conversely, the slower the transitions towards the *Depleted* state, the less likely that the EV usage unsuccessfully ends in that state. An increase of the charge speed implies considering a stronger transition probability towards states with higher energy levels in condition C. Finally, another relevant element is the frequency of charging points, which also directly captured by our model. We also stress that these aspects all have a direct translation into three system parameters, namely, the autonomy A, the time to charge T_{charge}, and the parameter f.

To show a sample result, in Fig. 2.12 we report the probability of successful service completion p_d as a function of the battery autonomy A, but also considering different values of f and T_{charge}. One can notice that A is the key factor to avoid range anxiety, since a reasonably high probability of service completion (in the figure, we highlighted a threshold of $1 - p_d = 70\%$) can be achieved only if A is large enough. However, the frequency of charging points impacts on this result as well, since if f

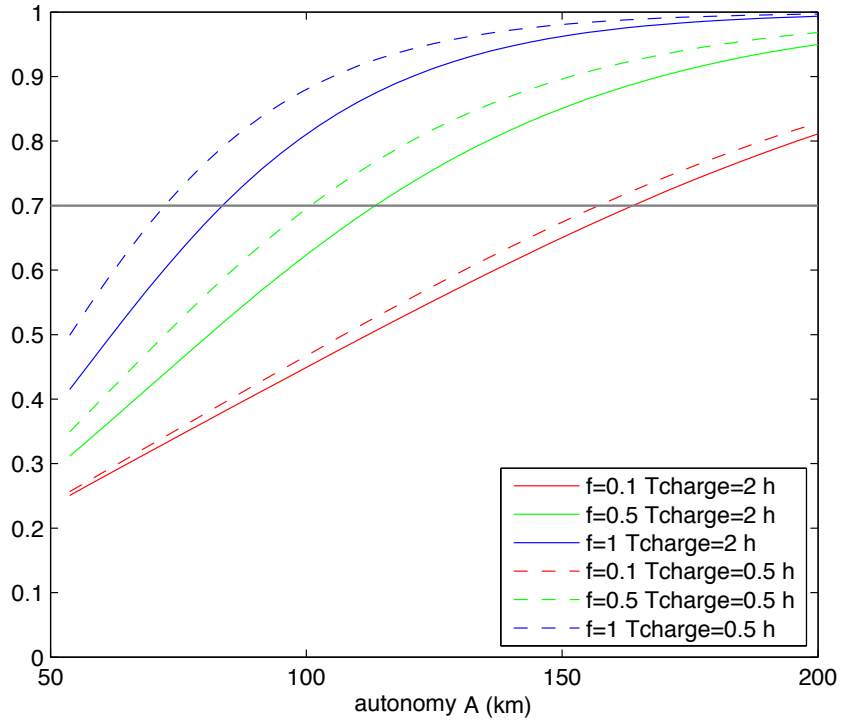

Figure 2.12: Probability of successful service completion within the day (i.e., the battery is not fully depleted), varying system parameters A, f, and T_{charge}.

is very low, the required autonomy might be too high: for example, $f = 0.1$ causes $1 - p_d$ to be below 70% unless A is very large.

Finally, we also focus on the impact of T_{charge}. From the considered model, this impact is less relevant, but still significant. According to the figure, a faster charging cycle can decrease the required autonomy by 10% or more; however, this happens only when f is high enough. This is because a faster charge can keep battery depletion sufficiently far even in the cases where the EV stops at the charging point only for a short while.

In addition, we must consider that the Markov chain presented here has only absorption to state *Depleted* as a (large) penalty, i.e., total failure. However, we can extend this point by introducing a reward process over the Markov chain, according to which the EV could cumulate a payoff depending on the condition it is in. In this case, we can consider an additional state, in which we force the vehicle's charging; this state involves no reward for the EV. More in general, several other investigations can exploit the proposed model, either expanding it, or including experimental evaluations to derive meaningful system parameters.

2.2.3 Conclusions

We proposed a Markov chain for assessing and possibly improving the performance of EVs, with particular reference to the evaluation of their autonomy and the resulting range anxiety related to the customers. Our chain builds up on a behavioral model of the EV, including possible actions such as "drive" and "park," as well as the battery status modeled as an energy queue. We showed how the model can easily integrate several elements of interest in the performance evaluation, namely the battery capacity, the density of the charging points, and the speed of charge for the battery.

As possible extension of this work, we could consider a relationship between the behavior of the users in the EVs and the charge level of the battery through a Markov decision process (MDP). We can further consider different conditions of motion; in particular, we can consider multiple states related to various motion kinds, each of which could have different levels of battery charge, and also

possibly a different reward in an MDP. Moreover, in our analysis we did not treat situations in which a deterioration of the battery or some malfunctions could imply a decrease in the EV autonomy over time. In future works, we might take care of these aspects considering a longer timescale. Furthermore, some additional battery effects (such as leakage) may be considered by defining other parameters describing the probability to move to lower level of charge even under *Park* conditions. Finally, an optimization framework for this reward collection can be formulated [38], so as to transparently implement intelligent algorithms for battery management.

Chapter 3

Game theory applied to telecommunications networks issues

In this Chapter we describe the application of game theory models to address some telecommunications issues with particular reference to management of a queueing system, jamming problems, and group recognition in a communications network. Moreover, in the following of the thesis we also discuss a game theoretic approach applied to a mobile computing setup. The purpose of the presentation of these investigations is to show how the joint combination of different theories born in different contexts can be useful enriching the evaluation of systems looking at them from a perspective that differs from the one commonly used.

3.1 Preliminaries on game theory

What economists call game theory, psychologists call the theory of social situations, which gives an accurate description of what game theory is about. Although game theory is relevant to games such as poker or bridge, most researchers in game theory focuses on how groups of people interact. There are two main branches of game theory: cooperative and non-cooperative game theory. Non-cooperative game theory deals mainly with how intelligent individuals interact with one another in an effort to achieve their own purposes.

In this setting the objective is to make predictions on the behavior of multiple agents that constitute the system under exam. For this reason, game theory is also used more and more commonly to address problems related to contexts that differ from the economic and psychological ones, such as telecommunications problems [52].

In general, game theory considers that individual agents, called *players*, perform actions according to their personal interests that may differ from the interests of someone else in the same system [41]. Each player acts towards the maximization of its own utility, for the assessment of which we must consider the actions played by all players. Moreover, each player has to create some beliefs about the actions performed by its opponents in the game, because it does not know them. The utility, called *payoff*, represents an arbitrary quantification of the goodness coming from a joint selection of actions. In general, a static game of complete information is conveyed by a triple $\mathcal{G} = (\mathcal{N}, \mathcal{S}, \mathcal{P})$, where $\mathcal{N}$ is the set of players, $\mathcal{S}$ is the set of all strategies allowed to players, and $\mathcal{P}$ represents the payoffs that depend on the actions chosen by the players. Considering this kind of game, a strategy can be defined as playing an action, but its definition become more complex if we consider more advanced setups.

In game theory the computation of equilibrium conditions is an important issue. We can define an equilibrium as a joint strategy profile where all players payoffs are locally maximized. In particular, we are interested in the computation of the Nash Equilibrium (NE) [72] defined as a strategy profile according to which each player does not have a stimulus to change on their side their path of action.

In this context, players can perform pure o mixed strategies, where the former defines tha action a player will take for any situation it could deal with, the latter considers a probability distribution over the set of pure strategies.

For our evaluations, we consider a *Bayesian game* that is a game of incomplete information in which each player can be of a *type*. The type of each player is different from its opponents type and has a different payoff function. This captures the fact that players may have different behaviors. Furthermore, we assume that distribution over types is common knowledge between players. Thus, each player knows its own type, but it does not know its opponents type. In this scenario, a strategy can be defined as a complete plan of actions in which every chance of the game, types included, are considered. The important aspect in a Bayesian context is that players form correct beliefs about their opponents action and type; indeed, equilibrium conditions hold whenever players beliefs are correct and robust. Considering all these assumptions, we can say that a NE describes a situation in which each player is playing a best response to its belief about the strategy chosen by the opponents and their type.

In the following, we will refer also to *Zero-sum Game* that is a mathematical representation of a situation in which each participant's gain or loss of utility is exactly balanced by the losses or gains of the utility of the other participants, which means that if the total gains of the participants are added up and, then, the total losses are subtracted, they will sum to zero. On the other hand, non-zero-sum describes a situation in which the interacting parties' aggregate gains and losses can be less than or more than zero. A zero-sum game is also named as *strictly competitive game* while non-zero-sum games can be either *competitive* or *non-competitive*. Most of the time, zero-sum games are solved by means of the *minimax theorem* which is closely related to linear programming duality, or with Nash equilibrium.

In the sequel of the present Chapter, we will exploit these concepts to capture the inherent uncertainty of distributed systems, which is very relevant to communication systems. We will show how this theoretical background enables a descriptively powerful evaluation of the system and paves the road to a useful characterization for many distributed network problems. In [46], nodes forward packets randomly and in an uncoordinated behavior. It may be interesting, for example, to evaluate how much efficiency is lost with respect to the case of coordinated management. In [47], multiple access techniques are integrated; this is a strong research topic also in view of upcoming 5G cellular networks. In this case, the access selection may be done with or without coordination among the controllers allowing a comparison between the different performance evaluations obtained. Finally, in [48] the authors consider the problem of optimizing the transmission strategy of two devices with energy harvesting capability that share a wireless channel, in order to maximize the long-term average importance of the transmitted data. It is assumed that a central controller is kept informed on the energy level and packet importance of both nodes. Actually, it may be useful to compare the case of a distributed behavior (either collaborative or competitive) of the nodes and compare the resulting performance with respect to the central controller case. Furthermore, in the same spirit also the coexistence of multiple uncoordinated energy sources is a relatively unexplored field that can be interesting to investigate in light of the strong interest received by energy harvesting as a way to achieve self-sustainable transmission and green networking.

3.2 Bayesian game analysis of a system with multiple candidate agents

The need for scalability of modern communication networks has led to the practical establishment of several distributed management algorithms.[1] Indeed, keeping the network intelligence spread in the entire network is both a low-cost management solution and also the proper way to involve the increased computational power of communication devices.

To mathematically characterize this aspect, we consider a joint application of queueing theory [40] and game theory [41]. In more detail, we consider a queueing system in two different cases: *uplink* and *downlink*. In the uplink case, we consider multiple candidate servers, whose clients, for example, can be thought of being packets arriving to the system for transmission. Each server represents an option available at the device, which is managed by its own controller, and has its own specific success probability for transmission. We model this situation as a game, where the servers are the players and they can decide to be inactive or active; staying active has a fixed local cost for the server, while a successful transmission or, more in general, service completion is beneficial for the whole system. It is worth noting that in a system with a centralized supervision, it would be best to only keep active the server with highest success probability. However, according to our analysis servers act selfishly, as a normal setup in any game theory applications, and servers do not even know who the best server is, since they do not know each other's characteristics. While the former is a classic ingredient of game theory capturing the lack of cooperation, the latter is due to the lack of *communication* between the agents, which is represented by modeling the problem as a Bayesian game [72]. In this setup, we compute the *social welfare* of our system as the sum of the individual expected gains. As a measure of inefficiency we compute the Price of Anarchy (PoA), one of the well known game theoretic parametes that indicates the loss due to the lack of cooperation and measures how the efficiency of a system degrades due to selfish behavior of its agents.

As well as for the uplink case just introduced, we evaluate at the same way also a *downlink case*, where we consider a system with candidate clients requiring services to a server that has the purpose of choosing the best client to which offer them in terms of maximizing the whole network gain and performance. We will explain in more details later on the two scenarios and the corresponding analysis.

Up to our knowledge, this work is the first to combine these two mathematical approaches in this way. Various works in the literature study different characterizations of a queueing model using game theory; most of them consider the point of view of the customers. Indeed, some research works include whether to avoid or follow the crowd [42], and the proper period of time in which to arrive to a queue in order to minimize waiting and tardiness costs [43]. Other papers study the network as a whole and its strategic structure as a complex system made of customers and servers [44, 45].

We remark that our analysis has strong consequences in modeling a transmission system with multiple alternatives controlled by distributed agents, a rationale that can be applied throughout the entire protocol stack. For example, at the network layer it can be exploited for a distributed routing selection in multi-hop environments [46]. At the datalink layer, multiple access techniques can be coordinated similarly [47]. Finally, at the physical layer, this can be applied for devices powered by multiple energy sources [48].

We refer to a game in which each player is characterized by a type, which is unknown to the others and we consider different levels of cooperation. Our goal is to compare the effects of cooperation and communication between the agents involved in the system. For this reason, we consider different scenarios and we compute the PoA quantifying the system inefficiency due to the selfish behavior of its members. In our case the PoA is evaluated as the ratio between the gain obtained in the best possible scenario, in which everything is known and there is cooperation, and the gain related to the

[1] This section is taken from "Bayesian Game Analysis of a Queueing System with Multiple Candidate Servers" published in IEEE CAMAD.

worst scenario, in which just a single agent works and the others are off. Moreover, we compute the gain that each agent has due to the fact that there are other agents in the system with whom it can cooperate. We call this measure *Maximum Diversity Gain*.

The rest of this Section is organized as follows. Sub-section 3.2.1 describes the system model and the game theory application; we compute the NEs in Section 3.2.2. Section 3.2.3 presents some numerical results and, finally, some concluding remarks can be found in Section 3.2.4.

3.2.1 System model

We focus on *downlink/uplink* systems. In particular, we consider our system in two different contexts: one in which two clients require services to a server that has to decide to which of them offer them (i.e., *downlink* case) and the other one in which there are two servers offering services and we need to determine which of the two servers is better to offer them to a client (i.e., *uplink* case).

3.2.1.1 Downlink case

In the downlink case we consider a system with two clients and a single server. The clients, client 1 and client 2, require a service offered by the server that has to establish to which of them is better to offer the service making some considerations regarding the system dynamics. Each client can either be *active* or *inactive*. Just to give an explanatory example, if the service required by the clients is the transmission of a content, it is reasonable to assume that the server sends data to the *active* client if just one client is *active*; it may be possible that then the active client could send the content to the *inactive* one. Instead, if both clients are *active*, the server sends the data to the best client and, as a consequence, this client may share the content with the other client for example via Bluetooth. We assume that to each client is associated a variable $\mu_i \in [0, 1]$, with $i \in [1, 2]$, that describes the interest of client i in having a certain service offered by the server. Moreover, we define c as the cost of being *active* for a client. The parameter c varies in the range $(0, 1)$. The value of c is equal for both clients. We assume that the probability of success, that is the probability that the service is accomplished, is 1 and, when both clients are *active*, the best one is choosen according to its value of μ_i; in particular, we assume that the server will choose the client with the higher interest level.

We can model this system in a game theoretic context, in which client 1 and client 2 are the two players, player 1 and player 2, respectively. From here on, we will use in an interchangeable way both terms client and player. The set of actions that players can do is constituted by being *active* and being *inactive*. In particular, to every pair of actions of the clients corresponds an arbitrary quantification of the goodness coming from performing those actions. In this way, each player can choose the best action considering the payoff associated to each possible move. It is worth noting that, in this case, each player acts towards the maximization of its own utility. We assume that successfully task completion involves a profit of 1, the profit is 0 otherwise, for both client (even the one not being *active*). As already discussed, if both client are *active*, the server chooses the client with the higher level of interest; however, the additional *active* client does not bring any additional benefit to the system. Proceeding with the analysis, since there are two possible players and two possible actions, we need to consider 4 different cases. If both clients are *inactive*, we reasonably assume that any task is required and, thus, any task is offered by the server. As a consequence, players payoffs are supposed to be 0. In the case in which client i is *active* and client j is *inactive*, the payoff of the former is $\mu_i - c$ and the one of the latter is μ_j. Finally, if both clients are *active*, the payoff of player 1 is $\mu_1 - c$ and that of player 2 is $\mu_2 - c$.

In Table 3.1 each entry shows the corresponding payoff for the two players associated to the pair of actions chosen, on rows for player 1 and columns for player 2.

		Player 2	
		active	**inactive**
Player 1	**active**	$\mu_1 - c,\ \mu_2 - c$	$\mu_1 - c,\ \mu_2$
	inactive	$\mu_1,\ \mu_2 - c$	0, 0

Table 3.1: Payoff of the players

		Player 2	
		active	**inactive**
Player 1	**active**	$\max(\mu_1, \mu_2) - c,$ $\max(\mu_1, \mu_2) - c$	$\mu_1 - c,\ \mu_1$
	inactive	$\mu_2,\ \mu_2 - c$	0, 0

Table 3.2: Payoff of the players

3.2.1.2 Uplink case

In the *uplink* case we consider a system with two servers, server 1 and server 2, and a single client. The client may require some services and it is necessary then to decide which of the two servers to choose to offer those services. We assume that each server can either be *active* or *inactive* and has a certain probability of successfully completing a service, μ_1 or μ_2, respectively, when it is *active*. Also in this scenario, we consider the parameter c as the cost of being *active*, with $c \in (0, 1)$, and its value is equal for both servers. Moreover, we consider that when neither server 1 nor server 2 is *active* or none of the two servers is able to complete the task even if *active*, the service is not offered and, in this case, the cost paid by servers is d. Without loss of generality, we set $d = 0$; for $d > 0$, it is sufficient to consider a rescaling of the utilities.

We can model this problem as a game in which the two servers are the players, player 1 and player 2, and their possible actions are being *active* or being *inactive*. In our evaluations successfully and incorrect task completion involve a profit of 1 and 0, respectively, for both servers (even the one not offering the service). If both servers are *active*, then the service is offered by the server with the higher successful probability assuming that the additional *active* server does not bring any benefit to the system. For each pair of actions it is possible to compute the payoff for each player and, then, players can choose their best move. Four different cases are to be considered. If both servers are *inactive*, neither attemps to offer the service and their payoffs are 0. If server i is *active* and server j is *inactive*, the payoff of the former is $\mu_i(1 - c) + (1 - \mu_i)(-c) = \mu_i - c$ and that of the latter is μ_i. Instead, if both servers are *active*, the value of their payoff is $\max(\mu_1, \mu_2) \cdot (1 - c) + (1 - \max(\mu_1, \mu_2)) \cdot (-c) = \max(\mu_1, \mu_2) - c$ for both of them.

In Table 3.2 each entry indicates the payoff associated to the pair of actions for the players.

3.2.2 Nash Equilibrium Computation

To analyze our systems, we consider a Bayesian setup. In particular, we assume that each player i, $i \in \{1, 2\}$, has a type that is the level of interest in the *downlink* case and the probability of correct task completion in the *uplink* case, represented as μ_i in both cases. The types of the players follow a joint distribution that is common knowledge between players. In more details, each player knows its own type, but it has to create some beliefs about its opponent type. To evaluate players payoff, we need to weigh the payoff expressions previously discussed with respect the types distributions, that is we need to compute the expected payoff. Furthermore, since our aim is to compare systems with and without cooperation and communication between agents, we consider different scenarios.

3.2.2.1 Scenario 1-Distributed service without signaling downlink case

Since we are considering a Bayesian context, a pure strategy s_i for player i represents the choice of being *active* or *inactive* for every possible type μ_i.

Client i will be surely *inactive* if $\mu_i = 0$ and surely *active* if $\mu_i = 1$. If we consider an intermediate case, client i will be *active* if its expected payoff when it is *active* is greater than the expected payoff when it is *inactive*. Focusing on a single client i, if a given value of μ_i involves that the server decide to offer the service to client i, then any other $\tilde{\mu_i} > \mu_i$ will allow the choice of client i. This is implied by the monotonicity of the expected payoff weighed on the distribution of the type as a function of μ_i. Indeed, client i is chosen by the server as the best client if $\mu_i > c$, thus, if this holds then also $\tilde{\mu_i} > c$ holds. Therefore, we can state that the optimal strategy follows a threshold policy.

Proposition. The best response of player i will be to be *active* and require the service if and only if

$$\mu_i \geq \frac{c}{1 - \rho_{-i}} \tag{3.1}$$

where ρ_{-i} is the probability that player $j \neq i$ is *active*. If we consider the distribution over types uniform in $[0, 1]$, then (3.1) becomes $\mu_i = c/\hat{\mu}_j$. Indeed, if player j chooses threshold $\hat{\mu}_j$ and it is *active* if and only if $\mu_j > \hat{\mu}_j$, then the probability that player j is *active* is equal to the probability that its type is greater than or equal to $\hat{\mu}_j$. For this reason $1 - \rho_{-i} = \hat{\mu}_j$. Moreover, if player i belief is that $\hat{\mu}_j < c$, then its best response is to never require the service to the server and, therefore, to set its threshold $\hat{\mu}_i = 1$. Conversely, player i's best response is to choose $\hat{\mu}_i = c/\hat{\mu}_j$.

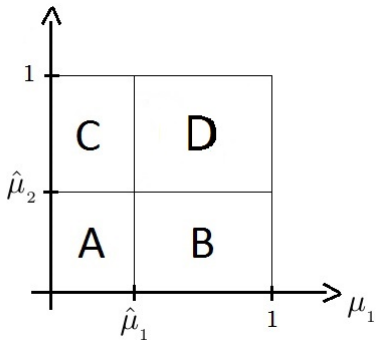

Figure 3.1: Areas for the players expected payoff computation downlink case.

Eq. 3.2 defines the best response threshold strategy $\hat{\mu}_i$ of player i assuming that player j chosen threshold is $\hat{\mu}_j$.

$$BR_i(\hat{\mu}_j) = \begin{cases} \frac{c}{\hat{\mu}_j}, & \text{if } \hat{\mu}_j \geq c \\ 1, & \text{if } \hat{\mu}_j < c \end{cases}. \tag{3.2}$$

Plotting the best response curves of the two players varying μ_1 and μ_2, it is possible to determine for which values of the pair (μ_1, μ_2) they intersect. We found that the curves coincide for $c \leq \mu_i \leq 1$ with $i \in \{1, 2\}$. As a consequence, the pairs (μ_1, μ_2) that satisfy $\mu_1 \mu_2 = c$ with $c \leq \mu_i \leq 1$ and $i \in \{1, 2\}$ are NEs.

Fig. 3.1 shows the areas considered for the computation of the players expected payoff. Indeed, since we consider a given distribution over types, it is necessary to weigh on this distribution considering different contributions and then summing their values. The following equations are the 4

contributions for the expected payoff of player 1.

$$A = 0 \tag{3.3}$$
$$B = \hat{\mu}_2 \left[\frac{1-\hat{\mu}_1^2}{2} - c(1-\hat{\mu}_1) \right] \tag{3.4}$$
$$C = \hat{\mu}_1^2 \left[\frac{1-\hat{\mu}_2}{2} \right] \tag{3.5}$$
$$D = (1-\hat{\mu}_2) \left[\frac{1-\hat{\mu}_1^2}{2} - c(1-\hat{\mu}_1) \right] \tag{3.6}$$
$$\tag{3.7}$$

As a consequence, the expected payoff of player 1 is given by $A + B + C + D$. Instead, for player 2 we obtained

$$A = 0 \tag{3.8}$$
$$B = \hat{\mu}_2^2 \left[\frac{1-\hat{\mu}_1}{2} \right] \tag{3.9}$$
$$C = \hat{\mu}_1 \left[\frac{1-\hat{\mu}_2^2}{2} - c(1-\hat{\mu}_2) \right] \tag{3.10}$$
$$D = (1-\hat{\mu}_2) \left[\frac{1-\hat{\mu}_2^2}{2} - c(1-\hat{\mu}_2) \right]. \tag{3.11}$$
$$\tag{3.12}$$

3.2.2.2 Scenario 2-Lazy client downlink case

This case refers to the scenario in which one client can be *active* or *inactive* and the other one is always *inactive*. It is as we have just a single client requiring services in the system and, for this reason, this represents the worst case due to the fact that there is neither cooperation nor communication between the clients. Since we consider two clients, there a two different sub-cases: case 2a that describes the situation in which client 2 is always *inactive*, case 2b that corresponds to the situation in which client 2 is actually the only one that can be *active*.

In the following analysis, we focus on case 2a. Indeed, the same results are obtained for case 2b after reversing clients roles. Given that player 2 is always *inactive*, the best strategy for player 1 is to be *active* if $\mu_1 - c > 0$. This case is a particular case of the previous Scenario 1 considering the pair $(\hat{\mu}_1, \hat{\mu}_2) = (c, 1)$ (similarly $(\hat{\mu}_1, \hat{\mu}_2) = (1, c)$ for case 2b) as NE.

Finally with these assumptions, player 1 expected payoff is

$$\int_0^1 d\mu_2 \int_0^{\hat{\mu}_1} 0 \; d\mu_1 + \int_0^1 d\mu_2 \int_{\hat{\mu}_1}^1 (\mu_1 - c) \; d\mu_1 = \frac{1-c^2}{2} - c(1-c) \tag{3.13}$$

considering that $\hat{\mu}_1 = c$. Whereas, for player 2 we obtained

$$\int_0^1 d\mu_2 \int_0^{\hat{\mu}_1} 0 \; d\mu_1 + \int_0^1 d\mu_2 \int_{\hat{\mu}_1}^1 \mu_2 \; d\mu_1 = \frac{1-c}{2}. \tag{3.14}$$

3.2.2.3 Scenario 3-Coordinated service downlink case

The coordinate service scenario refers to the case in which the game is completly known to the players; in particular, each player knows its opponent type. In this case both cooperation and communication are allowed between clients. Moreover, we assume that when both clients are *active*, the one with the highest interest μ_i requires the service to the server.

We assume now that player 1 knows the threshold value $\hat{\mu}_2$ of player 2.

Theorem If $\hat{\mu}_2 > c$, then $BR_1(\hat{\mu}_2 > c) < \hat{\mu}_2$ since the optimal strategy is a threshold policy. We prove this theorem by contradiction. Indeed, assuming that $BR_1(\hat{\mu}_2 > c) > \hat{\mu}_2$, then this involves that if $c < \mu_1 < \hat{\mu}_2$, player 1 does not require any service because *inactive*. However, as a counter example, we can prove that if $c < \mu_1 < \hat{\mu}_2$, for player 1 is better to be *active* in order to have a higher payoff. Indeed, defining q as $Prob\{\mu_2 > \hat{\mu}_2\}$, if the previous condition on the value of μ_1 holds, then the payoff of player 1 if it decides to be *inactive* depends on whether player 2 requires or not the service and it is $q\mu_1$, instead if player 1 decides to require the service its payoff is $q\mu_1 + (1-q)(\mu_1 - c)$. As a consequence, for player 1 it is better to be *active* if $q\mu_1 + (1-q)(\mu_1 - c) > q\mu_1$, that is if $\mu_1 > c$. This implies that $BR_1(\hat{\mu}_2) < \hat{\mu}_2$. This last result is in contrast with respect to what we have previously found.

At this point, we want to prove the following Lemma.

Lemma Assuming that player 1 knows the value of $\hat{\mu}_2$. If $\mu_1 \geq \hat{\mu}_2 \geq c$, then for player 1 it is better to decide to be *active* and require the service. As a consequence, $BR_1(\hat{\mu}_2) = c$.

We define $r = \chi_{(\mu_1,1)}(\mu_2)$ and $q = \chi_{(\hat{\mu}_2,1)}(\mu_2) - \chi_{(\mu_1,1)}(\mu_2)$, where the use of the indicator function χ means, for example, that $q = \begin{cases} 1, & \text{if } \hat{\mu}_2 \leq \mu_2 \leq \mu_1 \\ 0, & \text{otherwise} \end{cases}$. Assuming this, if player 1 decides to be *active* and require the service, then its payoff is $r\mu_1 + q(\mu_1 - c) + (1 - r - q)(\mu_1 - c)$, on the other hand, if it decides not to require it, its payoff is $r\mu_1 + q\mu_1 + (1 - r - q)0$. Then, for player 1 it is better to be *active* if

$$r\mu_1 + q(\mu_1 - c) + (1 - r - q)(\mu_1 - c) > r\mu_1 + q\mu_1 \tag{3.15}$$

holds. This means that $(\mu_1 - c)(1 - r) > 0$. Now, considering the expectation on μ_2

$$(\mu_1 - c)E_{\mu_2}[1 - r] > 0 \tag{3.16}$$

$$(\mu_1 - c)\int_0^1 1(1 - r)d\mu_2 > 0 \tag{3.17}$$

$$(\mu_1 - c)\int_0^{\mu_1} d\mu_2 > 0 \tag{3.18}$$

that is

$$\mu_1(\mu_1 - c) > 0. \tag{3.19}$$

This is always true because of the initial assumption of our Lemma. This means that player 1 reaches a higher payoff being *active* and requiring the service. In conclusion, since in general it must hold that $BR_i(\hat{\mu}_j) \geq c$, $BR_i(\hat{\mu}_j > c) < \hat{\mu}_j$, and $BR_i(\hat{\mu}_j < c) > \hat{\mu}_j > c$, in this setup, the NE, that is also a Pareto optimality, is given by the pair $(\hat{\mu}_1, \hat{\mu}_2) = (c, c)$.

It is worth noting actually that it is not necessary to have a complete a priori coordination between the agents operating in the system. Indeed, consider a scenario in which the system works as in Scenario 1 as previously discussed with the difference that when both clients are *active*, they can exchange some information about their type values in order to decide which of them is better to remain *active* and, on the other hand, which of them is better to switch off. With this assumption, the evaluation of the NE changes with respect to that scenario. Now, just some considerations follow to better explain this new setup. Focusing on player 1, it is reasonable to assume that if $\mu_1 < c$, if player 2 is *inactive* and player 1 decides to be *active* and request the service, its expected payoff is negative. Then, in this case, it is better to be *inactive* for player 1 gaining 0 as expected payoff. Therefore, it is reasonable to assume that player 1 can think to be *active* if $\mu_1 > c$. When this holds, three different cases can occur according to the value of μ_2

- *case a* $0 < \mu_2 < c$: this occurs with probability $Prob\{\mu_2 < \mu_1\} = \mu_1$ and the payoff for player 1 is $\mu_1 - c$ if it is *active* and request the service, 0 otherwise;

- *case b* $c < \mu_2 < \mu_1$: this occurs with probability $Prob\{\mu_2 < \mu_1\} = \mu_1$ and the payoff for player 1 is $\mu_1 - c$ if it is *active* and request the service, 0 otherwise;

- *case c* $\mu_2 > \mu_1$: this occurs with probability $Prob\{\mu_2 > \mu_1\} = 1 - \mu_1$ and the payoff for player 1 is μ_1 in any case.

Indeed, in *case a* and *case b* it holds that $\mu_1 > c$ and $\mu_2 < \mu_1$, then when clients tell each other the type values, player 1 knows that its type is higher, thus it has to decide whether being *active* and requiring the service or not according to the comparison of μ_1 and c. Instead, in *case c* player 1 knows a posteriori that its type is lower than its opponent type. Therefore, even if player 1 a priori decided to be *active*, player 2 will be *active* too and require the service since $\mu_2 > \mu_1$ holds. As a consequence, player 1 expected payoff will be μ_1. To evaluate the NE it is sufficient to compare the expected payoff when *active* with respect to the expected payoff when *inactive*; in more details, $\mu_1(\mu_1 - c) > 0$.

Same considerations hold reversing player 1 with player 2. Finally, we find that the NE is given by the pair $(\hat{\mu}_1, \hat{\mu}_2) = (c, c)$. This results is the same as the one obtained for the scenario with coordinated service as discussed at the beginning of this Sub-section. In conclusion, the best expected payoffs for the players is reached even just allowing a partial communication between clients, in particular when they are both *active*, without assuming complete a priori knowledge of the system.

3.2.2.4 Scenario 1-Distributed service without signaling uplink case

What previously said for the downlink still holds in the uplink case; in particular, server i will be *active* if the expected payoff when it is *active* is greater than the expected payoff when it is *inactive*. Moreover, also in this case it is still valid that the optimal strategy is a threshold policy for the same reason as previously discussed. The differences with the *downlink* case lies on the fact that for this scenario the evaluation of the NEs is significantly different. Focusing on player 1, we want that its payoff when it is *active* is greater than its payoff when it is *inactive*, therefore, defining q as the probability that player j is *active*

$$q\left[max(\mu_1, \mu_2) - c\right] + (1 - q)(\mu_1 - c) > q\mu_2 + (1 - q)0. \tag{3.20}$$

Doing some calculations, this means that

$$q\left[min(\mu_1, \mu_2)\right] < \mu_1 - c. \tag{3.21}$$

Player 1 knows the value of μ_1, but it does not know μ_2. On the other hand, distribution over types is common knowledge, therefore, we average on this distribution and solve

$$E_{\mu_2}\left[q\left[min(\mu_1, \mu_2)\right]\right] < E_{\mu_2}\left[\mu_1 - c\right]. \tag{3.22}$$

Since $\mu_1 - c$ is a constant with respect to E_{μ_2}, $E_{\mu_2}\left[\mu_1 - c\right] = \mu_1 - c$; the hardest part here is the computation of the other expectation. In particular, considering μ_1 and μ_2 uniformly distributed in $(0, 1)$, we know that

$$E_{\mu_2}\left[q\left[min(\mu_1, \mu_2)\right]\right] = \int_0^1 q \cdot min(\mu_1, \mu_2) d\mu_2. \tag{3.23}$$

At this point, we have to consider two different cases to solve the integral:

- case in which $\mu_1 < \hat{\mu}_2$

$$\int_0^{\mu_1} 0 \cdot min(\mu_1, \mu_2) d\mu_2 + \int_{\mu_1}^{\hat{\mu}_2} 0 \cdot min(\mu_1, \mu_2) d\mu_2 + \int_{\hat{\mu}_2}^1 1 \cdot \mu_1 \cdot d\mu_2 = \mu_1(1 - \hat{\mu}_2) \tag{3.24}$$

- case in which $\mu_1 > \hat{\mu}_2$

$$\int_0^{\hat{\mu}_2} 0 \cdot min(\mu_1, \mu_2) d\mu_2 + \int_{\hat{\mu}_2}^{\mu_1} 1 \cdot \mu_2 \cdot d\mu_2 + \int_{\mu_1}^{1} 1 \cdot \mu_1 \cdot d\mu_2 = \mu_1 - \hat{\mu}_2/2 - \mu_1^2/2. \tag{3.25}$$

As a consequence,

$$\mu_1 - c > \begin{cases} \mu_1 - \mu_1\hat{\mu}_2, & \text{if } \mu_1 < \hat{\mu}_2 \\ \mu_1 - \hat{\mu}_2/2 - \mu_1^2/2, & \text{if } \mu_1 > \hat{\mu}_2 \end{cases} \tag{3.26}$$

$$\mu_1 > \begin{cases} c/\hat{\mu}_2, & \text{if } \mu_1 < \hat{\mu}_2 \\ \sqrt{2c - \hat{\mu}_2^2}, & \text{if } \mu_1 > \hat{\mu}_2 \end{cases} \tag{3.27}$$

If $\mu_1 > \hat{\mu}_2$, we know that $\mu_1^2 + \hat{\mu}_2^2 > 2\hat{\mu}_2^2$, as a consequence, $\mu_1^2 + \hat{\mu}_2^2 > 2c$ is true if $\hat{\mu}_2 > \sqrt{c}$. In general,

$$\mu_i > \begin{cases} c/\hat{\mu}_j, & \text{if } \mu_i < \hat{\mu}_j \\ \sqrt{2c - \hat{\mu}_j^2}, & \text{if } \mu_i > \hat{\mu}_j \end{cases} \tag{3.28}$$

with $i, j \in \{1, 2\}$. If we plot the corresponding curves considering the two players, we obtain that the intersection is in $(\mu_1, \mu_2) = (\sqrt{c}, \sqrt{c})$. This represents the only NE of this scenario.

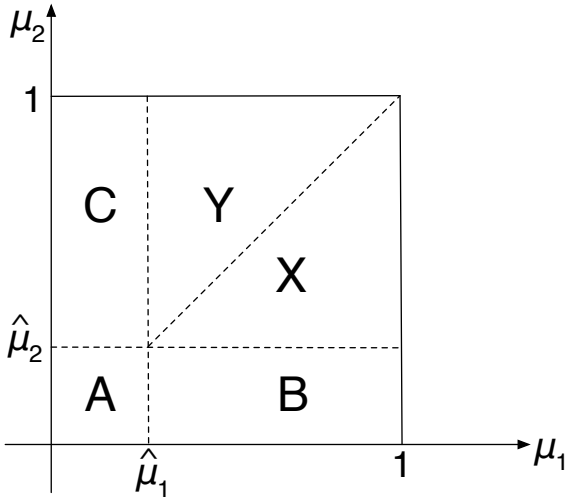

Figure 3.2: Areas for the players expected payoff computation uplink case.

Fig. 3.2 shows the areas considered for the computation of the players expected payoff. Indeed, since we consider a given distribution over types, it is necessary to weigh on this distribution considering different contributions and then summing their values. The following equations are the 5

contributions to sum for the expected payoff of player 1.

$$A = 0 \tag{3.29}$$

$$B = \hat{\mu}_2 \left[\frac{1-\hat{\mu}_1^2}{2} - c(1-\hat{\mu}_1) \right] \tag{3.30}$$

$$C = \hat{\mu}_1 \left[\frac{1-\hat{\mu}_2^2}{2} \right] \tag{3.31}$$

$$\begin{aligned} X &= \frac{(1-\hat{\mu}_1^3)(\hat{\mu}_2-1)}{3(\hat{\mu}_1-1)} + c\hat{\mu}_1(1-\hat{\mu}_2) \\ &- \frac{(1+\hat{\mu}_1)}{2}(c+\hat{\mu}_1)(1-\hat{\mu}_2) \end{aligned} \tag{3.32}$$

$$\begin{aligned} Y &= \frac{(1-\hat{\mu}_2^3)(\hat{\mu}_1-1)}{3(\hat{\mu}_2-1)} + c\hat{\mu}_2(1-\hat{\mu}_1) \\ &- \frac{(1+\hat{\mu}_2)}{2}(c+\hat{\mu}_2)(1-\hat{\mu}_1) \end{aligned} \tag{3.33}$$

The expected payoff of player 1 is given by $A+B+C+X+Y$. For player 2 we obtained similar results, it is sufficient to swap B with C and X with Y.

3.2.2.5 Scenario 2-Lazy server uplink case

This second scenario refers to the situation in which one server is always *inactive* and the other one can either be *active* or *inactive*. In this case, it is as there is just a single server in the system that works. For this reason, this represents the worst possible scenario. We will show that the obtained results confirm this fact.

Since there are two servers in the system, as before we define case 2a situation in which the only server that can be *active* in the system is server 1, case 2b the case in which server 1 is always *inactive*. We will focus on case 2a; similar results hold for case 2b after reversing servers roles.

Server 2 is always *inactive*, this means that $\hat{\mu}_2 = 1$. As a consequence, the best response threshold strategy for player 1 is to be *active* if and only if $\mu_1 - c > 0$, that is $\hat{\mu}_1 = c$. In this scenario the pair $(\mu_1, \mu_2) = (c, 1)$ does not represent a NE. Indeed, given $\hat{\mu}_2 = 1$, it is not true that the best response threshold strategy for player 1 is $\hat{\mu}_2 = c$. Under these considerations, we evaluate the expected payoff considering the pair $(\mu_1, \mu_2) = (c, 1)$ and its computation involves an unidimensional computation. In particular, the expected payoff of player 1 is

$$\int_0^{\hat{\mu}_1} 0 \; d\mu_1 + \int_{\hat{\mu}_1}^1 (\mu_1 - c) \; d\mu_1 = \frac{1-c^2}{2} - c(1-c) \tag{3.34}$$

considering that $\hat{\mu}_1 = c$. Whereas, the expected payoff of player 2 is

$$\int_0^{\hat{\mu}_1} 0 \; d\mu_1 + \int_{\hat{\mu}_1}^1 \mu_1 \; d\mu_1 = \frac{1-c^2}{2}. \tag{3.35}$$

3.2.2.6 Scenario 3-Coordinated service uplink case

Also in this case, it holds that the game is completly known to the players and both cooperation and communication are allowed to the servers. However, for the sake of clarity and explanation, since the payoffs of downlink and unplink could differ also when there is complete knowledge, we give the detailed analysis for the uplink case even if it could seem being very similar to the downlink situation.

In general, focusing on player 1, knowing that $\mu_1 > \mu_2$, player 1 will be *active* deciding to offer the service if and only if $\mu_1 > c$. Instead, if $\mu_2 > \mu_1$, then it will be *inactive*. Similar considerations hold for player 2.

We assume now that player 1 knows the threshold value $\hat{\mu}_2$ of player 2.

Theorem If $\hat{\mu}_2 > c$, then $BR_1(\hat{\mu}_2 > c) < \hat{\mu}_2$ since the optimal strategy is a threshold policy. We prove this theorem by contradiction. Indeed, assuming that $BR_1(\hat{\mu}_2 > c) > \hat{\mu}_2$, then this involves that if $c < \mu_1 < \hat{\mu}_2$, player 1 does not offer any service. However, as a counter example, we can prove that if $c < \mu_1 < \hat{\mu}_2$, then for player 1 is better to offer the service gaining a higher payoff. Indeed, defining $q = Prob\{\mu_2 > \hat{\mu}_2\}$, if the previous condition on the value of μ_1 holds, then the payoff of player 1 if it decides to be *inactive* depends on whether player 2 offer or not the service and it is $q\mu_2$, instead if player 1 decides to offer the service its payoff is $q\mu_2 + (1-q)(\mu_1 - c)$. As a consequence, for player 1 it is better to be *active* if $q\mu_2 + (1-q)(\mu_1 - c) > q\mu_2$, that is if $\mu_1 > c$. This implies that $BR_1(\hat{\mu}_2) < \hat{\mu}_2$ and it is in contrast with respect to what we have previously found.

We prove now the following Lemma.

Lemma Assuming that player 1 knows the value of $\hat{\mu}_2$. If $\mu_1 \geq \hat{\mu}_2 \geq c$, then for player 1 it is better to decide to be *active* and offer the service. As a consequence, $BR_1(\hat{\mu}_2) = c$.

We define $r = \chi_{(\mu_1,1)}(\mu_2)$ and $q = \chi_{(\hat{\mu}_2,1)}(\mu_2) - \chi_{(\mu_1,1)}(\mu_2)$, where the use of the indicator function χ means, for example, that $q = \begin{cases} 1, & \text{if } \hat{\mu}_2 \leq \mu_2 \leq \mu_1 \\ 0, & \text{otherwise} \end{cases}$. Assuming this, if player 1 decides to be *active* and offer the service, then its payoff is $r\mu_2 + q(\mu_1 - c) + (1-r-q)(\mu_1 - c)$, instead if it decides not to offer it, its payoff is $r\mu_2 + q\mu_2 + (1-r-q)0$. Then, for player 1 is better to be *active* if

$$r\mu_2 + q(\mu_1 - c) + (1-r-q)(\mu_1 - c) > r\mu_2 + q\mu_2 \tag{3.36}$$

holds. This means that $(1-r)(\mu_1 - c) > q\mu_2$. Now, considering the expectation on μ_2

$$(\mu_1 - c)E_{\mu_2}[1-r] > E_{\mu_2}[q\mu_2] \tag{3.37}$$

$$(\mu_1 - c)\int_0^1 1(1-r)d\mu_2 > \int_0^1 q\mu_2 d\mu_2 \tag{3.38}$$

$$(\mu_1 - c)\int_0^{\mu_1} d\mu_2 > \int_{\hat{\mu}_2}^{\mu_1} \mu_2 d\mu_2 \tag{3.39}$$

that is

$$(\mu_1 - c)\int_0^{\mu_1} d\mu_2 > \int_{\hat{\mu}_2}^{\mu_1} \mu_2 d\mu_2. \tag{3.40}$$

As a consequence,

$$\mu_1^2 - 2c\mu_1 + \hat{\mu}_2^2 > 0 \tag{3.41}$$

that is always true because of the negative discriminant. This means that player 1 reaches a higher payoff being *active* and offering the service. In conclusion, since in general it must hold that $BR_i(\hat{\mu}_j) \geq c$, $BR_i(\hat{\mu}_j > c) < \hat{\mu}_j$, and $BR_i(\hat{\mu}_j < c) > \hat{\mu}_j > c$, therefore, in this setup, the NE, that is also a Pareto optimality, is given by the pair $(\hat{\mu}_1, \hat{\mu}_2) = (c, c)$.

It is worth noting actually that still holds that it is not necessary to have a complete a priori coordination. Consider a scenario in which the system works as in scenario with distributed service without signaling with the difference that when both servers are *active* they can exchange some information about their type values to be able to decide which of them is better to offer services. Focusing on player 1, it is reasonable to assume that if $\mu_1 < c$, if player 2 is *inactive* and player 1 decides to be *active* and offer the service, its expected payoff is negative. Then, in this case, it is better to be *inactive* for player 1 and having a zero expected payoff. Therefore, it is reasonable to assume that player 1 decides to be *active* if $\mu_1 > c$. When this holds, three different cases can occur according to the value of μ_2

- *case a* $0 < \mu_2 < c$: this occurs with probability $Prob\{\mu_2 < \mu_1\} = \mu_1$ and the payoff for player 1 is $\mu_1 - c$ if it is *active* and offers the service, 0 otherwise;

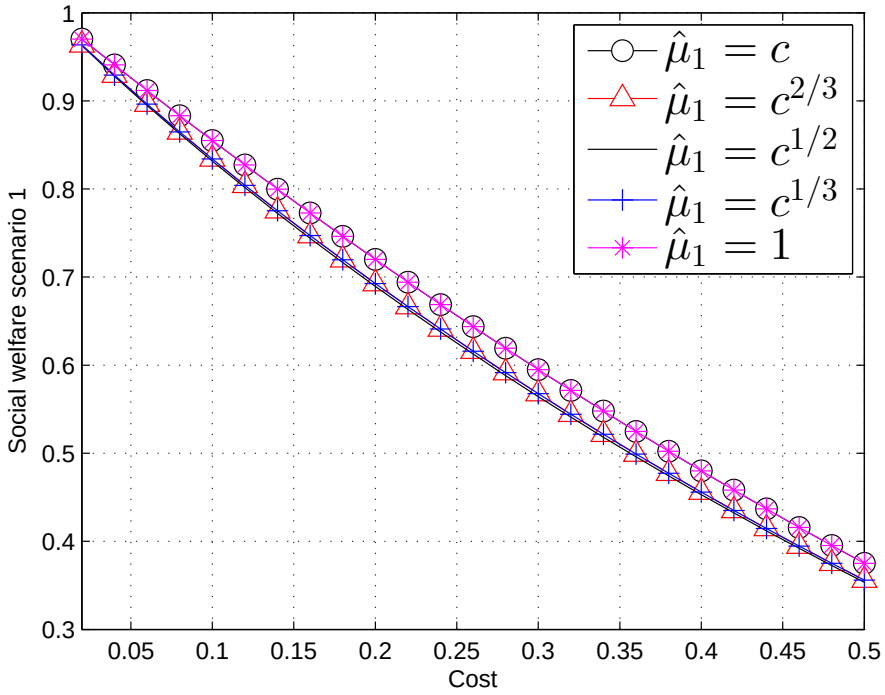

Figure 3.3: Total expected payoff for the distributed case without signaling (downlink case).

- *case b* $c < \mu_2 < \mu_1$: this occurs with probability $Prob\{\mu_2 < \mu_1\} = \mu_1$ and the payoff for player 1 is $\mu_1 - c$ if it is *active* and offers the service, 0 otherwise;
- *case c* $\mu_2 > \mu_1$: this occurs with probability $Prob\{\mu_2 > \mu_1\} = 1 - \mu_1$ and the payoff for player 1 is μ_2 in any case.

Indeed, in *case a* and *case b* it holds that $\mu_1 > c$ and $\mu_2 < \mu_1$, then when servers tell each other the type values, player 1 knows that its type is higher, thus it has to decide whether being *active* and offering the service or not according to the comparison of μ_1 and c. Instead, in *case c* player 1 knows a posteriori that its type is lower than its opponent type. Therefore, even if player 1 a priori decided to be *active*, player 2 will be *active* too and offers the service since $\mu_2 > \mu_1$ holds. As a consequence, player 1 expected payoff will be μ_2. To evaluate the NE it is sufficient to compare the expected payoff when *active* with respect to the expected payoff when *inactive*; in particular, $\mu_1(\mu_1 - c) > 0$.

We can drawn the same concluding remarks as the downlink case, and, in particular: (i) same considerations hold reversing player 1 with player 2; (ii) the NE is given by the pair $(\hat{\mu}_1, \hat{\mu}_2) = (c, c)$ (that is, same result obtained for the scenario with coordinated service). As a consequence we can state also for the uplink case that the best expected payoffs for the players cen be reached even just allowing a partial communication between servers without assuming complete a priori knowledge.

3.2.3 Performance evaluations

3.2.3.1 Downlink case

We consider the distribution over types uniform in the interval $(0, 1)$. For scenario 3.2.2.1, we take the following NEs: $(c, 1)$, $(c^{2/3}, c^{1/3})$, $(c^{1/2}, c^{1/2})$, $(c^{1/3}, c^{2/3})$, and $(1, c)$. Moreover, we define the social welfare as the sum of the expected payoff obtained for the two players.

Fig. 3.3 shows the social welfare obtained for scenario 3.2.2.1, considering the 5 NEs previously mentioned. As we can observe from these results, the highest value of the social welfare is given by

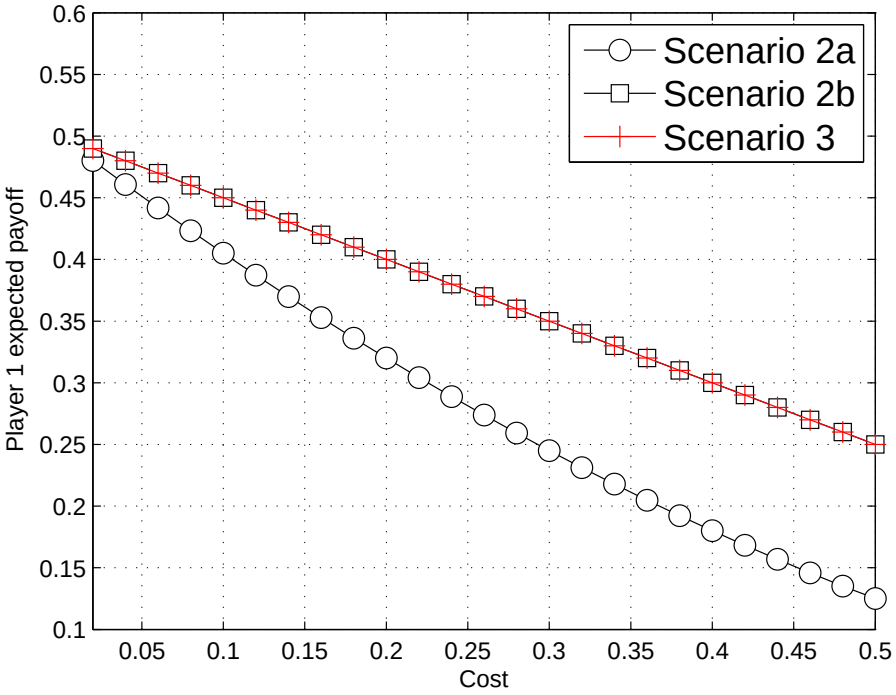

Figure 3.4: Player 1 expected payoff varying the cost of being *active* (downlink case).

the pairs $(c, 1)$ and $(1, c)$. The values of cost of being *active* c vary from 0.02 to 0.5 because for higher values of c we obtained degraded performances for all cases.

Fig. 3.4 shows the expected payoff of player 1 in three of the scenarios considered in the *downlink* case. Indeed, we have found that the best NEs for scenario 3.2.2.1, are the NEs of scenario 3.2.2.2, case 2a and case 2b, then, for this reason, we consider results for scenario 3.2.2.2 case 2a and case 2b, and scenario 3.2.2.3. As we can notice from this figure, the expected payoff for player 1 considering scenario 3.2.2.3 and scenario 3.2.2.2 case 2b are the same. It is worth noting that scenario 3.2.2.3 represents the best possible scenario. Therefore, from Fig. 3.4 we can state that the performances obtained when we assume client 1 always *inactive* are the same as the performances in the best possible case. Instead, looking at scenario 3.2.2.2 case 2a when client 2 is always *inactive*, we can observe that the expected payoff of player 1 is lower, in particular significantly lower as c increases, with respect to the results of the other 2 scenarios considered. For symmetry reasons, the expected payoffs of player 2 are the same as those shown in Fig. 3.4.

Since for this setup focusing on player 1 payoff, we find that a selfish behavior of player 1 implies the same payoff as the complete and perfect knowledge scenario, it can be stated that the computation of the PoA is meaningless.

3.2.3.2 Uplink case

Fig. 3.5 shows the expected payoff of player 1 in the NEs obtained for the scenarios considered in the *uplink* case. The cost c varies in the range [0.02 0.5] also for this results. In this figure, we can notice that the payoff for scenario 3.2.2.6 is an upper bound due to the assumption of complete a priori knowledge. On the other hand, the payoff for scenario 3.2.2.5 case 2a represents a lower bound. Looking at scenario 3.2.2.5 case 2b, we can state that for small values of c it is not always advantageous being always *inactive*: the player could have higher payoff cooperating with its opponent. Instead, for higher values of c, scenario 3.2.2.5 case 2b gives a higher expected payoff with respect to scenario

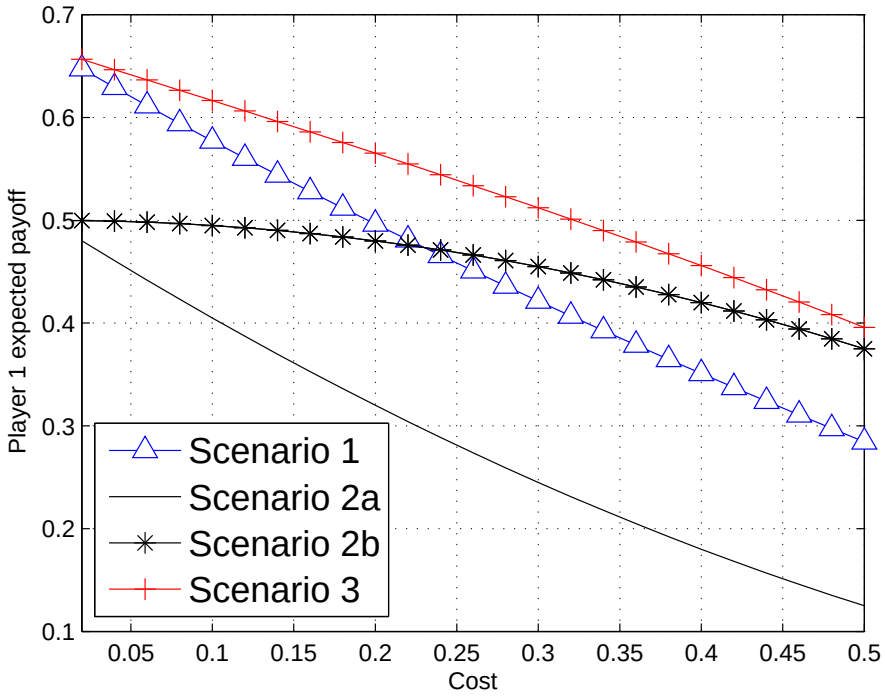

Figure 3.5: Player 1 expected payoff varying the cost of being *active* (uplink case).

3.2.2.4.

In Fig. 3.6 we show the PoA computed as the ratio between the social welfare obtained in scenario 3.2.2.6 (best case) and the social welfare in scenario 3.2.2.4. As we can notice, as c increases also the PoA increases. This means that increasing the cost c, the social welfare becomes more affected by non-cooperation in term of payoff.

In the same figure we show also what we have called the Maximum Diversity Gain, that is what a player gain due to the fact that there is another player in the system with which it can cooperate. We compute this quantity as the ratio between the social welfare in scenario 3.2.2.6 and the social welfare in scenario 3.2.2.5. As c increases, also the maximum diversity gain increases.

3.2.4 Conclusions

In this Section of the present thesis, we considered systems with multiple candidate strategic agents requiring or offering services (downlink or uplink case, respectively) that can decide to keep them active, and therefore available to require/offer the service, or inactive. We analyzed our systems under different cooperation and communication assumptions between the participiants and we applied game theory to evaluate the agents' behavior. Our main goal was to quantify the impact of the lack of cooperation and of communication among the agents in terms of system performance.

In general, the main result is that the a priori perfect knowledge of the system is not necessary. As a matter of fact, we found that additional partial information brings significant improvements in the system. In particular, considering a scenario in which it is allowed to the agents to share specific information about their types involves the same NE computation as the perfect knowledge case.

Considering a more dept reading of the numerical results, for the uplink case we found that staying inactive is not always advantageous, but it depends on the value of the cost of being active that the agent has to pay. On the other hand, for the downlink case it holds that the results related to the scenario in which the client is acting selfishly in terms of payoff are the same as the results obtained

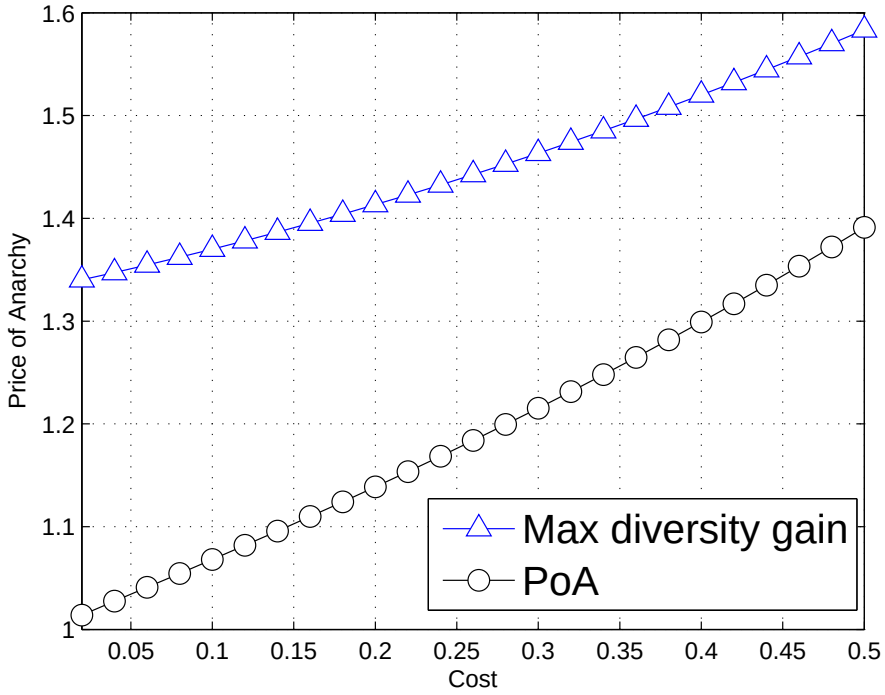

Figure 3.6: Price of anarchy and maximum diversity gain varying the cost of being *active* (uplink case).

considering a setup with complete and perfect knowledge. As a consequence, acting selfishly is not always a negative choice, but it depends on the environment considered for the evaluations.

As a possible extension of the present analysis, it might be considered a different value for the cost of the agents or a cost function that depends on some characteristic parameters of the system.

3.3 A zero-sum jamming game with incomplete position information in wireless scenarios

Jamming problems are a classic application of game theory to wireless networks. [2] The scenario where a legitimate transmitting network is contrasted by a malicious attacker acting on the purpose of disrupting communication can be faced in several contexts. For example, wireless ad hoc networking for military and civil purposes can be considered, where the jammer tries to disable the communication capabilities of the network [54]. The investigation can be extended to the physical layer, where the jammer is also able to corrupt the messages exchanged by the legitimate transmitters [55]. Also, cognitive spectrum access [56] can be investigated as another scenario of application, where the jammers can exploit vulnerabilities of reconfigurable cognitive radios.

From a modeling point of view, a jamming problem has a quite direct appeal in that, if properly formulated, it involves just two agents and, therefore, can be naturally framed as a two-player game between a legitimate network owner/user, from now on called the transmitter ($\mathbf{T}$), and the adversary that wants to cause disturbance or disruption in the communication, referred to as the jammer ($\mathbf{J}$). In this Section, we consider a simple setup where $\mathbf{T}$ can use multiple wireless channels for communicating and can select among them based on their quality, described, for example, through some capacity

[2] This section is taken from "A Zero-Sum Jamming Game with Incomplete Position Information in Wireless scenarios" published in IEEE European Wireless.

expressions that ultimately depend on the signal-to-interference-plus-noise ratio (SINR). Thus, in the case of fixed ambient noise, the data capacity of a channel only depends on the signal attenuation on it, and of course on the actions of **J**. On the other hand, we assume that **J** is only capable of brute-force attacks at the physical layer, aiming at raising the interference level on a given channel [57]. The interference that **J** can cause on a channel depends on the attenuation that its transmission gets on it.

For our evaluation, we adopt a standard formulation of the problem as a zero-sum game [55, 57], where **T** is the maximizer and **J** is the minimizer. The value of the game will simply be the sum capacity that **T** is able to achieve on the channels used for transmission. The final goal is to investigate the role of mutual positioning between **T** and **J**, since the attenuation can be related to the path loss experienced on the channel, which in the end is related to the distance. For the sake of simplicity, we consider a simple distance-based path loss model, but it is immediate to generalize the results to any situation where the channel quality is position-dependent.

We consider a Bayesian approach as done for jamming in [58] (and also in [59, 60] for other networking problems), where **T** has different types based on the positions of its nodes. This reflects the imperfect knowledge that **J** may have on the network structure. We aim to investigate the role of the position of **J**, and how this can impact on the resulting equilibrium. For this reason, **J** is not considered to be a player with type, this means that its position is known to all the players. Actually, with this assumption we evaluate whether the presence (or the knowledge thereof) of a jammer in a given position is a relevant element for the network and it changes its gameplay.

It turns out that, depending on the propagation scenario, there may be several situations where the effect of **J** is limited. One of these cases is when **J** is so far from the network that it cannot cause any damage; in this sense, our investigation includes physical layer security considerations [61], but it is not limited to them. In reality, the cause of **J**'s irrelevance is more game theoretic than physical. According to the structure of the game, if the resulting zero-sum formulation has a single NE in pure strategies for **J**, i.e., there is a single behavior that a rational jammer can adopt, its presence can be ignored. This is not because it does not cause any harm, but rather there is no effective countermeasure that can be taken against it.

One can also argue that such a jammer would not even be detected in the first place [57]. As a matter of fact, if **J**'s equilibrium move is to play along a certain pure strategy, **T** cannot tell whether **J** is really present in the network or there simply is a high interference level. Because of this ignorance, **T** has no margin of loss, and no margin for improvement either. On the other hand, there are positions of **J** where the resulting NE dictates that **J** plays a mixed strategy, meaning that **T** should counteract more than one possible jamming action. We label these positions as *critical*, and we identify them by looking at where the maximin of the game is different from the minimax and therefore, roughly put, there is something at stake for the communication network. As a general conclusion, we find that the choice of the proper countermeasures against jamming attacks should take into account the position of the jammers and possibly scan the interested area with different purposes, depending on whether a potential position of a jammer is critical or not.

The rest of this Section is organized as follows. In Sub-section 3.3.1 we describe the propagation scenario, with simplified fundamentals of wireless communications. In Sub-section 3.3.2 we give the game theoretic model for the problem, and in Sub-section 3.3.3 we compute the NEs. We present some numerical results in Sub-section 3.3.4. Finally, the concluding remarks can be found at the end of the next Section.

3.3.1 Wireless scenario

Radio waves propagate in different ways depending on the frequency used, and more in general on the physical scenario of communication [62]. However, the most important characteristic of interest in our analysis is that the perceived signal strength of a radio signal depends on the mutual positions

of transmitter and receiver. In many simplified models, the larger the distance, the weaker the signal. This is also the rationale that we adopt in the following analysis, which allows for a simple description by means of few parameters.

It is worthwhile noting, however, that radio propagation is much more complex than what will be discussed; it involves a thorough description of the frequency channel and the geometry of the area surrounding the transmitter and the receiver to account for factors such as: the presence or the absence of a direct path (line-of-sight) between the terminals; the effect of reflections, refractions, scattering, and related phenomena, from other objects present in the area; the characterization of the noise on said channel; the existence of other transmitters located close-by that can cause interference; and many other relevant issues. Also, these characteristics of the wireless channel are inherently time-varying [63]. Rapid fluctuations of the signal strength are possible, especially in mobile environments. Thus, the proper characterization of the wireless channel is that of a stochastic process and what we give in the following is to be meant as its statistical description derived from different realizations (which can be just samples at different time instants if the process is ergodic).

All these issues are outside the scope of the present work, where, for simplicity reasons, we consider a stationary channel with a straightforward distance-dependent attenuation through a power law, whose exponent is the only parameter that summarizes the scenario. More refined models are certainly possible but do not qualitatively change the conclusions that we draw later.

Thus, a signal transmitted with power P_T is received with a power attenuation $a(d_T)$ depending only on the distance d_T between the transmitter and the receiver, and therefore called the path loss at a distance d_T. We assume that $a(d_T)$ follows a power law with positive exponent α, usually $\alpha \in [2, 4]$, i.e.,

$$a(d_T) = K_0 \left(\frac{d_t}{d_0} \right)^{\alpha} \tag{3.42}$$

where d_0 is a reference distance (in particular, we can consider $d_0 = 1m$), so as to drop it from the equation) and K_0 is the attenuation at d_0. The received power will be $P_T/a(d_T)$.

We can assume a background noise with power spectral density N_0 to be present on the channel, whose bandwidth is equal to B. It is common to take the noise term as an additive white Gaussian noise (AWGN). The noise power will thus be N_0B. The meaning of this term can also be extended to include interference effects from other transmitters. Moreover, note that the background noise does not necessarily have to be white (and thus N_0 be a constant), nor Gaussian [64]; however, basic communication theory descriptions often regard the noise in terms of equivalent thermal noise characterizations, e.g., through noise temperature. Or alternatively, the term N_0B can be replaced with a more complicated expression where we compute the integral of the power spectral density over the channel band [62].

In short, we use N_0B to include both noise and also any unintentional interference. We can therefore compute the SINR at the receiver when the transmitter is at a distance d_T, denoted as $\Gamma(d_T)$, in the absence of jamming, as

$$\Gamma(d_T) = \frac{P_T}{a(d_T)N_0B}. \tag{3.43}$$

Instead, if a jammer is present on the same channel, located at a distance d_J from the receiver and using a jamming power P_J, we must consider it when computing the SINR; therefore we denote it as $\Gamma(d_T, d_J)$, and put it equal to

$$\Gamma(d_T, d_J) = \frac{P_T}{a(d_T)[N_0B + P_J/a(d_J)]}. \tag{3.44}$$

We can use 3.42 to model the attenuation of both the transmitter and the jammer. However, to take into account that the propagation models of the two may be different, we consider two different

parameters in the equation, i.e., we denote with α (as before) the path loss exponent of the transmitter, and, conversely, we use β for the jammer (for simplicity, we use the same K_0, though). From 3.44, we obtain

$$\Gamma(d_T, d_J) = \frac{P_T}{d_T^{\alpha}[K_0 N_0 B + P_J / d_J^{\beta}]}. \tag{3.45}$$

If noise, bandwidth, and transmission powers (both the useful and the jamming terms) are constants, the impact of the distance can be summarized as

$$\Gamma(d_T, d_J) = \frac{1}{d_T^{\alpha}(K_1 + K_2 d_J^{-\beta})}, \tag{3.46}$$

with K_1 and K_2 being suitable constants. An infinitely far jammer has no effect on the SINR, as $\Gamma(d_T) = \Gamma(d_T, \infty)$.

A suitable performance metric that may describe what a transmitter would like to maximize (and a jammer to minimize) is the channel capacity C. For example, we can use the formula of the Shannon capacity for an AWGN channel, which results in defining C as

$$C = B log_2[1 + \Gamma(d_T, d_J)], \tag{3.47}$$

which depends on the SINR (and, thus, also on the presence of a jammer).

If the transmitter operates over F multiple channels spanned by index $i = 1, 2, ..., F$, and each of them has bandwidth B_i, we take ξ_i to represent an indicator function that equals 1 whether the jammer is disturbing with power P_J the transmission on the ith channel, and 0 otherwise. The sum capacity available in the system in the presence of a jammer is therefore

$$C_{tot} = \sum_{i=1}^{F} \{\chi_i B_i log_2[1 + \Gamma(d_T, d_J)] + (1 - \chi_i) B_i log_2[1 + \Gamma(d_T)]\}. \tag{3.48}$$

Remarkably, the Shannon capacity is a good choice in terms of utility in the micro-economic sense [65], since it is a concave function of the SINR. In the following Sub-section, we will use it to characterize the payoff received by **T** in a zero-sum game.

3.3.2 Game theoretic model

We consider a wireless network with 2 transmitters, denoted as T_1 and T_2, sending data to a receiver (sink node), whose distances from the receiver are d_1 and d_2, respectively. The available spectrum is divided into 2 channels (c_1 and c_2) of equal bandwidth B. For the sake of simplicity, all propagation aspects of the channels will be represented through the path loss exponent of 3.42. In particular, we assume that c_1 and c_1 are characterized by parameters α_1 and α_2, respectively, when the useful transmitters operate on them. The entire network is represented by the single player **T** in the game, which thus comprehends T_1, T_2, and the receiver, as they are assumed to act towards the same goal, i.e., maximizing the total network capacity. To coordinate multiple access of T_1 and T_2, the network adopts a frequency division multiple access (FDMA) scheme, i.e., either of the channels c_1 and c_2 is assigned to T_1 and the other to T_2, without overlap. Nodes T_1 and T_2 use the same transmission power P_T.

However, the network activity is menaced by a malicious jammer **J** whose aim is to minimize the overall capacity of the network. The jammer is placed at distance d_J from the receiver, and can operate over only either c_1 or c_2, with a fixed power P_J, as per 3.44. Also, the path loss exponent perceived by **J** on channels c_1 and c_2 is equal to β_1 and β_2, respectively.

Our goal is to model the interaction between **T** and **J** as a zero-sum game with incomplete information. Thus, we consider a finite set $\mathcal{D}$ that has cardinality D and contains pairs of distances, i.e.,

$\mathcal{D} = ((d_1^{(1)}, d_2^{(1)}), ..., (d_1^{(D)}, d_2^{(D)}))$, where $d_i^{(k)}$ is the ith transmitter's distance in the kth pair. Each of the elements of $\mathcal{D}$ is considered to be a *type* of player **T**, denoted as $\Theta_k = (d_1^{(k)}, d_2^{(k)})$. **T** can be of type Θ_k with probability p_k, where the terms p_k are values between 0 and 1 for which $\sum_k p_k = 1$. For example, if a finite set of distances $\mathcal{Z} = \{z_j\}_{j=1,....,L}$ is available for both transmitters, and the transmitters can even have the same distance, then $\mathcal{D} = \mathcal{Z} \times \mathcal{Z}$ and $D = L^2$. For the analysis, we consider that d_J can only have one value (a possible extension of the present investigation is to allow also uncertainty for d_J). The distance d_J is known by both players. Conversely, type Θ_k is only known to player **T**, but the probability distribution $\mathbf{p} = (p_1, p_2..., p_D)$ is common knowledge in the game. This characterization with types follows that of Bayesian games.

Once the type Θ_k of **T** is given by a virtual player called $Nature$, **T** can perform either of these two actions: (A_1) assign c_1 to T_1 (and, consequently, c_2 to T_2); (A_2) the exact opposite, i.e., assign c_2 to T_1. Since the channels are fully described by the propagation parameter α_i, if A_1 is chosen, then the index i of α_i is the same of T_i; for A_2, they do not match. Hence, **T** has $N = 2^D$ pure strategies, since a strategy is defined as a D-tuple of actions, one per each type that **T** can be, and each action has two alternatives to choose from. We write the ith pure strategy of **T** as X_i, then the kth element of the associated D-tuple, referred to as $X_i(k)$, defines whether **T** plays action A_1 or A_2 when its type is Θ_k. **J** can instead perform either of the two actions: (Y_1) attack channel c_1 with attenuation parameter β_1, or (Y_2) attack c_2 with attenuation parameter β_2. Therefore, **J** has just two pure strategies, coinciding with its actions Y_1 and Y_2.

We denote the sets of all possible pure strategies of the players as $\mathcal{X} = \{X_i\}_{i=1,...,N}$ and $\mathcal{Y} = \{Y_1, Y_2\}$. We define a mixed strategy ξ for **T** as an N-tuple $(\xi_1, ..., \xi_N)$ that belongs to the space of probability distributions over $\mathcal{X}$, $\Delta\mathcal{X}$, i.e., $\xi_i \geq 0$ for all $i = 1, .., N$ and $\sum_{i=1,..,N} \xi_i = 1$. So, ξ_i denotes the probability that **T** plays X_i. Similarly, a mixed strategy η for **J** belongs to $\Delta\mathcal{Y}$ and is the pair of probabilities η_1 and $\eta_2 = 1 - \eta_1$ that **J** plays Y_1 and Y_2, respectively.

Given the prior probabilities $\mathbf{p} = (p_1, ..., p_D)$ for the type of **T**, we can put this Bayesian game in normal form using a $N \times 2$ matrix $\mathbf{M} = \{m_{ij}\}$, where entry m_{ij} with $i = 1, ..., N$ and $j = 1, 2$, represents the expected payoff for **T** when players **T** and **J** play their ith and jth pure strategy, respectively, computed as

$$m_{ij} = \sum_{k=1}^{D} p_k C_{tot}(X_i(k), Y_j) \tag{3.49}$$

where $C_{tot}(X_i(k), Y_j)$ is the sum capacity of the network according to Eq. 3.48 when **T** is of type Θ_k, and thus performs action $X_i(k)$ with probability p_k, while **J** chooses action Y_j.

Also note that since the game is zero-sum, we do not need to represent **J**'s payoff, which will be $-m_{ij}$. Finally, the expected payoff of a joint mixed strategy (ξ, η) can be computed by averaging the entries of **M** with weights equal to the probabilities of ξ and η.

3.3.3 Bayesian Nash Equilibria computation

The Bayesian Nash Equilibria (BNEs) of the zero-sum game, given the prior distribution **p** for the type of **T** and the resulting payoff matrix **M**, can be found via von Neumann's Minimax Theorem [66]. Since the game is a classic zero-sum game, it can be found to have at least one NE in mixed strategies, and actually all NEs yield the same payoffs. The mixed strategies played at NE will be *maximinimizer* strategies for both players, i.e., they assure to the players the highest payoff they can get in the worst-case scenario of the strategy played by the opponent.

We denote one of these equivalent NEs as (ξ^*, η^*), where ξ^* is the mixed strategy played by **T** and η^* is that played by **J**. There will be a unique quantity v, called the *value* of the game, such that each

NE yields a payoff equal to v to **T** (and correspondingly a payoff equal to -v to **J**), for which

$$v = \max_{\Delta\mathcal{X}} \min_{1\le j\le 2} \sum_{i=1}^{N} \xi_i^* m_{ij} = \min_{\Delta\mathcal{Y}} \max_{1\le i\le N} (m_{i1}\eta_1^* + m_{i2}\eta_2^*). \tag{3.50}$$

To solve numerically, we search for ω_1 and ω_2, with

$$\omega_1 = \min_{1\le j\le 2} \sum_{i=1}^{N} \xi_i^* m_{ij} \tag{3.51}$$

$$\omega_2 = \max_{1\le i\le N} (m_{i1}\eta_1^* + m_{i2}\eta_2^*), \tag{3.52}$$

so that ω_1 is maximized and ω_2 is minimized. The Minimax Theorem guarantees that the pair (ξ^*, η^*) is a NE and the value is given by $\omega_1 = \omega_2$. To solve the maximization of 3.51 and the minimization of 3.52, we reduce them to two linear programs with proper slack variables for ω_1 and ω_2. Thus, the problems become

$$\begin{aligned} \max \quad & \omega_1 \\ & s.t. \quad \omega_1 \le \sum_{i=1}^{N} \xi_i m_{i1}, \quad \omega_1 \le \sum_{i=1}^{N} \xi_i m_{i2} \\ & \qquad \xi_i \ge 0 \quad \forall i = 1, ..., N, \quad \sum_{i=1}^{N} \xi_i = 1 \end{aligned} \tag{3.53}$$

and, analogously,

$$\begin{aligned} \min \quad & \omega_2 \\ & s.t. \quad \omega_2 \ge \eta_1 m_{11} + \eta_2 m_{12} \\ & \qquad . \\ & \qquad . \\ & \qquad . \\ & \qquad \omega_2 \ge \eta_1 m_{N1} + \eta_2 m_{N2} \\ & \qquad \eta_1 \ge 0, \quad \eta_2 \ge 0, \quad \eta_1 + \eta_2 = 1. \end{aligned} \tag{3.54}$$

Both problems can be solved by means of optimization techniques; we used Dantzig's simplex algorithm [67]. We evaluate and compare the solution for different choices of the set $\mathcal{D}$, the prior p, the distance of the jammer d_J, and the propagation coefficients α_i and β_i.

We also compute the *maximin* and the *minimax* in pure strategies, which can be done by considering the same problems as above but imposing ξ and η to have all the elements equal to 0 but one, which is equal to 1. In this case, ω_1 gives the *maximin* and ω_2 the *minimax*. As a matter of fact, these values can be immediately found by scanning the matrix **M** and taking minima and maxima over rows and columns.

3.3.4 Numerical results

We evaluate a scenario where the propagation parameters α_1, α_2, β_1, and β_2 take different values in the range $2 \div 3$. We take N_0B, which represents the noise power plus the external unintentional interference, as equal to -120 dBm. We set the transmission power terms of the transmitter and the jammer to be the same, i.e., $P_T = P_J = 0$ dBm.

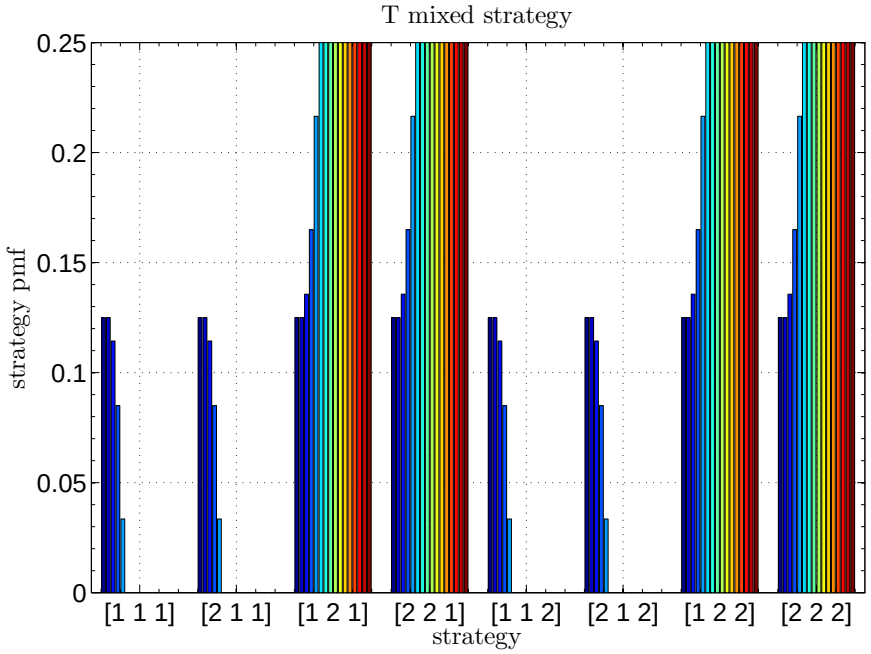

Figure 3.7: NE strategy of T as a function of $d_J \in [0.01, 15]$ m (α_1=α_2=β_1=2, β_2=2.5, prior distribution for T's type: [1/3 1/3 1/3]).

We set 3 types for **T** in $\mathcal{D} = \{(5,5),(5,10),(10,10)\}$ m. As a consequence, each of the 8 pure strategies of **T** is a triple of binary values (for brevity, we just write 1 or 2 instead of A_1 or A_2). For example, strategy [1 2 1] denotes that **T** assigns c_1 (i.e., the channel with attenuation parameter α_1) to transmitter T_1 when it is of type 1 or 3, while it assigns c_2 (i.e., the one with attenuation parameter α_2) to T_1 if it is of type 2; in other words, this strategy means that channel c_1 is assigned to T_1 when the transmitters are at the same distance, and to T_2 if T_1 is closer to the sink. Finally, we place the jammer at a distance d_J ranging from 0.01 to 15 m.

In this scenario, we evaluate the NE of the game, and its dependence on d_J. First, we considered the case of a uniform distribution for the types of **T**, i.e. $p_k = \frac{1}{3}$, $k = 1,2,3$, with attenuation parameters $\alpha_1 = \alpha_2 = 2$ for **T**, and $\beta_1 = 2$, $\beta_2 = 2.5$ for **J**. Figs. 3.7, 3.8, and 3.9 refer to this setting.

Figs. 3.7 and 3.8 show **T**'s mixed strategy and **J**'s mixed strategy, respectively, depending on d_J. In particular, Figs. 3.8 reveals that there are values of d_J for which the strategy of **J** at equilibrium is pure. For these cases, the corresponding strategy of **T** is a mixed strategy with probability 1/4 split over a support represented by all pure strategies $[\cdot\ 2\ \cdot]$, i.e., those for which action number 2 is played by **T** when its type is Θ_2. In other words, **T** surely plays A_2 when the nodes T_1 and T_2 are placed at different distances, otherwise it randomly chooses between its alternatives; indeed, when the strategy of **J** is pure, and the nodes are placed at identical distances, **T** is indifferent on which channel to assign to the nodes.

This result is also visible from figures such as Fig. 3.9, in which we plot the NE payoff for **T** (quantified as the capacity per unit of bandwidth: this is also what displayed in all similar plots afterwards), together with the *maximin* and *minimax* payoff in pure strategies. In the very region where **J**'s equilibrium move is a pure strategy, the three curves coincide. In these cases, the transmitter strategy can be regarded as *insensitive* to the presence of a jammer. From Fig. 3.9, the game has some degree of uncertainty in its outcome only when d_J is less than 4.484 m, which means that the jammer has an unpredictable behavior more or less only when closer to the receiver than the closest position available to the transmitters.

Fig. 3.10 shows the comparison between NE's payoff, *maximin*'s payoff and *minimax*'s payoff for a configuration slightly different from the previous one. We considered the same a priori probability

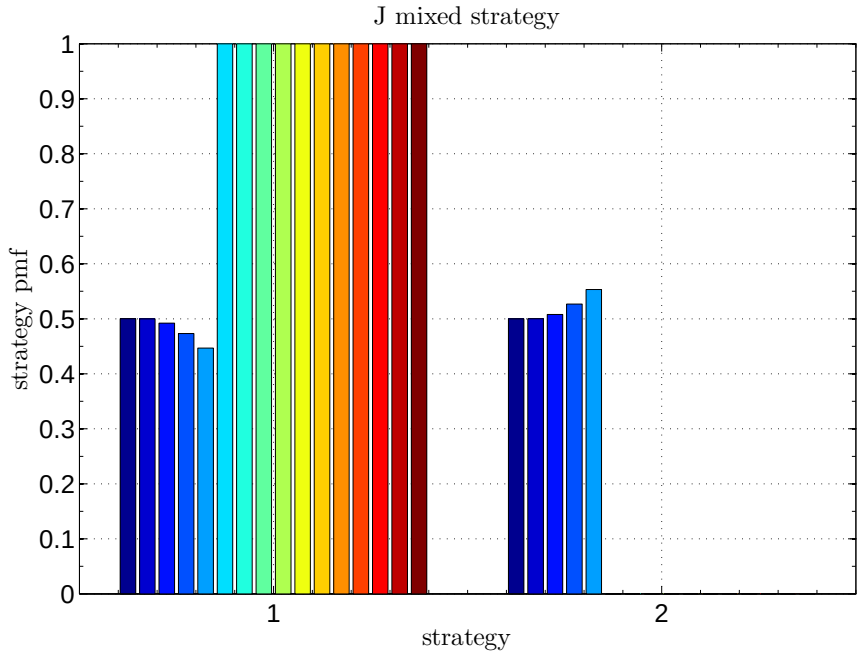

Figure 3.8: NE strategy of J as a function of $d_J \in [0.01, 15]$ m (α_1=α_2=β_1=2, β_2=2.5, prior distribution for T's type: [1/3 1/3 1/3]).

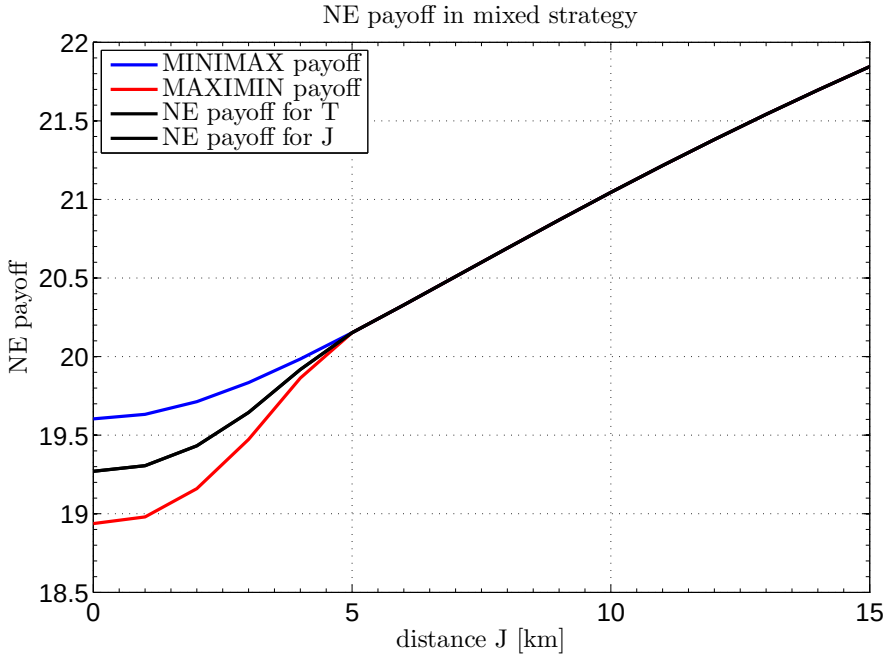

Figure 3.9: NE payoff in mixed strategies as a function of $d_J \in [0.01, 15]$ m (α_1=α_2=β_1=2, β_2=2.5, prior distribution for T's type: [1/3 1/3 1/3]).

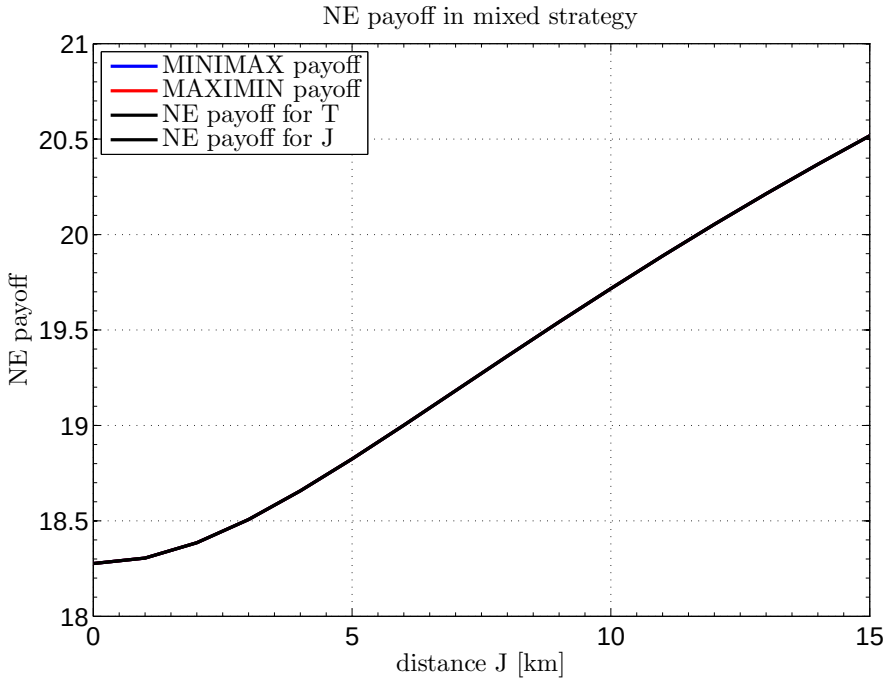

Figure 3.10: NE payoff in mixed strategies as a function of $d_J \in [0.01, 15]$ m (α_1=β_1=β_2=2, α_2=2.5, prior distribution for T's type: [1/3 1/3 1/3]).

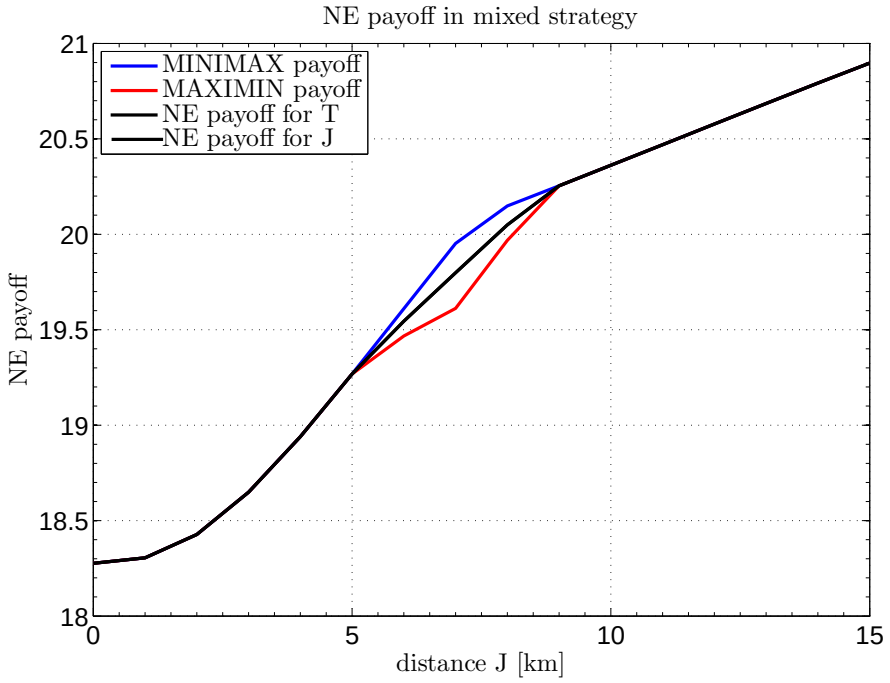

Figure 3.11: NE payoff in mixed strategy as a function of $d_J \in [0.01, 15]$ m (α_1=β_2=2, α_2=β_1=2.5, prior distribution for T's type: [1/3 1/3 1/3]).

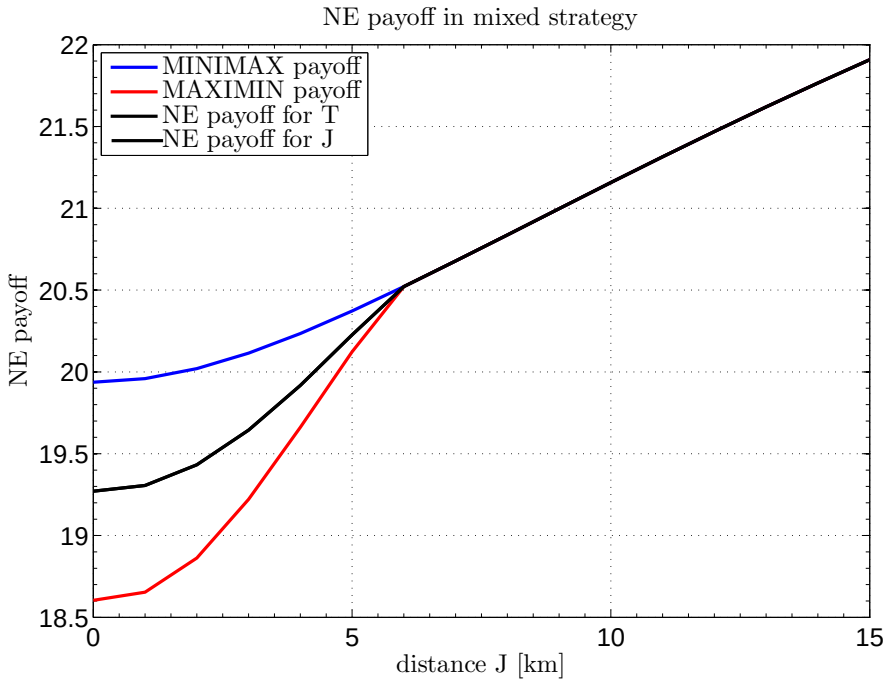

Figure 3.12: NE payoff in mixed strategy as a function of $d_J \in [0.01, 15]$ m (α_1=α_2=β_1=2, β_2=2.5, prior distribution for T's type: [1/6 2/3 1/6]).

but we set $\alpha_1 = \beta_1 = \beta_2 = 2$ and $\alpha_2 = 2.5$. In this case, the NE always imply a pure strategy for the jammer, regardless of the distance of **J** from the destination, since the *maximin* and *minimax*, and also the NE payoff, coincide for every d_J, and thus **T**'s strategy is always insensitive to **J**'s presence. This result is also correct since, in the presence of an unbalanced situation for the transmitter but not for the jammer (a channel has lower α_i and therefore has better quality, while the two β_i are identical), intuitively the jammer should always cause disturbance on the better channel.

Fig. 3.11 shows the comparison between NE's payoff, *maximin*'s payoff and *minimax*'s payoff for $\alpha_1 = \beta_2 = 2$ and $\alpha_2 = \beta_1 = 2.5$. In this case, the NE strategy of the jammer does not degenerate into a pure strategy for a whole region of intermediate distances, 5.298 m $< d_J <$ 8.730 m, which is more or less comprised between the available positions for the two transmitters.

Figs. 3.12, 3.13, and 3.14 show the results obtained considering the same values for the parameters used in Figs. 3.9, 3.10, and 3.11, respectively, for a non-uniform distribution of **T** types, where $p_2 = 2/3$, and $p_1 = p_3 = 1/6$. This leads to an expansion of the critical regions in which the jammer plays a mixed strategy. In particular, in Fig. 3.12 the border of the critical region is pushed to 5.830 m, i.e., beyond the smallest value in $\mathcal{D}$, i.e., 5 m, and a similar and even more relevant enlargement of the region happens in Fig. 3.14, where **J** plays a mixed strategy in the entire interval $0 < d_j <$ 10.012 m. Also, in Fig. 3.13, differently from the similarly shaped Fig. 3.10, the equilibrium strategy of the jammer is not a pure strategy for a very wide range of positions, namely, for $d_J <$ 11.740 m, even though the differences are minor.

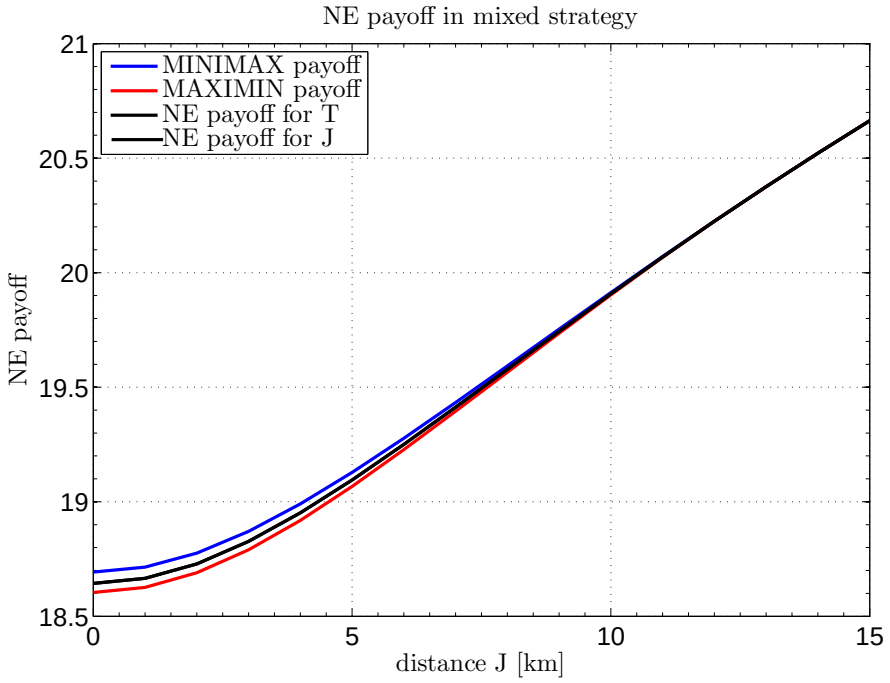

Figure 3.13: NE payoff in mixed strategy as a function of $d_J \in [0.01, 15]$ m (α_1=β_1=β_2=2, α_2=2.5, prior distribution for T's type: [1/6 2/3 1/6]).

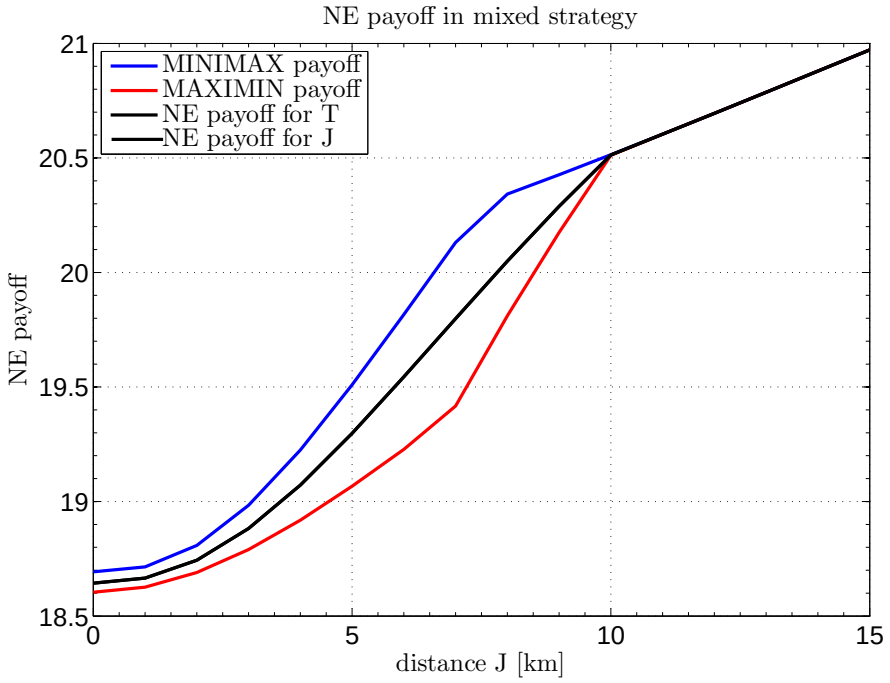

Figure 3.14: NE payoff in mixed strategy as a function of $d_J \in [0.01, 15]$ m (α_1=β_2=2, α_2=β_1=2.5, a priori probability [1/6 2/3 1/6]).

3.4 Jamming in underwater sensor network as a Bayesian zero-sum game with position uncertainty

We further apply the analysis just discussed to an underwater scenario.[3] Underwater acoustic sensor networks (UASNs) can be employed in a wide array of applications, from monitoring and prevention of seismic events, such as tsunamis and/or earthquakes, to equipment control and surveillance for autonomous systems operating undersea [68]. As any other kind of communication systems, they may be subject to malicious attacks. One of these is jamming. Since most of the practical solutions for counteracting jammers are designed with terrestrial radio networks in mind, they may be unsuitable for UASNs, which can therefore be extremely vulnerable to such attacks [69]. Also in considering this scenario, we tackle the investigation according to a game theoretic point of view. We consider a scenario, similar to [58], where the jammer creates noise-like interference with the aim of producing denial-of-service attacks. Indeed, underwater sensors do not usually possess sophisticated signal processing capabilities and, consequently, it is reasonable to assume that jamming attacks just consist of raising the noise level. In this setup as well as in the previus Section, the sensor nodes are able to use several communication channels and the resulting utility of the network is determined by its total transmission capacity. The jammer is only able to produce noise-like interference on a channel at a time and the interference that it causes depends on the attenuation perceived on it.

In the following, the sensors play together as the maximizer of the sum capacity that the network can reach on the channels involved in the transmission, and the jammer is the corresponding minimizer, and, in general, the analysis proceeds at most at the same way as discussed for the Wireless Sensor Networks (WSNs) case.

In more details, the rest of this Section is organized as follows. In Sub-section 3.4.1 we describe the propagation scenario, with simplified fundamentals of underwater wireless communications. We present some numerical results in Sub-section 3.4.2. Finally, we draw the general conclusions considering also the WSNs analysis in Sub-section 3.4.3.

3.4.1 Underwater scenario

Research on UASNs is somehow more limited compared to terrestrial sensor networks based on radio communications. These two kinds of networks share similarities for what concerns their many potential applications and their distributed nature; the main difference relates to the specific physical layer utilized, which relies on acoustic and radio waves, respectively, since it is generally accepted that radio signals do not propagate well underwater [73].

While the wireless medium is fairly understood in the literature, the acoustic channel for underwater communications is more difficult to characterize and utilize. Also, the standard uses of acoustic communications mostly involve echolocation (with applications such as the sonar and the fathometer), which, from a networking standpoint, have little interest as it only involves a single transmitter-receiver pair. The study of acoustic communications in a network context is more constrained, also because, still differently from terrestrial networks, equipment may be much more expensive.

Still, it may be expected that in specific environments and fields of application, submarine networking can find suitable exploitation. Moreover, due to the inherent difficulty of coordinating multiple nodes underwater, game theory investigations can be useful to devise distributed solutions. The major features and challenges that need to be faced in underwater environments include, but are not limited to, the following issues [74]. First of all, underwater channels have a small bandwidth compared to their terrestrial counterparts, resulting in lower bit rates. Also, the speed of acoustic waves in water is five orders of magnitudes lower than that of electro-magnetic waves in air (about $1.5 \cdot 10^3$ m/s versus

[3] This section is taken from "Jamming in Underwater Sensor Networks as a Bayesian Zero-Sum Game with Position Uncertainty" published in IEEE GLOBECOM.

$3 \cdot 10^8$ m/s, respectively); this results in a huge propagation delay in underwater channels. Thus, it is hinted in [65] that FDMA may be more attractive than its time division analog. However, underwater channels have much lower carrier frequencies than radio (kilohertz versus gigahertz), thus they cannot be considered as narrowband and frequency-selectivity must be accounted for even in a simple analysis. Actually, the use of cognitive and opportunistic access techniques can be a solution to adapt communication to the varying conditions at different times, distances, and channels.

All of these elements will be taken into account in our analysis. Other aspects that are not explicitly considered, but are worth mentioning, regard the higher unreliability of underwater networks, even in controlled scenarios: radio networks can be unreliable too, but to a lower extent and/or only if adverse conditions are assumed. Underwater links may lose connectivity due to propagation phenomena under the sea surface, or because of node mobility due to oceanic currents. Finally, underwater sensor nodes have severe energy constraints, since battery replacement or energy harvesting, e.g., through solar panels, may be extremely difficult or unavailable.

For these reasons, jamming attacks may be extremely harmful in underwater environments, and mechanisms to detect and prevent them are important. The huge propagation delay might forbid the sensor nodes from communicating with external controllers; as a consequence, an underwater network has to exploit its own resources to detect and mitigate the jamming attack [69].

The acoustic power attenuation of underwater channels is strongly dependent on the communication distance and on the signal frequency. An absorption loss is present, due to the conversion of acoustic pressure into heat, which increases with the signal frequency f as well as with the communication distance d. As a consequence, shorter communication links offer higher data rates. Attenuation $A(d, f)$ can be expressed in dB using Urick's model as [76]

$$10 \log_{10} A(d, f) = A_0 + k \log_{10} d + d 10 \log_{10} a(f) \tag{3.55}$$

where k is a spreading factor term, $a(f)$ is an absorpion coefficient, and A_0 is a normalization constant (the value for $A(d, f)$ at 1 m and very low frequencies). Formula 3.55 shares structural similarities with path loss expressions commonly used for the wireless case [77]. There are some relevant differences, though. First of all, since water is a much more dispersive medium for acoustic waves than what air is for electro-magnetic beams, there is a further dependence of distance: beyond the geometrical spreading, i.e., the first summand, d also appears in the second one, the absorption term. Also, the spreading factor k, describing the geometry of propagation, has lower values than what usually considered in radio environments [77]. Spherical spreading, that would lead to $k = 20$, is taken to be a best-case value in radio propagation, where the presence of obstacles lead to much higher values. Instead, for underwater acoustic propagation, shallow water scenarios may even have a more favorable spreading than spherical, since physical waveguide effects may produce a cylindrical spreading [78], and therefore $10 \leq k \leq 20$.

Absorption is expressed using Thorp's formula, giving $a(f)$ as a function of frequency f as [79]

$$10 \log_{10} a(f) = a_W f^2 + \alpha_1 \frac{f^2}{f_1^2 + f^2} + \alpha_2 \frac{f^2}{f_2^2 + f^2} + ... \tag{3.56}$$

where a_W is a pressure-dependent coefficient describing absorption in pure water, while the α_js, with $j = 1, 2, ...$ weigh further terms due to saline absorptions, and the terms f_j are the relaxation frequencies for these terms. For sea water, two such terms are usually included, $j = 1$ is for boric acid, especially relevant at low frequencies, and $j = 2$ for magnesium sulphate.

The oceanic noise can be modeled as the sum of several components, including turbulence, shipping, surface motion, and thermal noises [80]. Thus, we consider a power spectral density (PSD) of the noise $N(f) = N_t(f) + N_s(f) + N_w(f) + N_{th}(f)$, where $N_t(f)$, $N_s(f)$, $N_w(f)$, and $N_{th}(f)$ are noise terms corresponding to turbulence, shipping, surface motion, and thermal noise, respectively.

These components can be expressed in dB re μPa per Hz as a function of the frequency f in kHz as [75]

$$10\log_{10} N_t(f) = 17 - 30\log_{10} f \tag{3.57}$$

$$10\log_{10} N_s(f) = 40 + 20(s - 0.5) + 26\log_{10} f - 60\log_{10}(f + 0.3) \tag{3.58}$$

$$10\log_{10} N_W(f) = 50 + 7.5\omega^{\frac{1}{2}} + 20\log_{10} f - 40\log_{10}(f + 0.4) \tag{3.59}$$

$$10\log_{10} N_{th}(f) = -15 + 20\log_{10} f. \tag{3.60}$$

The parameters in 3.57-3.60 are the shipping activity s, ranging from 0 for lowest activity to 1 for most intense shipping and ω, i.e., the wind speed value in m/s, since surface motion noise is caused by wind-driven waves. In our numerical setup, we considered practical spreading with $k = 15$, $A_0 = 0$ dB, intermediate shipping activity $s = 0.5$ and no wind ($\omega = 0$), and a frequency range between 10 and 40 kHz. At these frequencies, absorption due to pure water and boric acid are negligible, while we consider the absorption associated to magnesium sulphate, with parameters $f_2 = 66$ kHz and $\alpha_2 = 48$ dB/km [81].

If a communication channel operates on a frequency band $\mathbf{B}_i$ with bandwidth $B_i = |\mathbf{B}_i|$, using a flat power profile, then the average SNR for a tone at frequency f can be expressed as [75]

$$SNR(d, f) = \frac{P_S}{A(d, f)N(f)B_i} \tag{3.61}$$

where P_S is the power of the transmitting sensor node, $A(d, f)$ is the attenuation PSD and $N(f)$ is the noise PSD. As it can be noticed, the expression of the SNR is the same as the previous Section, however the formulations of attenuation and backgroung noise are quite different because of the different communication channel considered. In particular, $A(d, f)$ increases with f while $N(f)$ decreases with f (at least in the relevant interval for acoustic communications). As a result, $[A(d, f)N(f)]^{-1}$ has a maximum for some frequency. Fig. 3.15 shows the frequency-dependent part of the SNR for a tone transmitted underwater with $d = \{1, 5\}$ km with the aforementioned choice of parameters.

For the transmission over $\mathbf{B}_i$, Shannon's capacity C_i is

$$C_i = \int_{\mathbf{B}_i} \log_2[1 + SNR(d, f)df]. \tag{3.62}$$

However, if a malicious node also causes noise-like interference on a specific channel, this as to be taken into account in the capacity's computation; consequently, we replace the SNR with the average SNJR which is

$$SNJR(d, f) = \frac{P_S}{A(d, f)[N(f)B_i + P_J A(d_J, f)^{-1}]} \tag{3.63}$$

where P_J is the power of the malicious node and d_J is its distance from the receiver. The channel capacity in the presence of a jammer becomes

$$C_i' = \int_{\mathbf{B}_i} \log_2[1 + SNJR(d, f)df]. \tag{3.64}$$

In the next Sub-section we will directly discuss the numerical results obtained considering different values of the parameters describing the setup under investigation. This is due to the fact that the game theoretic model and the BNEs computation are exactly the same as those described for the WSN case. Indeed, in this scenario the relevant aspect is that we change the nature of the communications channel, however the overall mathematical formulation is still the same.

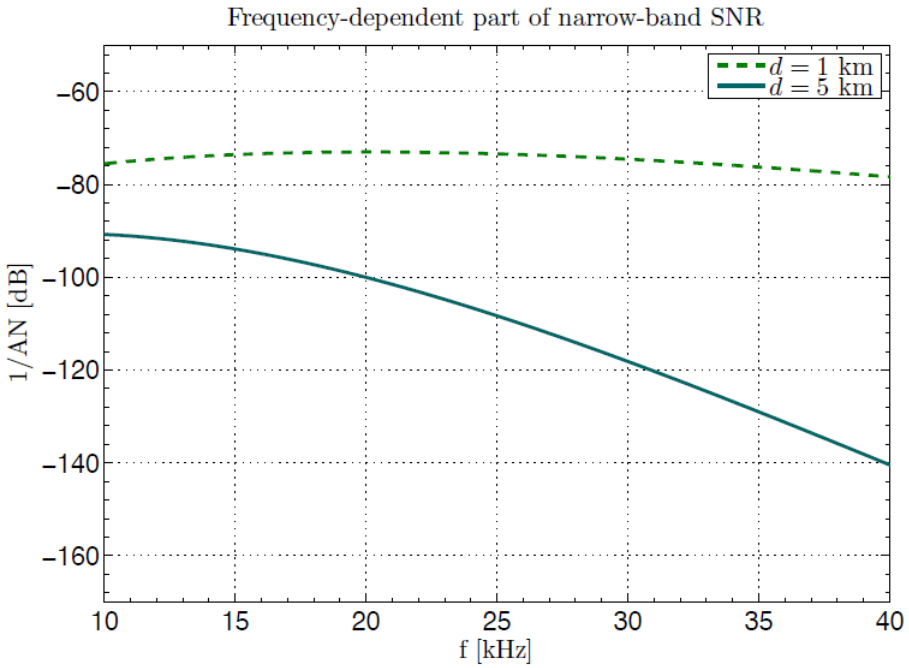

Figure 3.15: Frequency-dependent part of the SNR $[A(d,f)N(f)]^{-1}$ for a tone transmitted underwater with $d = 1,5$ km ($s = 0.5$, $w = 0$ m/s).

3.4.2 Numerical results

We consider a scenario with two sensors (T_1 and T_2), a receiver (included in **T** at the same way as previously discussed for the WSN scenario), and a jammer **J**. Given the matrix **M**, whose entry m_{ij} represents the expected payoff for **T** when player **T** is playing its ith pure strategy and player **J** is playing its jth pure strategy, to compute BNEs we use first von Neumann's Minimax Theorem and, then, we solve

$$\begin{aligned} \max \quad & \omega_1 \\ s.t. \quad & \omega_1 \leq \sum_{i=1}^{N} \xi_i m_{i1}, \quad \omega_1 \leq \sum_{i=1}^{N} \xi_i m_{i2} \\ & \xi_i \geq 0 \quad \forall i = 1, ..., N, \quad \sum_{i=1}^{N} \xi_i = 1 \end{aligned} \tag{3.65}$$

and

$$\begin{aligned} \min \quad & \omega_2 \\ s.t. \quad & \omega_2 \geq \eta_1 m_{11} + \eta_2 m_{12} \\ & . \\ & . \\ & . \\ & \omega_2 \geq \eta_1 m_{N1} + \eta_2 m_{N2} \\ & \eta_1 \geq 0, \quad \eta_2 \geq 0, \quad \eta_1 + \eta_2 = 1. \end{aligned} \tag{3.66}$$

by means of Dantzig's simplex algorithm, where ξ_i is the mixed strategy played by **T** and η_i is that played by **J**.

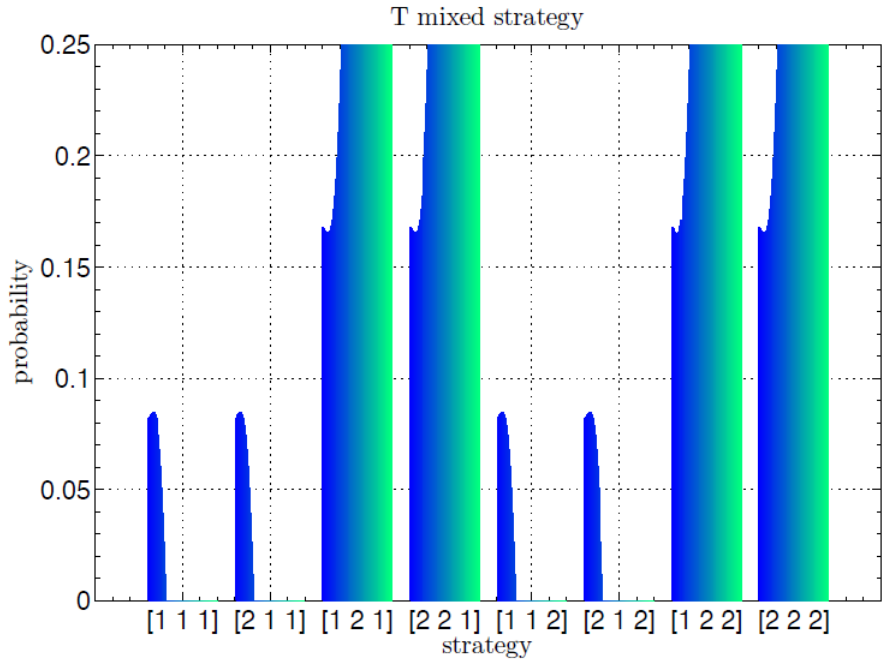

Figure 3.16: T mixed strategy as a function of $d_J \in [0.01, 6]$ km (prior distribution for T's type: [1/3 1/3 1/3]).

We assume that the transmission powers are constant $P_T = P_J = 95$ dB re μPa. We solve the game for d_J ranging from 0.01 to 6 km. We assume that T_1 and T_2 share a common spectrum at $[10, 40]$ kHz, divided into 2 channels (c_1 and c_2) of 15 kHz ($\mathbf{B}_1 = [10, 25]$ kHz and $\mathbf{B}_2 = [25, 40]$ kHz are the frequencies range considered for c_1 and c_2, respectively). Noise and attenuation over these channels can be determined as previously discussed obtaining

$$N_1 = \int_{\mathbf{B}_1} N(f)df = 37.44 dBre\mu Pa, \tag{3.67}$$

$$N_2 = \int_{\mathbf{B}_2} N(f)df = 32.87 dBre\mu Pa. \tag{3.68}$$

It can be noticed by looking at Fig. 3.15 that, although channel c_1 has a slightly higher noise, it is the better channel for a sensor that is far away.

The possible positions for the sensors are at 1 and 5 km. We could consider all pairs (4 alternatives) to be included in $\mathcal{D}$, but since two of them, i.e., $(1, 5)$km and $(5, 1)$km, give the same results, we consider just $\mathcal{D} = \{(1, 1), (1, 5), (5, 5)\}$ km. Consequently, $\mathbf{T}$ has 3 types and each of the $2^3 = 8$ pure strategies of $\mathbf{T}$ is a triple. For the sake of clarity, as seen for the wireless network case, [1 1 2] means that T assigns c_1 to T_1 if it is of type 1 or 2, while it assigns c_2 to T_1 if it is of type 3.

Given this setting, we plot the BNE of the game as a function of d_J. Figs. 3.16 and 3.17 report the BNE strategies of the players. We consider the case of a uniform prior distribution for $\mathbf{T}$'s type, i.e., $\mathbf{p} = [1/3\ 1/3\ 1/3]$. Fig. 3.16 shows that there exists a critical distance d_c for $\mathbf{J}$ such that all BNE strategies of $\mathbf{T}$ are equiprobable combinations over a support given by all pure strategies in the form $[\cdot, 2, \cdot]$. That means that $\mathbf{T}$ always plays A_2 (i.e., assigning c_1 to T_1) if its type is $(1, 5)$, which, in turn, means that it assigns the closer node to the worse channel (anticipating $\mathbf{J}$ will not jam it), and, furthermore, it blindly selects its move if it is of types $(1, 1)$ or $(5, 5)$, due to the fact that it is indifferent on its alternatives if the distances of the nodes are equal. Fig. 3.17 shows the same results

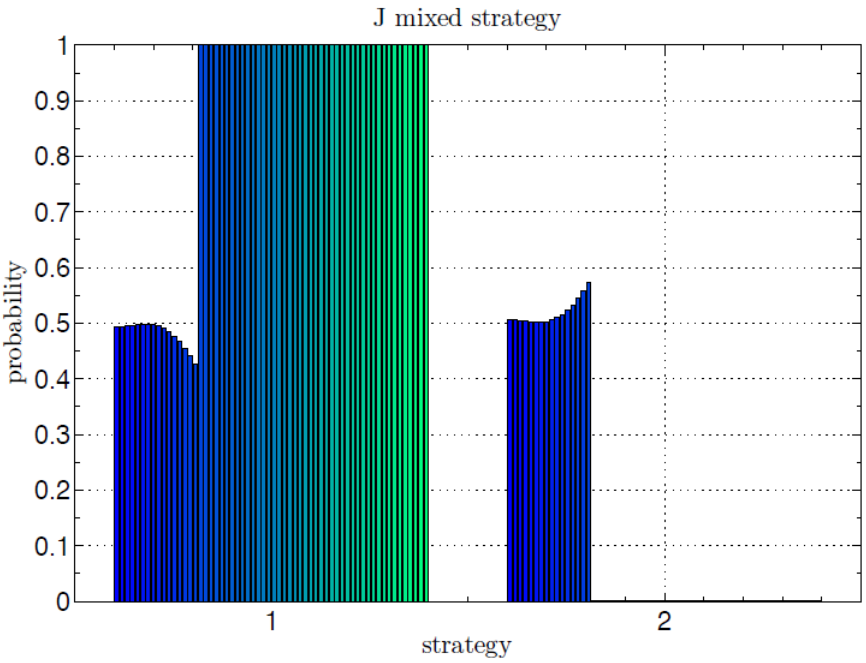

Figure 3.17: J mixed strategy as a function of $d_{\mathrm{J}} \in [0.01, 6]$ km (prior distribution for T's type: [1/3 1/3 1/3]).

from **J**'s standpoint, i.e., there exists a distance d_c for **J** at which its BNE strategies are pure, namely, **J** disrupts communication on c_1 with probability 1.

In Fig. 3.18 the payoff at BNE for **T** quantified as the sum capacity of the network in bit/s is shown. The BNE expected payoff for **T** is bound by the *maximin*'s payoff and the *minimax*'s payoff in pure strategies. These quantities are computed as the maximum of the minima and the minimum of the maxima over rows and columns of **M**. The three curves converge at d_c and, then, coincide for $d_J \geq d_c$. In this region the behavior of the sensor network is almost independently of the jammer's action, and vice versa. The Bayesian game is uncertain of its outcome at the equilibrium only when $d_J \leq 1.68$ km, that means that the jammer is relatively close to the receiver, closer or just slightly farther than the closer of the two sensors.

Furthermore, we consider a different configuration of the network, in particular with a non-uniform prior distribution for **T**'s type, such as $\mathbf{p} = [3/4\ 1/8\ 1/8]$ (Fig. 3.19). It is worth noting that considering this configuration, the transmitting sensor nodes are more likely to be close to the sink node and located at the same distance (this is also known to the jammer). Fig. 3.19 shows the BNE payoff for **T** and, also, the *maximin*'s payoff and the *minimax*'s payoff in pure strategies. We obtain performance similar to the previous case, i.e., the three curves converge if d_J is greater than d_c, but, now, d_c is smaller than before, it equals 1.01 km. The *maximin* and *minimax* bounds are tighter, consequently, the situation resembles a pure strategy case regardless of d_J.

Finally, we consider another non-uniform prior distribution for **T**'s type, $\mathbf{p} = [1/8\ 1/8\ 3/4]$. The BNE payoff for **T**, the *maximin* and *minimax* bounds coincide for every d_J ranging from 0.01 to 6 km (Fig. 3.20). As a consequence, if transmitting sensor nodes are likely to be far from the sink node, then the strategy of **T** is always independent of d_J. Intuitively, the jammer will always disrupt communication on the better channel (c_1). However, this does not mean that the jammer has no impact. Indeed, it can be noticed that the achieved capacity is much lower than what achieved in the previous cases (Figs. 3.18 and 3.19). Neverthless, the network performance is more predictable. Moreover, in this setup the sensor network actually knows that there is a jammer, but, in reality it

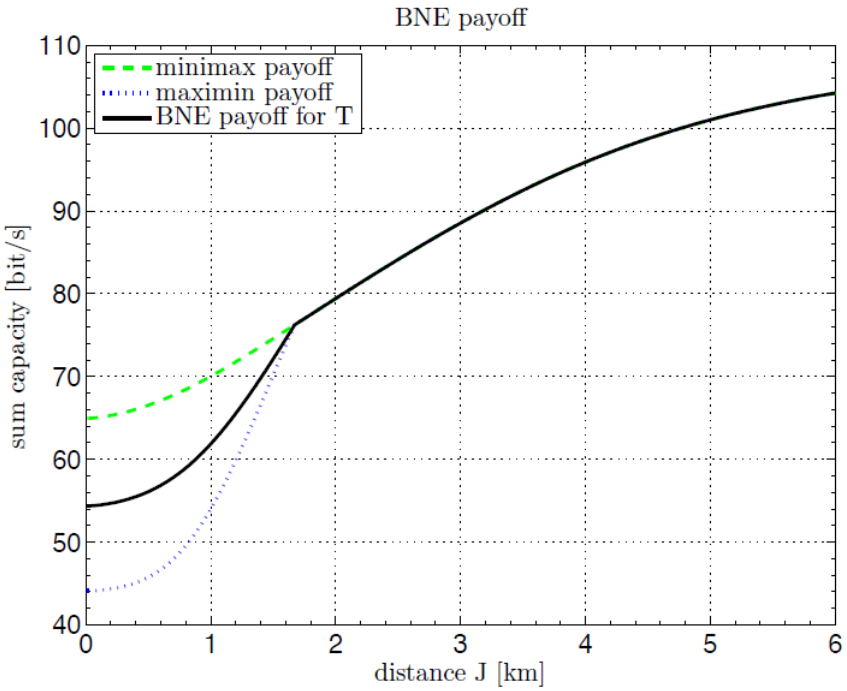

Figure 3.18: NE payoff in mixed strategies as a function of $d_J \in [0.01, 6]$ km (prior distribution for T's type: [1/3 1/3 1/3]).

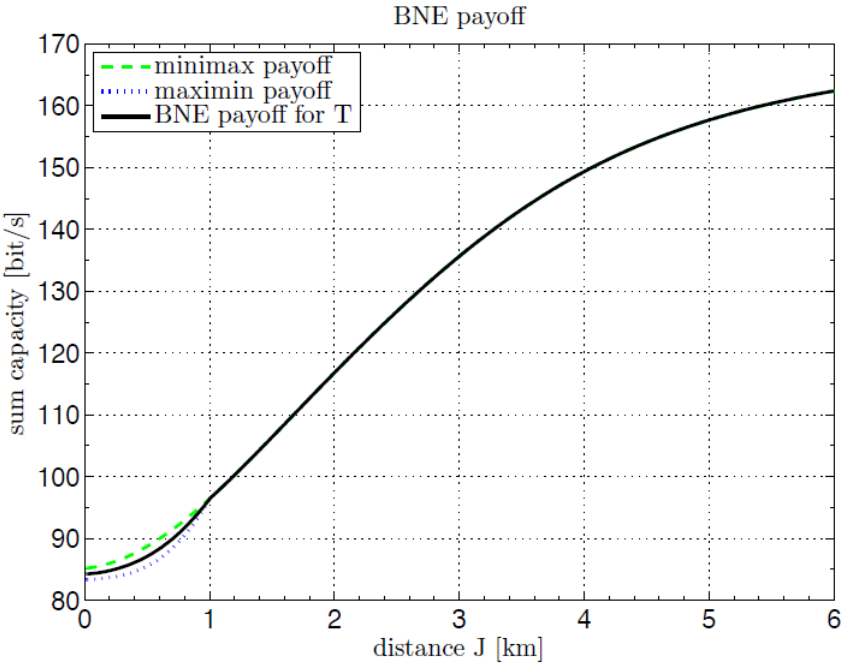

Figure 3.19: NE payoff in mixed strategies as a function of $d_J \in [0.01, 6]$ km (prior distribution for T's type: [3/4 1/8 1/8]).

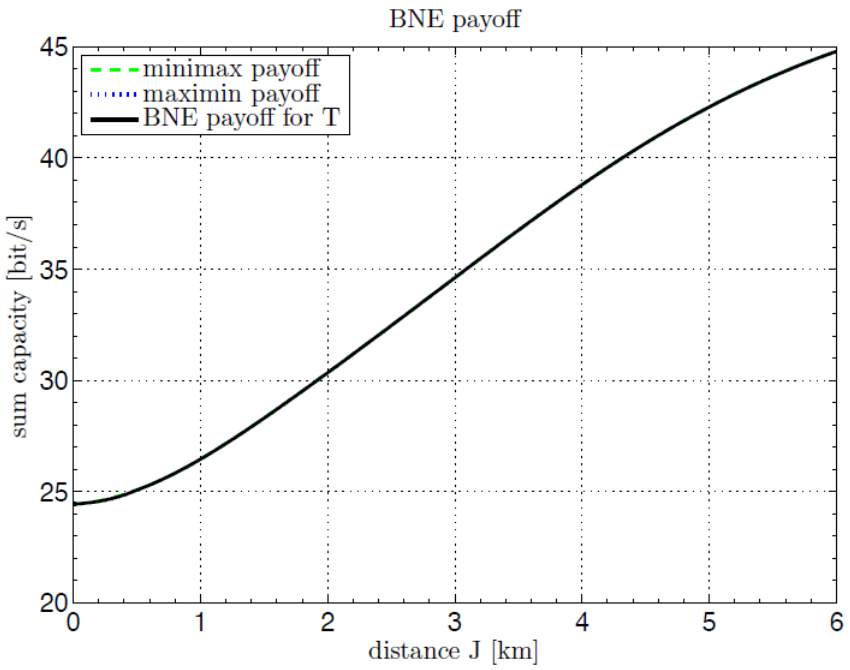

Figure 3.20: NE payoff in mixed strategies as a function of $d_J \in [0.01, 6]$ km (prior distribution for T's type: [1/8 1/8 3/4]).

would be actually difficult to detect it, since its actions would be identical to a higher noise (e.g., due to a more intense shipping or wind noise) on channel c_1.

3.4.3 Concluding remarks for the jamming problem evaluation in WSNs and UASNs

In these last two Sections, we investigated a game theoretic setup of the jamming problem with variable distances of the players involved. In particular, we formulated a Bayesian game where we framed the positions of the useful transmitters as the type of the maximizer player, whereas the jammer, i.e., the minimizer player, can only occupy a fixed position, which is characterized by a distance d_J from the intended receiver. In particular, we considered two possible different scenarios: wireless network and underwater acoustic sensor network. The difference between these two environments is due to the fact that the communication channels differ. For example, it is well known that underwater channels have a small bandwidth compared to terrestrial channels, meaning lower bit rates. Then, the speed of acoustic waves in water is several orders of magnitudes lower than that of the electromagnetic ones in air, consequently, this results in a huge propagation delay. Therefore, some medium access adjustments may be necessary. However, in general, it was possible to draw the same final observations in both cases. We investigated the dependence of the NEs and the resulting payoff on d_J. We obtained as the main result that, depending on the propagation parameters, there are intervals for d_J where the NE solution implies that the jammer adopts a pure strategy, that means that a given channel is jammed with probability 1. As a matter of fact, the network manager should especially control those situations where this does not happen. Those cases are the ones in which the jammer occupies a position according to which at the equilibrium its strategy mixes multiple jamming actions. Such scenarios have been classified as *critical positions* for the jammer. It can further be stated that any security enforcement should especially check those areas for jammers.

However, it would make sense to consider a deeper interaction between the network and the jammer,

where the game formulated here is used as a basis. For example, it can be thought of relaxing the assumption of knowing the jammer's position with certainty, and let this to be the type of the jammer. Our preliminary investigations indicate that the game becomes even more interesting. Especially, a more complicate interaction takes place and in the end the region where a jammer exhibits critical influence may change and even shrink further. Future analysis will be required to extend the analysis and identify challenges in an expanded setup with more advanced game theory instruments.

3.5 Analysis of strategic security through game theory for mobile social networks

Social mobile networking is rapidly expanding, as most of the users connected to social networks also enjoy wireless connectivity and the seamless integration brought by next generation networking [82].[4] However, this poses unprecedented challenges in terms of network security. Connecting to unprotected wireless hot-spots and/or interacting with other mobile nodes in a machine-to-machine communication may imply the risk of having sensible information stolen and/or services disrupted by malicious adversaries [83]. Furthermore, in the previous Section we addressed the problem of jamming in wireless and underwater acoustic sensor network, where a malicious node with the aim of disrupting network communications is present.

Mobile nodes are usually unaware of the intentions of the terminals they are interacting with. From a theoretical perspective, the network layer of a social mobile network operates assuming full cooperation and commonality of intents. However, not all the involved nodes may be benign: some can be adversaries pretending to collaborate, while instead pursuing some different purposes than the network wellbeing. In general, there exist multiple kinds of malicious clients with different purposes and abilities. These clients could act as hacker, cracker, cybercriminals, cyber terrorist, and malicious insiders [84]. As a consequence, we deal with several security problems in which the identity of a client is unknown to a legitimate node searching for collaboration. Thereafter, we refer to this scenario as a server-client interaction, even though this is done only to follow the common choices in the literature and by no means limited to this kind of interaction. Hence, in what follows *server* denotes a legitimate node of the network that interacts with a *client* of unknown intentions [89].

If the server trusts the clients to be benign and does not implement a surveillance procedure, attackers would be able to disrupt network operation by simply pretending to be legitimate clients. On the other hand, if the server considers each client as a potential malicious agent, it will implement some costly surveillance procedure that decreases the quality of service provided, not only for the server itself, but also for all the legitimate benign clients. Therefore, the most compelling network security problem is to correctly define a proper operation where both types of clients are considered and efficient defense strategies are designed with the purpose of preventing malicious activities and providing good quality of services to benign nodes [85].

Game theory has been widely used to tackle security problems in communication networks [94]. This approach enables low-cost distributed management of the network, as well as defining some theoretical performance bounds. However, most security issues are generally modeled as the interaction between a defender and a node that is certain to be a malicious attacker. In reality, the correct identification of a malicious client is challenging, especially if the attacker adopts a strategic behavior that tries to keep its true intent hidden from the network [88]. For this reason, it is not always possible to infer the identity of a malicious agent known to the other nodes of the network, but rather, only an estimate about the character of the client can be made; thus, the specific instrument to use in this scenario is that of Bayesian games [87].

[4]This section is taken from "Analysis of strategic security through game theory for mobile social networks" published in IEEE CAMAD.

Our purpose is to analyze a server/client game where the client can be either benign or malicious with a known prior probability. The nodes have an available set of possible actions that they can perform in the network. We remark that the existing literature usually considers just two actions available to each player, which enables a simple approach to the problem but on the other hand makes it easy to identify the client type (depending on whether he plays its collaborative action or not). We aim at expanding this scenario by including additional moves that enable a malicious client to get undetected, which in our opinion is a more realistic option.

A sample scenario could be a packet forwarding situation that is often used in the context of security. In this case, sensor nodes would have the option to transmit a packet, and supporting clients acting as relays can choose among forwarding it without damaging it, ignoring it, or adding some intentional errors to its transmission. This wider set of available options makes the analysis more realistic. Still, we are able to analyze the game in closed-form, and show some examples of analysis with given numerical values. Specifically, we consider a Bayesian game framework to capture the uncertainty about the client's nature, and identify the BNEs of this game, and discuss how they are affected by the numerical parameters. We also suggest some implications on the security strategies of the network.

In [89] and [87] authors provide a survey and classifications of existing game theoretic approaches to network security issues. They state that game theoretic approaches show that they are powerful tools for solving network security problems and that new game theoretic approaches should be a pool of research directions on network security. In [88] a new Bayesian hybrid detection approach has been suggested for a network defender. In this approach a lightweight monitoring system is used to estimate the defender opponent's actions, and a heavyweight monitoring system acts as a last resort of defense. The results obtained show that the dynamic game produces energy-efficient monitoring strategies for the defender, while improving the overall hybrid detection power.

We can find similar analysis in [91] and [92]. In particular, a new exact method called *DOBSS* for finding the optimal strategy for the leader in a Bayesian Stackelberg game is presented in [91]. In these kind of games, one agent, called the leader, must commit to a possibly mixed strategy that can be observed by other agents, called the followers, before they choose their own strategies. The leader is uncertain about the types of adversary it may face, therefore such games are extremely valuable in modeling domains involving security, including patrolling, setting up checkpoints, network routing, transportation systems and others. As a consequence, solution techniques such as *DOBSS* for efficiently solving such games are crucial. In [92], using a game-theoretic approach, authors propose a selective and dynamic mechanism for counter-fingerprinting. They first model and analyze the interaction between a fingerprinter and a target as a signaling game. Then, they derive the Nash equilibrium strategy profiles based on the information gain analysis and they design a mechanism to prevent or to significantly slow down fingerprinting attacks. Their game-theoretic approach appropriately distinguishes a fingerprinter from a benign client and mystifies packets to confuse the fingerprinter, while minimizing the effects on legitimate clients. This mechanism can reduce the probability of success of the fingerprinter significantly, without deteriorating the overall performance of other clients.

[86] presents an application of the Bayesian game theory to model node behaviors in trajectory privacy preservation activities in mobile Wireless Sensor Networks (mWSNs). The characteristics of autonomous nodes, including selfish, malicious and cooperative, have been formulated in the TPP game, and the trustworthiness of the unknown type node has been evaluated. Then, authors derive the equilibrium strategies of the game in both theoretical and simulation results.

In [90] authors study two-player security games which can be viewed as sequences of non zero-sum matrix games played by an attacker and a defender. It is assumed that at each stage of the game iterations, the players make imperfect observations of each other's previous actions. The underlying decision process can be seen as a fictitious play (FP) game, but in their analysis the communication channels that carry action information from one player to the other, or the sensor systems, are error

prone. Two possible scenarios are addressed: if the error probabilities associated with the sensor systems are known to the players, then the analysis provides guidelines for each player to reach a NE related to the NE of the underlying static game; if the error probabilities are not known to the players, then they evaluate the effect of observation errors on the convergence to the NE and the final outcome of the game. Moreover, both the classical FP and the stochastic FP have been discussed, where for the latter the payoff function of each player includes an entropy term randomizing its own strategy, which can be interpreted as a way of concealing its true strategy.

Security is a trouble of major importance to governments and companies throughout the world. Since resources are usually limited, complete coverage of potential points of attack is not possible. Deterministic allocation of available law enforcement agents adds predictable vulnerabilities that can be exploited by malicious adversaries. Strategic randomization is a game theoretic alternative that in [93] is implemented in Intelligent Randomization In Scheduling (IRIS) system, a software scheduling assistant for the Federal Air Marshals (FAMs) that provides law enforcement aboard U.S. commercial flights. The authors model the problem as a Stackelberg game, with FAMS as leaders that commit to a flight coverage schedule and terrorists as followers whose purpose is to attack a flight. The FAMS domain presents three challenges. First of all, with tens of thousands of commercial flights per day, the size of the Stackelberg game to solve is very large. Therefore, they use ERASERC, the fastest known algorithm for solving this class of Stackelberg games. Secondly, creating the game itself becomes a challenge due to number of payoffs needed for these large games. To address this issue, an attribute-based preference elicitation system to determine reward values is created. Thirdly, the complex scheduling constraints in transportation networks make it computationally very hard to model the game by explicitly modeling all combinations of valid schedules. Then, authors model the leader's strategy space by incorporating a representation of the underlying scheduling constraints. The scheduling assistant has been delivered to the FAMS and is currently undergoing testing and review for possible incorporation into their scheduling practices.

Finally, since in many security problems, service providers are basically unaware of the type of their clients that can potentially be an attacker (who will launch an attack at any time during their connections to service providers) or a legitimate agent, in [94] is provided a general framework for modeling security problems subject to different types of clients connected to service providers. Authors develop an incomplete information two-player game to capture the interaction between the service provider, the server, and an unknown client. In particular, they consider two types of clients, i.e. attacker and benign clients, and they analyze the game using perfect Bayesian Nash equilibrium (PBNE) with different conditions. As a result, they design an algorithm using the computed PBNE strategy profiles to find the best defense strategy that the server should use.

The rest of this Section is organized as follows. In Sub-section 3.5.1, we describe the system model and the game theory application; we compute the Bayesian Nash equilibrium analysis in Sub-section 3.5.2. Section 3.5.3 presents some numerical results and Section 3.5.4 draws the conclusions.

3.5.1 System model

We consider a Bayesian game, in which players can be of different types to capture different behaviors that the players may have.

For the sake of presentation, we consider the interaction between two nodes. This can be further extended to a larger number of nodes by repeating the pairwise interaction. In a mobile social network, each node can be either malicious or benign, depending on how they interact with the rest of the network. Malicious nodes damage communications in the network so as to disrupt its operation; we only focus on this kind of malicious attacks, that are aimed at denying service [85]. Moreover, we consider the typical interaction of multihop networks, where nodes exchange packets and require mutual collaboration in the form of relaying data to the end destination. In this setting, a server can decide to transmit a packet to another node, monitor the network in order to detect malicious nodes

		P2		
		Forward	**Ignore**	**Damage**
P1	**Nothing**	0,-1	0, 0	-1,-∞
	Packet	1, 1	-1, 0	-2, -∞
	Surveillance	-3, -2	-3, 0	2, -∞

Table 3.3: Normal-form (matrix) of the game considering Player 2 no malicious

without transmitting any packet, or do nothing and remain inactive. Furthermore, considering that some nodes may have malicious purposes, when a node is asked to forward a packet, it can really do so, or ignore the packet, or even forward a corrupted version of it, to cause harm.

We assume that one of the nodes, denoted as node 1, is a benign node (if both nodes are malicious, it is pointless to consider the defense from an adversary). The other node, denoted as node 2, may be either a legitimate node or a malicious attacker. We define p as the prior probability of being malicious for node 2. Note that the type of node 2 is private information, which means that node 2 is aware of being either malicious or not, while node 1 does not know (but it can estimate it via the probability p). Node 1 acts as a server that can transmit packets to a client or protect the network against malicious agents through surveillance. Node 2 acts as a client and it can forward a received packet without any damage, ignore a received packet, or forward a received packet corrupting it depending on its behavior. We can model this scenario using a two-player static Bayesian game in which the server and the client are the players, player 1 and player 2, respectively. The set of actions that can be taken is $\{Nothing, Packet, Surveillance\}$ for player 1 and $\{Forward, Ignore, Damage\}$ for player 2. These actions reflect the three types of possible interactions. Every pair of actions yields an arbitrary quantification of the goodness coming from its resulting outcome. Because of the Bayesian context, it is assumed that each player has a type Θ_i, with values in $\{0, 1\}$, that describes its being malicious. If a generic player i is malicious, its type is $\Theta_i = 1$, otherwise it is $\Theta_i = 0$. We assume that only player 2 has a type. As a consequence, $\Theta_1 = 0$ and $\Theta_i \in \{0, 1\}$; finally, we formally state that $p = Prob[\Theta_2 = 1]$.

Before analyzing the Bayesian game, we separately describe the cases in which player 2 is benign or malicious, as two different static games without any Bayesian element. We set arbitrary numbers for the utility of each outcome, that satisfy an ordinal criterion (most preferred situations have a higher utility). The actual numbers are chosen just for the sake of easy computations; the same analysis is still valid for other choices of values.

First, consider the scenario in which player 2 is not malicious. Table 3.3 shows the normal-form matrix describing this game. Player 2 will reach a payoff equal to $-\infty$ if it chooses to damage the transmission. Therefore, it will never choose that action that can be considered as a strictly dominated strategy. Indeed, a strategy is *dominated* if, regardless of what any other players do, the strategy brings to the player a strictly smaller payoff than some other strategy. For this reason, we can neglect this strategy in our analysis because it is dominated by both Forward and Ignore. Once we neglect the *Damage* action of player 2, a similar observation iteratively holds for the *Surveillance* strategy of player 1. In particular, this strategy is now strictly dominated by *Nothing* that allows to the player to earn a higher payoff regardless of what opponent may do. This is quite intuitive because, since player 2 is not malicious, it does not have any incentive to damage network, therefore, it is not necessary for player 1 to monitor and control the network against malicious agents. After these considerations, the 3x3 matrix can be simplified in a 2x2 matrix keeping the rows denoted by *Nothing* and *Packet*, and the columns *Forward* and *Ignore* from the original normal-form matrix. At this point, we can easily observe that two NEs in pure strategies can be found. In more details, these NEs are: (*Nothing*, *Ignore*) and (*Packet*, *Forward*). In addition, we investigate on the existence of NEs in mixed strategies. Defining α as the probability that player 1 chooses *Nothing* and β the probability

		P2		
		Forward	**Ignore**	**Damage**
P1	**Nothing**	0,-1	0, 0	-1,1
	Packet	1, -1	-1, 0	-2, 3
	Surveillance	-3, -2	-3, 0	2, -3

Table 3.4: Normal-form (matrix) of the game considering Player 2 malicious

that player 2 plays $Forward$, this game has a single mixed NE $(\frac{1}{2}, \frac{1}{2})$. This means that player 1 will plays $Nothing$ with probability $\frac{1}{2}$ and $Packet$ with probability $\frac{1}{2}$. In more details, we find that player 1 will play $Nothing$ if $\beta < \frac{1}{2}$, it will play $Packet$ if $\beta > \frac{1}{2}$, finally, it will be indifferent between playing $Nothing$ or $Packet$ if $\beta = \frac{1}{2}$. Similar observations hold for player 2; it will choose $Forward$ if $\alpha < \frac{1}{2}$, it will choose $Ignore$ if $\alpha > \frac{1}{2}$, and it will be indifferent if $\alpha = \frac{1}{2}$. 3.69 and 3.70 describe the best response strategy of player 1 and player 2, respectively.

$$BR_1 = \begin{cases} Nothing, & \text{if } \beta \leq \frac{1}{2}, \\ Packet, & \text{if } \beta \geq \frac{1}{2} \end{cases} \tag{3.69}$$

$$BR_2 = \begin{cases} Forward, & \text{if } \alpha \geq \frac{1}{2}, \\ Ignore, & \text{if } \alpha \leq \frac{1}{2} \end{cases} \tag{3.70}$$

Table 3.4 shows the normal-form matrix describing the simple game in which player 2 acts as a malicious player. With respect to Table 3.3, few meaningful changes have been made. In particular, acting to $Damage$ the network is now possible. Also, the mutual benefit of cooperation that was previously described by the outcome for $(Packet, Forward)$ has been altered for the malicious player. Focusing on player 2's payoffs, $Forward$ is strictly dominated by $Ignore$. Then, for player 1 it holds that $Packet$ is strictly dominated by $Nothing$. This is intuitive because, since player 2 is malicious, it does has incentive to damage nodes communication in order to gain a higher payoff; therefore, it is better for player 1 to monitor and control the network against malicious agents or to do nothing instead of transmitting a packet which will be corrupted. After these considerations, also in this case the 3x3 matrix can be simplified in a 2x2 matrix keeping the rows denoted by $Nothing$ and $Surveillance$, and the columns $Ignore$ and $Damage$ from the original normal-form matrix. At this point, we can observe that there are no BNE in pure strategies. Concerning the existence of BNEs in mixed strategies and defining α as the probability that player 1 chooses $Nothing$ and β the probability that player 2 plays $Ignore$, this game has a single mixed BNE denoted as $(\frac{3}{4}, \frac{1}{2})$, i.e., player 1 will plays $Nothing$ with probability $\frac{3}{4}$ and $Surveillance$ with probability $\frac{1}{4}$ and player 2 will choose $Ignore$ or $Damage$ with equal probability. The best response of players 1 and 2 is shown by the following equations.

$$BR_1 = \begin{cases} Nothing, & \text{if } \beta \leq \frac{1}{2}, \\ Surveillance, & \text{if } \beta \geq \frac{1}{2}. \end{cases} \tag{3.71}$$

$$BR_2 = \begin{cases} Ignore, & \text{if } \alpha \geq \frac{3}{4}, \\ Damage, & \text{if } \alpha \leq \frac{1}{4} \end{cases} \tag{3.72}$$

3.5.2 Bayesian Nash Equilibrium analysis

Now we consider an incomplete information game in which player 1 is not aware of the type of its opponent, i.e., benign or malicious. Either of the two games previously described is actually played with probability $1 - p$ or p respectively, with the parameter p (but not the actual type) being known in advance by player 1. That is, p is the prior probability of player 2 being of malicious type.

		P2		
	IF	**II**	**DF**	**DI**
N	0, p-1	0, 0	-p, 2p-1	-p,p
P1 **P**	1-2p, 1-p	-1, 0	1-3p, 2p+1	-p-1, 3p
S	-3, -2+2p	-3, 0	5p-3, -p-2	5p-3, -3p

Table 3.5: Normal-form (matrix) of the Bayesian game

	P2	
	DF	**DI**
N	-p, 2p-1	-p, p
P1 **P**	1-3p, 2p+1	-p-1, 3p

Table 3.6: Simplified normal-form (matrix) of the Bayesian game

Table 3.5 shows the payoff of each player according to the different strategies that it can take. For the sake of exposition, we shorten the action names by writing N, P, S, F, I, D, instead of "Nothing," "Packet," "Surveillance," "Forward," "Ignore," and "Damage," respectively. As previously stated for the two simple games, when player 2 is not malicious it actually plays only $Forward$ or $Ignore$, instead when it is malicious it can play $Ignore$ or $Damage$. Furthermore, under a Bayesian framework we represent strategies by defining an action for each player's type. Thus, while player 1's possible strategies are the same as the previous two games (i.e., they coincide with actions N, P, S), the strategies of player 2 are instead pairs of actions, since we need to specify what player 2 does depending on its type. This means that player 2 has four possible strategies in the Bayesian game, namely its strategy set is $\{IF, II, DF, DI\}$. We denote each strategy as a pair of actions to be played when the client is either malicious or benign, respectively. For example, strategy IF means that player 2 will play $Ignore$ if malicious, $Forward$ otherwise. Note that, for the sake of brevity, we already discarded player 2's strictly dominated strategies, depending on its type. To compute the payoffs earned by the players, we take expectations over beliefs for types. For example, for actions (N, IF): player 1 earns 0 if player 2 is not malicious, that is, with probability p, and 0 if player 2 is malicious, therefore the payoff is still 0; player 2 earns -1 if it is not malicious, that is, with probability p, and 0 otherwise, therefore its payoff is $0 \cdot p - 1 \cdot (1-p) = p - 1$. To compute the BNEs, we consider different cases depending on whether $p < \frac{1}{2}$ or $p > \frac{1}{2}$.

3.5.2.1 Likely benign client

This represents the case in which $p < \frac{1}{2}$. From Table 3.5, we notice that S is a strategy strictly dominated by N for player 1. As a consequence, we can neglect S as a possible action of player 1. Moreover, we can also state that II and IF are strictly dominated strategies for player 2; the former is strictly dominated by DI, the latter is strictly dominated by DF. Table 3.6 summarized the game considering these observations.

There exist two BNEs in pure strategies: (N, DI) and (P, DF). Defining α as the probability that player 1 plays N and β as the probability that player 2 chooses DF, we also find a mixed BNE: $(\frac{1}{2}, \frac{1}{2(1-p)})$. In more detail, the best strategy for player 1 is to choose N if $\beta < \frac{1}{2(1-p)}$, P if $\beta > \frac{1}{2(1-p)}$, and to be indifferent if $\beta = \frac{1}{2(1-p)}$. At the same time, the best strategy for player 2 is to play DF if $\alpha < \frac{1}{2}$, DI if $\alpha > \frac{1}{2}$, and to be indifferent if $\alpha = \frac{1}{2}$. The best response strategies of the two players are:

$$BR_1(\Theta_2) = \begin{cases} N, & \text{if } \beta \leq \frac{1}{2(1-p)}, \\ P, & \text{if } \beta \geq \frac{1}{2(1-p)}. \end{cases} \tag{3.73}$$

		P2	
		IF	**DI**
P1	**N**	0, 0	-p, p
	S	-3, 0	5p-3, -3p

Table 3.7: Simplified normal-form (matrix) of the Bayesian game

$$BR_2(\Theta_1) = \begin{cases} DF, & \text{if } \alpha \geq \frac{1}{2}, \\ DI, & \text{if } \alpha \leq \frac{1}{2} \end{cases} \tag{3.74}$$

3.5.2.2 Likely malicious client

In this case $p > \frac{1}{2}$. In Table 3.5, P is now a strategy dominated by N for player 1. As a consequence, we can neglect P as a possible action of player 1. We can also state that, focusing on player 2 payoff, IF is dominated by II. Moreover, it can be observed that there exists a linear combination of the payoffs that player 2 can reach playing DI and II that gives a higher payoff with respect to playing DF. In other terms, there exists μ such as $\mu \cdot u_2(DI) + (1-\mu) \cdot u_2(II) > u_2(DF)$, where u_i is the payoff of player i. 3.75 shows that, since $p > \frac{1}{2}$, $\frac{2p-1}{p} < \frac{p+2}{3p}$, there exists an interval for μ in which the condition on the payoffs is satisfied:

$$\frac{2p-1}{p} < \mu < \frac{p+2}{3p}. \tag{3.75}$$

Thus, we can neglect DF as a dominated strategy for player 2. Table 3.7 summarized the game considering these observations. In this case, the game has no BNEs in pure strategies. However, defining α as the probability that player 1 plays N and β as the probability that player 2 chooses II, there exists a mixed BNE: $(\frac{3}{4}, \frac{2p-1}{2p})$. In more details, the best strategy for player 1 is to choose N if $\beta > \frac{2p-1}{2p}$, S if $\beta < \frac{2p-1}{2p}$, and to be indifferent if $\beta = \frac{2p-1}{2p}$. At the same time, the best strategy for player 2 is to play II if $\alpha < \frac{3}{4}$, DI if $\alpha > \frac{3}{4}$, and to be indifferent if $\alpha = \frac{3}{4}$. The best responses are:

$$BR_1(\Theta_2) = \begin{cases} N, & \text{if } \beta \leq \frac{2p-1}{2p}, \\ S, & \text{if } \beta \geq \frac{2p-1}{2p}. \end{cases} \tag{3.76}$$

$$BR_2(\Theta_1) = \begin{cases} II, & \text{if } \alpha \geq \frac{3}{4}, \\ DI, & \text{if } \alpha \leq \frac{3}{4} \end{cases} \tag{3.77}$$

3.5.2.3 Uniform prior probability

The final case is when the server considers both types of the client to be equally likely ($p = \frac{1}{2}$), which may also mean that the server cannot make any assumption about the client's character. If we consider this situation of maximum uncertainty about player 2, we obtain the payoffs shown in Table 3.8. As it can be noted from the table, in this case there are no dominated strategies. Therefore, the analysis for the computation of the equilibria is much harder with respect to previous cases. However, a mixed equilibrium is bound to exist, and also continuity of the expected utility in the Bayesian case can be exploited (so that we can find the Nash equilibrium via the left and right limits that fall within the two previous cases).

		P2		
	IF	**II**	**DF**	**DI**
N	0, $-\frac{1}{2}$	0, 0	$-\frac{1}{2}$, 0	$-\frac{1}{2}$, $\frac{1}{2}$
P1 **P**	0, $\frac{1}{2}$	-1, 0	$-\frac{1}{2}$, 2	$-\frac{3}{2}$, $\frac{3}{2}$
S	-3, -1	-3, 0	$-\frac{1}{2}$, $-\frac{5}{2}$	$-\frac{1}{2}$, $-\frac{3}{2}$

Table 3.8: Normal-form (matrix) of the Bayesian game for $p = \frac{1}{2}$

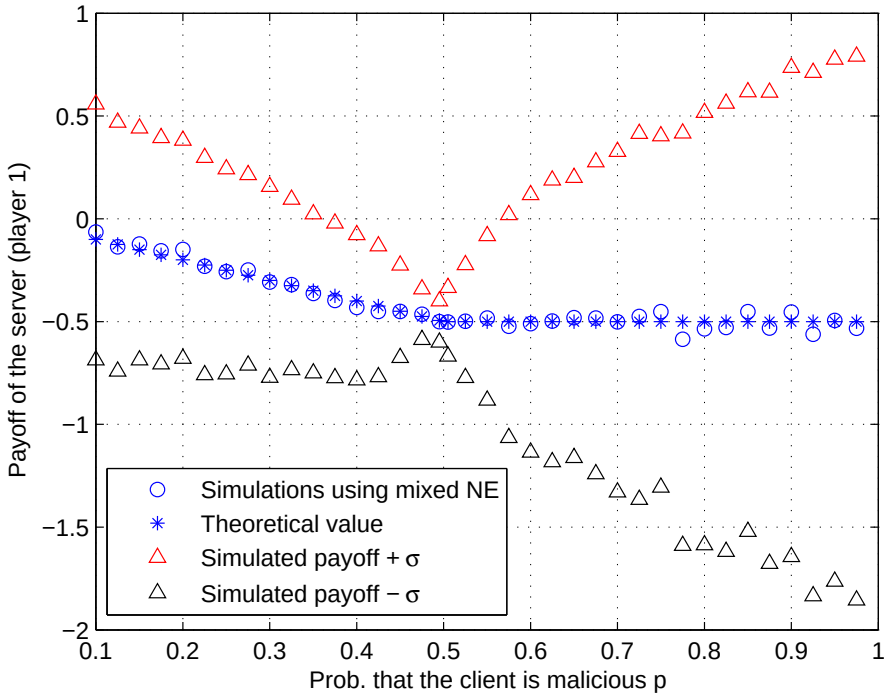

Figure 3.21: Comparison of player 1 payoff obtained via the theoretical analysis and simulations considering mixed NE.

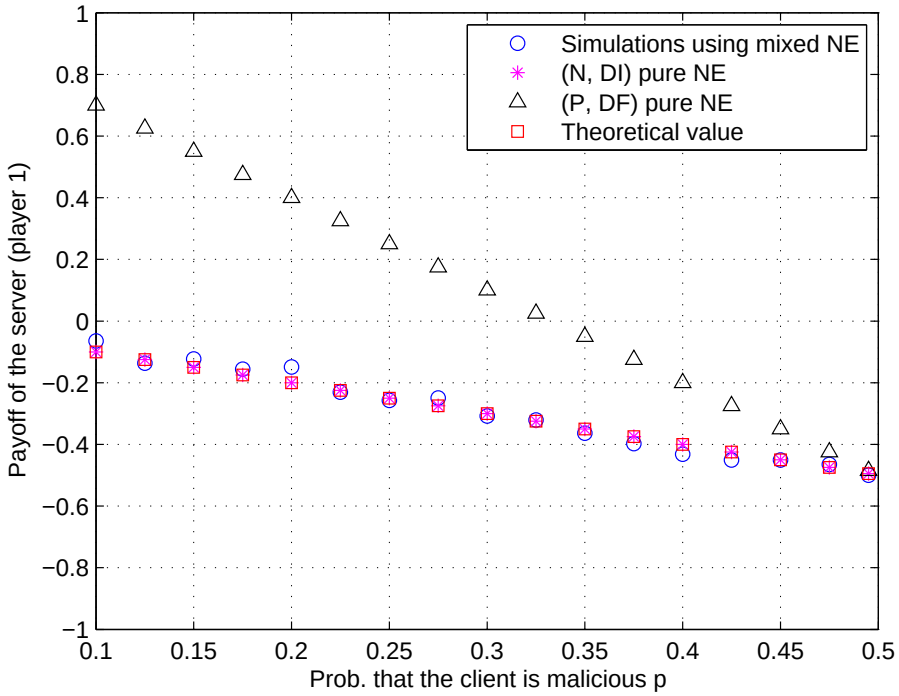

Figure 3.22: Comparison of player 1 payoff obtained via the theoretical analysis, simulations considering mixed NE, and considering pure NEs for $p < \frac{1}{2}$.

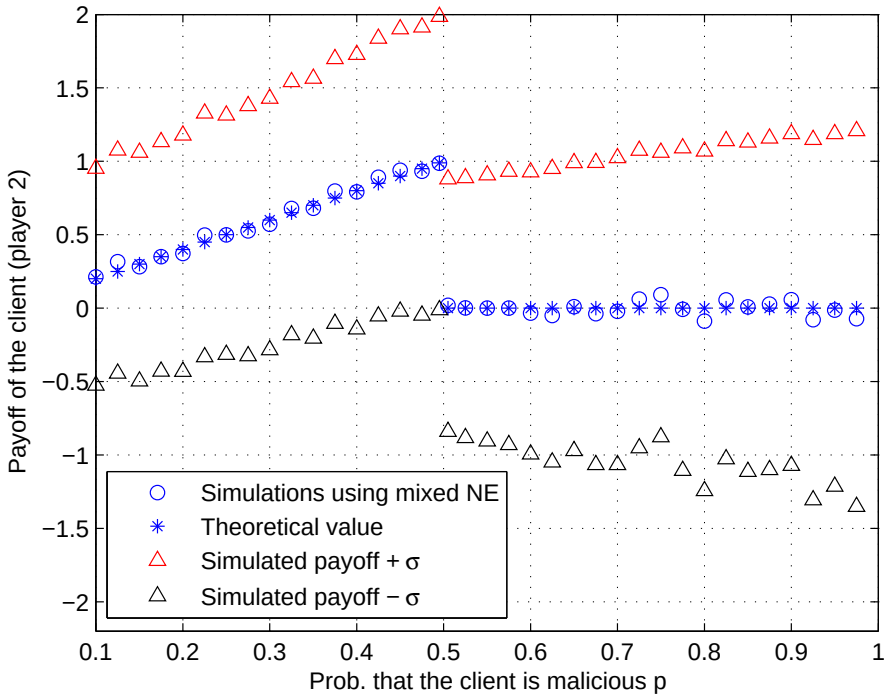

Figure 3.23: Comparison of player 2 payoff obtained via the theoretical analysis and simulations considering mixed NE.

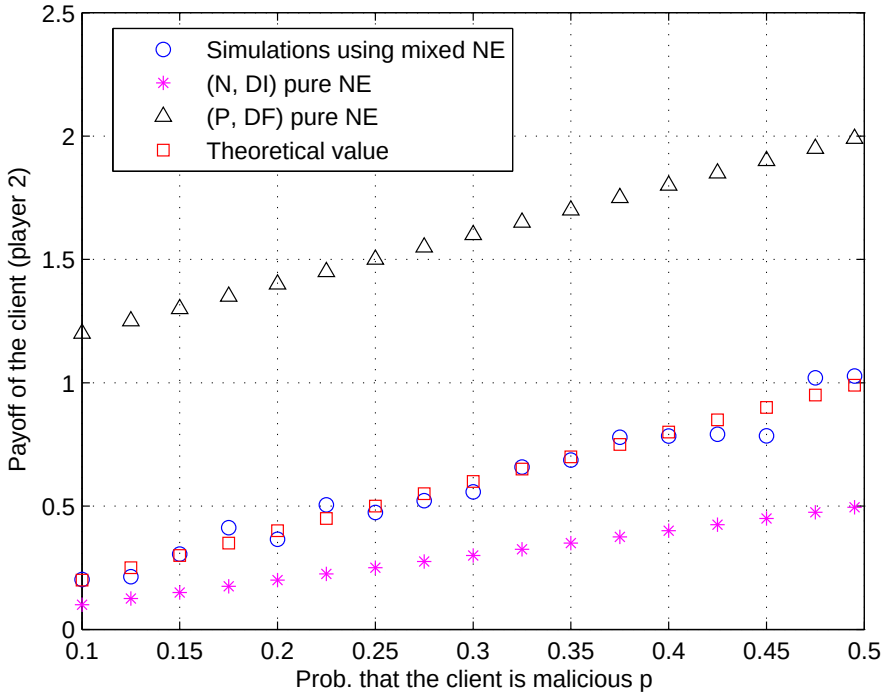

Figure 3.24: Comparison of player 2 payoff obtained via the theoretical analysis, simulations considering mixed NE, and considering pure NEs for $p < \frac{1}{2}$.

3.5.3 Numerical results

In this Sub-section, we discuss some numerical results, obtained by both analysis and simulation. We consider that each player plays a mixed equilibrium strategy. We limit our results to the repetition of a static Bayesian game, meaning that at each stage we do not consider the update of the belief that player 1 has on the type of its opponent. However, we can model this scenario through the repetition of a dynamic Bayesian game in which the game evolution is taken into account and the defender can dynamically update its beliefs based on new observations of actions chosen by its opponent and the game history in order to adjust its monitoring strategy accordingly. We will consider this aspect as a future work.

Figs. 3.21 and 3.23 show the payoff reached by player 1 and player 2, respectively, versus the value of p, i.e., the prior probability that player 2 is malicious. In these figures, we compare the payoff obtained through the theoretical analysis discussed in previous sections represented by the blue-dotted line with respect to the payoff obtained via simulations described by the blue-star line. As it can be observed by the figures, the simulations results follow very well the theoretical development. In particular, looking at Fig. 3.21 we can see that, for $p < \frac{1}{2}$, the lower the value of p, the higher the value of player 1 payoff. This is reasonable because the lower p, the less likely that player 2 is malicious, then it is not necessary to apply surveillance against a possible attacker in the network. As a consequence, player 1 can reach a higher payoff by transmitting packets. On the other hand, for $p > \frac{1}{2}$ the value of player 1's payoff is constantly equal to -0.5 (also confirmed by simulations). This is because players play the mixed BNE, then for player 1 is more likely to play N and, as a consequence, it is more likely that player 2 will play DI. Focusing on Fig. 3.23, we can notice that, for $p < \frac{1}{2}$, the lower p, the lower player 2's payoff. Indeed, the higher p, the lower the value of $(2(1-p))^{-1}$; therefore, player 2 will reach a higher payoff damaging the network. For $p > \frac{1}{2}$, the higher is p, the lower is the probability that player 2 will play strategy DI. Since player 1 is more likely to play N at

the equilibrium, player 2's payoff will be 0.

In Figs. 3.21 and 3.23 we also show the simulated payoff value plus or minus its standard deviation (obtained by simulation) with the red/black triangle lines. Looking at Fig. 3.21 we can observe that for too low and high values of p there is a greater dispersion of the individual observations around the average value. This aspect is less pronounced in Fig. 3.23.

Finally, Figs. 3.22 and 3.24 show the development of the players payoff considering theoretical analysis results with the red-square line, simulations results described by the blue-dotted line, and the results obtained considering that players play the two pure BNEs shown by magenta-star line and black-triangle line. In these figures, we consider p varying in the interval [0.10.5]; indeed, only in this interval there exists the pure BNEs. As we can notice, one of the two pure BNEs, that is (P, DF), outperforms the other cases. In particular, this is more evident for player 2's payoff shown in Fig. 3.24.

3.5.4 Conclusions

In this Section, we showed how game theory can be employed as an instrument to characterize interactions in social online networking. Especially, mobility of terminals poses several challenges in terms of identifying malicious players that aim at damaging the network operation.

To this end, we considered a Bayesian game between a server and a client where the server is operating with incomplete information and only has a prior belief on the client actual type. The analysis confirms practical aspects of network surveillance. In particular, it is found that malicious clients are hard to defeat without a proper detection and confirmation that they are indeed malicious. On the other hand, given the high cost of surveillance operation, the best strategy for the server would not be to force the identification of malicious clients, but rather to force a malicious client to strategically play some less harmful strategies. This would lead to an implicit surveillance without the need of actually putting them into operation. Our numerical findings confirm this trend, that is, under certain circumstances, it is more advantageous for the client (even a malicious one) not to harm the network in fear of retaliation. Especially, this may happen if a strategic client does not apply just a myopic optimization of its own payoff, but rather tries to avoid being identified. The best way to do so would actually be to occasionally cooperate with the network, which would lead to a transparent surveillance in which the client itself has the right incentive to behave correctly.

Beyond straightforward extensions, such as putting more players or changing the values of the game, there are several extensions that are left for future work, but still are worth discussing here.

For the specific choice of the numerical parameters made, we were able to find and discuss a detailed solution of the various cases depending on the prior p representing the likelihood of a malicious client. So, a first immediate extension is to investigate cases where the dominance of some actions does not apply at all and a three-fold mixed NE is found, i.e., the support of the mixed strategies include each action. This would complicate the analysis but will likely end up in a similar outcome of what discussed.

A more important application of game theory instruments concerns instead the derivation of an update rule for beliefs that is able to improve the social welfare. Notably, for the server it is not advantageous to have uncertainty on the client's type. This is visible from Figs. 3.21 and 3.23 where the server's payoff is shown to have the most desirable values for p around 0, i.e., whenever player 2 is guaranteed to be benign. On the other hand, even knowing with certainty that the client is malicious is preferable, as the payoff is actually the same than what received in the cases with a likely malicious player 2, which is not confirmed yet. This means that, from the server's standpoint, it would be overall preferable to know with certainty the status of the client than having no information about it.

Finally, the strategic choice of the adversary (a malicious client) here is always seen as a myopic maximization of the local value of its own utility. It would be certainly interesting to include more sophisticated strategies for the client, so that it can cheat the belief update rule of the server; for

example, it can occasionally forward some packets despite being malicious in order to gain trust from the server.

3.6 Social communication to improve group recognition in a network

Online social networks are still enjoying an unprecedented success and represent a very effective instrument for mass communication and content dissemination over the Internet.[5] From the scientific research standpoint, a strong theoretical component may be envisioned behind the pattern recognition and profiling engines that many online social networks adopt to offer better services to their users [95].

Profiling users can also be useful to discover communities of individuals sharing some attributes and therefore exploiting the inherent redundancy within the network, for example, to provide them with similar services or caching homogeneous contents [96, 116]. However, profiling procedures also pose several challenges about anonymity and privacy of the users [98, 99]. In particular, among the many challenges related to this problem, we focus on the detection of group structures, which is an interesting application of social network analysis. From the mathematical standpoint, the identification of group structures in social networks can be seen as a clustering optimization problem [100, 101, 102]. Also in the context of mobile networking, clustering has been widely investigated and is not an entirely new problem [103, 104]. However, what makes our investigation for social networks challenging is that we do not want to cluster mobile nodes based on their technical attributes (such as radio technologies or energy consumption) but rather on some independent application-driven parameters, such as their individual preferences or the societal relationship among them (e.g., who are their "friend nodes").

Most of the theoretical analysis in this field is implicitly based on the assumption that online social networks are able to collect massive amounts of information on their users. The problem resides in mining these data, rather than improving their availability, since the network owner is generally able to collect lots of data on every single user; most of the times, it happens that the users themselves are willingly sharing their preferences and attributes across the entire network [105].

In this Section, we adopt a different perspective by considering a mobile network where discovery of these individual traits of the users is only partial. There are several possible motivations for this scenario; we argue that mobility can be a primal cause. For example, it is reasonable to assume that mobility hinders communication and therefore limits the collection of data. At the same time, mobile networks can also have a temporary character and therefore most of the nodes only gain knowledge on their immediate neighbors only.

We remark that the two attributes of "mobile" and "social" networking have a complementary relationship, in that, for example, the latter can improve the former. In some papers [106, 101] it is studied how social relationships can help the routing algorithms. Again, this approach can be seen as a byproduct of context-aware networking. At the same time, social connections are used, for example by [96], as a way of further profiling users, since it can be assumed that users are likely to connect with each other if they share similar preferences, and their behavior is akin to those who they recognize as friends.

The novel aspect of this work is that we see mobility of the nodes as a *detrimental* to the information extraction, since it causes the network view to be only partial. In this sense, our claim is that the problems caused by such a partial information can only be overcome thanks to social collaboration among the nodes. Thus, we investigate how the collaborative exchange of information about each user's preferences can help recognizing the group structures in the network.

In particular, the scenario on which we focus, and that will be better detailed in the following, involves a network where nodes are element of a graph (representing a network snapshot) and are classified a priori as belonging to a group, which, in graph theory terms, is seen as a *color*. Colors

[5] This section is taken from "Social Communication to Improve Group Recognition in Mobile Networks" published in IEEE GLOBECOM.

have pre-defined bindings, which can be regarded as a binary friendship relationship over the social networks. However, nodes only have awareness of their relationship with their immediate neighbors on the graph. Since the network is not fully connected, the extraction of group information is therefore noisy. Here is where social collaboration applies. We devise a simple iterative procedure where the estimate about unknown nodes is further improved through periodic reporting that nodes make about their neighbors, on a random basis, as a social diffusion of context information.

We believe that such a procedure can be useful in any scenario where social exchange of information is useful, but a centralized coordination is difficult and therefore it is more convenient to resort to distributed exchange of signaling among the nodes. This may be the case for machine-to-machine communication in vehicular scenarios [107], that can be applied to exchanging road safety information, but where exchanges are only made among devices with compatible service (which represents our friendship relationship). More in general, delay-tolerant networks can experience disconnections but they can benefit from social relationships among the nodes to establish a routing backbone [108].

As a result, we show that, while estimating clusters from the initial incomplete data can be highly ineffective, the iterative procedure is much more accurate in identifying clusters and classifying individual nodes' preferences. Even better, a combination of this procedure used as a preliminary scan to improve the data, and a standard clustering approach applied on top, is even more effective. Since our goal is to show the effectiveness of social collaboration as a principle, both the social diffusion procedure and the clustering technique are intentionally kept simple; their detailed analysis would be out of the scope of the present analysis. However, both strategies can actually be refined and different choices of the pattern recognition technique can be made [102]. From our preliminary investigations we expect the effectiveness of social collaborative networking to hold with more complex strategies.

The problem of recognizing groups of similar nodes within a mobile social network can seen far away to what has been previously discussed in this Chapter. However, it is strongly related to the current topic. Indeed, this approach can be enriched considering the presence in the network of a given number of malicious nodes, and, this is the key factor that allows us to link this analysis to the previous investigations. The intent of these malicious nodes might be, for example, to forward erroneous social information to a chosen set of nodes in the network in order to compromise the network information that this set of nodes has. With this assumption, it is still possible to evaluate the effects of transmitting/forwarding malicious information in a network.

The rest of this Section is organized as follows. In Section 3.6.1 we formalize the model under investigation. In Section 3.6.2 we describe our proposed approach, as opposed to a standard k-means clustering, to recognize groups of nodes with similar preferences. Section 3.6.3 shows the numerical results. Finally, Section 3.6.4 concludes the analysis.

3.6.1 System model

We consider a network with N nodes spread over a planar area, that are labeled with integer numbers $1, 2, ..., N$. For simplicity, we consider that neighborhood relationships of the network nodes are based on a distance criterion. In particular, we define a coverage radius r and we define two nodes to be neighbors if and only if their Euclidean distance is lower than r. Note what follows. First of all, it is not restrictive to consider a higher number of dimensions, or a different distance than the Euclidean one. Also, our distance-based criterion can be directly linked with more realistic connectivity relationships based on path-loss and signal attenuation, which ultimately depends on the distance between the transmitter and the receiver. Naturally, more realistic radio communication models would also include other effects such as shadowing and fading, and capture node interference but the results will be analogous. In other words, we do not claim that a simple unit-disc model is particularly suitable for wireless communication; it is just that the specific investigations made in this work do not critically depend on this characterization, which however, offers the advantage of representing network connectivity with a simple parameter, the coverage radius r.

The network connectivity as a graph can be represented by an N x N adjacency matrix $\mathbf{A}$, where entry a_{ij} at the ith row and jth column of $\mathbf{A}$ is equal to 1 if i and j are neighbors and 0 otherwise.

Furthermore, we assume the existence (a priori) of C non-overlapping groups of nodes, which randomly partition the set of the N nodes. For the ease of terminology, we define each of the C groups as a "cluster" or also a "color" (we will use these two terms interchangeably), so that we can see the recognition of group structure as a clustering problem or a graph coloring problem. The color of each node is assumed to be randomly and independently determined. In the following, we will also assume that all the colors are equiprobable for a node, even though this is not necessary for our procedures. The color of each node can be described by vector $\mathbf{v}$ where ith element v_i is an integer between 1 and C which is the id of i's cluster.

Colors are related by a relationship, which will be referred to as "friendship." However, this naming is just again chosen for the sake of exposition, it can actually refer to any reflexive and symmetric (but not necessarily transitive) property that can relate a pair of nodes. In particular, we assume that a node is a friend of itself, and actually all nodes of the same colors are friends. Also, the same friendship relationship (or lack thereof) is symmetric and shared by each pair of nodes with the same colors. However, it is not transitive since we allow for colors a and b to be friends with each other, as well as for colors b and c to be friends with each other, without necessarily implying that two nodes of respective colors a and c are also friends. The specific aspect of our work is that, due to mobility, this relationship among an arbitrary pair of nodes is not known in general; it is so only for neighbor nodes, and the goal of our algorithms is to infer this relationship correctly also between non-neighbors [105, 96].

Importantly, the naming of this relationship just mimics an important relationship on online social communities (alternatively dubbed as belonging to the same "circle" or "professional network") but, at least to the extent of the present work, has nothing to do with collaborative behavior among the nodes, which we assume to exist regardless of their friendship relationship; indeed, we will implicitly show that it is beneficial also for non-friend nodes to collaborate. As a possible extension of the present work, it is possible to consider a scenario where social collaboration is limited to actual "friend" nodes. However, our connection of same color nodes as belonging to the same "logical" group is entirely separate from (and actually independent of) considering "physical" relationships of neighborhood [106].

We can define a C x C symmetric matrix $\mathbf{B}$ to describe the relationships between different clusters, in particular its entry b_{fg}, with $f, g \in \{1, 2, ..., C\}$, is set to $+1$ if the nodes in cluster f and those in cluster g are friends, and to -1 otherwise. Note that actually the choice of two values representing friendship and non-friendship are arbitrary, but using $+1$ and -1 allows for a consistent mathematical representation of the remaining procedures. In particular, value 0 will be used to represent indeterminacy between the two values.

We further remark that, in order to have an interesting problem, we require that all the rows in matrix $\mathbf{B}$ are different, since otherwise there were two colors that have identical relationship with the others, and therefore can be "merged" in a single one. Also, due to the reflexive requirement, matrix $\mathbf{B}$ must have all diagonal elements equal to 1. However, these properties still leave open the characterization of $\mathbf{B}$ for the off-diagonal elements. Intuitively speaking, a case where $\mathbf{B}$ contains many elements equal to -1 is easier to manage, since it means that nodes are only friends with those of their same color and, therefore, knowing that a neighbor node is a friend is more descriptive. In the following, we will consider two different choices to determine $\mathbf{B}$. We will always consider it to be an arbitrarily determined full-rank symmetric matrix with an all-1 diagonal, but we constrain it to have either 25% or 50% of its elements equal to 1. We refer to these cases as "low inter-color friendship" and "high inter-color friendship," respectively.

Generalizing the idea behind matrix $\mathbf{B}$, we can also define an N x N matrix $\mathbf{F}$ which describes friendship between each node of the network. Specifically, we can combine the information in v and

$\mathbf{B}$ to derive every entry in $\mathbf{F}$; for example, we can notice that

$$f_{ij} = b_{v_i v_j}. \tag{3.78}$$

However, as clear from the premises, such a matrix $\mathbf{F}$ is not available. We only know a partial estimate $\tilde{\mathbf{F}}$, where non neighbor do not have a 1 or -1 at their entry. Formally,

$$\tilde{\mathbf{F}} = \mathbf{F} \odot \mathbf{A} \tag{3.79}$$

where $\odot$ denotes the element-wise scalar multiplication.

3.6.2 Proposed social communication technique

The purpose of the present work is to identify, based only on $\tilde{\mathbf{F}}$, an estimate of the full-network matrix $\mathbf{F}$ denoted as $\hat{\mathbf{F}}$. Since the real $\mathbf{F}$ is not used but it is actually known, it can be compared with its estimate $\hat{\mathbf{F}}$ by determining the Frobenius norm $||\hat{\mathbf{F}} - \mathbf{F}||_F$. However, to have a normalized value and also since we can remark that the accuracy of the diagonal elements is always 100%, we define the following estimate efficiency parameter η as

$$\eta = 1 - \frac{||\hat{\mathbf{F}} - \mathbf{F}||_F}{2N(N-1)}, \tag{3.80}$$

so that the maximum efficiency of 1 is reached when all the elements of the estimate $\hat{\mathbf{F}}$ coincide with those of $\mathbf{F}$.

A straightforward solution to our problem is to apply an out-of-the-box clustering procedure. The elements of $\tilde{\mathbf{F}}$ can indeed be seen as points in an N-dimensional space. In this sense, indeterminate points have been set to 0, which is the intermediate value between possibilities $+1$ and -1; thus, a direct application of a clustering process makes sense. For example, we can apply a k-means clustering [103], which is a standard reference technique for this kind of investigation. As a side note, however, that this choice poses some theoretical questions, especially in that it requires to know in advance the number of clusters. However, we choose it due to its widespread knowledge and since it involves, as many other cluster techniques, a direct drawback if applied to this scenario. In fact, applying such a clustering scheme would totally ignore the underlying social structure of the network, treating each row of $\tilde{\mathbf{F}}$ as a different point in the data space. We expect that the conclusions drawn for the k-means technique would be applicable also to different and possibly more sophisticated clustering procedures, such as the Chinese restaurant clustering or affinity propagation [102, 111]. Also, note clustering actually does not directly determine $\hat{\mathbf{F}}$, which would be needed to apply 3.80 but rather gives a cluster id for all the nodes, which can be seen as an estimate $\hat{\mathbf{v}}$ of vector $\mathbf{v}$, and also an estimate of $\mathbf{B}$ by considering the centroids of the k-means. These points do not generally have values equal to either -1 or $+1$, but can also have intermediate values. Thus, it is required to round them (up or down, accordingly) to the closer one. Finally, $\hat{\mathbf{F}}$ is derived, see 3.78, as

$$\widehat{f_{ij}} = \widehat{b_{\hat{v}_i \hat{v}_j}}. \tag{3.81}$$

It will be shown in the next section that the k-means clustering does not achieve a very good performance. Thus, our goal is to see whether we can improve the efficiency of group detection by considering a system in which the nodes can communicate with each other and update their current friendship estimates based on the information that the other nodes spread in the network. To this end, we develop an iterative algorithm where we set an initial matrix $\mathbf{X}^{(0)} = \widetilde{\mathbf{F}}$ and we update its entries from the information communicated by a row (representing a node disseminating its data) chosen at random, so as to obtain matrix $\mathbf{X}^{(1)}$. After that, another row of $\mathbf{X}^{(1)}$ is chosen and the iteration is repeated to obtain $\mathbf{X}^{(2)}$ and so on. In principle, this can keep going on until a matrix $\mathbf{X}^{(T)}$ is obtained

where all the elements are either $+1$ or -1. However, the evaluation of the efficiency is based on the Frobenius norm that works element-wise and can be computed even if some elements have not reached the border values. We find out that it is more convenient for computational reasons to perform a given number of iterations; generally, we can get very close to the stopping point of the algorithm even in this way, but with a faster execution time.

We propose a policy based on a social collaborative exchange of information, where we also involve the following parameters: a threshold k chosen between 0 and 1, an integer value M, which jointly determine whether to update a value or not, and finally a real positive value Δ that describes the (initial) amount of the update.

Each iteration works in the following way. We choose at random the pth row of the temporary estimate $\mathbf{X}^{(t)}$ and we update from it all other rows (i.e., the friendship estimate of all other nodes) to determine $\mathbf{X}^{(t+1)}$. By looking at $\mathbf{X}^{(t)}$, we take a generic row i and we call those nodes j for which element $\widehat{f}_{ij} = +1$ as the *sure friends* of i, and similarly we define those for which $\widehat{f}_{ij} = -1$ as its *sure enemies*. Threshold k is used to label those nodes j that at the ith row have an entry $\widehat{f}_{ij} > +k$ as *likely friends* and similarly those for which $\widehat{f}_{ij} < -k$ are said to be *likely enemies*.

Note that these are just labels used while the algorithm is running. At the beginning of the iterations, all sure friends or enemies are identified correctly since they are based on authentic values of $\mathbf{F}$. After some iterations, there is no guarantee that this labeling is correct anymore.

To decide whether a specific row q different from p can be updated, we consider the element-wise product between the pth and qth rows. The result of this product can give three different outcomes: *o1)* node q likely has the same color of node p; *o2)* node q and node p likely belong to different clusters; *o3)* there is nothing that can be said. To call the first outcome, *o1*, we must have all the sure friends of p (i.e., their corresponding entry of the pth row is equal to $+1$) are not that sure enemies of q, and also the converse relationship must hold (sure enemies of p cannot be sure friends of q). Moreover, node q cannot have a likely friend that is a sure enemy for node p, or node q cannot have a likely enemy that is a sure friend for p. If any of these conditions is violated, then the outcome is *o2*. However, we do not consider sufficient not to violate any of these condition to have outcome *o1*; for example, the element-wise product can be entirely made by zeros (if node p and q do not share any neighbors) which is of little meaning but does not violate any constraint.

In our proposed procedure, *o2* is declared as the outcome if at least one vector element is negative. Else, *o1* is declared if at least M elements of the product vector are greater than k. Otherwise, the outcome is declared to be *o3*. Only if *o1* is declared, an update is performed for the pth row of the matrix, so that every qth element, for $q \in \{1, 2, .., N\}$ whose value $\mathbf{X}_{pq}^{(t)}$ is strictly between -1 and $+1$ is added the following quantity: $\Delta \cdot \mathbf{X}_{pq}^{(t)}$. As can be observed, being $\Delta \in (0, 1)$ this operation is actually an addition if nodes p and q are friends, it is a subtraction otherwise. Also, if the updated value exceeds the absolute value of 1, it is capped to either -1 or $+1$.

The procedure can be iterated until a matrix $\mathbf{X}^{(t)}$ is obtained with only $-1/+1$ values, or when $t = T_{\max}$. Then, we set $\widehat{\mathbf{F}} = \mathbf{X}^{(t)}$. Algorithm 1 shows the pseudocode considered for our evaluations, where the algorithm ends after $T_{\max}$ updates of the matrix. Note that the input value denoted as $X(:, :, 0)$ corresponds to $\mathbf{X}^{(0)} = \widetilde{\mathbf{F}}$ and is derived from the network topology and the real nodes' colors, in particular from parameters N, r, $\mathbf{A}$, $\mathbf{B}$ as per the aforementioned unit-disc model and equations (3.78) and (3.79). The output value $X(:, :, T_{\max})$ in the pseudocode corresponds therefore to $\widehat{\mathbf{F}} = \mathbf{X}^{(T_{\max})}$.

Another possibility of applying our rationale towards an improved estimate than that obtained by clustering the raw data is to still apply a clustering algorithm, in particular, we use again the k-means procedure, but after an initial phase where social communication has improved the data. In other words, we run our proposed heuristic iterative procedure for a given number of times. We update matrix $\mathbf{X}^{(t)}$ but (regardless of whether convergence is perfectly reached or not) we apply at the end a k-means clustering algorithm. Our goal with this last strategy is to verify whether the iterative

procedure of social collaboration improves the data per se, and enables the clustering algorithm to obtain a more efficient result.

Input : $N, M, k, \Delta, T_{max}, X(:,:,0)$
Output : $X(:,:,T_{max})$
$t \leftarrow 0$
while $t \leq T_{max}$ **do**
  randomly choose $n \in \{1, 2, \ldots, N\}$
  for *every* $m \in \{1, 2, \ldots, N\} \setminus \{n\}$ **do**
    $a(:) = X(n,:,t) \odot X(m,:,t)$
    $\ell \leftarrow 0$
    for $i \in \{1, 2, \ldots, N\}$ **do**
      if $a(i) > k$ **then**
        $\ell \leftarrow \ell + 1$
      end if
      if $a(i) < 0$ **then**
        $\ell \leftarrow 0$
        break
      end if
    end for
    if $\ell \geq M$ **then**
      for *every node* i **do**
        $X(n', i, t) = X(n', i, t) + \Delta \cdot X(n, i, t)$
        if $X(n', i, t) > 1$ **then**
          $X(n', i, t) = 1$
        end if
        if $X(n', i, t) < -1$ **then**
          $X(n', i, t) = -1$
        end if
      end for
    end if
  end for
  $t \leftarrow t + 1$
end while

Algorithm 1: Pseudocode of the iterative process

3.6.3 Performance analysis

We present some numerical results, all obtained for a scenario with a square area of side equal to 100 reference units. In particular, our purpose is to compare the performance considering a system that exploits the collaborative spreading of information in the network and another that does not, and just uses the clustering on the initial data.

We set the parameters introduced in the previous sections as $k = 0.4$, $M = 4$, and $\Delta = 0.01$. These values were chosen by heuristic trial-and-error procedures. Moreover, for this comparison we assume different values for the coverage radius r, the number C of clusters, and the number N of nodes in the entire networks.

All the figures shown consider the normalized efficiency parameter previously defined and compare three different approaches: the plain k-means algorithm; the heuristic iterative procedure based on collaborative exchange of information about friendship between nodes; finally, a joint approach where

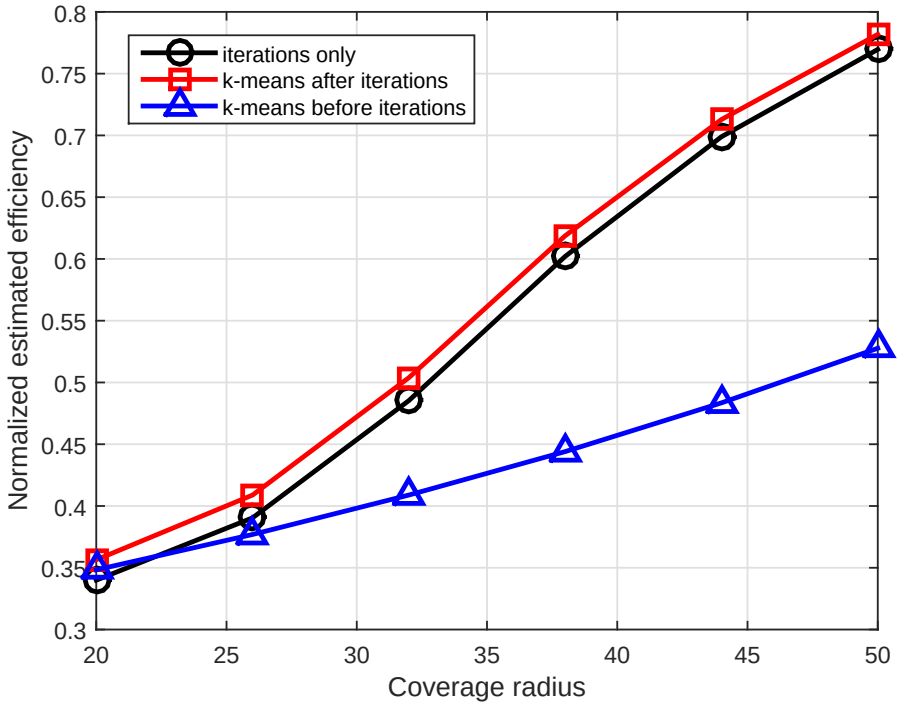

Figure 3.25: Normalized classification efficiency as a function of the coverage radius for $N = 200$ nodes, $C = 8$ colors, high inter-color friendship.

the iterative procedure is preliminary applied, and afterwards a k-means clustering is employed. Every result has been derived from a very large number of simulation runs, so that confidence intervals of the results, not shown in the plots, are extremely narrow.

Figs. 3.25 and 3.26 show the results obtained considering a network with 200 nodes, 8 clusters, and high and low inter-color friendship respectively. A general trend, found in all the results, is that an increase of the communication range r, which causes matrix $\mathbf{A}$ to become less sparse and therefore the initial estimate $\widetilde{\mathbf{F}}$ to be more similar to $\mathbf{F}$, generally improves the efficiency of the estimate; this conclusion holds true for all the three compared approaches, albeit to a different extent.

From the results, it is clearly visible that our proposed approach outperforms the standard k-means clustering by increasing the estimate efficiency. The application of the k-means algorithm in order to update again the estimate of $\mathbf{F}$ after the iterations improves the efficiency even more, albeit only slightly. Also, even though the differences are not that striking, the case with high inter-color friendship is characterized by a more difficult recognition of the clusters, especially for the k-means algorithm. In the following, we will report only results related to this case; we checked also the cases with low inter-color friendship and similar conclusions can be drawn there as well.

Fig. 3.27 allows the comparison of the results obtained changing only the number of clusters considered. Therefore, we consider not only the case with 8 clusters, but also the cases with 6 and 10 clusters. As it can be noted, considering a different number of clusters changes the corresponding efficiency value for each coverage radius. In particular, we can state that a higher number of clusters involves a lower efficiency, and therefore a higher error.

Finally, Fig. 3.28 compares the results obtained by changing the number of nodes from 200 to 500 in the network. Comparing Figs. 3.25 and 3.28, we infer that increasing the number of nodes does not significantly change the performance. Therefore, we can conclude that these algorithms are scalable with respect to the number of nodes in the network, and can be applied even to large scale scenarios

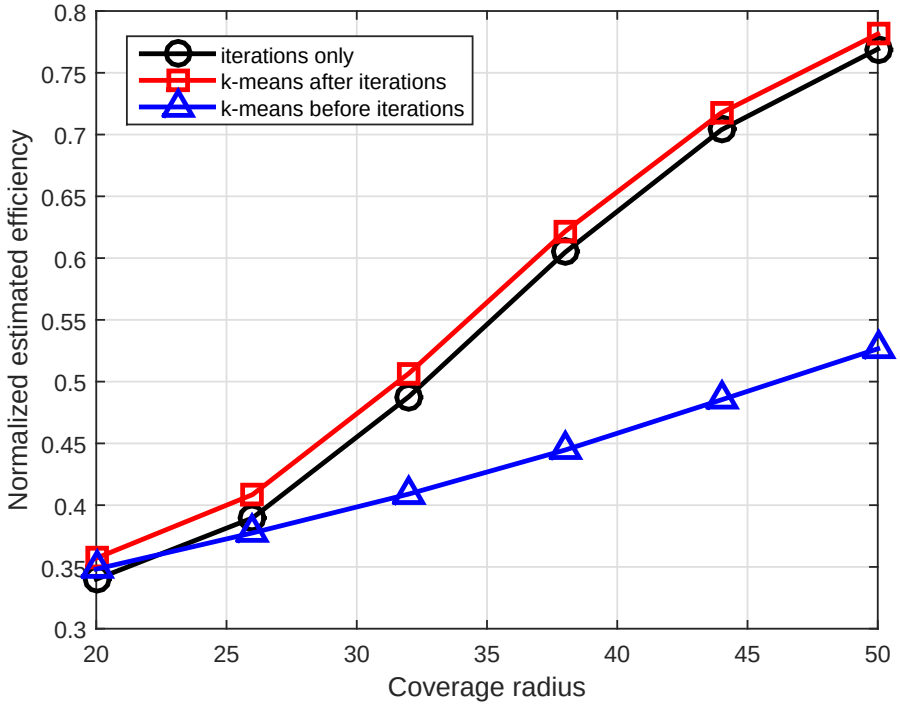

Figure 3.26: Normalized classification efficiency as a function of the coverage radius for $N = 200$ nodes, $C = 8$ colors, low inter-color friendship.

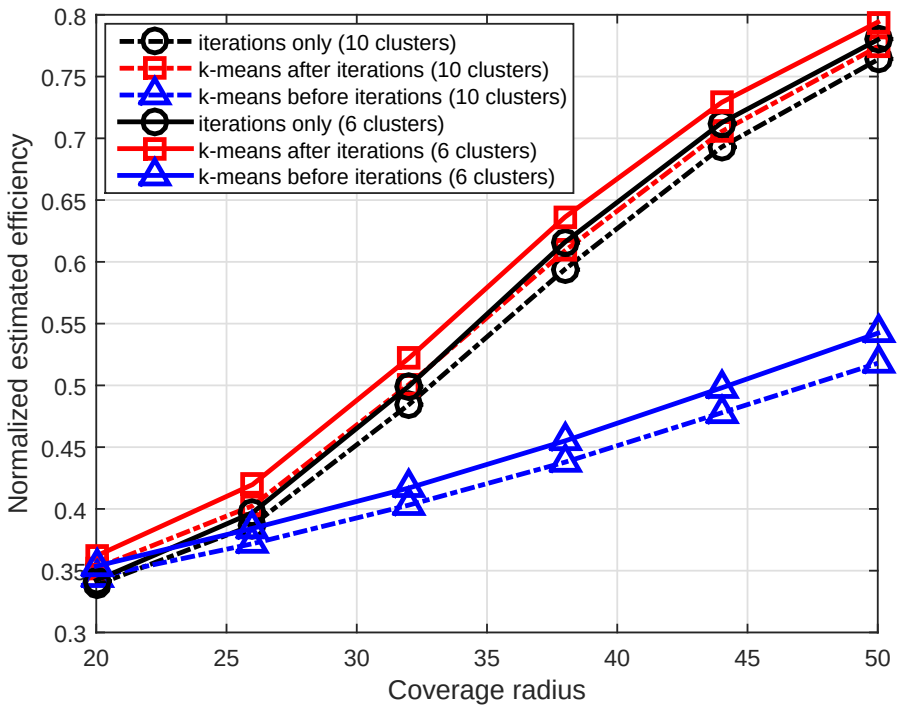

Figure 3.27: Normalized classification efficiency as a function of the coverage radius for $N = 200$ nodes, $C = 6; 10$ colors, high inter-color friendship.

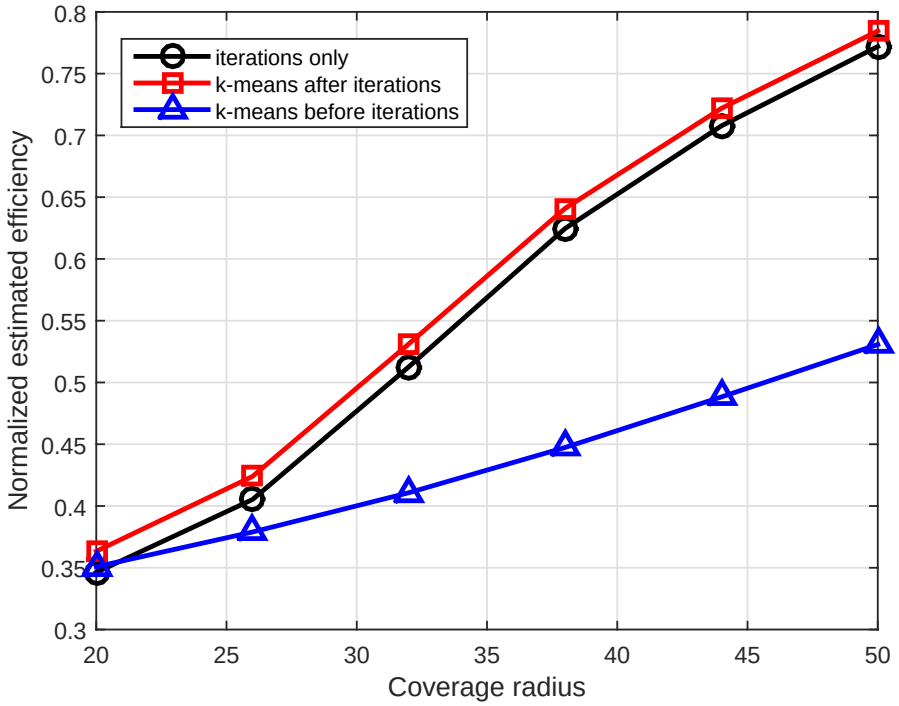

Figure 3.28: Normalized classification efficiency as a function of the coverage radius for $N = 500$ nodes, $C = 8$ colors, high inter-color friendship.

of the Internet of Everything.

3.6.4 Conclusions

We considered a problem of group detection in social mobile networks, where network mapping by each individual node is assumed to be partial, i.e., limited to its neighbors. We showed how traditional clustering procedures fail to efficiently identify the existing group structures, while a simple heuristic procedure based on the concept of social diffusion of information achieves a much higher efficiency of cluster recognition. Also, the efficiency is further enhanced by combining our proposed procedure with a standard clustering technique.

The work reports preliminary results related to a standard k-means clustering technique and a simple heuristic approach, since the purpose is to show the benefit of social communication. More results can be shown also exploring the parametric dependence of the inner values of the proposed technique (e.g., the update step Δ or threshold k). Future developments also include the evaluations of more sophisticated clustering techniques, especially avoiding the need of k-means clustering to know the number of colors in advance (an element that is, however, not required by our proposed original approach).

Moreover, different heuristic approaches can surely be investigated. While keeping the same rationale of a social communication where nodes collaboratively exchange information about their relationship so as to inform distant nodes, more complex techniques can be thought of, especially exploiting the inherent characteristics of the assumed friendship relationship. For example, contradictions in the self-declared friendship (node i reports being a friend of node j while node j reports the opposite about node i) should be identified and resolved.

Finally, the logical relationship of collaboration is (intentionally) kept separate from routing aspects and friendship connections. However, one can think of applying the same rationale to scenarios where

these aspects are interconnected, i.e., for example nodes only forward data coming from their friends, or they may even disseminate false or malicious information about their enemies. All these open challenges demonstrate the importance of this kind of quantitative investigations to realize efficient mobile Internet paradigms.

Chapter 4

Novel applications of Network Science

In this Chapter we give an overview of the future research interests. In particular, we continue the investigation by means of game theoretic approaches with particular reference to mobile computing scenarios. However, we also discuss some guidelines representing an effort to start a new research path where a telecommunications point of view might be used to deal with problems not directly related to telecommunications networks. In more details, one of our future aim is to study the brain connectivity using concepts and methods commonly related to an information technology background according to the basic principles of the Network Science.

4.1 A Bayesian game theoretic approach to task offloading in edge and cloud computing

The growing complexity of data analysis and processing algorithms makes their deployment in resource constrained devices (*e.g.*, sensors and mobile devices) increasingly challenging. The recent fog and edge computing paradigms [115] address this issue by placing compute-capable devices within low-latency one-hop wireless topologies.

Offloading local computation tasks to the edge processors can significantly speed-up their completion, but necessitates to transport the data over local wireless networks. Especially in modern architectures, where multiple technologies share the same spectrum resource, interference from exogenous wireless terminals, or from other mobile users offloading tasks, may heavily affect the capacity of the wireless links, so that the delivery of data to edge or cloud processors becomes a relevant component of the overall delay to completion.

Herein, we analyze a three-tiered communication/processing infrastructure, consisting of a local tier of mobile nodes, a middle tier of nearby computing nodes (i.e., edge servers), typically co-located with the wireless Base Stations (BS) and characterized by a limited amount of processing resources, and a remote tier of cloud servers connected to the BS through the core wired network. The mobile users can choose to locally process the data, or offload computation to edge or cloud resources. If the mobile devices decide to offload the processing task either to the edge or cloud server, then the associated data need to be transmitted over the local wireless network. As the wireless links have finite capacity, this first step introduces a delay, but also a coupling between the users, as the decision to offload the processing task of one user increases the network load and, thus, the delay to the completion of the task of all the other users.

The main challenge is that in practical cases, mobile users do not have a priori knowledge of the interference load and computation power of edge and cloud processors. Additionally, the decision of each mobile device influences the overall network load. In fact, unlike in-device processing, if a mobile user offloads a computational task to the edge or cloud resources through the BS, it creates interference that reduces the capacity of the wireless links of the other users.

To model and optimize this distributed decision making process with partial information, we propose a game theoretic framework. Specifically, due to the stochastic characterization of some of the influential variable of the system, such as exogenous interference load and channel gain, we adopt a Bayesian Game (BG) formulation. Each user can decide if locally execute the task on its mobile device, or offloading the task computation towards either the remote cloud or an edge server through the BS. The objective of each user is to minimize its computation cost, evaluated both in terms of computation time and energy needed to accomplish the task execution.

Under this game-theoretic analysis, we characterize the equilibrium for different parameter regions, as well as evaluate the impact of selfish actions by the users. Our result indicate that the uncertainty on network parameters of the other players can actually be beneficial to the overall social welfare as it deters users to aggressively cause interference to others, which would result in a low-efficiency equilibrium. This suggests that preventing the users from gaining information about the other nodes in the network may actually be a good strategy to avoid that the offloading option is abused by the terminals.

As already pointed out, game theory is a tool from applied mathematics that has been widely used to study how rational players, whose objective is usually seen as the maximization of a *utility function*, interact to determine an equilibrium point. In the context of network communication, this can be seen as the problem to obtain a distributed resource allocation procedure upon which nodes, seen as individual agents, agree. Recently, there has been soaring interest in this kind of applications to wireless communication and networking scenarios [116]. For instance, in [117] a game theoretic model for random access with carrier sensing is investigated. Games for resource management, network selection, and admission control in wireless systems were studied in [118, 119]. In [120], the authors investigate opportunistic communications in hierarchical cognitive networks. Finally, evolutionary coalition games for wireless networking and communications were studied in [121]. A comprehensive literature review of game theory formulations for energy efficiency in wireless sensor networks can be found in [122].

Closely related to this contribution, [123, 124] consider offloading problems and propose techniques to determine which tasks should be offloaded to improve the overall system performance. Most of the formulations presented in those papers focus in a single node scenario, where an application is represented as a weighted graph, whose nodes are tasks.

To the best of our knowledge, a relatively small number of contributions addressed a multi-users scenario in the context of edge and cloud computing. In [127], the authors propose a cooperative centralized optimization problems aiming at distributing the processing tasks of multiple users among the computation resources available locally at the mobile devices and globally at the cloud level. The objective is to minimize the average application delay for all users. A Mixed Integer Linear Programming formulation is used. In [128], the problem of distributing computation resources among data streams is studied. Multiple users share the wireless network as well as the computation resources in the cloud. The goal is that of maximizing the throughput of the data streams. Different from the present contribution, a heuristic genetic algorithm is used to solve the optimization problem, and a two-tier architecture composed of mobile users and remote cloud servers is considered.

Analogous to that adopted here, [125, 126] considers a three-tier architecture with multiple mobile users. The authors assume that the cloud resources are constrained. The optimization problem is solved using a greedy centralized heuristic. In [129], a three-tier architecture with no centralized control is studied, and game theory is used to study a scenario where multiple selfish users whether and where to offload their computation tasks. Different from our study, a non-cooperative, and non-Bayesian, formulation of the game is used, and there is no consideration of the interactions between the users from a wireless communications standpoint. In other words, all of the previous papers applying game theory to this scenario apparently do so from an idealized perspective where network nodes not only avoid causing congestion to each other but also are fully and instantaneously aware of

all the network parameters and can therefore make fully-informed rational (that is, selfish) decision. This aspect is particularly relevant for what concerns the contribution of the present work, since, as will be shown in the following, the Bayesian component of the game, used to determine incomplete information available to the users, actually lead to an improvement in the overall resulting efficiency of the allocation, an aspect related to the fact that selfish users only act for their own good.

The rest of the Section is organized as follows. Sub-section 4.1.1 and Sub-section 4.1.2 describe the system model and provide a game theoretic analysis, respectively. Numerical results and computation of the equilibria are presented in Sub-section 4.1.3. Sub-section 4.1.4 concludes the Section.

4.1.1 System model

We consider a scenario where a set of M mobile devices indicated as n_i, $i \in \{1, 2, .., M\}$, are connected to a BS s providing access to the global network infrastructure. The BS is attached via a high capacity link to an edge processor, which provides low-latency computation services to the users. The BS is also connected to a more powerful cloud computing resource through the Internet.

We assume that each user has a computationally intense task to be completed. A three-tier architecture is considered, where user can decide to compute the task locally in-device or to offload the task to the edge or cloud servers. We define a quasi-static scenario, in which the set of mobile device users remains unchanged for a period comparable to the completion of their tasks. We leave to future studies the analysis of scenario case where mobile users can depart and leave dynamically.

The mobile device users share the wireless channel to the BS s. $\mathcal{C}_{n_i} = (b_{n_i}, d_{n_i})$, $i \in \{1, 2, .., M\}$, describes the computation task of the node n_i, where b_{n_i} and d_{n_i} are the size of the input data and the total number of CPU cycles necessary to complete the task $\mathcal{C}_{n_i}$.

We denote the computation offloading decision of mobile device user n_i as a_{n_i}. Specifically, $a_{n_i} = 0$ if n_i computes the task locally, $a_{n_i} = 1$ if n_i offloads the computation task to the remote cloud server, finally, $a_{n_i} = 2$ if n_i offloads the computation task to the edge server. The vector $\mathbf{a} = (a_{n_1}, a_{n_2}, .., a_{n_M})$ is the decision profile of the mobile device users.

Since the users share the wireless resource, we adopt an interference model to capture the degradation of individual user links when other transmissions are active. In particular, we define the uplink data rate of n_i, i.e., r_{n_i}, as

$$r_{n_i} = W log_2 \left(1 + \frac{q_{n_i} g_{n_i}}{\omega_0 + \mathcal{I}}\right) \tag{4.1}$$

where $\mathcal{I} = \sum_{n_j \in \mathcal{M} - \{n_i\}} q_{n_j} g_{n_j} I\{a_{n_i}, a_{n_j} \in \{1, 2\}\}$, W is the channel bandwidth, q_{n_i} is n_i's transmission power, g_{n_i} is the channel gain between n_i and s, ω_0 is the background noise power, and $I\{a_{n_i}, a_{n_j} \in \{1, 2\}\}$, with $i, j \in \{1, 2, .., M\}$, is the indicator function representing the interference from the other user conditioned on its transmission decision.

We define $f_{n_i}^{LC}$, $f_{n_i}^{EC}$, and, $f_{n_i}^{CC}$, as the computation capability measured in terms of CPU cycles per second of the mobile devices, the computation capability assigned by the edge server to n_i, and the one assigned by the cloud, respectively. We assume that $f_{n_i}^{EC} < f_{n_i}^{CC}$. If n_i decides to locally compute C_{n_i}, the computation execution time is $t_{n_i}^{LC} = \frac{d_{n_i}}{f_{n_i}^{LC}}$. On the other hand, if n_i offloads the computation task it would incur the extra overhead for transmitting the input data either to the edge server or remote cloud through the wireless access behind the time needed to execute C_{n_i}.

To assess the offloading decision, we define two cost metrics corresponding to the time and energy consumption to complete the task execution. In particular, the total time to complete the task in the edge and cloud computing are

$$t_{n_i,off}^{EC} + t_{n_i,exe}^{EC} = \frac{b_{n_i}}{r_{n_i}} + \frac{d_{n_i}}{f_{n_i}^{EC}} \tag{4.2}$$

and

$$t^{CC}_{n_i,off} + t^{CC}_{n_i,exe} = \frac{b_{n_i}}{r_{n_i}} + D_i + \frac{d_{n_i}}{f^{CC}_{n_i}}, \tag{4.3}$$

where D_i is the delay caused by propagating the data through the wired data transmission to the cloud server.

If the task is completed locally, the energy expense is equal to $e^{LC}_{n_i} = \alpha_{n_i} d_{n_i}$, where α_{n_i} the consumed energy per CPU cycle. If the task is offloaded to the edge server, then the energy consumption is $e^{EC}_{n_i,off} = q_{n_i} \frac{b_{n_i}}{r_{n_i}} + L_{n_i}$, where L_{n_i} denotes the tail of the transmission energy due to the fact that the mobile device user will continue to occupy the channel for a while even after the data transmission. Finally, for the offloading towards the remote cloud we assume that $e^{CC}_{n_i,off} = q_{n_i} \left(\frac{b_{n_i}}{r_{n_i}} + D_i \right) + L_{n_i}$.

Consequently, we define the computation cost for each of the three possible computing decisions as

$$\begin{aligned} K^{LC}_{n_i} &= \lambda^t_{n_i} t^{LC}_{n_i} + \lambda^e_{n_i} e^{LC}_{n_i}, \\ K^{EC}_{n_i} &= \lambda^t_{n_i} \left(t^{EC}_{n_i,off} + t^{EC}_{n_i,exe} \right) + \lambda^e_{n_i} e^{EC}_{n_i,off}, \\ K^{CC}_{n_i} &= \lambda^t_{n_i} \left(t^{CC}_{n_i,off} + t^{CC}_{n_i,exe} \right) + \lambda^e_{n_i} e^{CC}_{n_i,off}. \end{aligned} \tag{4.4}$$

$\lambda^t_{n_i}, \lambda^e_{n_i}$ are positive weights in the continuous range $[0, 1]$ associated with the computational time and energy for n_i. The weights can be adapted to the state of the devices. For instance, if a mobile user's battery is close to depletion, $\lambda^e_{n_i}$ can be set to 1 and $\lambda^t_{n_i}$ to 0. Instead, when the tasks generated by a mobile device are delay-sensitive, then the delay can be set to $\lambda^t_{n_i} = 1$ and $\lambda^e_{n_i} = 0$. We neglect in our analysis the time needed to receive the outcome of processing. This component is typically smaller compared to cost of transporting the data due to the smaller size of feedback, but can be easily added to our metrics.

4.1.2 Bayesian game theoretic approach

In game theory, *players* perform actions purely based on their individual interests, which may differ from those of the other players [72]. Each player usually acts towards the maximization of its own utility; however, this is jointly determined by the actions played by all players. Throughout this Section, for readability reasons, we will actually consider an individual *cost* function that the players try to minimize; therefore, the same reasoning of classical setups apply but to consider a "utility function" or a "payoff" one should take the opposite value to what we consider here. Thus, in a first place we consider a *static game of complete information* as defined by a triple $\mathcal{G} = (\mathcal{A}, \mathcal{S}, \mathcal{K})$, where $\mathcal{A}$ is the set of players, $\mathcal{S}$ is the set of all strategies allowed to the players, and $\mathcal{K}$ is a set of cost functions, one per each user, depending on the strategies chosen by the players. Note that this reflects that a player's chosen strategy influences the cost paid by the other players; at the same time, rational players are in turn able to anticipate the effect of the strategies chosen by the other players. We search for a Nash Equilibrium (NE) seen as a joint strategy profile where all players locally minimize their paid cost.

However, we will also focus on a Bayesian game, i.e., a game of incomplete information in which rational anticipation of the game outcome made by the players is hindered by the lack of precise knowledge of the cost function of the other players. This is usually modeled by introducing a *type* for the players, which in turn translates in a different cost function; in our case the type will be given by a specific parameter that affects the transmission costs, and specifically we will consider the node distance from the BS as this parameter. Players are clearly aware of their own type, but as for the others they can only treat them as random variables; still, they can exploit a prior distribution on the other players' types, that is common knowledge. Note that this description is more accurate to describe mobile computing systems where many parameters such as the channel gain, can only be estimated but never known with certainty. Even though a mobile user can reasonably well estimate

its own channel gain, it is simplistic to assume that it knows with perfect precision that parameter for the other players; thus, a Bayesian setup is definitely more realistic.

In our scenario, we consider two mobile devices corresponding to the set of players, i.e., $\{n_1, n_2\}$. The set of actions for each player is {Local, Cloud, Edge}, where Local, Cloud, and Edge are associated with executing the task locally on the device, offloading the computation task to the remote cloud, and offloading the task execution to the edge server, respectively. Each player acts towards the minimization of its computation cost.

For the sake of simplicity, we consider a symmetric system, where all the following parameters are the same for both users (and thus we drop subscripts "n_1" and "n_2" for better readability: q, b, α, f^{LC}, f^{EC}, f^{CC}, λ^t, λ^e. Moreover, we assume L_{n_1} and L_{n_2} to be negligible.

In the Bayesian context, each player has a type defined by its corresponding channel gain, whose value is not known to its opponents. However, we assume that the prior distribution of the types is known, for instance based on historical data accumulated at the edge processor. Types of player 1 and 2 are channel gains g_{n_1} and g_{n_2}, respectively. In the literature, multi-path propagation is usually considered and modeled, e.g., as Rayleigh fading. For the sake of simplicity, we evaluate the channel gain as determined by path loss only, i.e., $g_{n_i} = \delta(n_i, s)^{-\gamma}$, for $i \in \{1, 2\}$, where $\delta(n_i, s)$ is the distance between n_i and s, and we choose exponent $\gamma = 4$ to describe a sub-urban scenario. We assume that distance $\delta(n_i, s)$ is uniformly distributed in $[\delta_{min}\ \delta_{max}]$. This assumption is made only to simplify the computations in what follows (especially to determine the Bayesian NE) but the conclusion we draw are actually valid as long as there is any kind of uncertainty on the channel gain. In particular, note that none of our conclusions are limited to the choice of uniform distribution for the positions and/or only considering the path loss in the evaluation; those are choices that can easily be relaxed and would just lead to more complex computations with analogous conclusions. Also for notational brevity, put

$$A = \frac{b}{W \log_2\left(1 + \frac{q g_{n_i}}{\omega_0 + q g_{n_j}}\right)} \tag{4.5}$$

$$B = \frac{b}{W \log_2\left(1 + \frac{q g_{n_i}}{\omega_0}\right)}. \tag{4.6}$$

Now, the cost paid by the two players depending on their moves can be directly written. Specifically:

– if both players choose Local, they both incur a cost equal to $\lambda^t \frac{d}{f^{LC}} + \lambda^e \alpha d$;

– if both players choose Cloud, their cost is also the same: $\lambda^t \left[A + D + \frac{d}{f^{CC}}\right] + \lambda^e \left[q\,(A + D)\right]$;

– if both players choose Edge, their identical cost is: $\lambda^t \left[A + \frac{d}{f^{EC}}\right] + \lambda^e q A$;

– if one player chooses Local and the other Cloud, then the cost paid by the former is $\lambda^t \frac{d}{f^{LC}} + \lambda^e \alpha d$, instead for the latter $\lambda^t \left[B + D + \frac{d}{f^{CC}}\right] + \lambda^e \left[q\,(B + D)\right]$;

– if one player chooses Local and the other Edge, then the cost paid by the former is $\lambda^t \frac{d}{f^{LC}} + \lambda^e \alpha d$, instead for the latter $\lambda^t \left[B + \frac{d}{f^{EC}}\right] + \lambda^e q B$;

– if one player chooses Cloud and the other Edge, then the cost paid by the former is $\lambda^t \left[A + D + \frac{d}{f^{CC}}\right] + \lambda^e \left[q\,(A + D)\right]$, instead for the latter $\lambda^t \left[A + \frac{d}{f^{EC}}\right] + \lambda^e q A$.

Importantly, the value of channel gain g_{n_i} in the numerator of (4.1) is known to player i. Conversely, the term g_{n_j} at the denominator is not known to player i as it represents the type of player j. In this Bayesian setup, we aim at the evaluation of the expected costs computed weighing the costs defined above with respect to the distribution of types. Before proceeding with the Bayesian evaluations, some considerations arisen from the complete knowledge case follow. In this case, we assume that players have complete knowledge of the system, meaning that each of them knows its opponent's type.

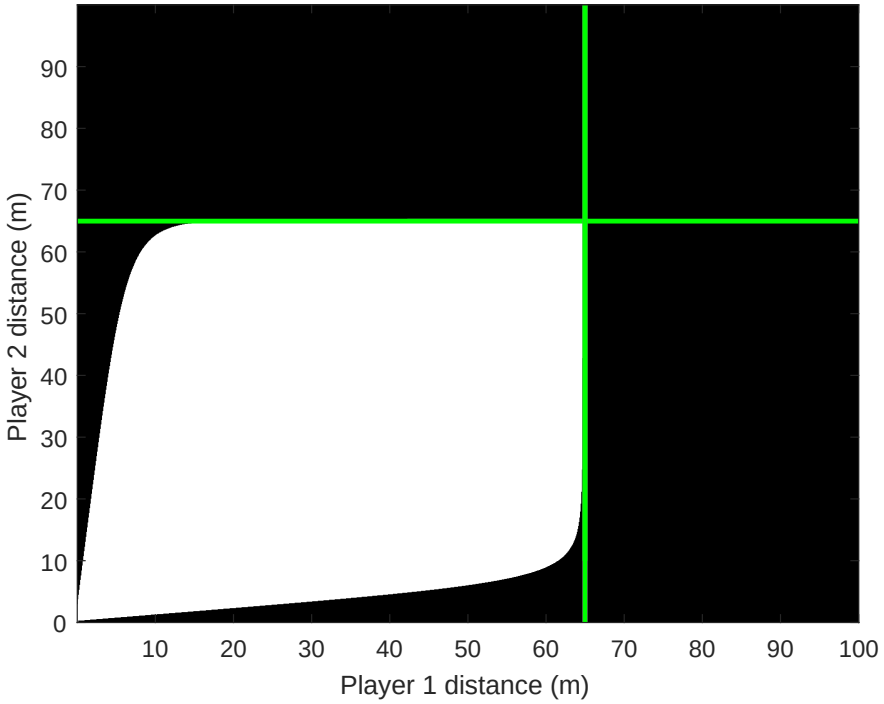

Figure 4.1: Validity regions for NEs.

For symmetry reasons, a NE in pure strategies must be to one of the three outcomes (Local, Local), (Cloud, Cloud), and (Edge, Edge), where the first action in the brackets refers to player 1 and the second to player 2. Moreover, a relationship between the value of D and the two outcomes (Cloud, Cloud) and (Edge, Edge) has been observed. If and only if $D < D_{thr}$, where

$$D_{thr} = \frac{d(f^{CC} - f^{EC})}{f^{CC} f^{EC}(1 + \Lambda q)}, \tag{4.7}$$

then (Cloud, Cloud) has lower computation cost than (Edge, Edge). Thus, we can compare possible outcome (Local, Local) with the "non-local" outcome (N,N) where N can stand for either "Cloud" or "Edge" depending on (4.7).

4.1.3 Equilibrium and Numerical results

We now consider a system with specific parameter choices reported in Table 4.1. According to the table, $\delta(n_i, s)$ is uniformly distributed between $\delta_{\min} = 10$ m and $\delta_{\max} = 100$ m. Moreover, we considered D in [4 13]ms.

First of all, we consider a baseline solution of the game with *complete* information, against which we assess the performance of our Bayesian setup. According to what discussed previously, rational players in this setup end up in playing a symmetric outcome. To determine whether in this scenario the players will eventually both play the Local strategy or strategy "N," we remark that the game is isomorphic to a Prisoner's dilemma [72]; however, the choice of which one of the symmetric allocations is the Nash equilibrium (and whether this is also Pareto efficient) depends on the channel gain, and in turn on the distances. Thus, we numerically computed the resulting equilibrium for all the possible values of $\delta(n_1, s)$ and $\delta(n_2, s)$. We recall that we are under the assumption of *full knowledge* on both users of their mutual positions, so both values are known to both players. The result is shown in Fig.

Table 4.1: Values of relevant parameters

Parameters	**Values**
b	40 kBytes
d	10^9 CPU cycles
f^{LC}	0.5 GHz
f^{EC}	10^2 GHz
f^{CC}	10^4 GHz
q	0.01 W
ω_0	5 μ W
W	1 GHz
λ^t	0.5
λ^e	0.5
α	4
g	30^{-4}
$\delta(n_i, \text{s})$	U([10 100] m)

4.1: the figure reports, for all pairs $(\delta(n_1, s), \delta(n_2, s))$, what would be the NE of rational (i.e., selfish) players, with the black region corresponding to the choice of locally executing the computation task, and the white region representing task offloading towards either the cloud or edge server, according to D.

Aside from some border effects, we can infer that a threshold behavior is present, meaning that the players will offload their computation only if they are close enough to the BS. Such a threshold δ^{thr}, which can be numerically computed (see later Fig. 4.2) to be around 65 meters, is also plotted in the figure. The presence of this threshold is not coincidental, as we will show next.

For the Bayesian case, it is possible to prove that a threshold behavior is indeed present, according to the following reasoning. Player i does not know whether player j is actually playing an offloading move; nevertheless, i may get a Bayesian belief that j will be playing according to a threshold strategy (meaning that j will offload only if close enough to the base station). Actually, this is the kind of self-enforcing assumption that automatically gets confirmed due to the symmetry of the players, and it is also easy to see that this threshold strategy would be the best response to itself. Hence, in Bayesian game terms, this is a Bayesian NE. Note that a similar reasoning has been formally proven in Section 3.2 of the present thesis.

This remark can serve to compute the expected cost obtained by the players in the Bayesian case. In particular, for each player i, if $\delta(n_i, s) > \delta^{thr}$, player i will decide for the local computation of the task execution, choosing offloading otherwise. The actual value of the threshold δ^{thr} can be found by imposing symmetry between the two outcomes as NEs, and therefore considering: $\delta(n_1, s) = \delta(n_2, s)$ and also that the cost of local computation is exactly equal to offloading. The value of δ^{thr} can be precisely found in this way.

Consequently, for the computation of the Bayesian expected cost we need to sum 4 different contributions denoted as K_1 – K_4. Specifically, looking at Fig. 4.1 and considering for example player 1, they are:

$$K_1 = \int_{\delta_{min}}^{\delta^{thr}} \int_{\delta_{min}}^{\delta^{thr}} \left(\lambda^t \left[A + D + \frac{d}{f^{CC}} \right] + \lambda^e \left[q(A+D) \right] \right) \mathrm{d}x \mathrm{d}y$$

if $D < D_{thr}$,

$$K_1 = \int_{\delta_{min}}^{\delta^{thr}} \int_{\delta_{min}}^{\delta^{thr}} \left(\lambda^t \left[A + \frac{d}{f^{EC}} \right] + \lambda^e q A \right) \mathrm{d}x \mathrm{d}y$$

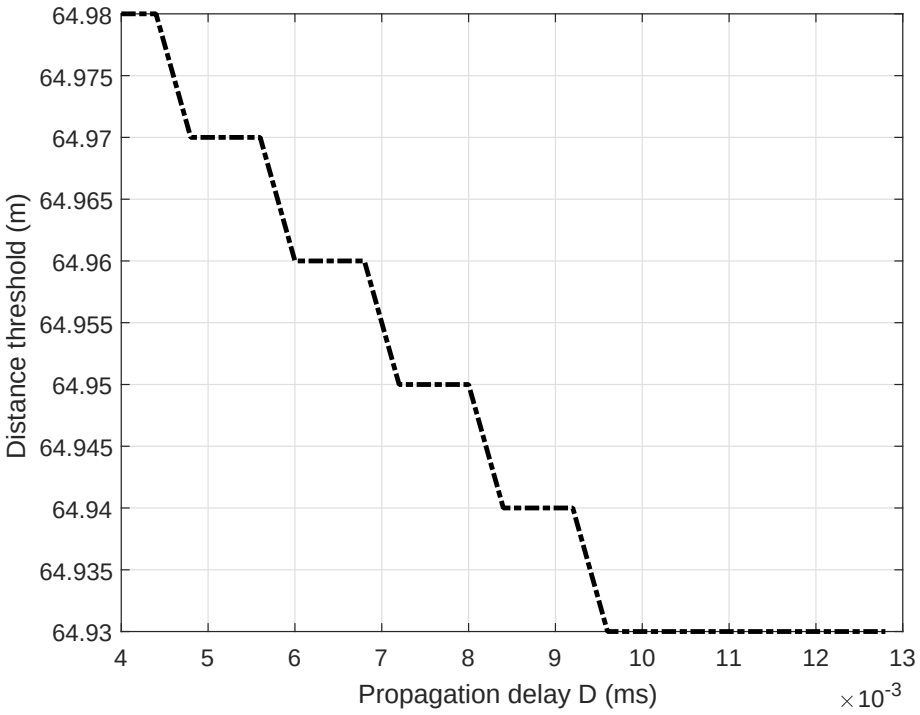

Figure 4.2: δ^{thr} development varying D.

otherwise,

$$K_2 = \int_{\delta_{min}}^{\delta^{thr}} \int_{\delta^{thr}}^{\delta_{max}} \left(\lambda^t \frac{d}{f^{LC}} + \lambda^e \alpha d \right) \mathrm{d}x\mathrm{d}y$$

$$K_3 = \int_{\delta^{thr}}^{\delta_{max}} \int_{\delta^{thr}}^{\delta_{max}} \left(\lambda^t \frac{d}{f^{LC}} + \lambda^e \alpha d \right) \mathrm{d}x\mathrm{d}y$$

and

$$K_4 = \int_{\delta^{thr}}^{\delta_{max}} \int_{\delta_{min}}^{\delta^{thr}} \left(\lambda^t \left[B + D + \frac{d}{f^{CC}} \right] + \lambda^e \left[q(B+D) \right] \right) \mathrm{d}x\mathrm{d}y$$

if $D < D_{thr}$,

$$K_4 = \int_{\delta^{thr}}^{\delta_{max}} \int_{\delta_{min}}^{\delta^{thr}} \left(\lambda^t \left[B + \frac{d}{f^{EC}} \right] + \lambda^e q B \right) \mathrm{d}x\mathrm{d}y$$

otherwise. Player 1 expected cost is given by $K_1 + K_2 + K_3 + K_4$. Player 2 expected cost can be evaluated in a similar way.

Fig. 4.2 shows how the distance threshold δ^{thr} varies considering several D's values. Figs. 4.3 and 4.4 depict player 1's cost considering the complete knowledge case and player 1 expected cost, respectively, as a function of D. In general, we can observe that as D increases, the computation cost increases until it reaches a saturation value. When the value of D is small enough (i.e., $D < D_{thr}$), the best action for the mobile device is to offload the task execution to the remote cloud instead of the edge server as the additional delay is compensated for by the larger computation speed. When the threshold D_{thr} is reached, the best action is to offload to the edge server. However, it is relevant to notice that the Bayesian case implies that the nodes incur a *lower* cost when they have imperfect knowledge on the distance of the other player. The reason for this apparently counterintuitive behavior is a consequence of multi-agent multi-objective optimization performed via game theory. Recalling that different users

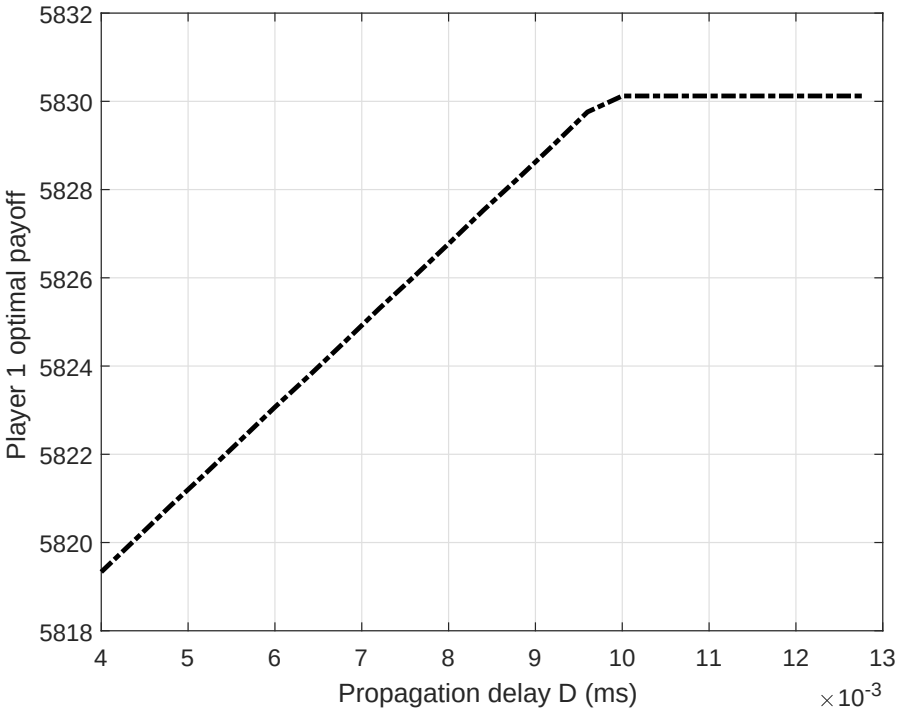

Figure 4.3: Player 1 cost in a complete knowledge scenario varying D.

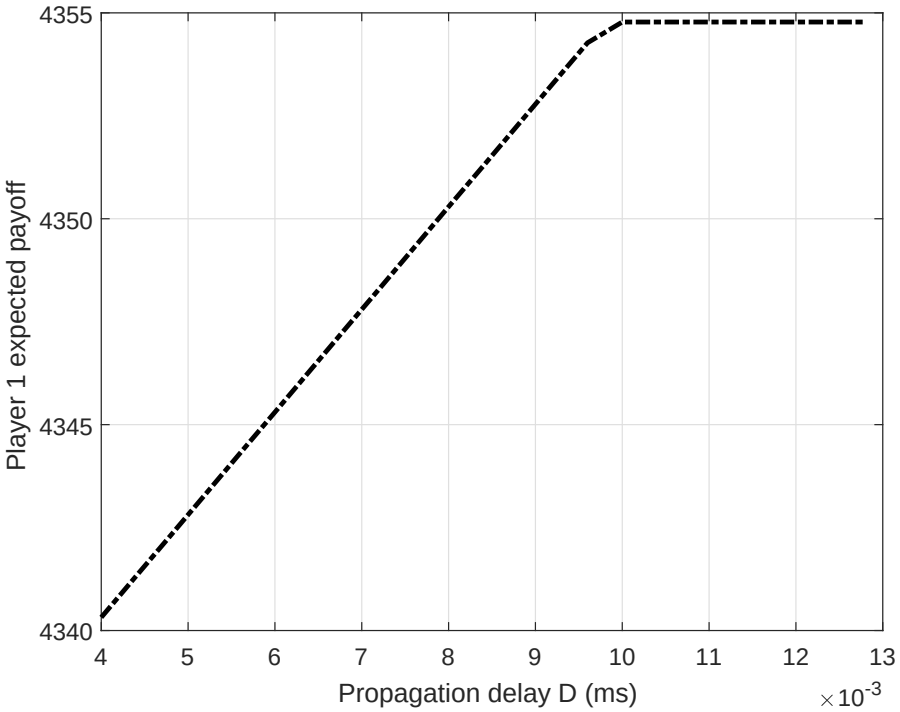

Figure 4.4: Player 1 expected cost varying D.

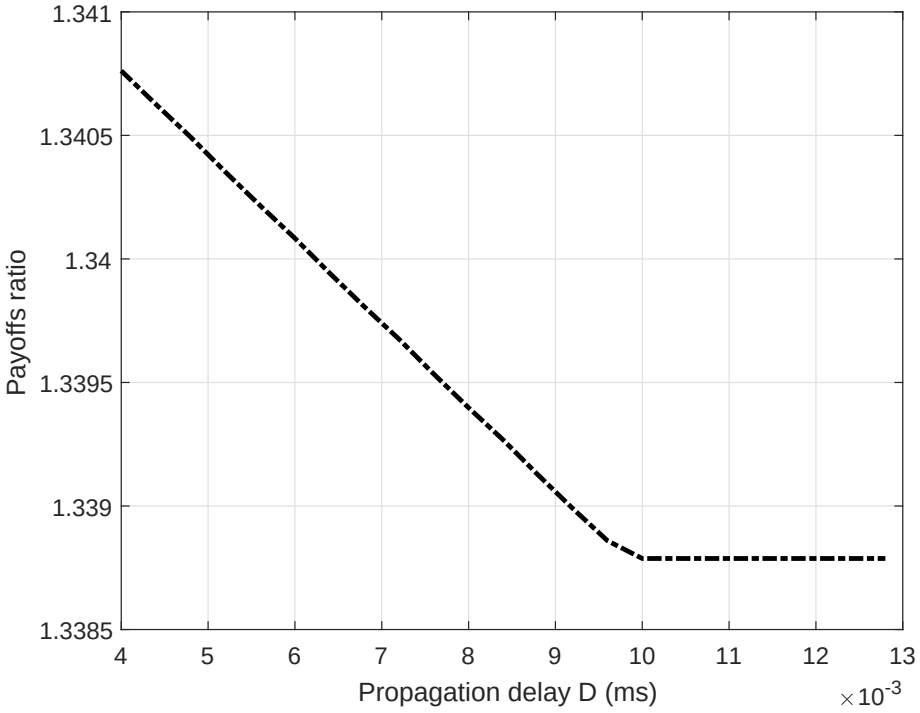

Figure 4.5: Ratio between player 1 optimal cost and player 1 expected cost varying D.

have a different objective in the game (i.e., minimization of their individual cost in a selfish way), the "ignorance is bliss" principle applies [72]. Differently from single-person optimization, where more knowledge always corresponds to a better outcome, in a game theoretic setup having less information about the other players may turn out, as in this case, to be advantageous, as players will be less aggressive and do not tend to abuse offloading if they are not sure that the other player is doing it too. Given the symmetry of the setup, it turns out that the best course of action for the players may be to abstain from unnecessary (or harmful for the other player) offloading operations.

Fig. 4.5 evaluates this further by considering the ratio between the ideal scenario with full knowledge and the expected cost in the Bayesian setup. Again there is a dependance on D that keeps increasing until a ceiling level is hit. In general, in the complete knowledge case, each player i knowing the opponent j distance $\delta(n_j, s)$ decides to offload the computation task only when this choice represents a NE, i.e., (Cloud, Cloud) or (Edge, Edge). In the Bayesian case, player i does not know $\delta(n_j, s)$, as a consequence, it might happen that it decides to offload the computation task even if the other player j choice is to locally execute its own task. In this way, player i has a lower computation cost. Indeed, the pairs of actions (Cloud, Local), (Edge, Local), (Local, Cloud), and (Local, Edge) give a lower computation cost with respect to (Local, Local) for the player that is choosing the task offloading. These asymmetrical pairs are not considered in the optimal case since they do not represent NEs, however they might arise in the Bayesian case due to the uncertainty on the players' distances from the BS.

4.1.4 Conclusions

We applied Bayesian game theory to a network scenario where mobile users can offload computations task to edge or cloud resources. Our objective was to make efficient offloading in a scenario where the mobile devices are unaware of the network load and mutual interference reduces the capacity of the wireless links connecting to the local base station. Numerical results illustrate regions where the

strategy of the devices converges to different points of equilibrium.

The remarkable finding of our analysis is that a Bayesian scenario, i.e., with imperfect information, actually achieves better welfare (or lower social cost) than one with full knowledge by the users. This is due to the competitive nature of the game, where selfish rational users would try offloading computational task even when it is not efficient for the entire network that they do so. Our results suggest an interesting guideline in the design for offloading strategies, i.e., to make network parameters less known to the users in order to improve their cooperative participation to resource sharing. However, it is worth underlining that this is only a preliminary study concerning this topic. It might be thought to empower the described analysis considering more sophisticated game theory approaches taking into account, for example, the human aspect behind the mobile device. This can be done by means of evolutionary games according to which the actions choices are influenced by the dynamics of the system in terms of what the other agents in the system may think that is the best choice to do. In this way, the dynamics of the system changes towards the direction of choosing, for example, the most popular action, i.e., the action that has been more frequently chosen.

Moreover, a combination of reinforcement learning, in particular dynamic programming, and game theory can be considered as well using the former to investigate on the internal system dynamics and define the set of possible policies by means of the latter.

4.2 Brain network analysis

In the literature, it can be found several examples of network structure analysis related to the nature of the living beings in terms of complex network. One of these is the cells network structure with particular reference to the investigation on the behaviors and interactions of the cells [133]. Above all, in the last years there has been an exponential increase in human neuroscientific research due to the extensive availability of non-invasive techniques for measuring brain activity and structure, such as neuroimaging and neurophysiological recordings, producing large datasets of spatio-temporal data. It is generally accepted by the scientific community that the brain can likely be modeled as a complex network and descriptions of the relationship between the brain system and a complex network are available in the literature.

One of the directions of our future path of investigations is related to the concept of *bio-inspired networking* according to which biological systems and network processes have similar interesting characteristics. As a consequence, it is possible to use solutions inspired by biological system for different networking paradigms associated to similar problems developed in the biological field and vice versa. The objective on which bio-inspired networking is based is to capture the dynamics and understand the fundamental characteristics of biological systems to design new methods and tools to manage communication systems and information networks. These must be suitable for dynamic environments that are able to self-management and that can easily evolve.

In this context, it is first necessary to determine the common aspects between the biological system and the computational (or network) system. Then, the model capturing the biological behavior can be designed, later, if needed, simplified and conformed to the system on which the analysis focuses. In the literature, we can find different examples of this kind of approach. An instance is the *Ant Colony Optimization* (ACO) based on the observation of the collective behavior of ants when they are searching food. This is an example of distributed self-organized system constituted by a population, whose components interact and communicate through changes in the surrounding environment, i.e., pheromones wake. We can find also several examples of applications of this ACO algorithm [135]. The most known in the ICT world is the *AntNet* routing protocol. At the same time, the integrated task for the allocation and the routing in Sensor Networks and in Actor Network are based on this concept. We further refer to biological principles even when we talk of *Artificial Immune System*, based on the mammalian immune system. It has the purpose to efficiently underline

in complex problems the changes in the environment or the deviations of the behavior from the normal system. This type of algorithm can be used for evaluations regarding computer or communication systems, or it can be applied to sensor networks [136]. Another example of bio-inspired networking is related to the concept of signaling, which accurately describes the interactions between certain molecules. Indeed, this is a case of efficient and specific communication that is used in *Rule-based Sensor Network*, programming scheme for SANETs. Recently, this research field is also growing in nano-scale communications and networks implying, in turn, that the communication techniques conventionally used, such as electromagnetic or acustic waves, are not applicable due to the limitations given by the channel and antenna size.

In general, techniques for metaeuristic optimization, such as *Genetic Algorithm* and *Simulated Appealing*, can be seen as bio-inspired methods. Indeed, they have been successfully used to solve networks problems; in particular, these models are suitable for solving problems on the cross-layer optimization in networks.

In this context, our main purpose is to concretize the study of several network intelligence paradigms, with a twofold meaning: analysis of the intelligence *of* the network referring, in particular, to the characterization of the neural systems, and analysis of the intelligence *in* the network, i.e., the possibility to insert in communication networks some processes similar to the human thinking, to improve their performance.

After a broad study of the structure and the behavior of complex networks, with particular reference to neural systems, a comparison between the advanced telecommunications techniques and complex network-based techniques might be useful. In this way, the key common points and the principal differences can be highlighted. In general, one of the goals might be to design distributed management and anomaly detection methods for neural systems; these methods may help understanding medical fenomena, such as schizofrenia and Alzheimer (typical brain diseases). It is not excluded that this comparison would involve an increase in the knowledge on telecommunications networks as well, implying the designing of new distributed communication protocols or expanding protocols already existing in the literature that can allow a better management of the networks being more robust and efficient. Therefore, there could be an improvement on the expertises in both scientific fields, neural and communication, in a interdisciplinary manner. Furthermore, it could be interesting to investigate machine learning techniques and genetic programming to design techniques with the purpose of optimizing and strengthening the actual interconnection between brain networks and telecommunications networks.

Nowadays, one of the areas that is raising significant relevance in the scientific community is that of brain connectivity. One of its goals is to make the most of the rich datasets that neuroscientists collect by evaluating the spatio-temporal dynamics present in the data [134]. In particular, we are interested in the investigation of *functional* and *effective* connectivity in the brain, that is on the temporal correlation in the activity of two brain regions, regardless of whether they have direct anatomic links (functional connectivity, FC), and the directed causal influences one brain area produces in another (effective connectivity, EC). The common denominator to these different types of brain connectivity is that, in all instances, the system can be characterized and described as a network and in this way brain properties can be examined under formal mathematical network theories. As it can be clearly noticed, complex network analysis has emerged as an important tool to characterize brain connectivity.

The rest of this Section is organized as follows. In Sub-section 4.2.1 we discuss some preliminary results obtained investigating on the brain FC using functional Magnetic Resonance Imaging (fMRI) data; in Sub-section 4.2.2 we describe an alternative EEG-based method to evaluate brain connectivity and we introduce more deeply our future interests on the study of the brain as a complex network.

4.2.1 Frequency-dependent functional connectivity of brain networks from resting-state fMRI

Network connectivity of the brain can be approached from several perspectives [140]. For the purposes of this work, we focus on FC, i.e., the analysis of how the activity of different (possibly distant) brain regions is sinchronized to accomplish to specific functions. This can be formally defined in terms of the correlation between signals, taken from different regions of interests (ROIs), describing neurophysiological events. Several electrophysiological and imaging techniques can be used to acquire this kind of signals; fMRI is one of the most widely employed. Common trends in these signals are checked against statistical independence, and the presence of relevant correlation can be interpreted as a measure of synchronization. The resulting pairwise value can be collected in a FC matrix, that gives a snapshot-like representation of how different regions in the brain supposedly interact.

The objective is to shed some light on the role of different frequency components in determining these FC relationships. In particular, we argue that the general approach of considering FC values on predefined frequency bands may neglect some aspects of the interaction among different brain regions. It seems sensible to think of this synchronism among different areas to happen via interactions at different timescales (and thus different frequencies). To better highlight this aspect, and also to give a richer description of the functional connectivity, it may be worth considering some proper filtering of the signals, from a resting-state fMRI experiment in our case, that are used in the FC analysis.

After a description of the context in which we frame our analysis, and the tools employed, we will detail our research contribution that consists in applying several filtering, with tunable parameters, to the fMRI signals, so as to highlight a possible differentiation based on frequencies in the resulting connectivity matrix. More specifically, we will show that the FC matrix that we can obtain via standard tools for the analysis is actually heavily dependent on filtering. For example, we are able to show that lower frequencies exhibit structural connectivity properties that are quite different from higher frequencies counterpart, to the point of configuring an entirely disjoint connection pattern, and these specific aspects are hidden when the entire frequency range is considered.

Methodological issues aside, this may also hint at a more colorful description than a mere FC matrix, where not only the plain connectivity relationship is considered, but also the frequencies involved in the connection (which, in turn, may hint at a faster or more slow-paced interaction among brain regions). Thus, it makes sense to think of this kind of analysis as a further research direction in modeling the brain network, possibly including frequency-differentiated interactions, which may lead to a better characterization and improved explanation of brain phenomena.

The remaining part of this Sub-section is organized as follows. In Sub-subsection 4.2.1.1 we give a general background of the topic; Sub-subsections 4.2.1.2 and 4.2.1.3 describe the toolbox and the dataset used, respectively; in Sub-subsection 4.2.1.4 some preliminary numerical results are shown; finally, Sub-subsection 4.2.1.5 draws some concluding observations and discussion on possible future development of the present analysis.

4.2.1.1 Background

FC has been studied with several electrophysiological and imaging techniques, ranging from local field potentials (LFP) to EEG, magnetoencephalography (MEG) and fMRI [141, 140, 137].

In over twenty years of fMRI experiments, FC has been quantified both in healthy and in pathological conditions. FC can explain relationship between different areas of the brain during task-related activities. This long-time research activity led to the identification of several functional networks: the sensorimotor, visual, amygdala, and hippocampus, among others[142]. Besides, FC studies further provided insights on the pathological behavior of these networks in case of diseases, e.g., schizophrenia[143], major depressive syndrome [144], Alzheimer's disease [145], as well as on changes in the normal healthy brain during development [146] and aging [147, 148].

FC has been correlated with the so-called *structural connectivity* (SC) [149]: generally, two regions that are physically connected (with significant SC values) usually show some degree of FC, too. Conversely, and even more intriguingly, literature has shown significant functional coupling between areas that are not directly connected; this strongly unravelled the underlying network organization of the brain that can exploits indirect paths to make effective communications between areas.

Another measure frequently associated with FC is the EC, that gives direction of the information flow between two areas where FC is established. This could represent an important outcome from the EC measure since it can provide support, e.g., to stimulation and neuromodulation [150] protocols targeting the normalization of a specific function, i.e. motor, cognitive or others.

Recently, increasing attention has been given to the behavior of the brain and its oscillatory activity during the *resting-state*, i.e. the condition in which no task is required to the subjects except for relaxing while staying awake. In this case, no particular task-related response is expected; however, an undergoing *default-mode network* (DMN) [147] has been robustly identified. It seems to account for an *active-idling state* where the subject is doing nothing, but can be reactive to any external stimulus.

FC largely served to the study of DMN in many kinds of studies: particularly promising is the use of FC for the investigation of the DMN at resting state. Indeed, this approach allows to dig into the functional segregated-integrated organization of the brain: specifically, high values of FC among some areas of the brain can identify them as a highly-connected, i.e. segregated, network. Such kind of networks are then functionally integrated each others through smaller FC values, giving rise to a complex *network-of-networks*[151].

Quantitatively, FC can be computed in many ways: correlation between time-series from pairs of ROIs has been firstly employed; then, other methods such as covariance and mutual information were exploited[140].

Some more recent works have hinted at the dependence of connectivity, especially meant as FC and EC, on frequency. In [152], the most interesting frequency bands were discussed, that can explain many neurophysiological human behaviors, from the ultra-slow frequencies (around 0.01 Hz) up to the ultra-fast oscillations (around 600 Hz). An inverse relationship was also pointed out between networks extension and frequency: high frequencies, i.e., small wavelengths, are usually confined in small neuronal areas, while low frequencies, i.e., large wavelengths, are generally involved in the functioning of larger-scale networks.

Reasonably, the latter implies the time-varying characteristic of FC: specifically, studies on LFP, EEG, and MEG made possible to follow FC changes in time at frequencies in a broad range between 0.01 Hz up to 600 Hz. Nevertheless, among non-invasive neurophysiological techniques, MEG and EEG are known to be affected by low spatial resolution: therefore, fMRI has been also employed in the study of FC of the brain. However, fMRI cannot provide such high frequency information as given by MEG and EEG (and, invasively, by LFP). The typical time-course of FC is sampled in the range of 5 to 10 minutes with the consequent possibility to only track very slow changes of the brain connectivity.

Recently, new studies are exploring the dynamic range of the fMRI signal during resting-state, assumed to be a *steady-state*. Along this way, the *chronnectome* of Calhoun et al. [153] has suggested the near-future direction and challenge of fMRI: in fact, time and frequency changes has to be tracked and quantified in order to unravel the spatial properties of "mutually informed activity" that is processed in the brain at any time, in any place [154].

Attempts in the same direction have been made also in the recent past by means of the decomposition of the fMRI signal in specific frequency bands related to physiology: $0.01 - 0.027$ Hz (slow-5) and $0.027 - 0.073$ Hz (slow-4) band [152] were considered in a study on resting-state FC to assess differences between normal subjects and a group of mild cognitive impaired patients[155]. With the investigation of FC, authors could suggest the involvement of a functional impairment rather than a structural difference in the amount of gray matter between the two groups.

Furthermore, the study of the five well-known functional brain networks mentioned above into the largest $0 - 0.24$ Hz available frequency band shows a higher value of correlation of cortical networks in the range $0.01 - 0.06$ Hz, whereas a limbic activity, i.e. deeper brain level, spread in the wider $0.01 - 0.14$ Hz frequency range [142].

Finally, low frequency fluctuations ($0.01 - 0.08$ Hz) of resting-state fMRI signal were reported to reflect spontaneous neuronal activity [156]. Moreover, it is known that low frequency oscillations ($0.01 - 0.073$ Hz) can be detected in the gray matter, while relatively high frequency oscillations ($0.073 - 0.25$ Hz) are related to white matter [157].

Therefore, our contribution represents an exploratory effort on the way to dig out the relationship between any possible pair of ROI in the brain in the full band of the fMRI signal.

4.2.1.2 DPARSF toolbox

Data Processing Assistant for Resting-State fMRI (DPARSF) is a MATLAB toolbox developed for pipeline data analysis of resting-state fMRI. This tool, available at [158], is an open source package based on some functions in Resting-State fMRI Data Analysis Toolkit (REST) and Statistical Parametric Mapping (SPM). Data are preprocessed by SPM and then entered into REST. SPM is known as a powerful tool, however lots of time-consuming and complex operations are required when analyzing a large data set.

The manual procedures needed to set (step-by-step and subject-by-subject) the SPM parameters may be cumbersome and could lead to making unintentional mistakes. DPARSF is designed to solve this problem and supply a user-friendly software. Indeed, after arranging the Digital Imaging And Communication in Medicine (DICOM) or Neuroimaging Informatics Technology Initiative (NIfTI) file formats, the user is required to click a few buttons to set parameters and DPARSF will give all the preprocessed data, i.e., by slice timing, realigning, normalizing, and smoothing, and eventually producing results for FC, Regional Homogeneity (ReHo), Amplitude of Low Frequency Fluctuation (ALFF), and Fractional ALFF (fALFF). As a matter of fact, while FC is used in resting-state fMRI studies to measure the signal synchrony among remote brain areas, other aspects of the regional spontaneous activity could be investigated using several metrics, such as the ReHo, ALFF, and fALFF. DPARSF may also exclude subjects with excessive noise due to head motion and generate a set of images to easily check the effect of normalization. Our detailed usage is as follows.

Convert DICOM files to NIfTI images – Most data are produced in DICOM format and, before data analysis, these DICOM format data are usually transformed into other formats, for example NIfTI file format. These kind of files contain affine coordinate definitions that relates voxel (i.e., a tidy cube of brain tissue) index to spatial location, in particular the noteworthy information of left hemisphere and right hemisphere. For this reason, DPARSF will convert the data by calling *dcm2nii* in MRIcroN software if users do not convert the data previously.

Remove first N time points – It is common to discard the first few volumes of the functional images to allow the subjects to get used to the scanning noise. If the user select this option, DPARSF will delete the number of time points specified for each subject.

Slice timing – Since most fMRI data are acquired using two-dimensional pulse sequences obtaining images one slice at a time, all brain slices are obtained at different time within a repeat time (TR). These timing differences can be a problem for a long TR. As a consequence, the differences in image acquisition time must be corrected. Specifying the number of slides, the slice order, and the reference slice, DPARSF will perform slice timing by calling some SPM functions.

Head motion correction – Motion correction is used to adjust the time series of images so as to have the brain in the same position in every image. If user select this option, DPARSF will motion-correct the time series of images by calling functions in SPM. DPARSF allows to exclude from further analysis subjects with excessive head motion; indeed, too much head motion may induce large artifact

in fMRI time series. As a consequence, DPARSF will create a report of head motion considering the realign parameters estimated by SPM.

Normalization – Different subjects have different brain size, shape, orientation, and gyral anatomy. Therefore, the individual brain is usually spatially normalized into a standardized template. Two optional normalization of the functional images into the Montreal Neurological Institute (MNI) space are provided: using echo-planar imaging (EPI) template and using unified segmentation on T1 image.

Smoothing – Since there could be residual differences in functional and gyral anatomy during inter-subject averaging, smoothing is usually used in pre-processing to suppress this residual noise. The Gaussian filter is the most common smoothing technique used. DPARSF will smooth the data with the specified width at half of the maximum value using SPM.

Remove linear tread – There could be a systematic increase or decrease in the signal with time due to long-term physiological shifts, movement related noise remaining after realignment or instrumental instability. For this reason, DPARSF will remove the systematic drift using a linear model by calling some REST functions.

Filtering – In [156], low fluctuations (0.01-0.08 Hz) of resting-state fMRI signal are reported to be of physiological importance reflecting spontaneous neuronal activity. Moreover, low frequency oscillations (0.01-0.073 Hz) are detected in the gray matter and, in contrast, relatively high frequency oscillations (0.073-0.25 Hz) are related to white matter [157]. Respiratory and cardiac signals fall within high frequency ranges [160]. DPARSF is able to filter the data, and its passband can be tuned at will, by calling ideal filter REST functions.

Remove effect of nuisance covariates – Recently, many researchers focused on the anti-correlation phenomenon of resting-state fMRI. A typical example is that significant anti-correlations between the components of the default-mode and attention networks are consistently observed, even though the global whole-brain signal is removed [161]. Therefore, this whole-brain signal would be removed by a regression analysis before the evaluation of the functional connectivity in order to reduce the effect of the physiological artifacts. Beyond this, the cerebrospinal fluid (CSF), six motion parameters, and the white matter signals could also be removed as nuisance variables to limit the effects of non-neuronal Blood Oxygenation Level Dependent (BOLD) fluctuations and head motion.

4.2.1.3 Dataset

The fMRI data that we used are all provided within the DPARSF tool. The full set of data is available at [159]. They were acquired using a SIEMENS TRIO 3-Tesla scanner in the Beijing Normal University Imaging Center for Brain Research from three subjects. They laid supine with the head fixed by straps and pads to minimize head motion. The subjects had to keep as motionless as possible and not to think systematically during the resting-state session.

The functional images are obtained using an EPI sequence with 33 axial slices, 3/0.6 mm thickness/gap, 64×64 in-plane resolution, TR of 2 ms, TE of 30 ms, flip angle of 90 degrees, 200×200 mm FOV. Moreover, a T1-weighted sagittal 3-dimensional magnetization-prepared rapid gradient echo (MPRAGE) sequence is acquired covering the entire brain with the following parameters 128 slices, TR of 2530 ms, TE of 3.39 ms, slice thickness of 1.33 mm, flip angle of 7 degrees, inversion time of 1100 ms, 256×256 mm FOV, and in-plane resolution of 256×192.

We use DPARSF pipeline analysis to process the data. After converting DICOM files to NIfTI files, the first 10 time points are discarded. Then, slice timing and head motion correction are performed and data are normalized according to the MNI space by using unified segmentation of T1 image and re-sampled to 3 mm isotropic voxels. Then, after smoothing with a 4 mm FWHM Gaussian kernel, the linear trend of time courses is removed and temporally low/high-pass filtering is performed.

Once this processed phase is finished, DPARSF extracts ROI time courses and compute the correlation matrix between the ROIs obtained. Since our purpose is to compare the ROI correlations obtained applying different filtering procedure to fMRI signals, we define several frequency bands with

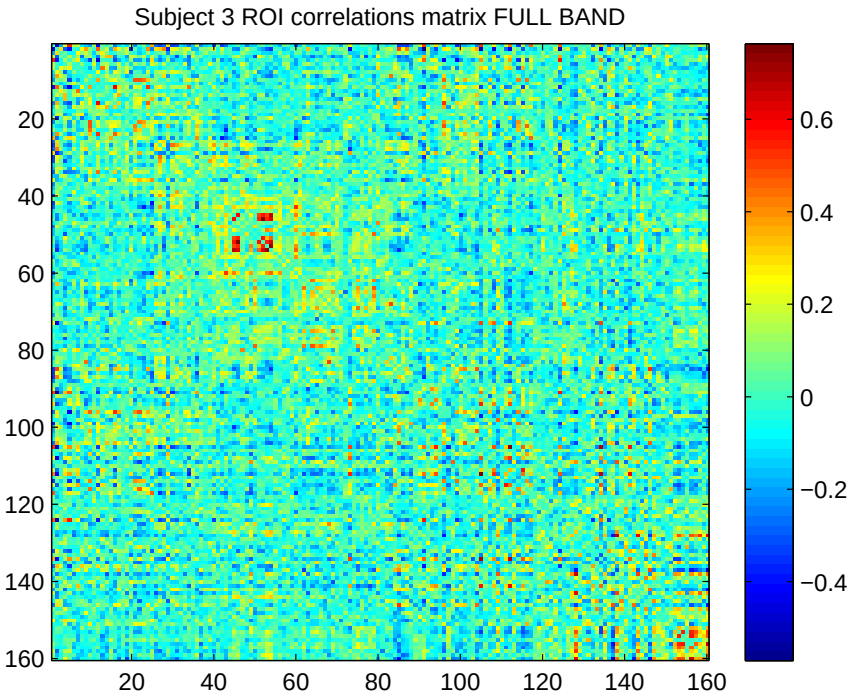

Figure 4.6: Subject 3 ROI correlation matrix considering the fMRI signal in its full band [0.01 0.5] Hz.

different cutoff frequencies. In particular, we consider a low-pass filter and a high-pass filter whose cutoff frequency (called β in both cases) is a tunable parameter, as detailed in the following.

4.2.1.4 Numerical Results

Once selected all the parameters required for the data processing, we can obtain the ROI correlations matrix. Prior to extracting the ROI signals, we filter our original fMRI data using low-pass and high-pass filter with different cutoff frequencies. Note that since $TR = 2$ ms, the sampling frequency F_s is 0.5 Hz; thus, in the frequency domain, the signals of interest can be found up to that value. In particular, we refer to [0.01 0.5] Hz as *full band*, since given the duration of our signals it is reasonable to ignore extremely low frequencies for functional interactions. Using a low-pass filter, we attenuate the signal outside the band [0.01 β], where, for our evaluations, we consider β as the independent variable, that goes up to 0.5 thus reaching the full band. Conversely, we also consider a high-pass filter in the band [β 0.5] with a similar approach.

Fig. 4.6 shows the 160×160 ROI correlation matrix obtained considering the full band fMRI signal related to subject 3. In the colorbar, we represent positive correlations with red-like pixels and negative correlation with blue-like pixels. Fig. 4.7 describes instead the ROI correlation matrix of the same subject 3, but after having filtered the relative fMRI signal with a low-pass filter with cutoff frequency 0.02. This comparison immediately shows that the two matrices are quite different, which means that correlations between ROI pairs may significantly change if we consider a filtered version of the signals, and the overall holistic connectivity description is heavily influenced. In other words, considering the fMRI signals at different frequency bands produce different connectivity relationships between different areas of the brain. Thus, depending on the frequency band to which the fMRI signals are considered, some functional links may or may not be present, and some links can even specifically appear stronger in a given frequency range.

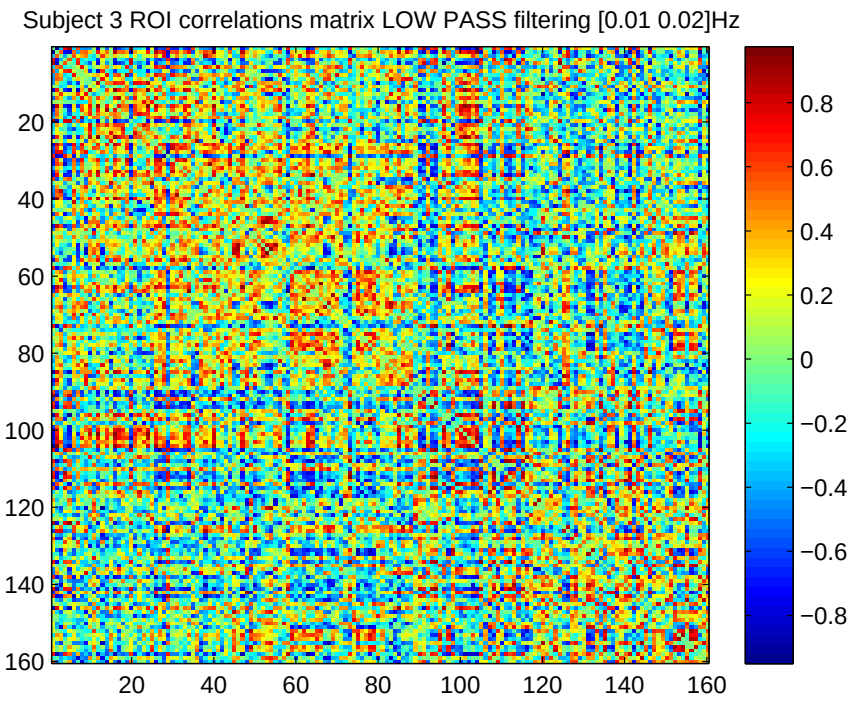

Figure 4.7: Subject 3 ROI correlation matrix considering fMRI signal filtered within [0.01 0.02] Hz.

To quantify the difference between ROI correlations corresponding to different bands of interest for the signal, we use the following approach. We take the ROI correlation matrix for the full band, denoted as $\mathbf{R}_{(\mathrm{FB})}$, and the same matrix obtained for any filtered version of the input signals, which we call $\mathbf{R}(\beta)$; this can actually either be $\mathbf{R}_{\mathrm{LP}}(\beta)$ or $\mathbf{R}_{\mathrm{HP}}(\beta)$, depending on the filtering being low-pass or high-pass, respectively. We compute the difference matrix $\Delta\mathbf{R}(\beta) = \mathbf{R}(\beta) - \mathbf{R}_{(\mathrm{FB})}$ that quantifies the difference between the connectivity description of the filtered version and the original full-band signals.

Once computed this difference, we define a Normalized Distance Index NDI as:

$$NDI = \frac{||\Delta\mathbf{R}(\beta)||_{\mathrm{F}}}{||\mathbf{R}_{(\mathrm{FB})}||_{\mathrm{F}}} \tag{4.8}$$

where $||\cdot||_{\mathrm{F}}$ denotes the Frobenius norm operator. In other words, we consider the Frobenius norm as a measure of the diversity of the two matrices, and we normalize the result to the Frobenius norm of the original full-band matrix. This value is meant to give a rough idea of the difference between the resulting connectivity matrix and the original full band case. Note that this value is "normalized" and therefore can be roughly seen as an index of separation (more or less as a percentage). However, correlation values of the FC can possibly be negative (and close to -1), and also the normalization factor, i.e., the Frobenius norm of the full band matrix, may be not too high. This would correspond to a case where the NDI is larger than 1, which simply means that the matrices are significantly different.

Fig. 4.8 shows the results obtained for each of the three subjects considering low-pass filters and varying the value of β. First of all, it is possible to notice that the three fMRI signals give quite consistent results for the same value of β. This seems to imply that the conclusion we have previously drawn for a specific subject are actually more general. For a low-pass filtering, it seems that most of the FC information is actually limited to the frequency range [0.01 0.25] Hz. In this case, indeed, if

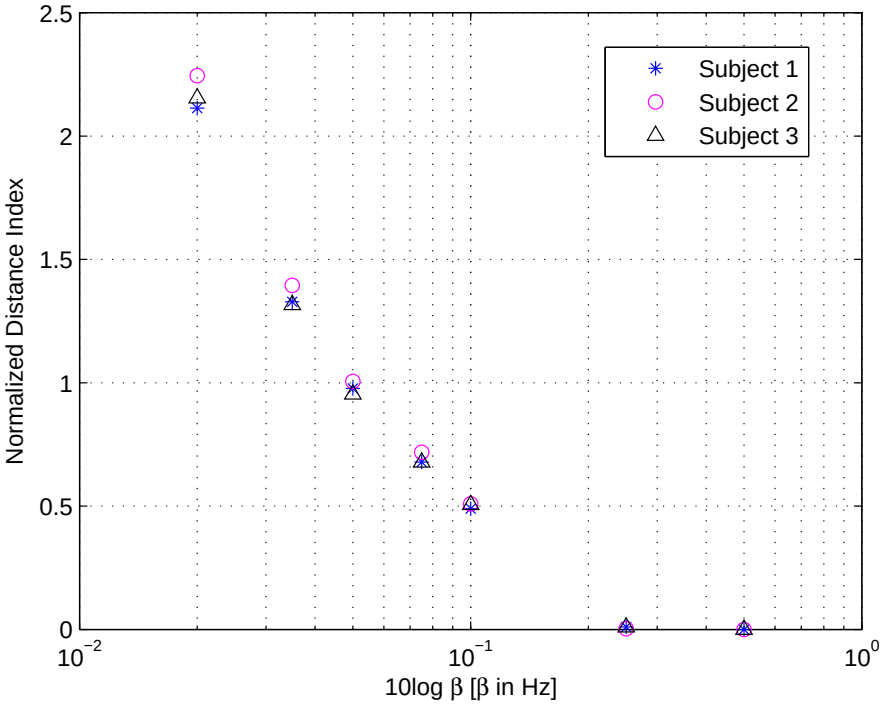

Figure 4.8: Low-pass filtering: comparison of the Normalized Distance Index.

$\beta = 0.25$ there is little difference with respect to the full band case. However, there are significant differences showing up when β is further decreased and only the low-pass components are kept. Already in the band [0.01 0.1], the figure shows a value of NDI quite higher than 0. Moreover, the lower is the cutoff frequency, the higher is the difference, in terms of NDI, between the functional connectivity related to the full band fMRI signal and the filtered fMRI signal. For extremely low values of β, the resulting connectivity matrix is significantly different, with an NDI larger than 1, which may suggest that there are entirely separate connectivity phenomena, which become evident if only low-frequency interactions among the brain regions are considered.

Fig. 4.9 considers instead a similar analysis, but for the case of high-pass filtering, with a tunable parameter β that still represents the cutoff frequency, so that, this time, the resulting passband is [β 0.5] Hz. Again, we plot NDI versus β and the results are analogous to those of Fig. 4.8: for example, there is a strong consistency of the results across different subjects. The maximum value of the NDI is even higher than before, which seems to suggest that a intra-region FC has a limited activity for higher frequencies. This was also visible from the low-pass filtering case showing almost no difference if $\beta = 0.25$. On the other hand, the values for relatively low cutoff frquency β, the high-pass filter may obtain better results.

Still, connectivity phenomena are significantly different at lower and higher frequency, to the point that they can be seen as entirely unrelated functional trends. While most of the FC relationship is captured by a filtered version of the signals with sufficiently large passband, on the other hand, just considering the full band of signals without any frequency differentiation may lead to hiding some existing correlation trends that only happen and are relevant at certain frequencies.

We remark that for the purpose of being systematic and since this is just a preliminary study on the topic, our analysis focuses on a variable β without searching for any specific physiological correlate. However, it may be worth considering specific frequency values or bands, with a precise physiological role: this kind of investigation, which is left for future work, may give an even better explanation of

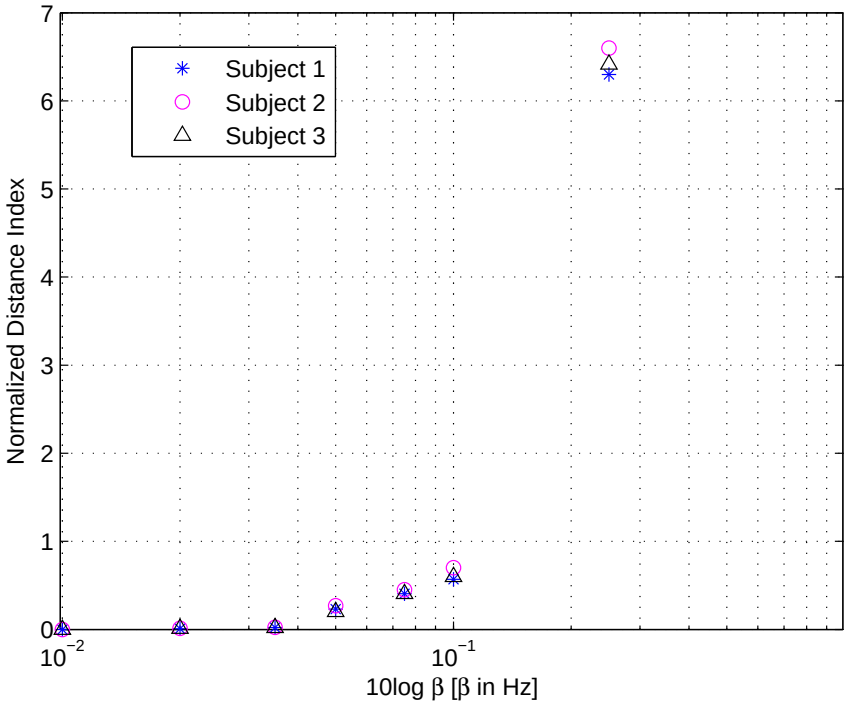

Figure 4.9: High-pass filtering: comparison of the Normalized Distance Index.

the difference of values existing across the entire frequency axis.

4.2.1.5 Discussion

To get a dataset of signals that are usable within a toolbox, several pre-processing procedures are required, most of the times including a filtering to limit the signals within a proper frequency band. The resulting "polished" signals feed the toolbox so as to achieve a quantification of FC (or any similar metric). So, a first immediate conclusion of our study is that this kind of preliminary operations on the signals requires special care, in particular it must be done avoiding filtering out some relevant frequencies, as this can strongly affect the conclusions on the undergoing physiological phenomena that the researcher desires to observe.

Moreover, it is worth noting that some other operations, e.g., avoiding head motion correction or similar adjustments on the signals, definitely play a role here. We verified that changes in the pre-processing pipeline lead to a slightly different FC matrices, the bulk of our conclusions, i.e., that the holistic representation of the FC matrix heavily changes at different frequencies, still holds true.

Beyond the importance of a correct pre-processing of fMRI signals, our analysis can also motivate the efforts towards gaining a systematic understanding of the role played by frequency components with respect to FC. The most striking aspect of our evaluation graphs is that, apparently, a linear relationship exists in the presence of links (i.e., what represented by the NDI) and the width of the considered frequency band. This result has also been validated for other kinds of filtering besides the low-pass and high-pass shown before.

Should this trend be confirmed by more investigations, a distribution law of FCs in the brain across different frequencies may be estimated. This aspect, if ultimately proven, would be extremely suggestive in implying that functional connectivity is not a static property of the brain, but rather is variegate and describes a plethora of different functions, that are themselves frequency-dependent.

An in-depth discussion of these features may therefore suggest interesting implications from signal processing to physiology that can open up further contributions in the fields of neurosciences.

4.2.2 Multiplexing applied to brain network

Over the past few decades, a variety of techniques for non-invasive measurement of brain activity have been developed. As mentioned before, one of these techniques is EEG, a high time resolution measurement of the voltage potential in the order of microvolts at various locations on the scalp. Using EEG and applying signal processing methods, it is possible to estimate the current sources inside the brain that best fit the measurements data. This estimation is known as *source localization* and it might be useful to investigate on the brain connectivity.

The neural activity can be modeled by currents and the activity can be well approximate by current dipoles. At any given time, the signal recorded at the scalp is a spatial summation of current density induced by synchronized post-synaptic potential occurring in large clusters of neurons. Therefore, it is clear that to detect an EEG signal at the scalp, many neurons must be activated synchronously. Indeed, in the generation of an EEG oscillation, tens of thousands of synchronously activated pyramidal cortical neurons are involved. The parallel orientation of their dendritic trunks to each other and the perpendicular orientation of them to the cortical surface, allow summation and propagation to the scalp surface. Several animal studies describe substantial synchronization among neighboring neurons (the so called large-scale synchronization). As a consequence, synchronization of oscillations is a key mechanism for neuronal communication between spatially distributed brain networks. It has been found that higher frequency oscillations (e.g., gamma oscillations) appear to originate from smaller neuronal assemblies, whereas low frequency oscillations (e.g., theta oscillations) span larger neuronal populations.

The procedure of source localization consists of two steps. First, the so called *forward problem* with the goal of finding the scalp potentials that would result from hypothetical dipoles (or, more generally, from a current distribution inside the head). Then, the second step is the *inverse problem* consisting in estimating the sources that fit the actual EEG data measured at specified positions of electrodes on the scalp. The accuracy with which a source can be located can be affected by several factors; for example, head modelling errors, source modelling errors, and EEG noise that can be instrumental or biological. It is worth noting that if the configurations of intracranial sources and the conductivity proprieties of the tissues are known, then the distribution of the scalp potential can be calculated using basic physical principles. As a consequence, the forward problem can be unambiguously solved. On the other hand, the inverse problem is ill-posed. Indeed, scalp-recorded electromagnetic measurements do not contain enough information about the 3-D distribution of the electric neuronal activity: the current distribution in a conducting volume can't be uniquely determinated by the field and potential information outside it. Therefore, it is clear that scalp-recorded EEG measurements can be described by an infinite number of different generating distributions (even if we consider an infinite numbers of recording electrodes). To explain better this point, we will proceed describing in more mathematical details the inverse problem formulation needed to solve source localization to investigate on the brain connectivity using EEG data.

The remaining part of this Sub-section is organized as follows. In Sub-subsection 4.2.2.1 we give a description of the inverse problem; in Sub-subsections 4.2.2.2 we examine the measures of connectivity considered; finally, in Sub-subsection 4.2.2.3 our future research interests are explained.

4.2.2.1 Inverse problem formulation

A dipole does not reflect the presence of a discrete and unique source, but it is rather a convenient representation of synchronized activation of a huge number of pyramidal cells likely extending larger patches of gray matter. In this context, the cortical pyramidal neurons are thought to be the in-

tracranial sources of scalp electric potential differences. These neurons are subjected to post-synaptic potentials that create an active impressed current density. The relationship between the current density vector field and the scalp potentials is

$$\mathbf{\Phi}_c = \mathbf{K}_c\mathbf{J} + c\mathbf{1}, \tag{4.9}$$

where $\mathbf{\Phi}_c$, denoting the potentials at N_E scalp electrodes all measured with respect to the same reference electrode, is a vector with N_E elements; $\mathbf{J}$ describes the current density at N_V cortical voxels and, therefore, it is a vector of N_V elements; c is a scalar value defined by the reference electrode arbitrarly chosen when the EEG signal is recorded; $\mathbf{1}$ is a vector of N_E ones; finally, the N_E x N_V matrix $\mathbf{K}_c$ is the lead field determined by the geometry and conductivity profile of the head. Eq. 4.9 represents the forward equation. For the sake of clarity, the subscript c is used to emphasizes that potentials are determined up to an arbitrary additive constant related to the reference electrode choice. Eq. 4.9 is an instantaneous discrete sampling of the measurement space (i.e., scalp electrodes) and the solution space (i.e., cortical voxels).

The estimation of the unknown electric neuronal activity $\mathbf{J}$ given the lead field $\mathbf{K}_c$ and the scalp potential measurements $\mathbf{\Phi}_c$ defined the inverse problem.

First of all, it is necessary to solve the so called *reference electrode problem* that correspond to solve

$$c = \arg\min_c ||\mathbf{\Phi}_c - \mathbf{K}_c - c\mathbf{1}||^2 \tag{4.10}$$

with $||\cdot||$ being the Euclidean norm. This means that c must satisfy, as best as possible, Eq. 4.9. Solving the problem in Eq. 4.10 and plugging the solution back into Eq. 4.9 we obtain

$$\mathbf{H\Phi}_c = (\mathbf{HK}_c)\mathbf{J} \tag{4.11}$$

where $\mathbf{H}$ is known in statistics as a centering matrix whose effect is to subtract the average value and it is defined as

$$\mathbf{H} = \mathbf{1} - \frac{\mathbf{1}\mathbf{1}^T}{\mathbf{1}^T\mathbf{1}}. \tag{4.12}$$

This has a relevant implication, since it demonstrates that inverse solutions are reference-independent as they must be obtained from the reference-independent forward equation 4.11, which is invariant to any change of reference. Given $\mathbf{H}$, it is possible to define $\mathbf{\Phi} = \mathbf{H\Phi}_c$ and $\mathbf{K} = \mathbf{HK}_c$ and, then

$$\mathbf{\Phi} = \mathbf{KJ}. \tag{4.13}$$

In the literature regarding the EEG, the effect of $\mathbf{H}$ is known as the average reference. It is worth noting that an inverse solution changes considering different samplings, which means that it will change if we consider a different number and different locations of the scalp electrodes. On the other hand, given the sampling, the solution to an inverse problem modeling the reference electrode will not depend on the choice of the reference electrode.

At this point, our goal is to solve the linear forward equation 4.9 for the unknown current density $\mathbf{J}$. This is a multivariate problem. It usually holds that $N_E << N_V$, meaning that the electrodes number is much smaller than the voxels number. As a consequence, the problem is undetermined with an infinite number of solutions.

In more details, we are looking for particular linear solutions of the form

$$\mathbf{J} = \arg\min_{\mathbf{J}} ||\mathbf{\Phi} - \mathbf{KJ}||^2 + \alpha\mathbf{J}^T\mathbf{WJ}. \tag{4.14}$$

This is a regularized, weighted minimum norm problem, where $\alpha \geq 0$ is the Tikhonov regularization paremeter, and $\mathbf{W}$ is a N_VxN_V symmetric positive definite weight matrix.

$$\mathbf{J} = \mathbf{W}^{-1}\mathbf{K}(\mathbf{KW}^{-1}\mathbf{K}^T + \alpha\mathbf{H})^+\mathbf{\Phi} \tag{4.15}$$

Eq. 4.15 is the general solution to this problem. The operator + on the top of the bracket represents the Moore-Penrose pseudo-inverse.

As shown in [163] both empirically and theoretically, the non-weighted minimum norm (i.e., Eq. 4.15 with $\mathbf{W} = \mathbf{1}$ the identity matrix) has very bad localization properties misplacing deep sources to the surface. This is due to the fact that this solution is an harmonic function attaining its extreme values only at the boundary of the solution space [164]. As a consequence, its use for localization is invalidated by this basic physics property of the minimum norm, regardless of the fact that it is the simplest solution.

Historically many attempts were made to improve the mislocalization of sources. The aim is to find an appropriate weigth matrix $\mathbf{W}$ in Eq. 4.15 so that the distributed linear inverse solution has zero localization error when tested with sources anywhere in the brain under ideal (i.e., no-noise) conditions.

The nonlinear system of equations shown in 4.16 can be used to obtain the weights for exact localization with zero error under ideal conditions.

$$\omega_i = [\mathbf{K}_i^T(\mathbf{K}\mathbf{W}^{-1}\mathbf{K}^T + \alpha\mathbf{H})^+\mathbf{K}_i]^{\frac{1}{2}} \tag{4.16}$$

ω_i, for $i = 1, ..., N_V$, are the elements of the diagonal weight matrix $\mathbf{W}$ and $\mathbf{K}_i \in \mathcal{R}^{N_E \times 1}$ denotes the ith column of the matrix $\mathbf{K}$. It is worth noting that, even if the weights are nonlinearly dependent from $\mathbf{K}$'s columns, the inverse solution remains linear. The following algorithm describes the way in which the weights (which do not depend on the measurements) computation can be solved:

1. initialize $\mathbf{W}$ with elements $\omega_i = 1$, for $i = 1, ..., N_V$;
2. compute $\mathbf{C} = (\mathbf{K}\mathbf{W}^{-1}\mathbf{K}^T + \alpha\mathbf{H})^+$;
3. keeping $\mathbf{C}$ fixed, for $i = 1, ..., N_V$, compute new weights $\omega_i = [\mathbf{K}_i^T\mathbf{C}\mathbf{K}_i]^{\frac{1}{2}}$;
4. using the new weights, go to step 2 until the change in the weight matrix is sufficiently small (i.e., convergence).

For the sake of exposition, the theoretical proof for the exact localization property of the linear inverse solution follows. The current density related to the ith voxel is

$$[\mathbf{J}]_i = \omega_i^{-1}\mathbf{K}_i^T(\mathbf{K}\mathbf{W}^{-1}\mathbf{K}^T + \alpha\mathbf{H})^+\Phi = [\mathbf{K}_i^T\mathbf{C}\mathbf{K}_i]^{-\frac{1}{2}}\mathbf{K}_i^T\mathbf{C}\Phi \tag{4.17}$$

where the second equality is obtained substituting the equation of the weights previously discussed. The squared current density $([\mathbf{J}]_i)^2$ reaches its maximum value when the actual scalp potential is generated by a point source at the target. For example, a point source with a representing its strenght at the jth voxel, gives $\Phi = a\mathbf{K}_j$ and $([\mathbf{J}]_i)^2 = a^2(\mathbf{K}_j^T\mathbf{C}\mathbf{K}_i)^2(\mathbf{K}_i^T\mathbf{C}\mathbf{K}_i)^{-1}$. The partial derivative of $([\mathbf{J}]_i)^2$ attains the zero value when $\mathbf{K}_i = \mathbf{K}_j$ proving that the linear tomography related to the equation of the weights considered at the beginning solves the multi-variate invers problem. Furthermore, it also achieves exact localization to test point sources under no-noise conditions. This method is known as *exact low-resolution electromagnetic tomography* (eLORETA).

4.2.2.2 Connectivity measures: coherence and phase synchronization

As we already pointed out discussing the brain connectivity analysis based on fMRI data, the *similarity* between time-varying signals recorded at two brain regions quantifies the dynamic functional connectivity between these two regions [165]. The term similarity is generic and it allows for a variety of measures that have been evaluated and used in the analysis of electric neuronal activity time series. Herein, we focus on two different definitions of similarity: *coherence*, which provides a measure of linear

similarity between signals, and *phase synchronization*, corresponding to a particular form of non-linear similarity. These measures are usually expressed as the sum of *lagged dependence* and *instantaneous dependence*. They are applicable to stationary and non-stationary time series and their values are non negative and defined in the frequency domain. In neurophysiology, the time series represent the electric neuronal activity at several brain locations. As a consequence, coherence and phase synchronization are to be interpreted as "connectivity" between locations. Neverthless, in this setting, any measure of dependence is substantially contaminated with an instantaneous, non-physiological contribution due to *volume conduction* (i.e., the complex effects of measuring electrical potentials at distance from their source generators) and *low spatial resolution*. Using eLORETA approach, the measures of dependence can be applied to any number of brain areas jointly (i.e. distributed cortical network) and the activity of these areas can be estimated.

Consider x_{jt} and y_{jt} as two stationary multi-variate time series, with $j = 1, 2, ..., N_R$, denoting the jth segment or epoch in which the EEG signal can be divided. Let $\mathbf{X}_{j\omega}$ and $\mathbf{Y}_{j\omega}$ be their discret Fourier transforms, Eqs. 4.18-4.21 define the cross-spectra, where $\mathbf{S}_{\mathbf{XX}\omega}$ and $\mathbf{S}_{\mathbf{YY}\omega}$ are Hermitian matrices.

$$\mathbf{S}_{\mathbf{XX}\omega} = \frac{1}{N_R}\sum_{j=1}^{N_R}\mathbf{X}_{j\omega}\mathbf{X}_{j\omega}^{*} \tag{4.18}$$

$$\mathbf{S}_{\mathbf{YY}\omega} = \frac{1}{N_R}\sum_{j=1}^{N_R}\mathbf{Y}_{j\omega}\mathbf{Y}_{j\omega}^{*} \tag{4.19}$$

$$\mathbf{S}_{\mathbf{XY}\omega} = \frac{1}{N_R}\sum_{j=1}^{N_R}\mathbf{X}_{j\omega}\mathbf{Y}_{j\omega}^{*} \tag{4.20}$$

$$\mathbf{S}_{\mathbf{YX}\omega} = \mathbf{S}_{\mathbf{XY}\omega}^{*} = \frac{1}{N_R}\sum_{j=1}^{N_R}\mathbf{Y}_{j\omega}\mathbf{X}_{j\omega}^{*} \tag{4.21}$$

For the phase-information cross-spectra the Fourier transforms must be normalized as shown in Eqs. 4.22-4.23.

$$\tilde{\mathbf{X}}_{j\omega} = (\mathbf{X}_{j\omega}^{*}\mathbf{X}_{j\omega})^{\frac{1}{2}}\mathbf{X}_{j\omega} \tag{4.22}$$

$$\tilde{\mathbf{Y}}_{j\omega} = (\mathbf{Y}_{j\omega}^{*}\mathbf{Y}_{j\omega})^{\frac{1}{2}}\mathbf{Y}_{j\omega} \tag{4.23}$$

Then, the definition of the cross-spectra is the same as previously discussed, with $\tilde{\mathbf{X}}_{j\omega}$ and $\tilde{\mathbf{Y}}_{j\omega}$ replacing $\mathbf{X}_{j\omega}$ and $\mathbf{Y}_{j\omega}$, respectively.

The real part of the Hermitian covariance matrix at frequency ω, i.e. $\mathcal{R}e(\mathbf{S}_\omega)$, represents the instantaneous, zero-phase, zero-lag covariance matrix corresponding to a multi-variate time series at frequency ω. Indeed, considering the multi-variate time series $\mathbf{X}_{jt} \in R^{p\times 1}$, for a discrete time $t = 0, ..., N_{T-1}$, with $j = 1, ..., N_R$, and filtering the time series to leave solely the frequency ω component, $\mathbf{X}_{jt}^{\omega Filtered}$ (note that the spectral density of $\mathbf{X}_{jt}^{\omega Filtered}$ is zero everywhere except at ω), the instantaneous, zero-lag, zero-phase shifted, time domain, symmetric covariance matrix for $\mathbf{X}_{jt}^{\omega Filtered}$ at frequency ω is

$$\mathbf{A}_\omega = \frac{1}{N_T N_R}\sum_{j=1}^{N_R}\sum_{t=1}^{N_t}(\mathbf{X}_{jt}^{\omega Filtered})(\mathbf{X}_{jt}^{\omega Filtered})^T \in \mathbf{R}^{r\times r}. \tag{4.24}$$

Finally, using the Parseval's theorem for the filtered time series, it holds

$$\mathcal{R}e(\mathbf{S}_{\mathbf{XX}\omega}) = \frac{N_T^2}{2}\mathbf{A}_\omega. \tag{4.25}$$

These considerations are still valid in the case we cosider the normalized time series for the phase synchronization evaluation, meaning that the instantaneous, zero-phase, zero-lag covariance matrix corresponding to a normalized multi-variate time series $\mathbf{X}$ at frequency ω, is easily the real part of the phase-information Hermitian covariance matrix at frequency ω, i.e. $\mathcal{R}e(\mathbf{S}_{\tilde{\mathbf{X}}\tilde{\mathbf{X}}\omega})$.

Eq. 4.26 shows the expression of the measure of linear dependence between time series $\mathbf{X}$ and $\mathbf{Y}$ at frequency ω, where $|\mathbf{M}|$ denotes the determinant of the matrix $\mathbf{M}$.

$$F_{X,Y}(\omega) = ln \frac{\begin{vmatrix} \mathbf{S}_{\mathbf{YY}\omega} & \mathbf{o} \\ \mathbf{o}^T & \mathbf{S}_{\mathbf{XX}\omega} \end{vmatrix}}{\begin{vmatrix} \mathbf{S}_{\mathbf{YY}\omega} & \mathbf{S}_{\mathbf{YX}\omega} \\ \mathbf{S}_{\mathbf{XY}\omega} & \mathbf{S}_{\mathbf{XX}\omega} \end{vmatrix}} \tag{4.26}$$

It is worth noting that the matrix in the numerator of Eq. 4.26 is a block diagonal matrix of dimension qxp, with $\mathbf{o}$ denoting a matrix of zeros. This linear dependence measure is expressed as the sum of the lagged linear dependence, called $F_{X \rightleftharpoons Y}(\omega)$, and instantaneous linear dependence, named $F_{X \cdot Y}(\omega)$, as follows

$$F_{X,Y}(\omega) = F_{X \rightleftharpoons Y}(\omega) + F_{X \cdot Y}(\omega). \tag{4.27}$$

Eq. 4.28 and Eq. 4.29 define the measure of instantaneous linear dependence and the measure of lagged linear dependence, respectively.

$$F_{X \cdot Y}(\omega) = ln \frac{\left| \mathcal{R}e \begin{pmatrix} \mathbf{S}_{\mathbf{YY}\omega} & \mathbf{o} \\ \mathbf{o}^T & \mathbf{S}_{\mathbf{XX}\omega} \end{pmatrix} \right|}{\left| \mathcal{R}e \begin{pmatrix} \mathbf{S}_{\mathbf{YY}\omega} & \mathbf{S}_{\mathbf{YX}\omega} \\ \mathbf{S}_{\mathbf{XY}\omega} & \mathbf{S}_{\mathbf{XX}\omega} \end{pmatrix} \right|} \tag{4.28}$$

$$F_{X \rightleftharpoons Y}(\omega) = F_{X,Y}(\omega) - F_{X \cdot Y}(\omega) = ln \frac{\left| \mathcal{R}e \begin{pmatrix} \mathbf{S}_{\mathbf{YY}\omega} & \mathbf{S}_{\mathbf{YX}\omega} \\ \mathbf{S}_{\mathbf{XY}\omega} & \mathbf{S}_{\mathbf{XX}\omega} \end{pmatrix} \right| \Big/ \left| \mathcal{R}e \begin{pmatrix} \mathbf{S}_{\mathbf{YY}\omega} & \mathbf{o} \\ \mathbf{o}^T & \mathbf{S}_{\mathbf{XX}\omega} \end{pmatrix} \right|}{\begin{vmatrix} \mathbf{S}_{\mathbf{YY}\omega} & \mathbf{S}_{\mathbf{YX}\omega} \\ \mathbf{S}_{\mathbf{XY}\omega} & \mathbf{S}_{\mathbf{XX}\omega} \end{vmatrix} \Big/ \begin{vmatrix} \mathbf{S}_{\mathbf{YY}\omega} & \mathbf{o} \\ \mathbf{o}^T & \mathbf{S}_{\mathbf{XX}\omega} \end{vmatrix}} \tag{4.29}$$

All these measures are non-negative and, moreover, they take the zero value only when there is independence of the pertinent type (lagged, instantaneous, or both).

In general, the measure of linear dependence $F_{X,Y}(\omega)$ can be interpreted as

$$\rho^2_{X,Y}(\omega) = 1 - e^{-F_{X,Y}(\omega)} \tag{4.30}$$

where $\rho_{X,Y}(\omega)$ is defined as the general coherence in [163]

$$\rho^2_{X,Y}(\omega) = \rho^2_c = 1 - \frac{\left| \mathbf{S}_{\mathbf{YY}\omega} - \mathbf{S}_{\mathbf{YX}\omega} \mathbf{S}^{-1}_{\mathbf{XX}\omega} \mathbf{S}_{\mathbf{XY}\omega} \right|}{|\mathbf{S}_{\mathbf{YY}\omega}|}. \tag{4.31}$$

In particular, we can define the instantaneous coherence $\rho_{X \cdot Y}(\omega)$ as

$$\rho^2_{X \cdot Y}(\omega) = 1 - e^{-F_{X \cdot Y}(\omega)} = 1 - \frac{\left| \mathcal{R}e \begin{pmatrix} \mathbf{S}_{\mathbf{YY}\omega} & \mathbf{S}_{\mathbf{YX}\omega} \\ \mathbf{S}_{\mathbf{XY}\omega} & \mathbf{S}_{\mathbf{XX}\omega} \end{pmatrix} \right|}{\left| \mathcal{R}e \begin{pmatrix} \mathbf{S}_{\mathbf{YY}\omega} & \mathbf{o} \\ \mathbf{o}^T & \mathbf{S}_{\mathbf{XX}\omega} \end{pmatrix} \right|} \tag{4.32}$$

Regarding the lagged coherence, it can be stated that the relationship shown in Eq. 4.33 holds.

$$\rho^2_{X \rightleftharpoons Y}(\omega) = 1 - e^{-F_{X \rightleftharpoons Y}(\omega)} = 1 - \frac{\begin{vmatrix} \mathbf{S}_{\mathbf{YY}\omega} & \mathbf{S}_{\mathbf{YX}\omega} \\ \mathbf{S}_{\mathbf{XY}\omega} & \mathbf{S}_{\mathbf{XX}\omega} \end{vmatrix} \Big/ \begin{vmatrix} \mathbf{S}_{\mathbf{YY}\omega} & \mathbf{o} \\ \mathbf{o}^T & \mathbf{S}_{\mathbf{XX}\omega} \end{vmatrix}}{\left| \mathcal{R}e \begin{pmatrix} \mathbf{S}_{\mathbf{YY}\omega} & \mathbf{S}_{\mathbf{YX}\omega} \\ \mathbf{S}_{\mathbf{XY}\omega} & \mathbf{S}_{\mathbf{XX}\omega} \end{pmatrix} \right| \Big/ \left| \mathcal{R}e \begin{pmatrix} \mathbf{S}_{\mathbf{YY}\omega} & \mathbf{o} \\ \mathbf{o}^T & \mathbf{S}_{\mathbf{XX}\omega} \end{pmatrix} \right|} \tag{4.33}$$

It is worth stressing the asymmetry in the results regarding the instantaneous coherence $\rho^2_{X\cdot Y}(\omega)$ and the lagged coherence $\rho^2_{X=Y}(\omega)$. Indeed, while the instantaneous coherence is the real part of the complex valued coherence, the lagged coherence is not the imaginary part of the complex valued coherence: the lagged coherence is ideally not affected by instantaneous dependence, whereas the imaginary part of the complex valued coherence is more affected by instantaneous dependence. As a consequence, the lagged coherence is a much more adequate electrophysiological connectivity measure. The reason is that it removes the confounding effect of instantaneous dependence due to low spatial resolution and volume conduction.

Phase synchronization has a rigorous physics definition that has been adapted and used in the neuroscience field. Other equivalent descriptive names for phase synchronization appear in the neuroscience, such as phase locking, phase locking value, phase locking index, phase coherence, etc. Consider two univariate stationary time series and $x_{j\omega}$, $y_{j\omega}$, with $j = 1, 2, ..., N_R$, their sample data in the frequency domain obtained using the discrete Fourier transform. Defining $\Delta\phi_j = \phi^x_j - \phi^y_j$ as the phase difference, it can be stated that if $\Delta\phi_j$ is stable over time segments j (independently from the amplitude), then there is a connection between the locations at which the measurements are made. This involves that phase synchronization can be seen as a measure of stability of phase difference. For the non-stationary case, a similar definition exists based on the concept of time-varying instantaneous phase and the definition of the stability over time instead of over segments. Furthermore, this measure can be seen as the absolute value of the complex valued (Hermitian) coherency between the normalized Fourier transforms. The normalization is done in a non-linear way before the calculation of the coherency such as removing from the outset any amplitude affects and leaving only phase information. This absolute value ranges between 0, i.e., no synchronization, and 1, i.e., perfect synchronization.

In the general case of two multi-variate time series, the measure of non-linear dependence $G_{X,Y}$ can be defined as the sum of lagged non-linear dependence $G_{X=Y}$ and instantaneous non-linear dependence $G_{X\cdot X}$. Similarly to what previously discussed, Eqs. 4.34-4.36 show the expressions of $G_{X,Y}$, $G_{X\cdot Y}$, and $G_{X=Y}$, respectively.

$$G_{X,Y}(\omega) = G_{X=Y}(\omega) + G_{X\cdot Y}(\omega) = ln\frac{\begin{vmatrix}\mathbf{S}_{\tilde{\mathbf{Y}}\tilde{\mathbf{Y}}\omega} & \mathbf{o} \\ \mathbf{o}^T & \mathbf{S}_{\tilde{\mathbf{X}}\tilde{\mathbf{X}}\omega}\end{vmatrix}}{\begin{vmatrix}\mathbf{S}_{\tilde{\mathbf{Y}}\tilde{\mathbf{Y}}\omega} & \mathbf{S}_{\tilde{\mathbf{Y}}\tilde{\mathbf{X}}\omega} \\ \mathbf{S}_{\tilde{\mathbf{X}}\tilde{\mathbf{Y}}\omega} & \mathbf{S}_{\tilde{\mathbf{X}}\tilde{\mathbf{X}}\omega}\end{vmatrix}} \tag{4.34}$$

$$G_{X\cdot Y}(\omega) = ln\frac{\left|\mathcal{R}e\begin{pmatrix}\mathbf{S}_{\tilde{\mathbf{Y}}\tilde{\mathbf{Y}}\omega} & \mathbf{o} \\ \mathbf{o}^T & \mathbf{S}_{\tilde{\mathbf{X}}\tilde{\mathbf{X}}\omega}\end{pmatrix}\right|}{\left|\mathcal{R}e\begin{pmatrix}\mathbf{S}_{\tilde{\mathbf{Y}}\tilde{\mathbf{Y}}\omega} & \mathbf{S}_{\tilde{\mathbf{Y}}\tilde{\mathbf{X}}\omega} \\ \mathbf{S}_{\tilde{\mathbf{X}}\tilde{\mathbf{Y}}\omega} & \mathbf{S}_{\tilde{\mathbf{X}}\tilde{\mathbf{X}}\omega}\end{pmatrix}\right|} \tag{4.35}$$

$$G_{X=Y}(\omega) = G_{X,Y}(\omega) - G_{X\cdot Y}(\omega) = ln\frac{\left|\mathcal{R}e\begin{pmatrix}\mathbf{S}_{\tilde{\mathbf{Y}}\tilde{\mathbf{Y}}\omega} & \mathbf{S}_{\tilde{\mathbf{Y}}\tilde{\mathbf{X}}\omega} \\ \mathbf{S}_{\tilde{\mathbf{X}}\tilde{\mathbf{Y}}\omega} & \mathbf{S}_{\tilde{\mathbf{X}}\tilde{\mathbf{X}}\omega}\end{pmatrix}\right| \Big/ \left|\mathcal{R}e\begin{pmatrix}\mathbf{S}_{\tilde{\mathbf{Y}}\tilde{\mathbf{Y}}\omega} & \mathbf{o} \\ \mathbf{o}^T & \mathbf{S}_{\tilde{\mathbf{X}}\tilde{\mathbf{X}}\omega}\end{pmatrix}\right|}{\begin{vmatrix}\mathbf{S}_{\tilde{\mathbf{Y}}\tilde{\mathbf{Y}}\omega} & \mathbf{S}_{\tilde{\mathbf{Y}}\tilde{\mathbf{X}}\omega} \\ \mathbf{S}_{\tilde{\mathbf{X}}\tilde{\mathbf{Y}}\omega} & \mathbf{S}_{\tilde{\mathbf{X}}\tilde{\mathbf{X}}\omega}\end{vmatrix} \Big/ \begin{vmatrix}\mathbf{S}_{\tilde{\mathbf{Y}}\tilde{\mathbf{Y}}\omega} & \mathbf{o} \\ \mathbf{o}^T & \mathbf{S}_{\tilde{\mathbf{X}}\tilde{\mathbf{X}}\omega}\end{vmatrix}} \tag{4.36}$$

These non-linear dependence measures can be associated to phase synchronization measures and Eqs. 4.37-4.39 define the relationships. In particular, Eqs. 4.37-4.39 show the general expression of the phase synchronization, the instantaneous phase synchronization, and the lagged phase synchronization, respectively, between two multi-variate time series.

$$\phi^2_{X,Y}(\omega) = 1 - e^{-G_{X,Y}(\omega)} = 1 - \frac{\left|\mathbf{S}_{\tilde{\mathbf{Y}}\tilde{\mathbf{Y}}\omega} - \mathbf{S}_{\tilde{\mathbf{Y}}\tilde{\mathbf{X}}\omega}\mathbf{S}^{-1}_{\tilde{\mathbf{X}}\tilde{\mathbf{X}}\omega}\mathbf{S}_{\tilde{\mathbf{X}}\tilde{\mathbf{Y}}\omega}\right|}{\left|\tilde{\mathbf{S}}_{\tilde{\mathbf{Y}}\tilde{\mathbf{Y}}\omega}\right|}. \tag{4.37}$$

$$\phi^2_{X \cdot Y}(\omega) = 1 - e^{-G_{X \cdot Y}(\omega)} = 1 - \frac{\left| \mathcal{R}e \begin{pmatrix} \mathbf{S}_{\tilde{\mathbf{Y}}\tilde{\mathbf{Y}}\omega} & \mathbf{S}_{\tilde{\mathbf{Y}}\tilde{\mathbf{X}}\omega} \\ \mathbf{S}_{\tilde{\mathbf{X}}\tilde{\mathbf{Y}}\omega} & \mathbf{S}_{\tilde{\mathbf{X}}\tilde{\mathbf{X}}\omega} \end{pmatrix} \right|}{\left| \mathcal{R}e \begin{pmatrix} \mathbf{S}_{\tilde{\mathbf{Y}}\tilde{\mathbf{Y}}\omega} & \mathbf{o} \\ \mathbf{o}^T & \mathbf{S}_{\tilde{\mathbf{X}}\tilde{\mathbf{X}}\omega} \end{pmatrix} \right|} \tag{4.38}$$

$$\phi^2_{X \rightleftharpoons Y}(\omega) = 1 - e^{-G_{X \rightleftharpoons Y}(\omega)} = 1 - \frac{\left| \begin{matrix} \mathbf{S}_{\tilde{\mathbf{Y}}\tilde{\mathbf{Y}}\omega} & \mathbf{S}_{\tilde{\mathbf{Y}}\tilde{\mathbf{X}}\omega} \\ \mathbf{S}_{\tilde{\mathbf{X}}\tilde{\mathbf{Y}}\omega} & \mathbf{S}_{\tilde{\mathbf{X}}\tilde{\mathbf{X}}\omega} \end{matrix} \right| \Big/ \left| \begin{matrix} \mathbf{S}_{\tilde{\mathbf{Y}}\tilde{\mathbf{Y}}\omega} & \mathbf{o} \\ \mathbf{o}^T & \mathbf{S}_{\tilde{\mathbf{X}}\tilde{\mathbf{X}}\omega} \end{matrix} \right|}{\left| \mathcal{R}e \begin{pmatrix} \mathbf{S}_{\tilde{\mathbf{Y}}\tilde{\mathbf{Y}}\omega} & \mathbf{S}_{\tilde{\mathbf{Y}}\tilde{\mathbf{X}}\omega} \\ \mathbf{S}_{\tilde{\mathbf{X}}\tilde{\mathbf{Y}}\omega} & \mathbf{S}_{\tilde{\mathbf{X}}\tilde{\mathbf{X}}\omega} \end{pmatrix} \right| \Big/ \left| \mathcal{R}e \begin{pmatrix} \mathbf{S}_{\tilde{\mathbf{Y}}\tilde{\mathbf{Y}}\omega} & \mathbf{o} \\ \mathbf{o}^T & \mathbf{S}_{\tilde{\mathbf{X}}\tilde{\mathbf{X}}\omega} \end{pmatrix} \right|} \tag{4.39}$$

To sum up before proceeding, coherence and phase synchronization can be used as a measure of connectivity between two brain areas (more in general cortices) described by the time series of scalp electric potential differences, i.e., EEG. In this context, volume conduction effect might induce significantly high coherence or phase synchronization even if the two underlying cortices are not actually connected: the activity at any cortical area will be observed instantaneously (with zero-lag) by all scalp electrodes. To deal with this problem using EEG signals and eLORETA as imagining technique, it is necessary to estimate the electric neuronal activity distributed throughout the cortex. In particular, a 3D component vector corresponding to the current density vector with dipole moments along the X, Y, and Z axes is computed. This tomography has zero location error and it is linear, but at the same time it has low spatial resolution. This means that the time series will suffer from non-physiological values of zero-lag coherence and phase synchronization.

The analysis previously shown has been done considering two multi-variate time series, however it can be easily extended to estimate the similarity between groups of multi-variate time series. Indeed, it would be sufficient to consider the cross-spectra matrix between each time series and, then, a higher dimension for the matrices, i.e., corresponding to the number of time series considered, for the evaluation of the total, instantaneous, and lagged coherence and/or phase synchronization.

In the literature, it can be found several recent examples of application of the LORETA procedures to evaluate brain networks connectivity. It is worth noting that several version of the LORETA-based software exist each of them aiming at solving the source localization problem. For our future works we are interested in using eLORETA described in this Chapter. In [166], the use of group-ICA (i.e., independent component analysis) to decompose resting state EEG signals into a certain number of independent components (ICs) is proposed. The authors use LORETA to find the cortical location of these ICs into spatially well-defined sources (or nodes). Through the estimation of the spectral power cross-correlation between different ICs within subjects, they obtain a functional relationship between such EEG source nodes. As a results of their work it is possible to state that since changes in α-band connectivity between eye close and eye open can be observed, it's feasible to study neuronal resting-state networks considering the existence of functional connectivity between ICA components in EEG data. Furthermore, the detection of EEG resting-state independent networks (EEG RS-independent-Ns) and their interactions in all frequency bands have been also investigated [167]. In this paper, the author apply eLORETA and ICA to resting-state EEG data in healthy subjects considering δ, θ, α, β, and γ frequency bands and they find five RS-independent-Ns in the α, β, and γ frequency bands.

A similar analysis is carried in [168], in which the authors do not consider resting state EEG data, but EEG data recorded during listening of music. The goal is to process sleep spindles with ICA in order to investigate the opportunity of extracting spindle components (SCs) corresponding to different EEG activity patterns during a spindle. This has been done by means of visual analysis of the spindle EEG and visual selection of ICs. Furthermore, LORETA is used to define the intracranical current sources underlying these SCs.

4.2.2.3 eLORETA and multiplexing approach

It is clearly evident looking at the literature that the quantitative analysis of networks is fundamental for the study of systems throughout the biological, social, information, engineering, and physical sciences. Indeed, several examples of networks analysis can be found across different disciplines: networks have been used to represent interactions between proteins, friendships between people, hyperlinks between Web pages, and much more. In addition to this, several features arise in a diverse variety of networks. Networks constructed from empirical data exhibit heavy tailed degree distributions, the small-world property, and/or modular structures. These structural features can have relevant implications, e.g. for information diffusion and robustness against component failure.

Traditional networks studies assumed that nodes are connected to each other by a single type of static link that encapsulates all connections between them. Most of the time this assumption can be a gross oversimplification, and it can led to misleading results and even the inability to address certain problems. As an example, consider the transmission of diseases [169]. If time dependence is ignored with the consequence of loosing the order of pairwise human contacts, the presence of multiple layers would be ignored making it difficult to unravel the relevance of multiple transportation and communication modes [170]. To incorporate multiple channels of connectivity in a system, a multilayer (and, more specifically, *multiplex*) network model is needed [171]. For this reason, nowadays, an increasing number of researchers with diverse expertise have turned their attention to studying multiplex networks [172, 173, 174, 175, 176]. This kind of networks provide a natural description for systems in which entities have a different set of neighbors in each layer, which can represent, for example, a task, an activity, a category. An important aspect in describing multilayer networks is defining and quantifying the interconnectivity between different categories of connections. Multiplex networks could also be suggestive for extended holistic representations of the whole network, where the underlying connectivity structure is abstracted by multiple layers and where specialized (functional) behaviors may emerge, a feature that is typically attributed to neural and social systems. As an instance in a telecommunications context, this can lead to advanced representations of smart cities as complex systems with bio-inspired approaches.

In [162] the author gives a review of the main achievements obtained from interdisciplinary research based on fMRI and establishes the birth of multilayer network analysis and modeling of the human brain. According to the definition of multilayer network that he gives, it consists of several distinct classical networks, each one encoding a specific type of information about the system. There are different types of multilayer brain networks where layers' connectivity, measured with respect to a specific definition of similarity (e.g., cross-correlation, spectral coherence, phase synchronization) might encode: (i) activity in different frequency bands; (ii) time-varying activity; (iii) activity with respect to different tasks; (iv) structural and functional connectivity. Moreover, some examples of applications of frequency-based decomposition related to fMRI and MEG data are discussed. It is shown that the choice of the frequency band might have a relevant impact on the functional representation of the brain, result that are in agreement with what we discussed Sub-section 4.2.1. As a consequence, considering a multilayer approach might be useful to distinguish the contributions coming from different frequency bands.

In the literature, other interesting investigations focusing on the study of the brain connectivity in different frequency bands using fMRI data can be found. In particular, in [177], the authors show that, in investigating the coherence spectrum among 87 brain regions using fMRI data, two frequency bands, 0.01–0.03 Hz (very low frequency, VLF, band) and 0.07–0.09 Hz (low frequency, LF, band), mainly contributed to functional connectivity. Comparing graph theoretical indices for the VLF and LF bands reveals that the network in the former case has a higher capacity for information segregation between identified communities than the latter case. Hubs in the VLF band are mainly located within the anterior cingulate cortices, whereas those in the LF band are located in the posterior cingulate cortices and thalamus. In [178] and [179], the authors show that each functional layer in a

range between 0.01 Hz and 0.25 Hz, in steps of 0.02 Hz, provides unique information and should be neither aggregated with other layers nor neglected. The result is based on the analysis of structural reducibility, a modern technique grounded on information entropy. The irreducibility of the multilayer functional representation of human brain raises the necessity for multilayer analysis of the underlying architecture and a few first results have been recently reported about the identification of hubs. It has been shown that hubs in a multilayer network might be dramatically different from hubs in each layer of the system. In this context, hubs can be used to distinguish, with high accuracy and sensitivity (above 80% in both cases), the brain of a schizophrenic patient from a healthy brain in resting state.

In [180, 181, 182, 183], MEG data are used in a similar way as previously said regarding fMRI data. In particular, layers are used to encode the connectivity between neural oscillations within four frequency bands, namely alpha ($8-13$ Hz), beta ($13-30$ Hz), low gamma ($30-50$ Hz) and high gamma ($50-100$ Hz) [180]. In this context, the mean connection strength, averaged across the network where the functional connectivity between schizophrenic patients and controls differs most, has been used to gain new insights about within and between oscillatory frequencies. In [181], two regimes of multilayer network behavior have been identified in a system with 5 layers (bands $1-4$ Hz, $4-8$ Hz, $8-13$ Hz, $13-30$ Hz and $30-48$ Hz): in the first regime layers are independent, while in the second regime they are highly dependent. Results suggest that healthy human brain operates at the transition point between these two regimes. These studies provide evidence for and support the hypothesis that functional layers do not act as independent entities, suggesting the existence of mechanisms for integration and segregation of brain activity within and across different frequency bands [182]. Moreover, MEG recordings during resting states in subjects affected by the Alzheimer's disease have been used to build a multilayer network where layers represent functional connectivity in different frequency bands ($2-4$ Hz, $4-8$ Hz, $8-10.5$ Hz, $10.5-13$ Hz, $13-20$ Hz, $20-30$ Hz, $30-45$ Hz). The study provides evidence that regional connectivity in unhealthy subjects is abnormally distributed across frequency bands (a feature with no counterpart in healthy individuals) revealing an abnormal loss of inter-frequency centrality in memory-related association areas. The proposed methodology has led to high classification accuracy (78.4%) and sensitivity (91.1%) of subjects, confirming the superior performance of multilayer analysis as compared to more traditional approaches [183].

However, to the best of our knowledge any investigations based on multiplexing/multilayer analysis applied to EEG data can be found in the scientific literature. Some works analyze EEG data considering different frequency bands, but without any reference to a multiplexing approach. In [184] authors combined simultaneous MEG and EEG (MEEG) recordings with minimum-norm-estimate-based inverse modeling to investigate the structure of oscillatory phase synchronized networks that are active during visual working memory (VWM) maintenance. The resulting networks are characterized with a number of network metrics that are then compared between delta/theta, alpha, beta, and gamma frequency bands. Several salient differences between frequency bands have been found. Alpha- and beta-band networks are more clustered and small-world like but have smaller global efficiency than the networks in the delta/theta and gamma bands. Alpha- and beta-band networks also have truncated-power-law degree distributions and high k-core numbers. The data converge on showing that during the VWM-retention period, human cortical alpha- and beta-band networks have a memory-load dependent, scale-free small-world structure with densely connected core-like structures. These data further show that synchronized dynamic networks underlying a specific cognitive state can exhibit distinct frequency-dependent network structures that could support distinct functional roles.

In [185], the authors examine changes in functional brain networks during normal development in young children using graph theoretical concepts. Resting-state eyes-closed EEG was recorded (14 channels) from 227 children twice at 5 and 7 years of age. Synchronization likelihood (SL) is calculated in three different frequency bands and between each pair of electrodes to obtain SL-weighted graphs. Mean normalized clustering index, average path length and weight dispersion are then calculated to characterize network organization. Repeated measures analysis of variance test for time and gender

effects. For all frequency bands mean SL decreases from 5 to 7 years; clustering coefficient increases in the alpha band; path length increases in all frequency bands; mean normalized weight dispersion decreases in beta band. Moreover, it has be found that girls show higher synchronization for all frequency bands and a higher mean clustering in alpha and beta bands.

In [186], considering EEG data during sleep, the relationship between the activities in different frequency bands is evaluated calculating the cross correlation coefficient. The procedure used allows an objective and automated quantitative analysis of the sleep EEG. The purpose of the authors is the characterization of the sleep cycle as a dynamic and continuous process. In [187], the effects of ten 10Hz-wide sub-bands between 0 and 100Hz on mental tasks classification are studied. An investigation on the interaction of different EEG frequency bands and their effects on the SPM systematically by comparing different correlation models with various numbers of degrees of freedom is done in [188]. In EEG/fMRI correlation studies it is common to consider the fMRI BOLD as filtered version of the EEG alpha power. Therefore, in this paper the question that is addressed is whether EEG frequency components may affect the correlation between alpha band and BOLD. This is done comparing the statistical parametric maps (SPMs) and considering the EEG data in different frequency bands. Finally, in [189], the authors compare resting-state functional connectivity derived across frequency bands from EEG with resting-state functional connectivity derived from BOLD fMRI. They investigate the relationship between synchronous fMRI and EEG connectomes across frequency bands in a whole-brain, using source space analysis. Based on such analysis, fMRI connectivity is dominated by the inter-hemispheric connections between homologous areas, whereas brain connectivity derived from EEG shows a more complex pattern of connections composed by both intra-hemispheric and inter-hemispheric connections. Moreover, they find that EEG connectomes in low frequency bands are the most similar to resting-state fMRI connectomes.

According to what just discussed, our purpose is to analyze brain network connectivity using EEG signals, coherence and phase-synchronization as a measure of similarity between the different brain areas. Our aim is to base the analysis on a multiplexing perspective as a network representation in which each layer defines a different network, for example, constructed from a different subject, patient group, experimental condition, cognitive task, or time point. It might be conceived to combine multiple aspects, thus creating a network with more than one multilayer dimension; for example, a multilayer network in which one dimension is pazient and a second dimension is time. In this kind of network structure, a node can exist in all layers or in a subset of layers and it is linked throughout the layers by an edge representing its identity. Different edges types can also link nodes within and between layers representing different types of relationships between network elements. This framework is particularly appealing in the context of understanding statistically significant similarities and differences in network structure between experimental scenarios or across time, a traditionally difficult enterprise.

In this background, we aim at creating connectomes obtained in terms of connectivity matrices using some source localization tools, such as eLORETA, for each frequency band of interest. Before defining the connectivity matrices, it would be necessary to apply some pre-processing analysis to the raw data in order to clean the signals in the sense described in Sub-section 4.2.1. Moreover, it would be interesting to design a multi-frequency band characterization of the patients used to get the EEG data. Some features of the connectomes obtained might be extracted for each patient and for each frequency band, with particular reference to local community paradigm (LCP) usually used for link prediction in bipartite network, small-world and scale-free properties, average node degree, path length, clustering coefficient, rich-club structure, and others. To do so, we need to extend and generalize the mathematical formulations of these network features from a monoplex point of view (i.e., classical network) to a multiplexing perspective addressing the inherent dependencies between networks and offering a more suitable framework for statistical inference.

We firmly believe that using a mathematical framework incorporating the interconnected nature of the system is needed to understand the intricacies of the neuroscientific data and their utility in

uncovering relevant principles of brain function. Indeed, this is a natural consequence of the fact that as technology advances, the neuroscience community is becoming significantly overwhelmed by rich data sets reflecting complex spatio-temporal interactions across multiple scales of the brain. Network analysis, especially dynamic neural networks built on multiplexing approaches, might be a powerful tool to describe the complex evolution and organization of the human brain and its relationship to cognition. In this way, it might be possible to increasingly tease apart the complex relationships between the structure and the function of the brain, make predictions on the evolution of disease state, and understand how dynamc interactions through remote brain areas give rise to cognitive states defining human function.

Chapter 5

General conclusions

The research investigations presented in this thesis are strongly related to the recent development of the Network Science. The key factor combining all the evaluations discussed is that, despite the obvious diversity of the systems investigated, the structure and the evolution of the networks behind each system is driven by a common set of central laws and organizing principles. Therefore, disregarding the nature of the components and the precise nature of their interactions, it's possible to use a common set of mathematical tools to explore them. The basic architecture of networks emerging in various domains of science, technology, and nature are similar to each other. Consequently, theories and models belonging to different fields can be used and jointly applied to investigate on networks problems spanning different scientific contexts.

The research path discussed here started dealing with ICT issues addressed using classical telecommunications investigations. In particular, an error detection/correction mechanism based on the selective retransmissions of erroneous packets has been designed to video flow transmissions by means of a Markov analysis. The aim was to evaluate the system perfomance in terms of throughput, packet dropping probability, and average number of transmissions taking care of the incremental nature of the source coding used for video flow packets and the real-time aspect related to multimedia transmissions. According to the numerical results, the channel correlation may be beneficial to increase throughput and, therefore, the transmission speed. Moreover, we found that the correlation has a worsening effect on the average number of transmissions and the dropping probability, since these quantities increase as the channel burstiness increases. In video transmissions, retransmissions lead to undesirable delays and dropped independent packets cause an irreversible loss of information, which, in turn, compromises the quality of the video. A tradeoff between transmission speed and reproduction quality has thus emerged.

A Markov analysis has been further applied for the management of EVs networks. In particular, we investigated on how the so-called range anxiety can be avoid considering the impact of the battery charge, charging time, and number of charging spots on the network performance in terms of probability of successful service completion. Indeed, the daily usage of EVs has been considered and the previously mentioned probability refers to the case in which the car user is able to reach home at the end of the day. In this setup, the range anxiety describes the situation in which customers are wary of EVs practicality due to their limited autonomy, long recharging time, and the still small number of recharging points. It has been found that the EV autonomy is the key factor to avoid the range anxiety. In particular, a reasonable high probability of sevice completion can be achieved only if the value of the autonomy is large enough. Moreover, the frequency of the recharging spots has a relevant impact as well: if the number of charging points is too low, then the required autonomy might be too high.

One of the other relevant aspects that unites any network type is that it might be made up of several different entities. In a communications network these entities may refer to different technologies

with the aim to provide or require different services with likely different purposes. Consequently, the joint combination of theories and models not directly related to the telecommunications world may be useful to solve communications network problems. In particular, some game theoretic-based analysis have been decribed and discussed. Indeed, despite game theory is born in an economic context, it has been used to evaluate communications network issues since it works towards goals similar to some purposes of telecommunications methods. In particular the management of queueing system, jamming problems, and group recognition in a telecommunications network have been addressed by means of game theory.

Systems with multiple candidate strategic agents requiring or offering services (downlink or uplink case, respectively) that can decide to keep them active, i.e., available to require/offer the service, or inactive have been considered. We analyzed our systems under different cooperation and communication assumptions and we applied a Bayesian game theoretic approach to evaluate the agents' behavior. Our principal purpose was to quantify the impact of the lack of cooperation and communication among the agents in terms of system performance. The main result is that the a priori perfect knowledge of the system is not necessary. In fact, we found that additional partial information brings significant improvements in the system. In particular, considering a scenario in which it is allowed to the agents to share specific information about their types involves the same NE computation as the perfect knowledge case. Looking for a more dept reading of the results, for the uplink case we found that staying inactive is not always advantageous, but it depends on the value of the cost of being active payed by the agent. On the other hand, for the downlink case it holds that the results related to the scenario in which the client is acting selfishly are the same as the results obtained considering a setup with complete and perfect knowledge. Therefore, acting selfishly is not always a negative choice, but it depends on the environment considered for the evaluations.

To futher support the idea that theories referring different environments can be jointly combined towards a common goal, the security issue known as jamming problem has been investigated by means of game theory. Two possible scenarios have been investigated: wireless sensor network and underwater acoustic sensor network. The difference between them is in the communication channels. Indeed, it is well known that underwater channels have a small bandwidth compared to terrestrial channels, meaning lower bit rates. Then, the speed of acoustic waves in water is several orders of magnitudes lower than that of the electromagnetic ones in air, consequently, this results in a huge propagation delay. Threfore, some medium access adjustments may be necessary to deal with these two different environments. However, in general, it was possible to draw the same final observations in both cases. We investigated the dependence of the NEs and the resulting payoff on the distance between a legittimate receiver and a jammer. The main result is that, depending on the propagation parameters, there are some range of values for this distance for which the NE solution implies that the jammer adopts a pure strategy, meaning that a given channel is jammed with probability 1. As a matter of fact, the network manager should especially control those situations where this does not happen. Those cases are the ones in which the jammer occupies a position according to which at the equilibrium its strategy mixes multiple jamming actions. Such scenarios have been classified as critical positions for the jammer. It can further be stated that any security enforcement should especially check those areas for jammers.

In addition to this, we showed how a game theoretic approach can be employed to characterize interactions in social online networking, with particular reference to the several challenges pose by terminals mobility in terms of identifying malicious players aiming at damaging the network operation. In this context, we considered a Bayesian game between a server and a client where the server is operating with incomplete information and only has a prior belief on the client actual type. The analysis confirmed practical aspects of network surveillance. It has been found that malicious clients are hard to defeat without a proper detection and confirmation that they are indeed malicious. Moreover, given the high cost of surveillance operation, the best strategy for the server would not be forcing the

identification of malicious clients, but rather to force a malicious client to strategically play some less harmful strategies. An implicit surveillance without the need of actually putting them into operation would be led. The numerical results confirm this trend: under certain circumstances, it is more advantageous for the client (even a malicious one) not to harm the network in fear of retaliation. This may happen if a strategic client does not apply just a myopic optimization of its own payoff, but rather tries to avoid being identified. To do so the malicious client might occasionally cooperate with the network, leading to a transparent surveillance in which the client itself has the right incentive to behave correctly.

Strongly related to the previous works investigated, but on a different matter, we considered a problem of group detection in social mobile networks, where network mapping by each individual node is assumed to be limited to its neighbors. Our aim was to show how traditional clustering procedures fail to efficiently identify the existing group structures, while a simple heuristic procedure based on the concept of social spreading of information achieves a much higher efficiency of cluster recognition. The system efficiency could be further enhanced by combining our proposed procedure with a standard clustering technique. The relationship with the previous investigations lies on the fact the malicious agents can be in the network with the purpose of disseminating corrupted social information. In this case, it would be useful to identify the malicious nodes before the exchange of social information is hopelessly corrupted.

In addition to the several extensions of the analysis described in details, some future reaserch interests have been discussed as well. In particular, if on one hand these interests aim at continuing on the path traced by the already tackled research topics, on the other hand they represent the will to start a new research path where an ICT point of view might be used to address problems not directly related to telecommunications networks.

Following the same path of the current research, we considered a mobile computing context. The key aspect of the system model considered is that there are advantages and disadvantages in offloading towards the remote cloud or the network edge. In particular, the edge server usually is nearest with respect to the remote cloud to the final user, however it has less computation capabilities in comparison with it. In this setup, our purpose was to address the management of computational offloading in a three-tier hierarchical architecture comprising mobile devices, edge computing, and cloud computing. Although edge and cloud devices have lower data processing time than mobile devices, the simultaneous transmission of heavy data streams may overload the local wireless network, resulting in an overall larger delay. Therefore, a game theoretic framework is proposed for the distributed decision making in a scenario where mobile users share the same network resource and do not have a priori information in the wireless links. We evaluated at first the rational gameplay of the nodes in a scenario with complete knowledge, and we compared it with a scenario with incomplete information modeled as a Bayesian game. In particular, we considered network positions, and consequently channel gain and distance-related parameters, to be uniformly distributed within a given range, and the nodes only have this knowledge available as a prior. The analysis demonstrated that rationality (implying selfish behavior) of the mobile users does not necessarily lead to a more efficient allocation and actually the scenario of incomplete information leads to a socially better outcome, thereby suggesting an interesting guideline for the design of computational offloading strategies in realistic scenarios. Future investigations on this topic aim at empowering the analysis done considering more sophisticated game theory approaches. It might be conceived to take into account, for example, the human aspect behind the mobile device. This can be done through evolutionary games according to which the actions choices are influenced by the dynamics of the system in terms of choosing, e.g., the action that has been more frequently chosen. Furthermore, a combination of reinforcement learning, with particular reference to dynamic programming, and game theory can be considered. The former can be used to investigate on the internal system dynamics, the latter to define the set of possible policies.

In the light of the scientific evolution and the key concepts of the Network Science, we further

suggested the investigation on brain connectivity using a ICT standpoint. It is generally accepted that the brain can be modeled as a complex network and, in the literature, there can be found several descriptions of the relationship between the brain system and a complex network. In particular, some preliminary investigations that we have done confirmed the idea that the brain connectivity can be evaluated using a multiplexing approach. Indeed, using fMRI data, we found that considering the brain signals in different frequency bands implies having different connectivity matrices. As a consequence, according to a multiplexing point of view, our purpose is to analyze the brain connectivity in terms of features and properties that the brain shows as a network of networks, where each layer can be associated to a different frequencies band. It is worth underline that other "meanings" can be assigned to the layers obtaining several networks of networks the combination of which might allow a more detailed evaluation of the brain connectivity. For these future investigations, several data sources can be used, with particular reference to EEG data.

Acknowledgments

I'd like to thank my supervisor Leonardo for the support that he gave me during these three years, Dr. Carlo Vittorio Cannistraci and Dr. Marco Levorato that allowed me to do some of my research work abroad spending time in wonderful environments and meeting amazing and interesting people, and, the last but not least, my family and all my friends that always encouraged me in this path.

Bibliography

[1] A. L. Barabasi, "Network Science," 2016.

[2] D. Towsley, and J. Wolf, "On the statistical analysis of queue lengths and waiting times for statitical multiplexers with ARQ retransmission schemes," *IEEE Trans. Commun.*, vol. 27, no. 4, pp. 693–702, 1979.

[3] A. G. Konheim, "A queueing analysis of two ARQ protocols," *IEEE Trans. Commun.*, vol. 28, no. 7, pp. 1004–1014, 1980.

[4] M. Rossi, L. Badia, and M. Zorzi, "Exact statistics of ARQ packet delivery delay over Markov channels with finite round-trip time delay," *IEEE Trans. Wireless Commun.*, vol. 4, no. 4, pp. 1858–1868, 2005.

[5] W. Luo, K. Balachandran, S. Nanda, and K. Chang, "Delay analysis of selective-repeat ARQ with applications to link adaptation in wireless packet data systems," *IEEE Trans. Wireless Commun.*, vol. 4, no. 3, pp. 1017–1029, 2005.

[6] X. Zhang, and Q. Du, "Adaptive low-complexity erasure-correcting codebased protocols for QoS-driven mobile multicast services over wireless networks," *IEEE Trans. Veh. Technol.*, vol. 55, no. 5, pp. 1633–1647, 2006.

[7] F. Zhai, Y. Eisemberg, T. N. Pappas, R. Berry, and A. K. Katsaggelos, "Rate-distortion optimized hybrid error control for real-time packetized video transmission," *IEEE Trans. Image Process.*, vol. 15, no. 1, pp. 40–51, 2006.

[8] A. Larno, M. Lindstrom, M. Meyer, G. Pelletier, J. Torsner, and H. Wiemann, "The LTE link-layer design," *IEEE Comm. Mag.*, vol. 47, no. 4, pp. 52–59, 2009.

[9] F. Fitzek, and M. Reisslein, "MPEG4 and H.263 video traces for network performance evaluation," *IEEE Netw.*, vol. 15, no. 6, pp. 40–54, 2001.

[10] *Cisco White Paper*. Available online at www.cisco.com.

[11] L. Badia, N. Baldo, M. Levorato, M. Zorzi, "A Markov framework for error control techniques based on selective retransmission in video transmission over wireless channels," *IEEE Journal on Selected Areas in Communications*, vol. 28, no. 3, pp. 488-500, 2010.

[12] S. Lin, D. J. Costello, M. J. Miller, "Automatic-Repeat-reQuest error control schemes," IEEE Commun. Mag., vol. 22, no. 12, pp. 5-17, 1984.

[13] H. O. Burton, D. Sullivan,"Errors and error control," *Proc. of IEEE*, vol. 60, no. 11, pp. 1293-1301, 1972.

[14] K. Takahata, N. Uchida, N. Y. Shibata, "QoS control for real time video stream over hybrid network by wired and wireless LANs, " *Proc. of the IEEE AINA*, pp. 45-51, 2003.

[15] T. Sikora, "MPEG digital video-coding standards," *IEEE Sign. Proc. Magazine*, vol. 14, no. 5, pp. 82-100, 1997.

[16] L. Badia, M. Levorato, M. Zorzi, "Analysis of selective repeat retransmission techniques for differentially encoded data," *Proc. of the IEEE ICC*, pp. 1-6, 2009.

[17] J. B. Seo, Y. S. Choi, S. Q. Lee, N. H. Park, and H. W. Lee, "Performance analysis of a type-II Hybrid-ARQ in a TDMA system with correlated arrival over a non-stationary channel," *Proc. ISWCS*, pp. 59-63, 2005.

[18] K. Stuhlmüller, N. Färber, M. Link, and B. Girod, "Analysis of video transmission over lossy channels," *IEEE J. Sel. Areas Commun.*, vol. 18, no. 6, pp. 1012-1030, 2000.

[19] I. Ahmed, L. Badia, D. Munaretto, and M. Zorzi, "Analysis of PHY/ application cross-layer optimization for scalable video transmission in cellular networks," *Proc. IEEE WoWMoM*, 2013.

[20] L. Badia, A. V. Guglielmi, "A Markov analysis of automatic repeat request for video traffic transmission," *Proc. IEEE WoWMoM*, 2014.

[21] C. C. Li, S. C. S. Chen, "Providing unequal reliability for transmitting layered video streams over wireless networks by multi-ARQ schemes," *ICIP*, vol.3, pp. 100-104, 1999.

[22] H. C. Wei, Y. C. Tsai, C. W. Lin, "Prioritized retransmission for error protection of video streaming over WLANs," *Proc. of the 2004 ISCAS*, vol.2, 2004.

[23] P. Pérez and N. Garcia, "Lightweight multimedia packet prioritization model for unequal error protection," *IEEE Trans. on Consumer Electronics*, vol. 57, no. 1, pp. 132-138, 2011.

[24] H. Lee, T. Jung, K. Seo, and C.K. Kim, "Delay constrained ARQ mechanism for MPEG media transport protocol based video streaming over Internet," *Proc. AFIN*, 2015.

[25] H. Ha, J. Park, S. Lee, and A. C. Bovik, "Perceptually unequal packet loss protection by weighting saliency and error propagation," *IEEE Trans. Circ. Sys. Video Tech.*, vol. 20, no. 9, pp. 1187-1199, 2010.

[26] C. H. Lin, Y. C. Wang, C. K. Shieh, and W. S. Hwang, "An unequal error protection mechanism for video streaming over IEEE 802.11e WLANs," *Computer Networks*, vol. 56, no. 11, pp. 2590-2599, 2012.

[27] J. Lu, C. K. Wu, S. Xiao, and J. C. Du, "A network coding based hybrid ARQ algorithm for wireless video broadcast," *Science China Information Sciences*, vol. 54, no. 6, pp. 1327-1332, 2011.

[28] M.-F. Tsai, T.-C. Huang, C.-H. Ke, C. K. Shieh, and W. S. Hwang, "Adaptive hybrid error correction model for video streaming over wireless networks," *Multimedia Systems*, vol. 17, no. 4, pp. 327-340, 2011.

[29] L. Badia, N. Baldo, M. Levorato, M. Zorzi, "A Markov framework for error control techniques based on selective retransmission in video transmission over wireless channels," *IEEE Journal on Selected Areas in Communications*, vol. 28, no. 3, pp. 488-500, 2010.

[30] L. Badia, "On the effect of feedback errors in Markov models for SR ARQ packet delay," *Proc. IEEE Globecom*, 2009.

[31] M. Zorzi and R. R. Rao, "Lateness probability of a retransmission scheme for error control on a two-state Markov channel," *IEEE Trans. Comm.*, vol. 47, no. 10, pp. 1537-1548, 1999.

[32] M. Rossi, L. Badia, and M. Zorzi, "On the delay statistics of SR ARQ over Markov channels with finite round-trip delay," *IEEE Trans. On Wireless Comm.*, vol. 4, no. 4, pp. 1858–1868, 2005.

[33] P. Richardson, D. Flynn, and A. Keane, "Optimal charging of electric vehicles in low voltage distribution systems," *IEEE Trans. Power Syst.*, vol. 27, no. 1, pp. 268–279, 2012.

[34] H.Y. Mak, Y. Rong, Z.J.M. Shen, "Infrastructure planning for electric vehicles with battery swapping," *Manage. Sci.*, vol. 59, pp. 1557–1575, 2012.

[35] Z. Liu, W. Tao, L. Jiang, and C. Zhu, "Design and application on electric vehicle real-time condition monitoring system by Internet of Things technology," *IEEE Trans. Software Engineering and Service Science*, pp. 744–747, 2014.

[36] S. Skippon, M. Garwood, "Responses to battery electric vehicles: UK consumer attitudes and attributions of symbolic meaning following direct experience to reduce psychological distance," *Transportation Research Part D*, vol. 16, pp. 525–531, 2011.

[37] F. J. Soares, J. A. Pecas Lopes, P. M. Rocha Almeida, C. L. Moreira, L. Seca, "A stochastic model to simulate electric vehicles motion and quantify the energy required from the grid," *Proc. Power Systems Computation Conference*, Stockholm, Sweden, 2011.

[38] E. B. Iversen, J. M. Morales, H. Madsen, "Optimal charging of an electric vehicle using a Markov decision process," *Applied Energy*, vol. 123, pp. 1–12, 2014.

[39] L. Badia, "On the impact of correlated arrivals and errors on ARQ delay terms," *IEEE Trans. Commun.*, vol. 57, no. 2, pp. 334-–338, 2009.

[40] L. Kleinrock, "Queueing Systems," vol. 1, Theory, Wiley, 1975.

[41] M. J. Osborne and A. Rubinstein, "A Course in game theory," *Cambridge, USA: The MIT Press*, 1994.

[42] R. Hassin and M. Haviv, "To queue or not to queue: Equilibrium behavior in queues," *Kluwer Academic Publishers*, Boston, 2003.

[43] M. Haviv, "When to arrive at a queue with tardiness costs?," *Performance Evaluation*, vol. 70, no. 6, pp. 387–99, 2013.

[44] A. Galeotti, S. Goyal, M. O. Jackson, F. Vega-Redondo, and L. Yariv, "Network games," *Review of Economic Studies*, Mimeo, Caltech, 2006.

[45] A. Galeotti and F. Vega-Redondo, "Complex networks and local externalities: a strategic approach," *Int. J. Ec. Theory*, vol. 7, pp. 77-–92, 2011.

[46] M. Zorzi and R. R. Rao, "Geographic random forwarding (GeRaF) for ad hoc and sensor networks: multihop performance," *IEEE Trans. Mob. Comput.*, vol. 2, no. 4, pp. 337–48, 2003.

[47] J. Buhler and G. Wunder, "Traffic-aware optimization of heterogeneous access management," *Communications, IEEE Trans. Commun.*, vol. 58, no. 6, pp. 1737–47, 2010.

[48] D. Del Testa, N. Michelusi, and M. Zorzi, "On optimal transmission policies for energy harvesting devices: the case of two users," *Proc. Int. Symp. on Wirel. Commun. Syst. (ISWCS)*, 2013.

[49] A. K. Erlang, "The theory of probabilities and telephone conversations," *Nyt Tidsskrift for Matematik B*, 1909.

[50] A. H. Kolmogorov, "Sur le probleme d'attente," *Mat. Sbornik*, vol. 38, pp. 101–6, 1931.

[51] C. D. Crommelin, "Delay probability formulae when the holding times are constant," *P. O. Elect. Engrs' J.*, vol. 25, pp. 41–50, 1932.

[52] G. Quer, F. Librino, L. Canzian, L. Badia, and M. Zorzi, "Using game theory and Bayesian networks to optimize cooperation in ad-hoc wireless networks," *Proc. IEEE ICC*, pp. 5178-–5184, 2012.

[53] T. Roughgarden, "Selfish routing and price of anarchy," *Cambridge, MIT Press*, 2005.

[54] C. W. Commander, P. M. Pardalos, V. Ryabchenko, S. Uryasev, G. Zrazhevsky, "The wireless network jamming problem," *J. Comb. Optim.*, vol. 2007, no. 14, pp. 481–498, 2007.

[55] A. Kashyap, T. Bas¸ar, and R. Srikant, "Correlated jamming on MIMO Gaussian fading channels," *IEEE Trans. Inf. Th.*, vol. 50, no. 9, pp. 2119-– 2123, Sep. 2004.

[56] K. Dabcevic, A. Betancourt, L. Marcenaro, and C. S. Regazzoni, "Intelligent cognitive radio jamming - a game-theoretical approach," *EURASIP Journal on Advances in Signal Processing*, vol. 2014, no. 171, 2014.

[57] X. Xu, K. Gao, X. Zheng, I. Zhao, "A zero-sum game theoretic framework for jamming detection and avoidance in wireless sensor networks," *Proc. IEEE CSIP*, 2012.

[58] A. Garnaev, Y. Hayel, and E. Altman, "A Bayesian jamming game in an OFDM wireless network," *Proc. WiOpt, Paderborn, Germany*, 14-18 May 2012.

[59] Y. Liu, C. Comaniciu, and H. Man, "A Bayesian game approach for intrusion detection in wireless ad hoc networks," *Proc. ACM Gamenets*, Pisa, Italy, 14 Oct. 2006.

[60] K. Akkarajitsakul, E. Hossain, and D. Niyato, "Distributed resource allocation in wireless networks under uncertainty and application of Bayesian game," *IEEE Commun. Mag.*, vol. 49, no. 8, pp. 120-–127, Aug. 2011.

[61] M.H. Manshaei, Q. Zhu, T. Alpcan, T. Bas¸ar, and J.-P. Hubaux, "Game theory meets network security and privacy," *ACM Computing Surveys*, vol. 45, no. 3, no. 25, June 2013.

[62] A. Goldsmith, "Wireless communications," CambridgeUniv.press, 2005.

[63] W. C. Jakes, "Microwave mobile communications," New York: John Wiley & Sons Inc., Feb. 1975.

[64] E. Akyol, K. Rose, and T. Bas¸ar, "On optimal jamming over an additive noise channel," *Proc. IEEE CDC*, Florence, Italy, pp. 3079–3084, Dec. 10-13, 2013.

[65] M. J. Osborne and A. Rubinstein, "A course in game theory," MITpress, 1994.

[66] J. von Neumann, "Zur Theorie der Gesellschaftsspiele," *Math. Annalen*, vol. 100 pp. 295-–320, 1928.

[67] S. J. Wright and J. Nocedal, "Numerical optimization," vol. 2, Springer, New York, 1999.

[68] J. Heidemann, W. Ye, J. Wills, A. Syed, and Y. Li, "Research challenges and applications for underwater sensor networking," *Proc. IEEE WCNC*, pp. 228-–235, Las Vegas, NV, 3-6 Apr. 2006.

[69] S. Misra, S. Dash, M. Khatua, A.V. Vasilakos and M.S. Obaidat, "Jamming in underwater sensor networks: detection and mitigation," *IET Communications*, vol. 6, no. 14, pp. 2178-–2188, Sep. 2012.

[70] A. B. MacKenzie, L. A. DaSilva, "Game theory for wireless engineers," *Morgan & Claypool Publishers*, 2006.

[71] M. Zuba, Z. Shi, Z. Peng, J.-H. Cui, "Launching denial-of-service jamming attacks in underwater sensor networks," *Proc. ACM WUWNet*, no. 12, Seattle, WA, 1-2 Dec. 2011.

[72] S. Tadelis, "Game theory: an introduction," *Princeton Univ. Press*, 2013.

[73] M. Stojanovic, "Recent advances in high-speed underwater acoustic communications," *IEEE J. Ocean. Eng.*, vol. 21, no. 2, pp. 125-–136, Apr. 1996.

[74] L. Badia, M. Mastrogiovanni, C. Petrioli, S. Stefanakos, and M. Zorzi, "An optimization framework for joint sensor deployment, link scheduling and routing in underwater sensor networks," *ACM SIGMOBILE Mob. Comput. Commun. Rev.*, vol. 11, no. 4, pp. 44–56, Oct. 2007.

[75] N. Baldo, P. Casari, and M. Zorzi, "Cognitive spectrum access for underwater acoustic communications," *Proc. IEEE ICC Workshops*, pp. 518-–523, Beijing, PRC, 19-23 May 2008.

[76] L. Badia, P. Casari, M. Levorato and M. Zorzi, "Analysis of an automatic repeat request addressing long delay channels," *Proc. WUnderNET*, Bradford, UK, 26 May 2009.

[77] R. Urick, "Principles of Underwater Sound," McGraw-Hill, 1983.

[78] J. Partan, J. Kurose, B. N. Levine, and J. Preisig, "Low spreading loss in underwater acoustic networks reduces RTS/CTS effectiveness," *Proc. ACM WUWNet*, no. 5, Seattle, WA, 1-2 Dec. 2011.

[79] L. Berkhovskikh, and Y. Lysanov, "Fundamentals of Ocean Acoustics," New York: Springer, 1982.

[80] M. Stojanovic, "On the relationship between capacity and distance in an underwater acoustic communication channel," *Proc. ACM WUWNet*, Los Angeles, CA, pp. 41—47, 25 Sep. 2006.

[81] H. F. Bezdek, "Pressure dependence of the acoustic relaxation frequency associated with MgSO4 in the ocean," *J. Acoust. Soc. Am.*, vol. 54, pp. 1062–1065, 1973.

[82] N. Vastardis, and K. Yang, "Mobile social networks: architectures, social properties, and key research challenges," *IEEE Commun. Surv. & Tut.*, vol. 15, no. 3, pp. 1355–1371, 2013.

[83] G. Quer, F. Librino, L. Canzian, L. Badia, and M. Zorzi, "Inter-Network cooperation exploiting game theory and bayesian networks," *IEEE Trans. on Comm.*, vol. 61, no. 10, pp. 4310—4321, 2013.

[84] R. Sabillon, J. Cano, V. Cavaller, and J. Serra, "Cybercrime and cybercriminals: A comprehensive study," *Int. J. Comp. Netw. Commun. Sec.*, vol. 4, no. 6, pp. 165–176, 2016.

[85] M. Jain, B. An, M. Tambe, "Security games applied to real-world: Research contributions and challenges," *Moving Target Defense II*, pp. 15—39, Springer, 2013.

[86] X. Jin, N. Pissinou, S. Pumpichet, C.A. Kamhoua, K. Kwiat, "Modeling cooperative, selfish and malicious behaviors for trajectory privacy preservation using Bayesian game theory," *Local Computer Networks (LCN)*, pp. 835—842, IEEE, 2013.

[87] X. Liang, Y. Xiao, "Game theory for network security," *IEEE Communications Surveys and Tutorials*, vol. 15, n. 1, pp. 472—486, 2013.

[88] Y. Liu, C. Comaniciu, H. Man, "A Bayesian game approach for intrusion detection in wireless ad hoc networks," *Proceeding from the 2006 Workshop on game theory for Communications and Networks*, ACM, 2006.

[89] M.H. Manshaei, Q. Zhu, T. Alpcan, T. Bac¸sar, J.P. Hubaux, "Game theory meets network security and privacy," *ACM Comput. Surv.*, vol. 45, n. 3, pp. 1—39, 2013.

[90] K.C. Nguyen, T. Alpcan, T. Basar, "Security games with incomplete information," *International Conference on Communications (ICC)*, pp. 1-–6, 2009.

[91] P. Paruchuri, J.P. Pearce, J. Marecki, M. Tambe, F. Ordonez, S. Kraus, "Playing games for security: an efficient exact algorithm for solving bayesian stackelberg games," *Proceedings of AAMAS*, pp. 895-–902, 2008.

[92] M.A. Rahman, M.H. Manshaei, E. Al-Shaer, "A game-theoretic approach for deceiving remote operating system fingerprinting," *IEEE CNS*, pp. 73-–81, 2013.

[93] J. Tsai, C. Kiekintveld, F. Ordonez, M. Tambe, S. Rathi, "Iris-a tool for strategic security allocation in transportation networks," 2009.

[94] S. Farhang, M. H. Manshaei, M. N. Esfahani, Q. Zhu, "A dynamic bayesian security game framework for strategic defense mechanism design," *R. Poovendran and W. Saad (eds.) GameSec 2014, LNCS*, vol. 8840, pp. 317-–326, Springer, 2014.

[95] J. Golbeck, "Trust and nuanced profile similarity in online social networks," *ACM Transactions on the Web*, vol. 3, no. 4, art. 12, Sept. 2009.

[96] R. Li, C. Wang, and K. C.-C. Chang, "User profiling in an ego network: co-profiling attributes and relationships," *Proceedings ACM WWW*, pp. 819–830, 2014.

[97] Z. Wang, D. Zhang, X. Zhou, D. Yang, Z. Yu, and Z. Yu, "Discovering and profiling overlapping communities in location-based social networks," *IEEE Trans. Syst., Man, and Cyb.*, vol. 44, no. 4, pp. 499–509, Apr. 2014.

[98] C. Diaz, C. Troncoso, and A. Serjantov, "On the impact of social network profiling on anonymity," *Lect. Notes in Comput. Science*, vol. 5134, pp. 44-62, 2008.

[99] L.A. Cutillo, R. Molva, and T. Strufe, "Safebook: A privacy-preserving online social network leveraging on real-life trust," *IEEE Commun. Mag.,* vol. 47, no. 12, pp. 94–101, Dec. 2009.

[100] Q. Cai, M. Gong, L. Ma, S. Ruan, F. Yuan, and L. Jiao, "Greedy discrete particle swarm optimization for large-scale social network clustering," *Information Sciences*, vol. 316, pp. 503–516, Sept. 2015.

[101] S. Sharma and S. K. Jena, "Cluster based multipath routing protocol for wireless sensor networks," *ACM SIGCOMM Comp. Commun. Rev.*, vol. 45, no. 2, pp. 14–20, Apr. 2015.

[102] B. J. Frey and D. Dueck, "Clustering by passing messages between data points," *Science*, vol. 315, no. 5814, pp. 972–976, 2007.

[103] P. Sasikumar and S. Khara, "K-means clustering in wireless sensor networks," *Proc. Int. Conf. Comput. Intellig. Commun. Netw.*, pp. 140–144, Nov. 2012.

[104] M. Rossi, L. Badia, P. Giacon, M. Zorzi, "Energy and connectivity performance of routing groups in multi-radio multi-hop networks," *Wirel. Commun. Mob. Comput.*, vol. 8, no. 3, pp. 327–342, Mar. 2008.

[105] L. Gou, M. X. Zhou, H. Yang, "KnowMe and ShareMe: understanding automatically discovered personality traits from social media and user sharing preferences," *Proc. ACM CHI*, pp. 955–964, 2014.

[106] M. Xiao, J. Wu, L. Huang, "Community-aware opportunistic routing in mobile social networks," *IEEE Trans. Comp.*, vol. 63, no. 7, pp. 1682–1695, July 2014.

[107] I. Lequerica, M. García Longaron, P. M. Ruiz, "Drive and share: efficient provisioning of social networks in vehicular scenarios," *IEEE Commun. Mag.*, vol. 48, no. 11, pp. 90–97, Nov. 2010.

[108] E. M. Daly, M. Haahr, "Social network analysis for information flow in disconnected delay-tolerant MANETs," *IEEE Trans. Mob. Comput.*, vol. 8, no. 5, pp. 606–621, May 2009.

[109] L. Badia, A. Erta, L. Lenzini, M. Zorzi, "A general interference-aware framework for joint routing and link scheduling in wireless mesh networks," *IEEE Network*, vol. 22, no. 1, pp. 32–38, Jan. 2008.

[110] M. M. Halldórsson, "Modeling reality algorithmically: the case of wireless communication," *Lect. Notes in Comput. Science*, vol. 8243, pp. 1–5, Dec. 2013.

[111] C. Jiang, Y. Chen, Y. Yang, C. Wang, and K. J. R. Liu, "Dynamic Chinese restaurant game: theory and application to cognitive radio networks," *IEEE Trans. Wirel. Commun.*, vol. 13, no. 4, pp. 1960–1973, 2014.

[112] N. Fernando, S. Loke, and W. Rahayu, "Mobile cloud computing: A survey," *Future Generation Computer Systems*, vol. 29, no. 1, pp. 84—106, 2012.

[113] Y. C. Hu, M. Patel, D. Sabella, N. Sprecher, and V. Young, "Mobile edge computing-A key technology towards 5G," *ETSI White Paper*, vol. 11, 2015.

[114] J. Weibull, "Evolutionary game theory," *Cambridge, MA: The M.I.T Press*, 1995.

[115] F. Bonomi, R. Milito, J. Zhu, S. Addepalli, "Fog computing and its role in the Internet of Things," *Proc. Mobile Cloud Comput.*, pp. 13–16, 2012.

[116] W. Wang, A. Kwasinski, D. Niyato, and Z. Han, "A survey on applications of model-free strategy learning in cognitive wireless networks, *IEEE Commun. Surv.& Tut.*, vol. 18, no. 3, pp. 1717-1757, Jan. 2016.

[117] M. Ghazvini, N. Movahedinia, K. Jamshidi, and N. Moghim, "Game theory applications in CSMA methods," *IEEE Commun. Surv.& Tut.*, vol. 15, no. 3, pp. 1062-1087, 2013.

[118] D. Niyato and E. Hossain, "Radio resource management games in wireless networks: an approach to bandwidth allocation and admission control for polling service in IEEE 802.16," *IEEE Wirel. Commun.*, vol. 14, no. 1, pp. 27-–35, 2007.

[119] R. Trestian, O. Ormond, and G.-M. Muntean, "Reputation-based network selection mechanism using game theory," *Phys. Commun.*, vol. 4, no. 3, pp. 156-171, 2011.

[120] G. Scutari and D. P. Palomar, "MIMO cognitive radio: a game theoretical approach," *IEEE Trans. Sig. Proc.*, vol. 58, no. 2, pp. 761-–780, Feb. 2010.

[121] M. A. Khan, H. Tembine, and A. V Vasilakos, "Evolutionary coalitional games: design and challenges in wireless networks," *IEEE Wirel. Commun.*, vol. 19, no. 2, pp. 50-56, 2012.

[122] T. AlSkaif, M. G. Zapata, and B. Bellalta, "Game theory for energy efficiency in wireless sensor networks: latest trends," *J. Netw. Comput. Appl.*, vol. 54, pp. 33-61, 2015.

[123] E. Abebe and C. Ryan, "Adaptive application offloading using distributed abstract class graphs in mobile environments," *J. Syst. Softw.*, vol. 85, no. 12, pp. 2755–2769, 2012.

[124] B. G. Chun, S. Ihm, P. Maniatis, M. Naik, and A. Patti, "Clonecloud: elastic execution between mobile device and cloud," *Proc. EuroSys*, pp. 301–314, 2011.

[125] R. Rahimi, N. Venkatasubramanian, S. Mehrotra, and A. Vasilakos, "MAPCloud: mobile applications on an elastic and scalable 2-tier cloud architecture," *Proc. IEEE UCC*, pp. 83–90, 2012.

[126] R. Rahimi, N. Venkatasubramanian, and A. Vasilakos, "MuSIC: on mobility-aware optimal service allocation in mobile cloud computing," *Proc. IEEE Cloud*, 2013.

[127] L. Yang, J. Cao, and H. Cheng, "Resource constrained multi-user computation partitioning for interactive mobile cloud applications," *tech. rep., Dept. of Computing*, Hong Kong Polytechnic Univ., 2012.

[128] L. Yang, J. Cao, Y. Yuan, T. Li, A. Han, and A. Chan, "A framework for partitioning and execution of data stream applications in mobile cloud computing," *Sigmetrics Perf. Eval. Rev.*, vol. 40, no. 4, pp. 23–32, 2013.

[129] V. Cardellini, V. De Nitto Personé, V. Di Valerio, F. Facchinei, V. Grassi, F. Lo Presti, and V. Picialli, "A game-theoretic approach to computation offloading in mobile cloud computing," *Math. Progr.*, vol. 157, no. 2, pp. 421–449, 2016.

[130] P. Erdos, and A. Renyi, "On random graph," *Publ. Math. Debrecen 6*, pp. 290, 1959.

[131] R. Albert, H. Jeong, and A. L. Barabasi, "Diameter of the World Wide Web," *Nature*, vol. 401, pp. 130–131, 1999.

[132] F. Dressler, O. B. Akan, "Bio-inspired networking: from theory to practice," *New R and D Tools for Wireless Communications*, 2010.

[133] F. Ferreira-Santos, " Complex network analysis of brain connectivity: an introduction," *Lab. Neuropsychophysiology - Univ. Porto*, 2012.

[134] M. Rubinov, and O. Sporns, "Complex network measures of brain connectivity: uses and interpretations," *Neuroimage*, vol. 52, pp. 1059–1069, 2010.

[135] G. Di Caro, and M. Dorigo, "AntNet: distributed stigmergeticcontrol for communication networks," *J. Artificial intelligence research*, vol. 9, pp. 317–365, 1998.

[136] B. Atakan, and O. B. Akan, "Immune system based distributed node and rate selection in wireless sensor networks," *Proc. IEEE/ACM BIONETICS*, 2006.

[137] D. Mantini, M. G. Perrucci, C. Del Gratta, G. L. Romani, and M. Corbetta, "Electrophysiological signatures of resting state networks in the human brain," *Proceedings of the National Academy of Sciences of the United States of America*, vol. 104, no. 32, pp. 170–5, 2007.

[138] Q. K. Telesford, S. L. Simpson, J. H. Burdette, S. Hayasaka, and P. J. Laurienti, "The brain as a complex system: using network science as a tool for understanding the brain," *Brain Connect.*, vol. 1, no. 4, pp. 295-308, Oct. 2011.

[139] M. Rubinov and O. Sporns, "Complex network measures of brain connectivity: uses and interpretations," *Neuroimage*, vol. 52, pp. 1059-1069, 2010.

[140] R. M. Hutchison, T. Womelsdorf, E. A. Allen, P. A. Bandettini, V. D. Calhoun, M. Corbetta, S. Della Penna, J. H. Duyn, G. H. Glover, J. Gonzalez-Castillo, D. A. Handwerker, S. Keilholz, V. Kiviniemi, D. A. Leopold, F. de Pasquale, O. Sporns, M. Walter, and C. Chang, "Dynamic functional connectivity: Promise, issues, and interpretations," *NeuroImage*, vol. 80, pp. 360–378, 2013.

[141] S. M. Smith, "The future of fMRI connectivity," *NeuroImage*, vol. 62, no. 2, pp. 1257–1266, 2012.

[142] C. W. Wu, H. Gu, H. Lu, E. A. Stein, J. H. Chen, and Y. Yang, "Frequency specificity of functional connectivity in brain networks," *NeuroImage*, vol. 42, no. 3, pp. 1047–1055, 2008.

[143] J. Fitzsimmons, M. Kubicki, and M. Shenton, "Review of functional and anatomical brain connectivity findings in schizophrenia," *Curr. Opin. Psychiatry*, vol. 26, no. 2, pp. 172-187, Mar. 2013.

[144] P. C. Mulders, P. F. van Eijndhoven, A. H. Schene, C. F. Beckmann, and I. Tendolkar, "Resting-state functional connectivity in major depressive disorder: A review," *Neuroscience & Biobehavioral Reviews* vol. 56, pp. 330-344, 2015.

[145] Y. I. Sheline and M. E. Raichle, "Resting state functional connectivity in preclinical Alzheimer's disease," *Biological Psychiatry*, vol. 74, no. 5, pp. 340–347, 2013.

[146] N. U. F. Dosenbach, S. E. Petersen, and B. L. Schlaggar, "The teenage brain: functional connectivity," *Curr. Dir. in Psychol. Science*, vol. 22, pp. 101-107, Apr. 2013.

[147] R. Sala-Llonch, D. Bartrés-Faz, and C. Junqué, "Reorganization of brain networks in aging: a review of functional connectivity studies," *Frontiers in psychology*, vol. 6, no. May, p. 663, 2015.

[148] L. K. Ferreira and G. F. Busatto, "Resting-state functional connectivity in normal brain aging," *Neuroscience & Biobehavioral Reviews*, vol. 37, no. 3, pp. 384–400, 2013.

[149] J. S. Damoiseaux and M. D. Greicius, "Greater than the sum of its parts: a review of studies combining structural connectivity and resting-state functional connectivity." *Brain structure & function*, vol. 213, no. 6, pp. 525–33, 2009.

[150] K. Friston, R. Moran, and A. K. Seth, "Analysing connectivity with Granger causality and dynamic causal modelling," *Current Opinion in Neurobiology*, vol. 23, pp. 172 – 178, 2013.

[151] O. Sporns, "Network attributes for segregation and integration in the human brain," *Current Opinion in Neurobiology*, vol. 23, no. 2, pp. 162–171, 2013.

[152] G. Buzsáki and A. Draguhn, "Neuronal oscillations in cortical networks," *Science*, vol. 304, pp. 1926 – 1929, 2004.

[153] V. D. Calhoun, R. Miller, G. Pearlson, and T. Adali, "The Chronnectome: time-varying connectivity networks as the next frontier in fMRI data discovery," *Neuron*, vol. 84, no. 2, pp. 262–274, 2014.

[154] V. D. Calhoun and T. Adali, "Time-varying brain connectivity in fMRI data: whole-brain data-driven approaches for capturing and characterizing dynamic states," *IEEE Sig. Proc. Mag.*, vol. 33, no. 3, pp. 52–66, 2016.

[155] Y. Han, J. Wang, Z. Zhao, B. Min, J. Lu, K. Li, Y. He, and J. Jia, "Frequency-dependent changes in the amplitude of low-frequency fluctuations in amnestic mild cognitive impairment: A resting-state fMRI study," *NeuroImage*, vol. 55, no. 1, pp. 287–295, 2011.

[156] B. Biswal, F. Z. Yetkin, V. M. Haughton, and J. S. Hyde, "Functional connectivity in the motor cortex of resting human brain using echo-planar MRI," *Magn. Reson. Med.*, vol. 34, pp. 537 – 541, 1995.

[157] X. N. Zuo, A. Di Martino, C. Kelly, Z. E. Shehzad, D. G. Gee, D. F. Klein, F. X. Castellanos, B. Biswal, and M. P. Milham, "The oscillating brain: complex and reliable," *NeuroImage*, vol. 49, pp. 1432 – 1445, 2010.

[158] DPARSF toolbox, available at: `http://rfmri.org/DPARSF`.

[159] fMRI data, available at: `http://rfmri.org/DemoData`.

[160] D. Cordes, V. M. Haughton, K. Arfanakis, J. D. Carew, P. A. Turski, C. H. Moritz, M. A. Quigley, and M. E. Meyerand, "Frequencies contributing to functional connectivity in the cerebral cortex in resting state data ," *AJNR Am. J. Neuroradiol.*, vol. 22, pp. 1326 – 1333, 2001.

[161] P. Fransson, "Spontaneous low-frequency BOLD signal fluctuations: an fMRI investigation of the resting-state default mode of brain function hypothesis," *Hum. Brain Mapp.*, vol. 26, pp. 15 – 29, 2005.

[162] M. De Domenico, "Multilayer modeling and analysis of human brain networks," *GigaScience*, vol. 6, no. 5, pp. 1—8, 2017.

[163] R. Pascual, and D. Marqui, "Review of methods for solving the EEG inverse problem," *Int. J. Bioelectromagnetism*, vol. 1, pp. 75—86, 1999.

[164] S. AxleR, P. Bourdon, and W. Ramey, "Harmonic function theory," *Springer*, New York, 1992.

[165] K. J. Worsley, J.-I. Chen, J. Lerch, and A. C. Evans, "Comparing functional connectivity via thresholding correlations and singular value decomposition,", *Phil. Trans. R. Soc. B*, issue 360, pp. 913—920, 2005.

[166] J. L. Chen, T. Ros, and J. H. Gruzelier, "Dynamic changes of ICA derived EEG functional connectivity in the resting state," *Human Brain Mapping*, vol. 34, no. 4, pp. 852-–868, 2013.

[167] Y. Aoki, R. Ishii, R. D. Pascual-Marqui, et al., "Detection of EEG-resting state independent networks by eLORETA-ICA method," *Front Hum Neurosci*, 2016.

[168] L. Jancke and N. Alahmadi, "Detection of independent functional networks during music listening using electroencephalogram and sLORETA–ICA," *Neuroreport*, no. 27, pp. 455-–461, 2016.

[169] P. Holme and J. Saramaki, "Temporal networks," *Phys. Rep.*, vol. 519, no. 97, 2012.

[170] M. Kivela, A. Arenas, M. Barthelemy, J. P. Gleeson, Y. Moreno, and M. A. Porter, "Multilayer networks."

[171] S. Wasserman and K. Faust, "Social network analysis: methods and applications, structural analysis in the social sciences," vol. 8, *Cambridge University Press*, Cambridge, England, 1994.

[172] J. Gao, S. V. Buldyrev, H. E. Stanley, and S. Havlin, "Networks formed from interdependent networks," *Nat. Phys*, vol. 8, pp. 40, 2012.

[173] S. V. Buldyrev, R. Parshani, G. Paul, H. E. Stanley, and S. Havlin, "Catastrophic cascade of failures in interdependent networks," *Nature*, vol. 464, pp. 1025, 2010.

[174] K. Lewis, J. Kaufman, M. Gonzalez, A. Wimmer, and N. Christakis, "Tastes, ties, and time: a new social network dataset using Facebook.com," *Soc. Networks*, vol. 30, pp. 330, 2008.

[175] E. A. Leicht and R. M. D'Souza, "Percolation on interacting networks."

[176] P. J. Mucha, T. Richardson, K. Macon, M. A. Porter, and J.-P. Onnela, "Community structure in time-dependent, multiscale, and multiplex networks," *Science*, vol. 328, pp. 876, 2010.

[177] S. Sasai, F. Homae, H. Watanabe, A. T. Sasaki, H. C. Tanabe, N. Sadato, and G. Taga, "Frequency-specific network topologies in the resting state human brain," *frontiers in Human Neuroscience*, vol. 8, pp. 1022, 2014.

[178] M. De Domenico, S. Sasai, and A. Arenas, "Mapping multiplex hubs in human functional brain networks," vol. 10, pp. 326, 2016.

[179] M. De Domenico, V. Nicosia, A. Arenas, and V. Latora "Structural reducibility of multilayer networks," *Nature Communication*, vol. 6, no. 6864, 2015.

[180] M. J. Brookes, P. K. Tewarie, B. A. E. Hunt, S. E. Robson, L. E. Gascoyne, E. B. Liddle, P. F. Liddle, and P. G. Morris, "A multilayer network approach to meg connectivity analysis," *Neuroimage*, vol. 132, pp. 425–438, 2016.

[181] P. Tewarie, A. Hillebrand, B. W. van Dijk, C. J. Stam, G. C. O'Neill, P. V. Mieghem, J. M. Meier, M. W. Woolrich, P. G. Morris, and M. J. Brookes, "Integrating cross-frequency and within band functional networks in resting-state meg: a multilayer network approach," *Neuroimage*, vol. 142, pp. 324–336, 2016.

[182] G. Deco, J. Cabral, M. W. Woolrich, A. B. A. Stevner, T. J. van Hartevelt, and M. L. Kringelbach, "Single or multi-frequency generators in on-going brain activity: a mechanistic whole-brain model of empirical meg data," *Neuroimage*, vol. 152, pp. 538–550, 2016.

[183] J. Guillon, Y. Attal, O. Colliot, V. La Corte, B. Dubois, D. Schwartz, M. Chavez, and F. De Vico Fallani, "Loss of inter-frequency brain hubs in alzheimer's disease," *Scientific Reports*, vol. 7, no. 10879, 2017.

[184] S. Palva,S. Monto, and J. M. Palva, "Graph properties of synchronized cortical networks during visual working memory maintenance," *Neuroimage* vol. 49, no. 4, pp. 3257–3268, 2009.

[185] M. Boersma, D. J. A. Smit, H. M. A. de Bie, G. C. M. Van Baal, D. I. Boomsma, E. J. C. de Geus, H. A. D. van de Waal, and C. J. Stam, "Network analysis of resting state EEG in the developing young brain: structure comes with maturation," *Human Brain Mapping*, vol. 32, no. 3, pp. 413–425, 2011.

[186] K. Mann, P. Backer, and J. Roschke, "Dynamical properties of the sleep eeg in different frequency bands," *International Journal of Neuroscience*, vol. 73, no. 3, pp. 161–169, 1993.

[187] H. Liu, J. Wang, C. Zheng, and P. He, "Study on the effect of different frequency bands of EEG signals on mental tasks classification," *IEEE-EMBS*, 2005.

[188] J. C. Munck, S. I. Gonçalves, R. Mammolit, R. M. Heethaar, and F. H. Lopes da Silva, "Interactions between different EEG frequency bands and their effect on alpha-fMRI correlations," *Neuroimage*, vol. 47, no. 1, pp. 69–76, 2009.

[189] F. Deligianni, M. Centeno, D. W. Carmichael, and J. D. Clayden, "Relating resting-state fMRI and EEG whole-brain connectomes across frequency bands," *Front Neurosci.*, vol. 8, pp. 258, 2014.